For Reference

NOT TO BE TAKEN FROM THIS ROOM

Ex libris
universitatis
albertaensis

THE UNIVERSITY OF ALBERTA

RELEASE FORM

NAME OF AUTHOR DAVID T. LYNCH

TITLE OF THESIS OSCILLATORY BEHAVIOR IN CATALYTIC REACTIONS: A MATHEMATICAL AND EXPERIMENTAL INVESTIGATION

DEGREE FOR WHICH THESIS WAS PRESENTED DOCTOR OF PHILOSOPHY

YEAR THIS DEGREE GRANTED SPRING, 1982

Permission is hereby granted to THE UNIVERSITY OF ALBERTA LIBRARY to reproduce single copies of this thesis and to lend or sell such copies for private, scholarly or scientific research purposes only.

The author reserves other publication rights, and neither the thesis nor extensive extracts from it may be printed or otherwise reproduced without the author's written permission.

THE UNIVERSITY OF ALBERTA

OSCILLATORY BEHAVIOR IN CATALYTIC REACTIONS: A MATHEMATICAL AND EXPERIMENTAL INVESTIGATION

by

© DAVID T. LYNCH

A THESIS

SUBMITTED TO THE FACULTY OF GRADUATE STUDIES AND RESEARCH

IN PARTIAL FULFILMENT OF THE REQUIREMENTS FOR THE DEGREE

OF DOCTOR OF PHILOSOPHY

IN

CHEMICAL ENGINEERING

DEPARTMENT OF CHEMICAL ENGINEERING

EDMONTON, ALBERTA

SPRING, 1982

Digitized by the Internet Archive
in 2022 with funding from
University of Alberta Libraries

https://archive.org/details/Lynch1982

THE UNIVERSITY OF ALBERTA

FACULTY OF GRADUATE STUDIES AND RESEARCH

The undersigned certify that they have read, and recommend to the Faculty of Graduate Studies and Research, for acceptance, a thesis entitled OSCILLATORY BEHAVIOR IN CATALYTIC REACTIONS: A MATHEMATICAL AND EXPERIMENTAL INVESTIGATION submitted by DAVID T. LYNCH in partial fulfilment of the requirements for the degree of DOCTOR OF PHILOSOPHY in CHEMICAL ENGINEERING.

ABSTRACT

In recent years many theoretical and experimental examinations of the stability of chemically reacting systems have shown that these systems can display oscillatory behavior. In this work, a combined modelling and experimental investigation of oscillatory behavior in the oxidation of CO over supported metal catalysts was performed.

The initial modelling studies were of a general nature, and from them it was found that the use of simplifying assumptions in reactor models can result in transient and steady-state violations of mass conservation. It was also found that complex periodic and chaotic behavior are possible when a reactor model consists of more than two ordinary differential equations.

From the experimental work, the detailed effects of operating conditions on oscillatory behavior in the oxidation of CO over supported Pt and Pt-Pd catalysts were determined. This experimental work enabled some insight to be gained into the underlying mechanism responsible for oscillatory behavior.

Using the experimental insights, a specific model for the catalytic oxidation of CO was developed. For certain parameter values, this model successfully reproduced many of the fine structural details of the experimentally observed oscillations.

Table of Contents

Chapter Page

1. INTRODUCTION AND OBJECTIVES 1

1.1 Introduction 1

1.2 Research Objectives 3

1.3 Thesis Layout 4

1.4 References 5

2. EFFECT OF SIMPLIFYING ASSUMPTIONS ON A NON-OSCILLATORY MODEL 8

2.1 Introduction 8

2.2 A Simple Model 9

2.3 Exact Solution 11

2.4 Steady-State Assumption 13

2.5 Equilibrium Assumption 14

2.5.1 Elimination of [X] from Eq. 2.9 15

2.5.2 Elimination of [X] and [AX] from Eq. 2.10 .16

2.5.3 Elimination of [AX] and [BX] from Eq. 2.11 17

2.6 Conditions for Pairwise Equivalence 18

2.7 Conclusions 20

2.8 Nomenclature 21

2.9 References 22

3. EFFECT OF THE EQUILIBRIUM ASSUMPTION ON A MODEL FOR AN OSCILLATORY REACTION 23

3.1 Introduction 23

3.2 Eigenberger's Model 23

3.3 Elimination of [X] — System #1 27

3.3.1 Uniqueness Analysis 28

3.3.2 Stability Analysis 32

3.3.2.1 Trace Condition 32
3.3.2.2 Determinant Condition 35
3.4 Elimination of [AX] — System #2 36
3.4.1 Uniqueness Analysis 36
3.4.2 Stability Analysis 39
3.4.2.1 Trace Condition 39
3.4.2.2 Determinant Condition 40
3.5 Elimination of [BX] — System #3 40
3.5.1 Uniqueness Analysis 40
3.6 Comparison of Systems #1, #2, and #3 43
3.7 Isolation of the Equilibrium Assumption 48
3.7.1 Elimination of [AX] — System #1A 49
3.7.2 Elimination of [AX] — System #2A 51
3.7.3 Elimination of [BX] — System #3A 53
3.8 Conclusions 55
3.9 Nomenclature 55
3.10 References 56
4. EFFECT OF THE REMOVAL OF THE EQUILIBRIUM ASSUMPTION ..58
4.1 Introduction 58
4.2 General Model 58
4.3 Stability Analysis 59
4.4 Numerical Results and Discussion 65
4.5 Conclusions 68
4.6 Nomenclature 68
4.7 References 69
5. CHAOS AND RELATED PHENOMENA 70
5.1 Introduction 70

5.2 Model Development 71
5.3 Stability Analysis 74
5.4 Hopf Bifurcation from a Unique Steady State 75
5.5 Complex Oscillations and Chaotic Behavior 79
5.6 Chaos and Fractal Curves 88
5.7 Trajectories in T-Y-Z Space 91
5.8 Conclusions 94
5.9 Nomenclature 94
5.10 References 96
6. DESCRIPTION OF THE EXPERIMENTAL APPARATUS 98
6.1 General Description of the Equipment 98
6.2 Feed Metering and Mixing 99
6.3 Heated Recycle Compartment 103
6.4 Catalytic Reactor in Heated Fluidized Sandbath ..106
6.5 Auxiliary Reactor 110
6.6 Gas Composition Analysis 113
6.6.1 Gas Chromatograph 114
6.6.2 Infrared Spectrophotometer 118
7. OSCILLATORY BEHAVIOR IN THE OXIDATION OF CARBON MONOXIDE 123
7.1 Literature Review 123
7.2 Preliminary Experimental Work 128
7.3 Effects of Operating Conditions 137
7.3.1 CO_2, CO and Combined Oscillations 138
7.3.2 Recycle Ratio 142
7.3.3 Bulk Temperature 144
7.3.4 Concentration of CO in the Feed 146
7.3.5 Volumetric Feed Rate - CO/O_2 Constant 148

7.3.6 Volumetric Feed Rate - Molar CO Flow Constant 148

7.3.7 Nitrogen and Helium Diluents 151

7.3.8 Reactor Pressure 154

7.4 Qualitative Effects of Temperature 156

7.5 Chaos and Nitrogen Dilution at 423 K 158

7.6 Reproducibility of Oscillations 159

7.7 Conclusions 168

7.8 References 170

8. A MODEL FOR OSCILLATORY BEHAVIOR FOR CO OXIDATION ...172

8.1 Model Development 172

8.2 Stability and Uniqueness 177

8.3 Numerical Integration Results 178

8.4 Conclusions 186

8.5 Nomenclature 187

8.6 References 188

9. RECOMMENDATIONS 190

Appendix A Computer Programs for Chapters 3 and 4 192

Appendix B Computer Programs for Chapter 5 202

Appendix C Rotameter and Flowmeter Calibrations 224

Appendix D Gas Chromatograph Calibration 230

Appendix E Computer Programs for Chapter 8 235

VITA 248

LIST OF TABLES

Table	Page
2.1 Conditions for Pairwise Steady-State Equivalence	18
2.2 Conditions for Pairwise Dynamic Equivalence	19
3.1 Sign of the Discriminant and Quartic Root Types	29
4.1 Types of Solutions to Equations 4.1 - 4.3	64
7.1 Description of Oscillations Shown in Figure 7.3	141
8.1 Parameter Values for Figures 8.1 and 8.2	181
8.2 Parameter Values for Figure 8.3	185
D.1 GC Calibration Data for CO_2-N_2 Mixtures	231
D.2 GC Calibration Data for O_2-N_2 Mixtures	232
D.3 GC Calibration Data for CO-N_2 Mixtures	232

LIST OF FIGURES

Figure		Page
3.1	System #1 - Regions of Uniqueness and Multiplicity as a Function of K_{23} and K_4	31
3.2	System #1 - Trace Condition and Stability Regions as a Function of K_{23} and K_4	34
3.3	System #1 - Combined Stability and Uniqueness Regions as a Function of K_{23} and K_4	37
3.4	System #3 - Regions of Differing Numbers of Steady-States	44
3.5	Steady-State Differences between Systems #1, #2, and #3	45
3.6	Dynamic Differences between Systems #1, #2, and #3	47
3.7	System #1A - Effect of K_2/K_{-2} on [AX]	50
3.8	System #2A - Effect of K_2/K_{-2} on [AX]	52
3.9	System #3A - Effect of K_2/K_{-2} on [AX]	54
4.1	Predictions of Eigenberger's Model	62
4.2	Stability Regions for the General Model as a Function of K_2 and K_{-2}	63
4.3	Predictions of the General Model	66
4.4	Predictions of the General Model	67
5.1	Stability Regions as a Function of Da_1 and β_2	77
5.2	Hopf Bifurcation	78
5.3	Four Maxima per Cycle Oscillation	80
5.4	Chaotic Oscillation	81
5.5	Chaotic Oscillation	82
5.6	Six Maxima per Cycle Oscillation	83
5.7	Chaotic Oscillation with Emergence of a Third Curve on the Next-Amplitude Plot	89
5.8	Fractal Curves in the Next-Amplitude Plot	90

5.9 Two-Dimensional Views of the Three-Dimensional Attractor 93

6.1 General Description of the Experimental Apparatus 100

6.2 Feed Metering and Mixing Schematic 101

6.3 Heated Recycle Compartment Schematic 104

6.4 Reactor in Sandbath 107

6.5 Reactor Detail 109

6.6 Auxiliary Reactor 111

6.7 Gas Chromatograph Column Arrangement 116

6.8 Typical GC Chromatograms 117

6.9 Infrared Spectrophotometer Sample Cell 120

6.10 IR Calibration Curves for CO and CO_2 122

7.1 Preliminary Observations — GM Pt-Pd Catalyst 132

7.2 Preliminary Observations — 0.05% Pt Catalysts 135

7.3 Simple Oscillatory Behavior 139

7.4 Effect of Recycle Ratio 143

7.5 Effect of Bulk Temperature 145

7.6 Effect of Molar Percent CO in the Feed 147

7.7 Effect of Volumetric Feed Rate (Constant CO/O_2 in the Feed) 149

7.8 Effect of Volumetric Feed Rate (Constant CO Molar Flow in the Feed) 150

7.9 Effect of Nitrogen and Helium Diluents on CO Oscillations 152

7.10 Effect of Reactor Pressure 155

7.11 Qualitative Effects of Temperature 157

7.12 Effect of Dilution of Oxygen With Nitrogen 160

7.13 Reproducibility of the Oscillatory Behavior 162

7.14 Catalyst Activity Changes at 473 K 163

8.1 Oscillations Similar to Experimental Observations 180

8.1 Extreme Forms of the CO Oscillations 183

8.3 Multipeak Oscillations 184

C.1 Rotameter Calibration Curves for Oxygen 225

C.2 Rotameter Calibration Curves for Helium 226

C.3 Rotameter Calibration Curves for Nitrogen 227

C.4 Calibration Curves for Matheson Model ALL-100 Linear Mass Flowmeter (0-100 SCCM) 228

C.5 Calibration Curves for Matheson Model 8116-0153 Linear Mass Flowmeter (0-5000 SCCM) 229

1. INTRODUCTION AND OBJECTIVES

1.1 Introduction

Initiated by the early work of Liljenroth [1.1] and van Heerden [1.2], a considerable amount of research has been directed at analyzing the stability of chemically reacting systems. Theoretical and experimental studies, summarized in several review articles [1.3 - 1.7], have shown that under certain conditions, chemical and catalytic reaction systems can display oscillatory behavior. In a continuous flow reactor, oscillatory behavior is normally manifested through periodic changes in the reaction temperature and/or the concentrations of reacting species with respect to time. In heterogeneously catalyzed reactions oscillations in concentrations of adsorbed species and/or oscillations in the temperature of the catalyst's surface can occur as well. These oscillations can occur without accompanying oscillations in the bulk fluid phase.

The recent interest in oscillatory phenomena in chemical reactors is due to several factors:

1. The fundamental processes occurring in chemical reactors can be more fully understood through a knowledge of the mechanisms by which oscillatory behavior occurs.
2. Large temperature fluctuations on catalyst surfaces can result in rapid catalyst deactivation.
3. Large temperature fluctuations in a chemical reactor can

present safety problems, hence, a knowledge of how to predict, and suppress, this behavior is necessary for proper design and operation.

4. Increased conversion of reactants to products, and isolation of low yield intermediates, can sometimes be obtained by operating a chemical reactor in a cyclical fashion.

In the field of heterogeneously catalyzed reactions, reports of oscillatory behavior have been mainly restricted to oxidation reactions, e.g. oxidation of ammonia [1.8], hydrogen [1.9 - 1.11], carbon monoxide [1.12 - 1.19], and hydrocarbons [1.19 - 1.21], catalyzed by bulk (wire, gauze or foil) or supported platinum or nickel. Self-sustained ocillations have been observed in recycle, fixed-bed and single-pellet reactors under isothermal and nonisothermal conditions. Various causes for the oscillatory behavior have been postulated; these include competing mechanisms [1.13, 1.14], variations in activation energy with surface coverage [1.22, 1.23], non-reacting adsorbed species [1.24], presence of impurities [1.15], formation of surface oxides [1.21, 1.25], variations in catalyst surface temperature [1.26], and local heat and mass transfer effects [1.27].

Many mathematical models which display oscillatory behavior have been constructed using the above postulates. Unfortunately, a large chasm has separated the theoreticians from the experimentalists, as none of the models which have

appeared in the literature have been validated through systematic experimentation. There are two main reasons for this: firstly, an experimental study which systematically examines the effects of the various operating conditions (temperature, concentration, space velocity, etc.) on oscillatory behavior has yet to appear in the literature, and secondly, most models have been so reduced in complexity through the use of simplifying assumptions that only a tenuous connection with physical reality remains.

1.2 Research Objectives

As originally conceived, this research project was to encompass a general mathematical and experimental examination of oscillatory behavior in heterogeneous catalytic reactors. Since a total description of this phenomena would indeed be a formidable task, a number of specific research areas, generally consistent with the overall objectives, were chosen.

As a starting point, models which have appeared in the literature were examined with the particular aim of investigating the effects of simplifying assumptions, such as the equilibrium assumption. Also, in order to gain modelling experience, simple models displaying oscillatory behavior were developed. In parallel with this work, an experimental apparatus was constructed and oscillatory behavior of carbon monoxide oxidation over supported metal catalysts was

examined.

Building on the experience thus gained, a systematic experimental investigation of the effects of operating conditions on oscillatory behavior was performed. In parallel with the experimental study, a new model for carbon monoxide oxidation was developed. The new model was kept as physically realistic as possible, so that all parameters in the model had actual physical counterparts, and thus the model behavior could be directly compared with the actual experimental behavior. However, in a model, increased complexity is the price which is exacted for physical realism, and thus a total delimiting of the model behavior has not yet been achieved.

1.3 Thesis Layout

Since the research project was approached from several directions, this thesis is composed of several quite distinct though related pieces of work. For this reason, references are cited at the end of each chapter.

In Chapter 2, a simple catalytic reaction is examined so as to develop the groundwork for determining the effects of simplifying assumptions on reaction models. Building on this development, the effects of the equilibrium assumption on a model of an oscillatory reaction are presented in Chapter 3, and in Chapter 4 the consequences of removing the equilibrium assumption, and going to a higher order system

(three ordinary differential equations), are examined. In Chapter 5, an interesting property of high order systems, namely chaos, is introduced, and is shown to exist in a very simple reaction model.

The next two Chapters, 6 and 7, are devoted to a description of the experimental equipment, and a presentation of experimental observations for carbon monoxide oxidation on supported metal catalysts. These experimental observations are then used in Chapter 8 to qualitatively examine the predictions of a new model for carbon monoxide oxidation. Finally in Chapter 9 possible directions for future work are presented.

1.4 References

1.1 Liljenroth, F.G., Chem. Met. Eng., 1918 19 287.

1.2 van Heerden, C., Ind. Eng. Chem., 1953 45 1242.

1.3 Nicolis, G. and Portnow, J., Chem. Rev., 1973 73 365.

1.4 Schmitz, R.A., Adv. Chem. Ser., 1975 148 156.

1.5 Sheintuch, M. and Schmitz, R.A., Catal. Rev. Sci. Eng., 1977 15 107.

1.6 Franck, U.F., Angew. Chem. Int. Ed. Engl., 1978 17 1.

1.7 Slin'ko, M.G. and Slin'ko, M.M., Catal. Rev. Sci. Eng., 1978 17 119.

1.8 Flytzani-Stephanopoulos, M., Schmidt, L.D. and Caretta, R., J. Catal., 1980 64 346.

1.9 Zuniga, J.E. and Luss, D., J. Catal., 1978 53 312.

1.10 Belyaev, V.D., Slin'ko, M.M. and Slin'ko M.G., Proc. Int. Congr. Catal., 6th (London 1976), p. 758, Chem. Soc., London, 1977.

1.11 Kurtanjek, Z., Sheintuch, M. and Luss, D., J. Catal., 1980 66 11.

1.12 Beusch, H., Fieguth, P. and Wicke, E., Chem. Ing. Techn., 1972 44 445.

1.13 Hugo, P. and Jakubith, M., Chem. Ing. Techn., 1972 44 383.

1.14 McCarthy, E., Zahradnik, J., Kuczynski, G.C. and Carberry, J.J., J. Catal., 1975 39 29.

1.15 Varghese, P., Carberry, J.J. and Wolf, E.E., J. Catal., 1978 55 76.

1.16 Plichta, R.T. and Schmitz, R.A., Chem. Eng. Commun., 1979 3 387.

1.17 Sheintuch, M., AIChE J., 1981 27 20.

1.18 Rathousky, J., Kira, E. and Hlavacek, V., Chem. Eng. Sci., 1981 36 776.

1.19 Cutlip, M.B. and Kenney, C.N., Chemical Reaction Engineering - Houston, ACS Symp. Ser. 65, p.475, ACS, Washington, 1978.

1.20 Hawkins, J.R. and Wanke, S.E., Can. J. Chem. Eng., 1979 57 621.

1.21 Vayenas, C.G., Lee, B. and Michaels, J., J. Catal., 1980 66 36.

1.22 Pikios, C.A. and Luss, D., Chem. Eng. Sci., 1977 32

191.

1.23 Ivanov, E.A., Chumakov, G.A., Slin'ko, M.G., Bruns, D.D., Luss, D., Chem. Eng. Sci., 1980 35 795.

1.24 Eigenberger, G., Chem. Eng. Sci., 1978 33 1263.

1.25 Renola, G.T., Ph.D. Thesis, University of Illinois, 1979.

1.26 Dagonnier, R., Dumont, M. and Nuyts, J., J. Catal., 1980 66 130.

1.27 Jensen, K.F. and Ray, W.H., Chem. Eng. Sci., 1980 35 241.

2. EFFECT OF SIMPLIFYING ASSUMPTIONS ON A NON-OSCILLATORY MODEL

2.1 Introduction

In the modelling of heterogeneously catalyzed reactions, whether it be steady-state or dynamic modelling, it is common to begin with fairly complex models which consist of many equations. These large models result from the need to describe the many variables (bulk and surface phase temperatures, bulk and surface phase concentrations of the reactants and products, surface phase concentrations of intermediates, etc.) which are present in heterogeneous catalytic systems.

Since the analytical or numerical solution of large systems of simultaneous non-linear algebraic or differential equations is a non-trivial task, it is common to reduce the size of the system of equations by making simplifying assumptions. In the modelling of heterogeneously catalyzed reactions, the two most commonly used simplifying assumptions are the steady-state assumption and the equilibrium assumption.

These two assumptions have been used, usually without question, throughout virtually the entire history of heterogeneous catalysis, as shown by examination of the early works [2.1, 2.2] in the field. It is only as of late that any questioning of the validity of the assumptions [2.3],

and examination of their effects [2.4 - 2.6] has been performed. However, even in systems in which it can be shown that the surface reaction is the controlling step, the use of the equilibrium assumption in a model can have some unexpected effects. These insidious effects result from the very manner in which the equilibrium assumption is used to eliminate variables from a model.

In the following, it will be shown that for a very simple model, extremely different, and in some cases contradictory, results can be obtained depending on how the equilibrium assumption is used to eliminate variables from the model. For comparison purposes, the exact analytical solution, and a solution using the steady-state hypothesis, are also presented.

2.2 A Simple Model

The irreversible isomerization of A will be used as an example. The overall reaction is

$$A \longrightarrow B \tag{2.1}$$

and the following reaction mechanism will be considered:

$$A + X \underset{k_{-1}}{\overset{k_1}{\rightleftharpoons}} AX \tag{2.2}$$

$$B + X \underset{k_{-2}}{\overset{k_2}{\rightleftharpoons}} BX \tag{2.3}$$

$$AX \xrightarrow{k_3} BX \tag{2.4}$$

If the catalytic sites, X, are conserved,then mass balances on AX, BX, and X give:

$$\frac{d[AX]}{dt} = k_1[A][X] - k_{-1}[AX] - k_3[AX] \tag{2.5}$$

$$\frac{d[BX]}{dt} = k_2[B][X] - k_{-2}[BX] + k_3[AX] \tag{2.6}$$

$$\frac{d[X]}{dt} = - k_1[A][X] + k_{-1}[AX] - k_2[B][X] + k_{-2}[BX] \tag{2.7}$$

where the normalized site conservation equation is given by:

$$[AX] + [BX] + [X] = 1 \tag{2.8}$$

In dimensionless form, Eqs. 2.5-2.7 are written as:

$$\frac{d[AX]}{dT} = K_1[X] - K_{-1}[AX] - [AX] \tag{2.9}$$

$$\frac{d[BX]}{dT} = K_2[X] - K_{-2}[BX] + [AX] \tag{2.10}$$

$$\frac{d[X]}{dT} = - K_1[X] + K_{-1}[AX] - K_2[X] + K_{-2}[BX] \tag{2.11}$$

where,

$$K_1 = k_1[A]/k_3 \tag{2.12a}$$

$$K_{-1} = k_{-1}/k_3 \tag{2.12b}$$

$$K_2 = k_2[B]/k_3 \tag{2.12c}$$

$$K_{-2} = k_{-2}/k_3 \tag{2.12d}$$

$$T = k_3t \tag{2.12e}$$

In the following it will be assumed that [A] and [B] in the gas phase are held constant. Conceptually, this could

be achieved by having only a very small amount of catalyst in a large reactor, or alternatively, it could be accomplished by regulating the flows of A and B to and from the reactor.

2.3 Exact Solution

Since Eq. 2.8 forces the sum of the derivatives to be equal to zero, i.e.:

$$\frac{d[AX]}{dT} + \frac{d[BX]}{dT} + \frac{d[X]}{dT} = 0 \tag{2.13}$$

then Eqs. 2.9-2.11 are not linearly independent, and any two of these equations are sufficient to completely describe the behavior of the surface concentrations. For example, if [X] is eliminated from Eqs. 2.9 and 2.10 by using Eq. 2.8, then the following system of two ordinary differential equations results:

$$\frac{d[AX]}{dT} = -(1+K_1+K_{-1})[AX] - K_1[BX] + K_1 \tag{2.14}$$

$$\frac{d[BX]}{dT} = (1-K_2)[AX] - (K_2+K_{-2})[BX] + K_2 \tag{2.15}$$

From linear systems theory, the solution of Eqs. 2.14 and 2.15 is given by:

$$[AX] = -\frac{K_1(a+K_{-2})(1-e^{aT})}{a(a-b)} + \frac{K_1(b+K_{-2})(1-e^{bT})}{b(a-b)} \tag{2.16}$$

$$+\left\{\frac{(a+K_{-2}+K_2)e^{aT}}{(a-b)} - \frac{(b+K_{-2}+K_2)e^{bT}}{(a-b)}\right\}[AX]_o - \frac{K_1(e^{aT}-e^{bT})}{(a-b)}[BX]_o$$

$$[BX] = -\frac{\{K_1+K_2(a+1+K_{-1})\}(1-e^{aT})}{a(a-b)} + \frac{\{K_1+K_2(b+1+K_{-1})\}(1-e^{bT})}{b(a-b)}$$

$$+\frac{\{(a+1+K_1+K_{-1})e^{aT} - (b+1+K_1+K_{-1})e^{bT}\}}{(a-b)}[BX]_o$$

$$+\frac{(1-K_2)(e^{aT}-e^{bT})}{(a-b)}[AX]_o \qquad (2.17)$$

where,

$$a = -\frac{(1+K_1+K_{-1}+K_2+K_{-2})}{2}\left[1-\sqrt{1-4\frac{\{K_1(1+K_{-2})+(1+K_{-1})(K_2+K_{-2})\}}{(1+K_1+K_{-1}+K_2+K_{-2})^2}}\right] \qquad (2.18a)$$

$$b = -\frac{(1+K_1+K_{-1}+K_2+K_{-2})}{2}\left[1+\sqrt{1-4\frac{\{K_1(1+K_{-2})+(1+K_{-1})(K_2+K_{-2})\}}{(1+K_1+K_{-1}+K_2+K_{-2})^2}}\right] \qquad (2.18b)$$

From Eqs. 2.16 and 2.17, the values of [AX] and [BX] at a steady-state are readily found to be:

$$[AX] = -\frac{K_1(a+K_{-2})}{a(a-b)} + \frac{K_1(b+K_{-2})}{b(a-b)}$$

$$[AX] = \frac{K_1K_{-2}}{K_1(1+K_{-2}) + (1+K_{-1})(K_2+K_{-2})} \qquad (2.19)$$

$$[BX] = \frac{K_1 + K_2(1+K_{-1})}{K_1(1+K_{-2}) + (1+K_{-1})(K_2+K_{-2})} \qquad (2.20)$$

Thus, Eqs. 2.16-2.20 completely describe the dynamic and steady-state behavior of the reaction system.

2.4 Steady-State Assumption

In the previous reaction system, the steady-state assumption could take the form of assuming that the concentration of either of surface species AX or BX is always at a steady-state. If, for example, surface species BX is always at a steady-state, then mathematically this is equivalent to setting Eq. 2.10 equal to zero,

$$K_2[X] - K_{-2}[BX] + [AX] = 0 \tag{2.21}$$

If Eq. 2.21 is used in conjunction with the site conservation equation, Eq. 2.8, then the system of Eqs. 2.9-2.11 can be reduced to a single equation in one variable. Eliminating [X] and [BX] from Eq. 9 gives:

$$\frac{d[AX]}{dT} = \frac{K_1K_{-2}}{K_2+K_{-2}} - [AX]\frac{\{K_1(1+K_{-2})+(1+K_{-1})(K_2+K_{-2})\}}{(K_2+K_{-2})} \tag{2.22}$$

Equation 2.22 is solved to yield:

$$[AX] = \frac{K_1K_{-2}(1-e^{-T\{K_1(1+K_{-2})+(1+K_{-1})(K_2+K_{-2})\}/(K_2+K_{-2})})}{K_1(1+K_{-2})+(1+K_{-1})(K_2+K_{-2})} + [AX]_o e^{-T\{K_1(1+K_{-2})+(1+K_{-1})(K_2+K_{-2})\}/(K_2+K_{-2})} \tag{2.23}$$

It should be noted that this result can also be obtained if Eqs. 2.8 and 2.21 are used to eliminate [AX] and [BX] from Eq. 2.11, as the same expression for [AX] always occurs irrespective of the solution path which is followed when the steady-state assumption is used.

A comparison of Eq. 2.23 with the exact solution given by Eqs. 2.16 and 2.19 shows that these equations have

identical steady-state behavior. Also, if $K_2+K_{-2} \gg 1+K_1+K_{-1}$, then the dynamic behavior of Eq. 2.16 will be similar to that of Eq. 2.23, as the constants **a** and **b** in the exponential terms of Eq. 2.16 become:

$$a \simeq -\frac{(K_2+K_{-2})}{2}\left[1-\sqrt{1-4\frac{\{K_1(1+K_{-2})+(1+K_{-1})(K_2+K_{-2})\}}{(K_2+K_{-2})^2}}\right]$$

$$a \simeq -\frac{\{K_1(1+K_{-2})+(1+K_{-1})(K_2+K_{-2})\}}{(K_2+K_{-2})} \qquad (2.24)$$

$$b \simeq -(K_2+K_{-2}) + \frac{\{K_1(1+K_{-2})+(1+K_{-1})(K_2+K_{-2})\}}{(K_2+K_{-2})} \qquad (2.25)$$

From Eqs. 2.24 and 2.25 it is seen that **b** is a much larger negative number than **a** when $K_2+K_{-2} \gg 1+K_1+K_{-1}$, thus the exponential terms containing **b** in Eq. 2.16 will rapidly approach zero, and hence the dynamic behavior of Eq. 2.16 will be controlled by the exponential terms which contain **a**. This will result in the exponential terms of Eqs. 2.16 and 2.23 being identical, hence the dynamic behavior of Eq. 2.16 will be similar to that of Eq. 2.23.

2.5 Equilibrium Assumption

The equilibrium assumption for this simple reaction system could take the form of assuming that either of AX or BX is at equilibrium with the gas phase. In order to maintain consistency with the preceeding development for the steady-state hypothesis, it will be assumed that BX is always at equilibrium with the gas phase, which

mathematically is equivalent to:

$$K_2[X] = K_{-2}[BX] \tag{2.26}$$

By using Eqs. 2.26 and 2.8, it is possible to eliminate two of the [AX], [BX], and [X] concentrations from Eqs. 2.9-2.11, and thus reduce the system to a single equation in one variable. In the following it will be shown that extremely different solutions can be arrived at depending on which two variables are eliminated.

2.5.1 Elimination of [X] from Eq. 2.9

Combination of Eqs. 2.8 and 2.26 yields [X] as a function of [AX],

$$[X] = \frac{K_{-2}(1-[AX])}{(K_2+K_{-2})} \tag{2.27}$$

Using Eq. 2.27 to eliminate [X] in Eq. 2.9 gives:

$$\frac{d[AX]}{dT} = \frac{K_1K_{-2}}{K_2+K_{-2}} - [AX]\frac{\{K_1K_{-2}+(1+K_{-1})(K_2+K_{-2})\}}{(K_2+K_{-2})} \tag{2.28}$$

Solving Eq. 2.28 for [AX] yields:

$$[AX] = \frac{K_1K_{-2}\left(1-e^{-T\{K_1K_{-2}+(1+K_{-1})(K_2+K_{-2})\}/(K_2+K_{-2})}\right)}{K_1K_{-2}+(1+K_{-1})(K_2+K_{-2})} + [AX]_0 e^{-T\{K_1K_{-2}+(1+K_{-1})(K_2+K_{-2})\}/(K_2+K_{-2})} \tag{2.29}$$

Comparing Eq. 2.29 with 2.23 reveals that the [AX] from the equilibrium assumption will be similar to that from the steady-state assumption if $K_{-2} \gg 1$.

2.5.2 Elimination of [X] and [AX] from Eq. 2.10

Combination of Eqs. 2.8 and 2.26 can be used to yield [AX] as a function of [BX], such that,

$$[AX] = 1 - [BX](K_2+K_{-2})/K_2 \tag{2.30}$$

Using Eq. 2.24 to eliminate [X], and Eq. 2.30 to eliminate [AX] in Eq. 2.10 yields:

$$\frac{d[BX]}{dT} = 1 - [BX]\frac{(K_2+K_{-2})}{K_2} \tag{2.31}$$

Solving Eq. 2.31 for [BX] gives:

$$[BX] = \frac{K_2(1-e^{-T(K_2+K_{-2})/K_2})}{(K_2+K_{-2})} + [BX]_o e^{-T(K_2+K_{-2})/K_2} \tag{2.32}$$

The behavior of [AX] can now be determined by substituting Eq. 2.32 into Eq. 2.30 to yield:

$$[AX] = [AX]_o e^{-T(K_2+K_{-2})/K_2} \tag{2.33}$$

In order to remain consistent with the equilibrium assumption, Eq. 2.30 has also been used to convert $[BX]_o$ to $[AX]_o$ in Eq. 2.32.

It is seen that the steady-state and dynamic behavior for [AX] predicted by Eq. 2.33 is extremely different from that given by Eq. 2.29, as Eq. 2.33 predicts a steady-state value of [AX] equal to zero, which will only occur in Eq. 2.29 if $K_1K_{-2} \neq 0$. However, even if this condition is met, the dynamic behavior of Eq. 2.33 will only be similar to that of Eq. 2.29 if the additional conditions $K_{-1} \ll 1$ and

$K_{-2} << K_2$ are met. It is interesting to note that these above conditions are necessary to secure dynamic and steady-state agreement between Eqs. 2.29 and 2.33 even though both equations were derived from Eqs. 2.9-2.11 using the same equilibrium assumption.

2.5.3 Elimination of [AX] and [BX] from Eq. 2.11

Substitution of Eq. 2.26 into Eq. 2.8 yields [AX] as a function of [X],

$$[AX] = 1 - [X](K_2+K_{-2})/K_{-2} \tag{2.34}$$

Using Eqs. 2.26 and 2.34 to respectively eliminate [BX] and [X] in Eq. 2.11 gives:

$$\frac{d[X]}{dT} = K_{-1} - [X]\frac{\{K_1K_{-2}+K_{-1}(K_2+K_{-2})\}}{K_{-2}} \tag{2.35}$$

Solving Eq. 2.35 for [X] yields:

$$[X] = \frac{K_{-1}K_{-2}(1-e^{-T\{K_1K_{-2}+K_{-1}(K_2+K_{-2})\}/K_{-2}})}{(K_1K_{-2}+K_{-1}(K_2+K_{-2})} + [X]_o e^{-T\{K_1K_{-2}+K_{-1}(K_2+K_{-2})\}/K_{-2}} \tag{2.36}$$

The behavior of [AX] can now be determined by substituting Eq. 2.36 into Eq. 2.34 to give:

$$[AX] = \frac{K_1K_{-2}(1-e^{-T\{K_1K_{-2}+K_{-1}(K_2+K_{-2})\}/K_{-2}})}{(K_1K_{-2}+K_{-1}(K_2+K_{-2})} + [AX]_o e^{-T\{K_1K_{-2}+K_{-1}(K_2+K_{-2})\}/K_{-2}} \tag{2.37}$$

A comparison of Eqs. 2.37 and 2.29 shows that if $K_{-1}>>1$ and $K_{-2}>>K_2$, then similar steady-state and dynamic behavior for [AX] will be predicted by both equations. As in the previous derivation, these conditions are necessary even though both of Eqs. 2.29 and 2.37 were derived from Eqs. 2.9-2.11 using the same equilibrium assumption.

2.6 Conditions for Pairwise Equivalence

Listed in Tables 2.1 and 2.2 are the various conditions necessary for pairwise equivalent behavior between the expressions derived for [AX] using the exact solution, the steady-state approximation, and the equilibrium assumption.

Table 2.1 Conditions for Pairwise Steady-State Equivalence

	Eq. 2.23 (S.-S.)	Eq. 2.29 (Equil.)	Eq. 2.33 (Equil.)	Eq. 2.37 (Equil.)
Eq. 2.19 (Exact)	None	$K_{-2}>>1$	$K_1K_{-2}\simeq 0$	$K_{-2}>>1$ $K_{-1}>>1$
Eq. 2.23 (S.-S.)	—	$K_{-2}>>1$	$K_1K_{-2}\simeq 0$	$K_{-2}>>1$ $K_{-1}>>1$
Eq. 2.29 (Equil.)	$K_{-2}>>1$	—	$K_1K_{-2}\simeq 0$	$K_{-1}>>1$
Eq. 2.33 (Equil.)	$K_1K_{-2}\simeq 0$	$K_1K_{-2}\simeq 0$	—	$K_1K_{-2}\simeq 0$
Eq. 2.37 (Equil.)	$K_{-2}>>1$ $K_{-1}>>1$	$K_{-1}>>1$	$K_1K_{-2}\simeq 0$	—

An inspection of the conditions listed in Table 2.2 reveals some additional complications which result from the equilibrium assumption. Not only do the forms of Eqs. 2.29,

Table 2.2 Conditions for Pairwise Dynamic Equivalence

	Eq. 2.23 (S.-S.)	Eq. 2.29 (Equil.)	Eq. 2.33 (Equil.)	Eq. 2.37 (Equil.)
Eq. 2.19 (Exact)	$K_2+K_{-2}>>1+K_1+K_{-1}$	$K_{-2}>>1$ $K_2+K_{-2}>>1+K_1+K_{-1}$	$K_{-1}<<1$ $K_{-2}<<K_2$ $K_2+K_{-2}>>1+K_1+K_{-1}$	$K_{-1}>>1$ $K_{-2}>>K_2$ $K_2+K_{-2}>>1+K_1+K_{-1}$
Eq. 2.23 (S.-S.)	—	$K_{-2}>>1$	$K_{-1}<<1$ $K_{-2}<<K_2$ $K_1<<K_2$	$K_{-1}>>1$ $K_{-1}>>K_2$ $K_{-2}>>1$
Eq. 2.29 (Equil.)	$K_{-2}>>1$	—	$K_{-1}<<1$ $K_{-2}<<K_2$ $K_1K_{-2}<<K_2$	$K_{-1}>>1$ $K_{-2}>>K_2$
Eq. 2.33 (Equil.)	$K_{-1}<<1$ $K_{-2}<<K_2$ $K_1<<K_2$	$K_{-1}<<1$ $K_{-2}<<K_2$ $K_1K_{-2}<<K_2$	—	$K_{-1}\doteq 1$ $K_{-2}\doteq K_2$ $K_1<<1$
Eq. 2.37 (Equil.)	$K_{-1}>>1$ $K_{-2}>>K_2$ $K_{-2}>>1$	$K_{-1}>>1$ $K_{-2}>>K_2$	$K_{-1}\doteq 1$ $K_{-2}\doteq K_2$ $K_1<<1$	—

2.33, 2. 37 differ from each other, but, contradictory conditions are necessary in order to have agreement between Eqs. 2.29 and 2.33, or Eqs. 2.29 and 2.37. For example, Eqs. 2.29 and 2.33 will be dynamically similar if $K_{-1}<<1$, $K_{-2}<<K_2$ and $K_1K_{-2}<<K_2$, however, Eqs. 2.29 and 2.37 will be dynamically similar if $K_{-1}>>1$ and $K_{-2}>>K_2$. Clearly these conditions are contradictory.

2.7 Conclusions

The preceeding derivations were not performed with the intention of illustrating that certain conditions are necessary to secure agreement between an exact solution, and solutions based on steady-state or equilibrium assumptions. This is intuitively obvious, and needs no proof. Rather, they were intended to illustrate that the steady-state approximation does not introduce any inconsistencies into the solution of a reaction model, while the equilibrium assumption does introduce inconsistencies. The inconsistencies introduced by the equilibrium assumption appear in the form of different, and contradictory, solutions to the reaction model depending on which variables are eliminated from the model by the use of this assumption.

The question whose answer must now be attempted is: "What is the 'best' way of using the equilibrium assumption?". A tentative answer to this question can be provided by examining the following equations which result from directly introducing the equilibrium assumption into Eqs. 2.9-2.11.

$$\frac{d[AX]}{dT} = K_1[X] - K_{-1}[AX] - [AX] \tag{2.38}$$

$$\frac{d[BX]}{dT} = [AX] \tag{2.39}$$

$$\frac{d[X]}{dT} = - K_1[X] + K_{-1}[AX] \tag{2.40}$$

As was previously shown, the solution of Eq. 2.38 was given by Eq.2.29, and it is this equation, of the solutions based on the equilibrium assumption, which most closely agrees with either the exact solution or the solution based on the steady-state approximation. A comparison of Eqs. 2.38-2.40 with Eqs. 2.9-2.11 shows that Eq. 2.38 is the only equation which has not been explicitly altered by the equilibrium assumption (an implicit alteration occurs in the site conservation equation). Hence, a very casual rule-of-thumb is to only use those equations which have been altered the 'smallest amount' by the application of the equilibrium assumption.

For this model, with the analytical derivation completed, it can be confidently said that the implicit alteration of one term in Eq. 2.38 is a smaller alteration than the total elimination of two terms which has occurred in each of Eqs. 2.39 and 2.40. However, in general there is no way of determining if one type of alteration is smaller than another.

2.8 Nomenclature

Roman

a,b constants in the analytical solution of Eqs. 2.14-2.15

[A] gas phase concentration of A

[AX] normalized surface phase concentration of A

[B] gas phase concentration of B

[BX] normalized surface concentration of B

k_i rate constant for the i-th forward reaction

k_{-i} rate constant for the i-th forward reaction

K_i dimensionless rate constants for the forward reactions

K_{-i} dimensionless rate constants for the forward reactions

t time

T dimensionless time

[X] normalized active site surface concentration

2.9 References

2.1 Rideal, E.K. and Taylor, H.S., Catalysis in Theory and Practice, MacMillan, London, 1926.

2.2 Schwab, G.-M., Taylor, H.S. and Spence, R., Catalysis, Van Nostrand, New York, 1937.

2.3 Bilimoria, M.R., Bruns, D.D. and Bailey, J.E., AIChE J., 1980 26 319.

2.4 Elnashaie, S.S. and Cresswell, D.L., Chem. Eng. Sci., 1974 29 753.

2.5 Herz, R.K. and Marin, S.P., J. Catal., 1980 65 281.

2.6 Lynch, D.T. and Wanke, S.E., accepted Can. J. Chem. Eng.

3. EFFECT OF THE EQUILIBRIUM ASSUMPTION ON A MODEL FOR AN OSCILLATORY REACTION

3.1 Introduction

In the previous chapter it was seen that the use of the equilibrium assumption can have unexpected effects on both the steady-state and the dynamic behavior of a reaction model. Since these effects were present in even a very simple model, they should also be present in the more complex models which are used to describe oscillatory behavior in chemical reactions. In order to determine the effects of the equilibrium assumption on a model of an oscillatory reaction it was decided to examine a model presented by Eigenberger [3.1].

3.2 Eigenberger's Model

Eigenberger proposed that oscillatory behavior in catalytic reactions could be caused by the existence of an inert surface species which alternately acts as a source of, and a sink for catalytic sites. For the overall reaction $2A + B \longrightarrow 2C$, Eigenberger proposed the following mechanism:

$$A + X \underset{k_{-1}}{\overset{k_1}{\rightleftharpoons}} AX \qquad (3.1)$$

$$B + 2X \underset{k_{-2}}{\overset{k_2}{\rightleftharpoons}} BXX \qquad (3.2)$$

$$2AX + BXX \xrightarrow{k_3} 2C + 4X \qquad (3.3)$$

$$B + X \underset{k_{-4}}{\overset{k_4}{\rightleftharpoons}} BX \qquad (3.4)$$

The adsorbed species BX is unreactive in this mechanism and acts as a capacitance which makes oscillations possible.

In several papers [3.1 - 3.3] devoted to describing this model, it was always assumed that the BXX species was at equilibrium with the gas phase. In this way, a reaction model describing this system can be reduced to a system of two ordinary differential equations, as two of [AX], [BX], [BXX] and [X] can be eliminated through the use of the equilibrium assumption, and the site conservation equation. However, based on the work in the previous chapter, the question must arise as to which two variables should be eliminated.

A general model for this system based on mass balances on the surface species is as given below:

$$\frac{d[AX]}{dt} = k_1[A][X] - k_{-1}[AX] - 2k_3[AX]^2[BXX] \qquad (3.5)$$

$$\frac{d[BX]}{dt} = k_4[B][X] - k_{-4}[BX] \qquad (3.6)$$

$$\frac{d[BXX]}{dt} = k_2[B][X]^2 - k_{-2}[BXX] - k_3[AX]^2[BXX] \qquad (3.7)$$

$$\frac{d[X]}{dt} = k_{-1}[AX] - k_1[A][X] + 2k_{-2}[BXX] - 2k_2[B][X]^2 + k_{-4}[BX] - k_4[B][X] + 4k_3[AX]^2[BXX] \qquad (3.8)$$

where it is assumed that [A] and [B] in the gas phase are held constant by some means or other, and where the normalized site conservation equation is given by:

$$[AX] + [BX] + 2[BXX] + [X] = 1 \tag{3.9}$$

In dimensionless form, this system of equations is given by:

$$\frac{d[AX]}{dT} = K_1[X] - K_{-1}[AX] - 2K_3[AX]^2[BXX] \tag{3.10}$$

$$\frac{d[BX]}{dT} = K_4[X] - [BX] \tag{3.11}$$

$$\frac{d[BXX]}{dT} = K_2[X]^2 - K_{-2}[BXX] - K_3[AX]^2[BXX] \tag{3.12}$$

$$\frac{d[X]}{dT} = K_{-1}[AX] - K_1[X] + K_{-2}[BXX] - 2K_2[X]^2 + [BX] - K_4[X] + 4K_3[AX]^2[BXX] \tag{3.13}$$

where,

$$K_1 = k_1[A]/k_{-4} \tag{3.14a}$$

$$K_{-1} = k_{-1}/k_{-4} \tag{3.14b}$$

$$K_2 = k_2[B]/k_{-4} \tag{3.14c}$$

$$K_{-2} = k_{-2}/k_{-4} \tag{3.14d}$$

$$K_3 = k_3/k_{-4} \tag{3.14e}$$

$$K_4 = k_4[B]/k_{-4} \tag{3.14f}$$

$$T = k_{-4}t \tag{3.14g}$$

Eigenberger eliminated two of the variables from this model by assuming equilibrium for the BXX species, i.e.:

$$K_2[X]^2 = K_{-2}[BXX] \tag{3.15}$$

and by using the normalized site conservation equation,

$$[AX] + [BX] + [X] = 1 \tag{3.16}$$

In the site conservation equation, Eigenberger assumed that [BXX] was always very small, and thus was insignificant compared to the other terms. However, the development in the preceeding chapter has shown that the model performance is affected by the choice of variables which are eliminated through the use of the simplifying assumptions. Thus, it is necessary to decide which two of [AX], [BX], [X] or [BXX] should be eliminated through the use of Eqs. 3.15 and 3.16. This decision can be partially resolved by examining the resultant forms of Eqs. 3.10-3.13 if the equilibrium assumption is assumed to hold, i.e.

$$\frac{d[AX]}{dT} = K_1[X] - K_{-1}[AX] - 2K_3[AX]^2[BXX] \tag{3.17}$$

$$\frac{d[BX]}{dT} = K_4[X] - [BX] \tag{3.18}$$

$$\frac{d[BXX]}{dT} = - K_3[AX]^2[BXX] \tag{3.19}$$

$$\frac{d[X]}{dT} = K_{-1}[AX] - K_1[X] + [BX] - K_4[X] + 4K_3[AX]^2[BXX] \tag{3.20}$$

Clearly, Eq. 3.19 should not be used, as use of this equation will have one of two results; either [BXX] will be driven to a stable steady-state at zero, or some of the other concentrations will be driven into physically impossible regions, i.e. outside of the interval (0,1). Thus, as was done by Eigenberger, Eq. 3.15 will be used to eliminate

[BXX], with the following set of equations resulting:

$$\frac{d[AX]}{dT} = K_1[X] - K_{-1}[AX] - K_{23}[AX]^2[X]^2 \qquad (3.21)$$

$$\frac{d[BX]}{dT} = K_4[X] - [BX] \qquad (3.22)$$

$$\frac{d[X]}{dT} = K_{-1}[AX] - K_1[X] + [BX] - K_4[X] + 2K_{23}[AX]^2[X]^2 \qquad (3.23)$$

where, $K_{23} = 2K_3K_2/K_{-2}$ (3.24)

However, the choice is still unclear as to which of the remaining three variables should be eliminated by Eq. 3.16. In the following, the three possible different systems, each consisting of two ordinary differential equations, will be examined. In particular, the steady-state and dynamic differences between these systems will be illustrated.

3.3 Elimination of [X] — System #1

If Eq. 3.16 is used to eliminate [X] from Eqs. 3.21-3.23, then the following system, to be known as System #1, results:

$$\frac{d[AX]}{dT} = K_1(1-[AX]-[BX]) - K_{-1}[AX] - K_{23}[AX]^2(1-[AX]-[BX])^2 \qquad (3.25)$$

$$\frac{d[BX]}{dT} = K_4(1-[AX]-[BX]) - [BX] \qquad (3.26)$$

In order to better understand the behavior of this system, both a uniqueness, and a stability analysis will be

performed.

3.3.1 Uniqueness Analysis

A uniqueness analysis consists of determining when the system of Eqs. 3.25 and 3.26 has a unique steady-state.This can be determined by performing the following steps:

1. The left-hand sides of the differential equations are set equal to zero.
2. The resulting algebraic equations are combined to obtain a single algebraic equation in one variable.
3. The conditions for which this algebraic equation has a unique zero are determined.

Setting the left-hand sides of Eqs. 3.25 and 3.26 equal to zero gives:

$$K_1(1-[AX]-[BX]) - K_{-1}[AX]^2 - K_{23}^2(1-[AX]-[BX])^2 = 0 \quad (3.27)$$

$$K_4(1-[AX]-[BX]) - [BX] = 0 \quad (3.28)$$

Solving Eq. 3.28 for [BX], and substituting this into Eq. 3.27 gives upon rearrangement:

$$[AX]^4 - 2[AX]^3 + [AX]^2 + [AX]\{K_1+K_{-1}(1+K_4)\}(1+K_4)/K_{23} - K_1(1+K_4)/K_{23} = 0 \quad (3.29)$$

Applying Descartes Rule of Signs to Eq. 3.29 reveals that it has one or three positive real roots, and one negative real root. Since only roots in the interval $0 \leq [AX] \leq 1$ are physically reasonable, it is necessary to check the number of positive roots which are outside of this range. This is

done by substituting [AX]=Z+1 into Eq. 3.29 to get:

$$Z^4 + 2Z^3 + Z^2 + Z\frac{\{K_1+K_{-1}(1+K_4)\}(1+K_4)}{K_{23}} + \frac{K_{-1}(1+K_4)^2}{K_{23}} = 0 \quad (3.30)$$

An application of Descartes Rule of Signs to Eq. 3.30 shows that there are no roots in the region Z>0, hence there are no roots in the region [AX]>1. Thus, the region $0 \leq [AX] \leq 1$ can contain either one or three positive real roots.

The conditions under which only a single positive real root will exist can be determined by examining the discriminant of Eq. 3.29. For the general quartic equation

$$x^4 + bx^3 + cx^2 + dx + e = 0 \quad (3.31a)$$

the discriminant is given by [3.4] :

$$\Delta = -4p^3 - 27q^2 \quad (3.31b)$$

where, $$p = bd - 4e - c^2/3 \quad (3.31c)$$

and $$q = -b^2e + bcd/3 + 8ce/3 - d^2 - 2c^3/27 \quad (3.31d)$$

The type of roots of the quartic equation can be determined from the sign of the discriminant as shown in Table 3.1.

Table 3.1 Sign of the Discriminant and Quartic Root Types

	Types of Roots of the Quartic Equation
$\Delta < 0$	2 distinct real roots; 2 complex conjugate roots
$\Delta = 0$	repeated roots
$\Delta > 0$	4 distinct roots, or no real roots

Since Eq. 3.29 always has one negative root, then the necessary and sufficient conditions for the existence of a

single positive real root is that the discriminant of Eq. 3.29 should always be negative. Of greater interest is the situation where the discriminant is equal to zero, as this delimits the boundary between the regions of unique steady-states and multiple steady-states.

The discriminant of Eq. 3.29 is found by substituting the coefficients of Eq. 3.29 into Eq. 3.31 to give after considerable manipulation:

$$\Delta = -27(P+Q)^4 + 4(P-Q)(P^2+34PQ+Q^2) - 16PQ \qquad (3.32a)$$

where,

$$P = K_1(1+K_4)/K_{23} \qquad (3.32b)$$

$$Q = K_{-1}(1+K_4)^2/K_{23} \qquad (3.32c)$$

Setting the discriminant equal to zero and rearranging the terms gives:

$$-16K_1K_{-1}K_{23}^2 + 4\{K_1-K_{-1}(1+K_4)\}\{K_1^2+34K_1K_{-1}(1+K_4)+K_{-1}^2(1+K_4^2)\}K_{23} - 27(1+K_4\{K_1+K_{-1}(1+K_4)\}^4 = 0 \qquad (3.33)$$

Thus, Eq. 3.33 can be used to define the boundary between the regions of uniqueness and multiplicity. The easiest way to use Eq. 3.33 is to notice that it is a quadratic in terms of K_{23}. If K_1, K_{-1} and K_4 are specified, then the values (if any) of K_{23} for the uniqueness - multiplicity boundary can be calculated. If the solution of Eq. 3.33 results in complex conjugates for K_{23} then uniqueness is guaranteed. Shown in Figure 3.1 are typical regions of uniqueness and multiplicity in the K_{23} - K_4 parameter space, where K_1=48 and K_{-1}=2 were held constant.

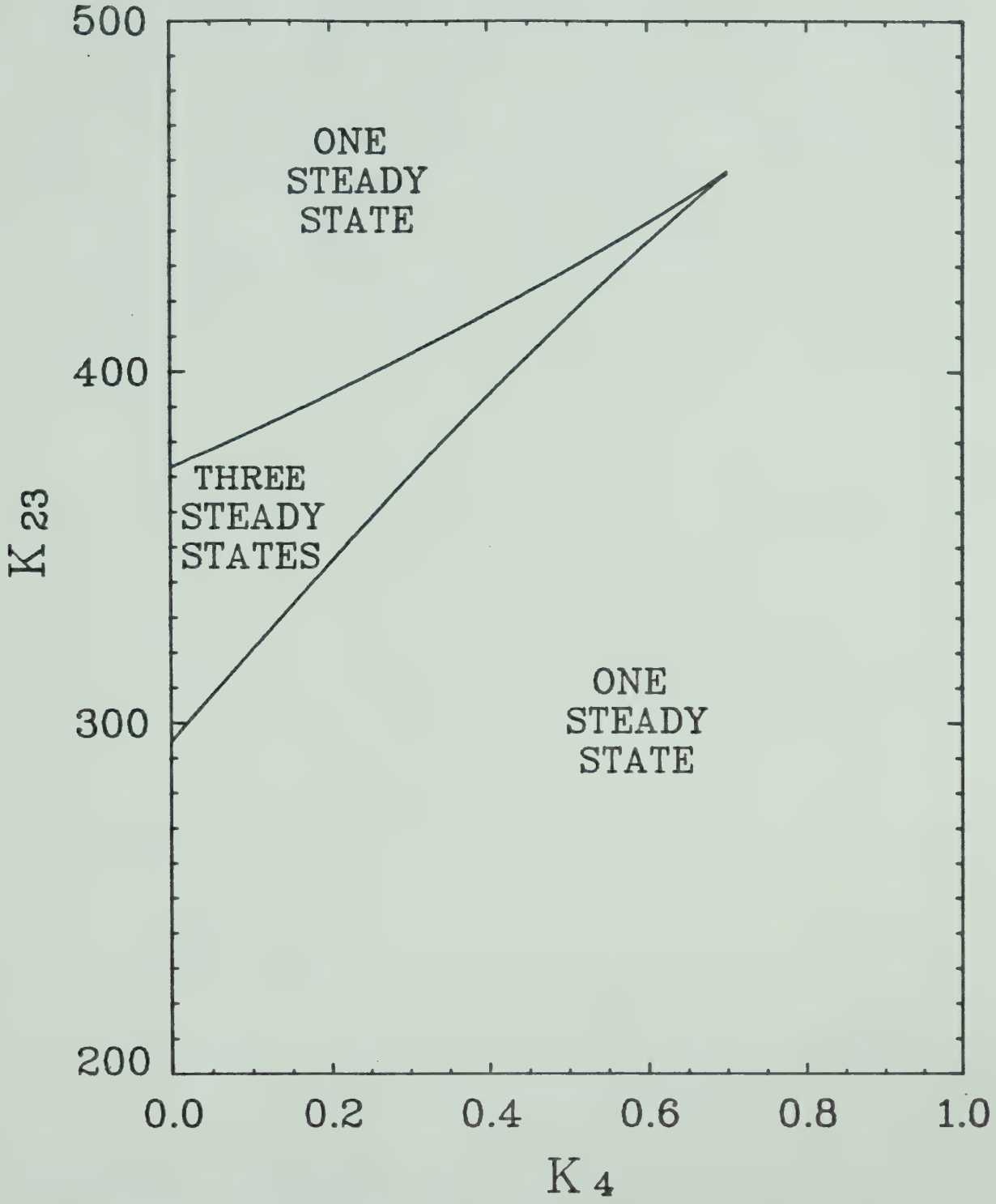

Figure 3.1 System #1 - Regions of Uniqueness and Multiplicity as a Function of $K_{2,3}$ and K_4 (K_1=48, K_{-1}=2)

3.3.2 Stability Analysis

A stability analysis for the system of Eqs. 3.25 and 3.26 can be performed by examining the signs of the trace and the determinant of the Jacobian matrix, where for this system the Jacobian matrix is given by:

$$J = \begin{bmatrix} -K_1 - K_{-1} & 2K_{23}[AX]^2(1-[AX]-[BX]) \\ -2K_{23}[AX](1-[AX]-[BX])^2 & -K_1 \\ +2K_{23}[AX]^2(1-[AX]-[BX]) & \\ -K_4 & -1-K_4 \end{bmatrix} \quad (3.34)$$

A steady-state will be asymptotically stable if all of the eigenvalues (roots of the characteristic equation) have negative real parts. For a system of two ordinary differential equations, the two eigenvalues will have negative real parts if the trace of the Jacobian is negative, and the determinant positive, where the trace and the determinant are evaluated at the steady-state. If either of these two conditions are violated, then the steady-state is unstable.

3.3.2.1 Trace Condition

From the Jacobian matrix the trace is given by:

$$Tr(J) = -K_1 - K_{-1} - 1 - K_4 - 2K_{23}[AX](1-[AX]-[BX])^2 + 2K_{23}[AX]^2(1-[AX]-[BX]) \quad (3.35)$$

The number of unknowns in Eq. 3.35 can be reduced by two through the use of Eqs. 3.27 and 3.28. These equations are most conveniently used to eliminate [BX] and K_{23}, as solving Eq. 3.28 for [BX] gives:

$$[BX] = K_4(1-[AX])/(1+K_4) \tag{3.36}$$

which upon substitution into Eq. 3.27, and solving for K_{23} yields:

$$K_{23} = \frac{(1+K_4)\{K_1(1-[AX])-K_{-1}[AX](1+K_4)\}}{[AX]^2(1-[AX])^2} \tag{3.37}$$

Inserting Eqs. 3.36 and 3.37 into Eq. 3.35 gives:

$$Tr(J) = K_1+K_{-1}-1-K_4 - \frac{2K_1(1-[AX])}{(1+K_4)[AX]} - \frac{2K_{-1}(1+K_4)[AX]}{1-[AX]} \tag{3.38}$$

In order to determine the boundary at which the trace changes sign, Eq. 3.38 is set equal to zero and rearranged to give:

$$[AX]^2\{(1-2K_{-1})(1+K_4)^2-(1+K_4)(K_1+K_{-1})-2K_1\}$$
$$+ [AX]\{4K_1+(1+K_4)(K_1+K_{-1})-(1+K_4)^2\} - 2K_1 = 0 \tag{3.39}$$

For any set of values for K_1, K_{-1} and K_4, Eq. 3.39 can be solved for two values of [AX] at which the trace is equal to zero. These values can then be used in Eq. 3.37 to determine the corresponding values of K_{23} for which the trace is equal to zero. If the values of [AX] from Eq. 3.39 are complex conjugates, then the trace is always negative, and for the selected values of K_1, K_{-1} and K_4 it cannot change sign for any K_{23}. Shown in Figure 3.2 are the points in K_{23} - K_4 parameter space at which the trace of the Jacobian is equal to zero, where the values of K_1 and K_{-1} are those which were previously used in constructing Figure 3.1.

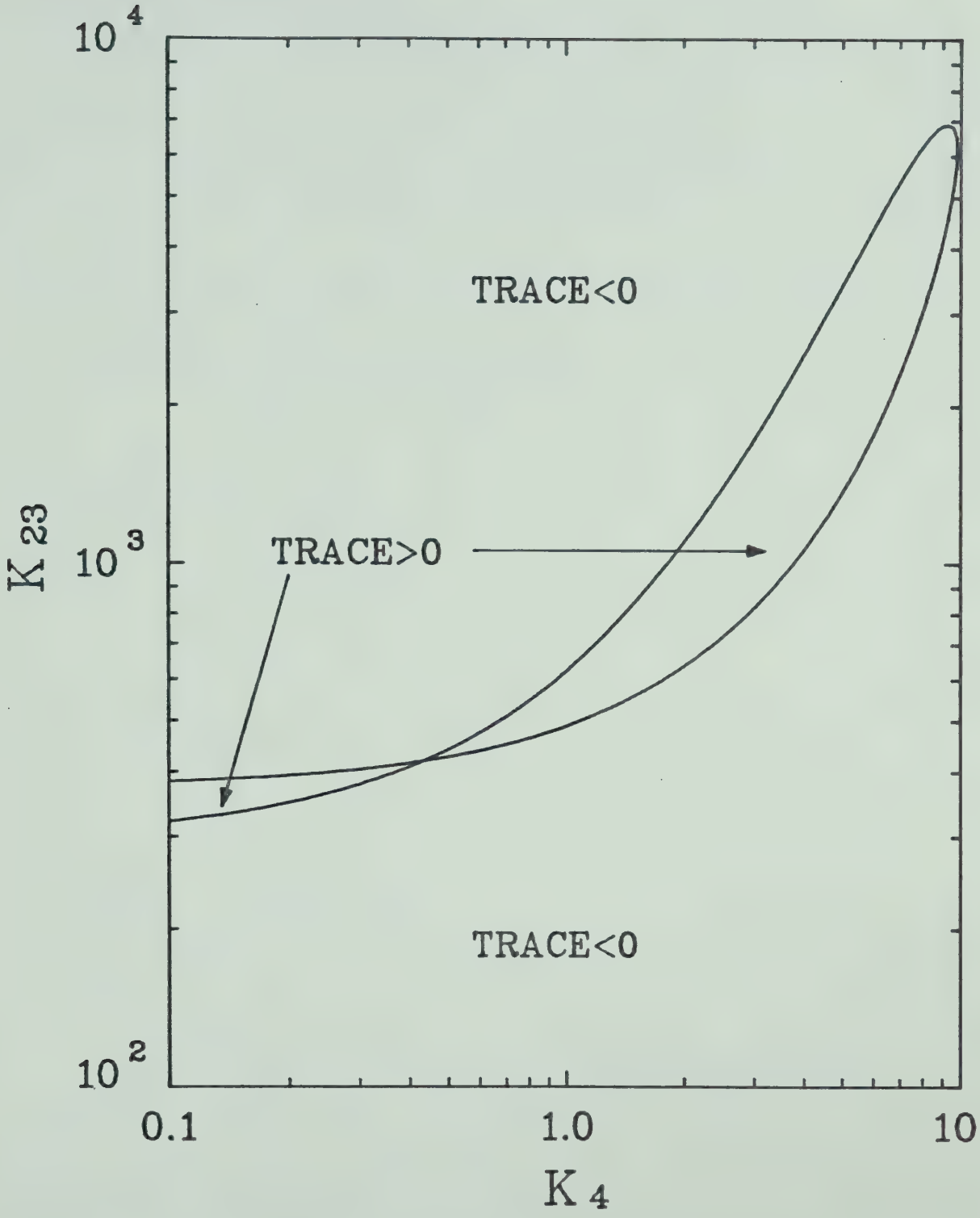

Figure 3.2 System #1 - Trace Condition Stability Regions as a Function of K_{23} and K_4 (K_1=48, K_{-1}=2)

3.3.2.2 Determinant Condition

From Eq. 3.34 the determinant of the Jacobian is given by:

$$\mathrm{Det}(J) = (1+K_4)\{K_{-1}+2K_{23}[AX](1-[AX]-[BX])_2\} + K_1 - 2K_{23}[AX]_2(1-[AX]-[BX]) \quad (3.40)$$

Substituting Eqs. 3.36 and 3.37 into Eq. 3.40 gives:

$$\mathrm{Det}(J) = \frac{2K_1}{[AX]} + \frac{2K_{-1}(1+K_4)[AX]}{1-[AX]} - K_{-1}(1+K_4) - 3K_1 \quad (3.41)$$

Setting Eq. 3.41 equal to zero and rearranging gives:

$$3\{K_1+K_{-1}(1+K_4)\}[AX]^2 - \{5K_1+K_{-1}(1+K_4)\}[AX] + 2K_1 = 0 \quad (3.42)$$

For any given set of parameters K_1, K_{-1} and K_4, Eq.3.42 can be used to determine two values of [AX] for which the determinant of the Jacobian is equal to zero. These values can then be used in Eq. 3.37 to determine the corresponding values of K_{23} for which the determinant is equal to zero. If complex conjugates result from the use of Eq. 3.42, then for the selected values of K_1, K_{-1} and K_4, the determinant is positive for all values of K_{23}.

When the above procedure was numerically implemented, it was found that the locus of points at which the determinant was equal to zero, was identical to the locus of points which separate the regions of uniqueness and multiplicity. Hence, the curves in Figure 3.1 represent the locus of points for which the determinant is equal to zero, as well as separating the regions of uniqueness and

multiplicity. This result is consistent with the theoretical findings of Gavalas [3.5], who showed that for systems obeying conservation equations, the number of steady-states will be equal to 2m+1 (m=0,1,2,etc.) where at least m of the steady-states will be unstable.

In order to show the overall multiplicity and stability properties of System #1, a combination of Figures 3.1 and 3.2 as shown in Figure 3.3 is necessary.

3.4 Elimination of [AX] — System #2

If Eq. 3.16 is used to eliminate [AX] from Eqs. 3.21-3.23, then the following system, to be known as System #2, results:

$$\frac{d[X]}{dT} = [BX] - (K_1+K_4)[X] + K_{-1}(1-[BX]-[AX]) + 2K_{23}(1-[BX]-[X])^2[X]^2 \qquad (3.43)$$

$$\frac{d[BX]}{dT} = K_4[X] - [BX] \qquad (3.44)$$

3.4.1 Uniqueness Analysis

Setting the left-hand sides of Eqs. 3.43 and 3.44 equal to zero gives:

$$[BX] - (K_1+K_4)[BX] + K_{-1}(1-[BX]-[X]) + 2K_{23}(1-[BX]-[X])^2[X]^2 = 0 \qquad (3.45)$$

$$K_4[X] - [BX] = 0 \qquad (3.46)$$

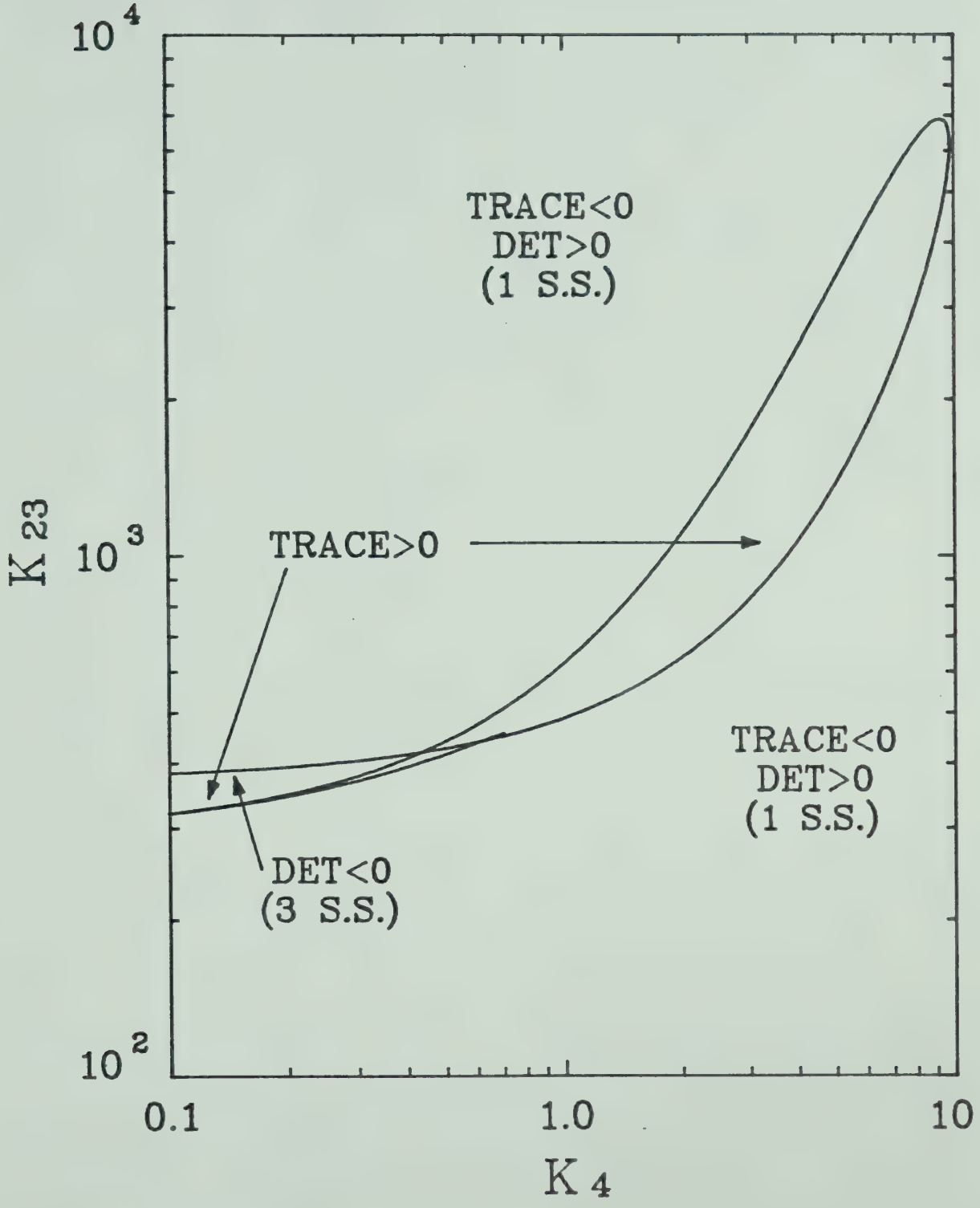

Figure 3.3 System #1 - Combined Stability and Uniqueness Regions as a Function of K_{23} and K_4 (K_1=48, K_{-1}=2)

Solving Eq. 3.46 for [BX], and substituting into Eq. 3.45 gives upon rearrangement:

$$2K_{23}(1+K_4)^2[X]^4 - 4K_{23}(1+K_4)[X]^3 + 2K_{23}[X]^2 - \{K_1+K_{-1}(1+K_4)\}[X] + K_{-1} = 0 \qquad (3.47)$$

However, at a steady-state, combination of Eqs. 3.16 and 3.43 yields a relationship between [X] and [AX] such that:

$$[X] = (1-[AX])/(1+K_4) \qquad (3.48)$$

Substitution of Eq. 3.48 into 3.47 gives upon rearrangement:

$$[AX]^4 - 2[AX]^3 + [AX]^2 + [AX]\{K_1+K_{-1}(1+K_4)\}(1+K_4)/2K_{23} + K_1(1+K_4)/2K_{23} = 0 \qquad (3.49)$$

A comparison of Eqs. 3.49 and 3.29 shows that these equations are virtually identical, with the only difference being that the K_{23} terms in Eq. 3.29 are multiplied by a factor of two in Eq. 3.49. Thus, the results of a uniqueness analysis for System #2 will be identical to that which was performed for System #1, with the only change being that the values of K_{23} necessary for multiplicity will be one-half of those previously determined for System #1. If the values on the K_{23} axis in Figure 3.1 are divided by a factor of two, then the modified figure would describe the uniqueness - multiplicity regions for System #2.

3.4.2 Stability Analysis

From Eqs. 3.43 and 3.44, the Jacobian matrix for System #2 is given by:

$$J=\begin{bmatrix} 4K_{23}(1-[BX]-[X])^2[X]-K_1-K_4 & 1-K_{-1} \\ -K_{-1}-4K_{23}(1-[BX]-[X])[X]^2 & -4K_{23}(1-[BX]-[X])[X]^2 \\ K_4 & -1 \end{bmatrix} \quad (3.50)$$

If the Jacobian is written in terms of [AX] and [BX] through the use of Eqs. 3.48 and 3.16, then it becomes:

$$J=\begin{bmatrix} 4K_{23}[AX]^2(1-[AX]-[BX]) & 1-K_{-1} \\ -4K_{23}[AX](1-[AX]-[BX])^2 & -4K_{23}[AX](1-[AX]-[BX])^2 \\ -K_1-K_{-1}-K_4 & \\ K_4 & -1 \end{bmatrix} \quad (3.51)$$

3.4.2.1 Trace Condition

From Eq. 3.51 the trace of the Jacobian is given by:

$$Tr(J) = -K_1 - K_{-1} - K_4 - 1 - 4K_{23}[AX](1-[AX]-[BX])^2 \\ 4K_{23}[AX]^2(1-[AX]-[BX]) \quad (3.52)$$

Comparing Eq.3.52 with 3.35 shows that the trace of the Jacobian for System #2 is identical with that of System #1, except that all the K_{23} terms have been multiplied by a factor of two. Thus, if the values on the K_{23} axis of Figure 3.2 are reduced by a factor of two, then this figure can also be used for determining the stability of System #2.

3.4.2.2 Determinant Condition

From Eq. 3.51 the determinant of the Jacobian is given by:

$$\mathrm{Det}(J) = (1+K_4)\{K_{-1}+4K_{23}[AX](1-[AX]-[BX])^2\} + K_1 - 4K_{23}[AX]^2(1-[AX]-[BX]) \quad (3.53)$$

Comparing Eq. 3.53 with 3.40 shows that the determinant of the Jacobian for System #2 is identical with that of System #1, except that all of the K_{23} terms have been multiplied by a factor of two. Hence, if Figure 3.1 is modified by dividing the values on the K_{23} axis by a factor of two, then it can be used to depict those points at which the determinant is equal to zero for System #2.

3.5 Elimination of [BX] — System #3

Using Eq. 3.16 to eliminate [BX] from Eqs. 3.21-3.23 gives System #3:

$$\frac{d[AX]}{dT} = K_1[X] - K_{-1}[AX] - K_{23}[AX]^2[X]^2 \quad (3.54)$$

$$\frac{d[X]}{dT} = -K_1[X] + K_{-1}[AX] - K_4[X] + 1 - [X] - [AX] + 2K_{23}[AX]^2[X]^2 \quad (3.55)$$

3.5.1 Uniqueness Analysis

Setting the left-hand sides of Eqs. 3.54 and 3.55 equal to zero gives:

$$K_1[X] - K_{-1}[AX] - K_{23}[AX]^2[X]^2 = 0 \quad (3.56)$$

$$- K_1[X] + K_{-1}[AX] - K_4[X] + 1 - [X] - [AX] + 2K_{23}[AX]^2[X]^2 = 0 \quad (3.57)$$

Combining Eqs. 3.56 and 3.57 gives [X] in terms of [AX] such that

$$[X] = \{[AX](1+K_{-1})-1\}/(K_1-K_4-1) \quad (3.58)$$

Substitution of Eq. 3.58 into 3.56 yields upon rearrangement:

$$K_{23}(1+K_{-1})^2[AX]^4 - 2K_{23}(1+K_{-1})[AX]^3 + K_{23}[AX]^2 - \{K_1+K_{-1}(1+K_4)\}(K_1-K_4-1)[AX] + K_1(K_1-K_4-1) = 0 \quad (3.59)$$

Through the use of Descartes Rule of Signs, it is seen that Eq. 3.59 can possibly have zero, two or four positive real roots if $K_1>K_4+1$, or it can have one or three positive real roots if $K_1<K_4+1$. As previously explained, it is necessary to determine how many of the positive roots are in the interval $0\leq[AX]\leq1$. Substituting $[AX]=Z+1$ into Eq. 3.59 gives:

$$K_{23}(1+K_{-1})^2Z^4 + K_{23}(1+K_{-1})(4K_{-1}+2)Z^3 + K_{23}\{6K_{-1}(1+K_{-1})+1\}Z^2 + \{2K_{-1}K_{23}(2K_{-1}+1)-\{K_1+K_{-1}(1+K_4)\}(K_1-K_4-1)\}Z + \{K_1^2K_{23}-K_{-1}(1+K_4)(K_1-K_4-1)\} = 0 \quad (3.60)$$

If $K_1<K_4+1$ then all of the coefficients in Eq. 3.60 are positive, and hence there will be no roots in the region $Z>0$ ($[AX]>1$). Thus, the region $0\leq[AX]\leq1$ will contain one or three positive real roots when $K_1<K_4+1$. However, if $K_1>K_4+1$, then depending on the value of K_{23} there can

possibly be zero, one or two roots in the region [AX]>1.

Obviously, these results indicate that something is drastically wrong with System #3, as roots in the region [AX]>1 are physically impossible. Also, as stated previously, Gavalas has shown that systems which obey conservation principles must have an odd number of steady-states. Since, for certain conditions, System #3 can have an even number of steady-states, then the conclusion which must be reached is that the use of the simplifying assumptions has resulted in a violation of mass conservation.

In order to further illustrate some of the unusual features of System #3, the boundaries separating the regions of differing numbers of steady-states are determined by examining the discriminant of Eq. 3.59. Substituting the coefficients of Eq. 3.59 into Eq. 3.31 yields after considerable manipulation:

$$\Delta = 16K_1K_{-1}P^3K_{23}^2/Q^9 - 27R^4P^4/Q^8 + 4(30K_1R^2/Q^8+R^3/Q^9-96K_1^2R/Q^7+64K_1^3/Q^6)P^3K_{23} \quad (3.61a)$$

where,

$$P = K_1 - K_4 - 1 \quad (3.61b)$$

$$Q = K_{-1} + 1 \quad (3.61c)$$

$$R = K_1 + K_{-1}(1+K_4) \quad (3.61d)$$

Setting the discriminant equal to zero and rearranging the terms gives:

$$16K_1K_{-1}K_{23}^2 + 4(30K_1R^2Q + R^3 - 96K_1^2RQ^2 + 64K_1^3Q^3)K_{23}$$
$$- 27PQR^4 = 0 \qquad (3.62)$$

Since Eq. 3.62 is a quadratic equation in terms of K_{23}, then if K_1, K_{-1} and K_4 are specified, the values of K_{23} for which the discriminant is equal to zero are readily determined. These boundaries are shown in Figure 3.4 which has been constructed using the same values of K_1 and K_{-1} as in Figure 3.1. It is interesting to note that in Figure 3.4 there is a region of parameter space for which System #3 does not have any real steady-states. This is obviously physically impossible.

3.6 Comparison of Systems #1, #2, and #3

Through the use of Figures 3.3 and 3.4 it is possible to choose parameter values for K_{23} and K_4 such that interesting differences between the three systems are illustrated. In all cases, the parameters K_1=48 and K_{-1}=2 are used, and the computer programs used for the integrations are included in Appendix A.

For the parameter values K_{23}=20000 and K_4=50 an examination of Figures 3.3 and 3.4 shows that all three systems possess a single, stable, steady-state. However, as shown in Figure 3.5, the location of the steady-states differ significantly from each other. Thus, despite the three systems being qualitatively similar, they are quantitatively dissimilar. In some respects, this type of

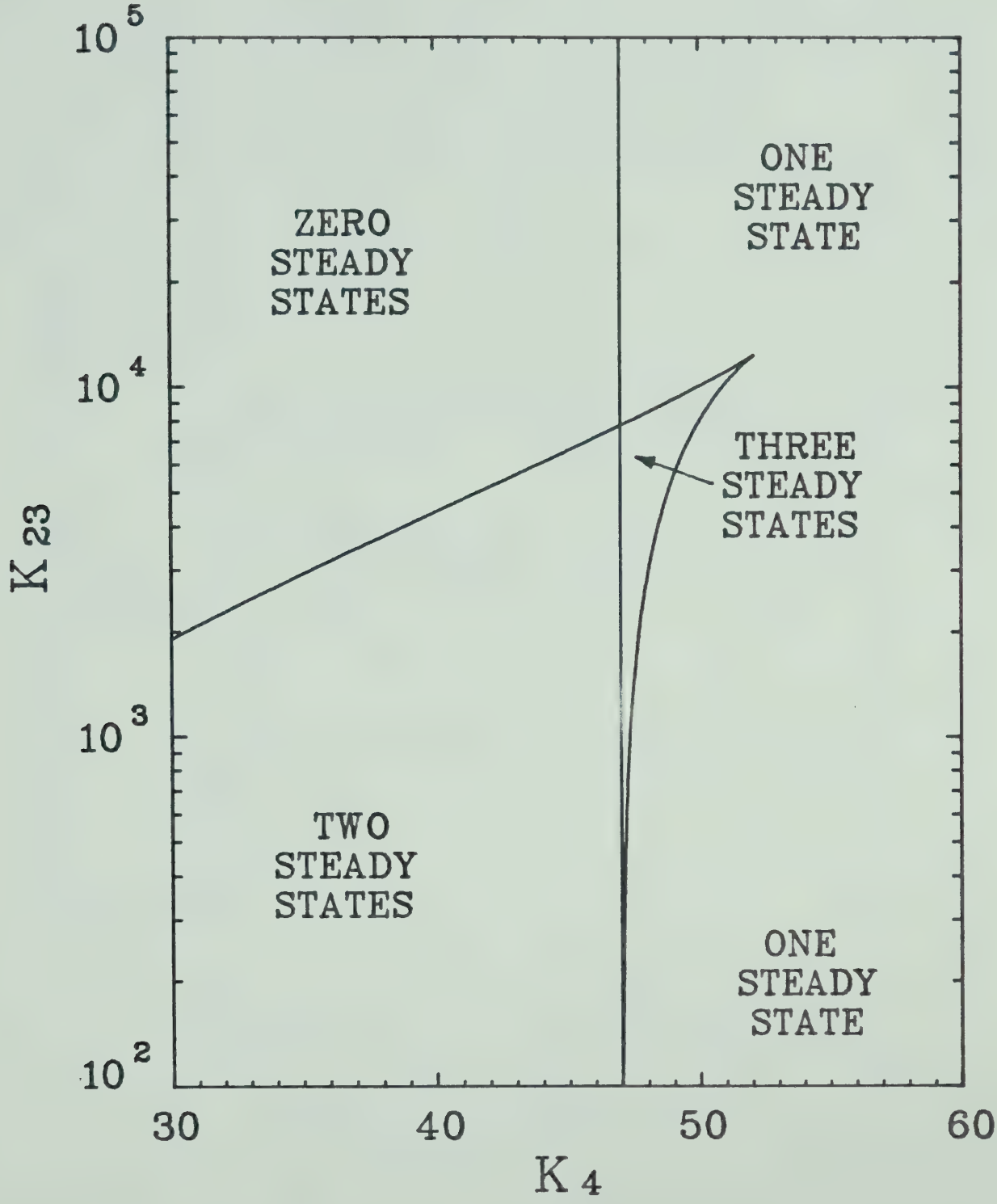

Figure 3.4 System #3 - Regions of Differing Numbers of Steady-States (K_1=48, K_{-1}=2)

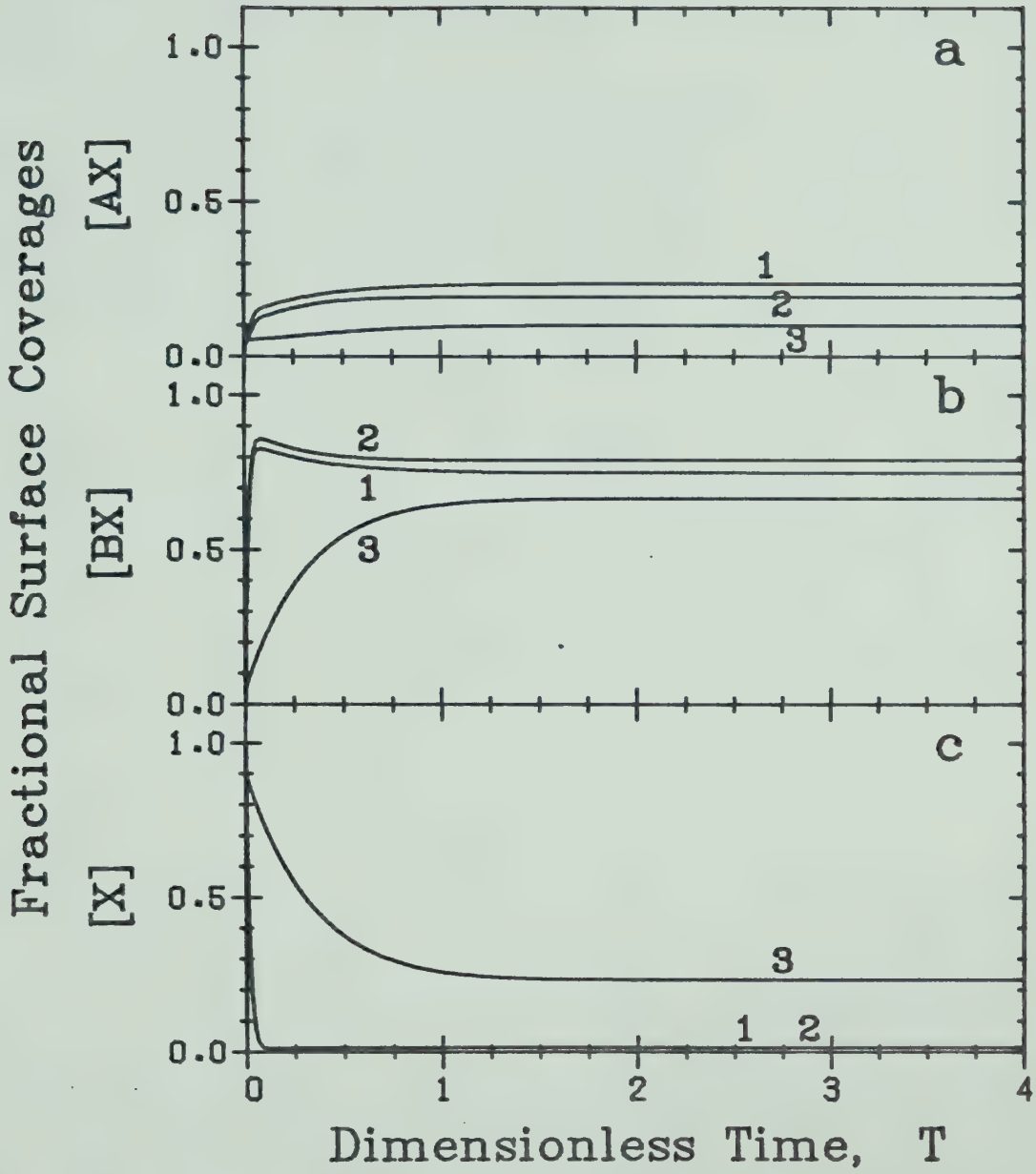

Figure 3.5 Steady-State Differences Between Systems #1, #2, and #3 (K_1=48, K_{-1}=2, $K_{2,3}$=20000, K_4=50)

behavior is analogous to that depicted in the previous chapter, where it was analytically shown that the location of a steady-state could change depending on the manner in which the equilibrium assumption was used to simplify a model.

Perhaps a more interesting situation is shown in Figure 3.6 where the parameters $K_{23}=1250$ and $K_4=5$ were used with the previously stated values of K_1 and K_{-1}. From the uniqueness and stability analysis it is found that System #1 has a single, stable, steady-state; System #2 has a single, unstable, steady-state; and System #3 does not have any real steady-states. From Figure 3.6 it is seen that these differences result in dramatic qualitative, as well as quantitative, differnces between the three systems, as System #1 is stable, System #2 oscillates, and System #3 'explodes'.

It is the behavior of System #3 which is particularly interesting, as if the integration is continued past that shown in Figure 3.6, then the value of [X] approaches positive infinity, and that of [BX] approaches negative infinity. This behavior is a direct violation of mass conservation as all the concentrations have been normalized to be in the range of zero to one.

While it is apparent that these effects are due to the use of simplifying assumptions in the derivation of the three systems, it must be remembered that <u>two</u> simplifying assumptions were used. These assumptions were the assumption of equilibrium given by Eq. 3.15,

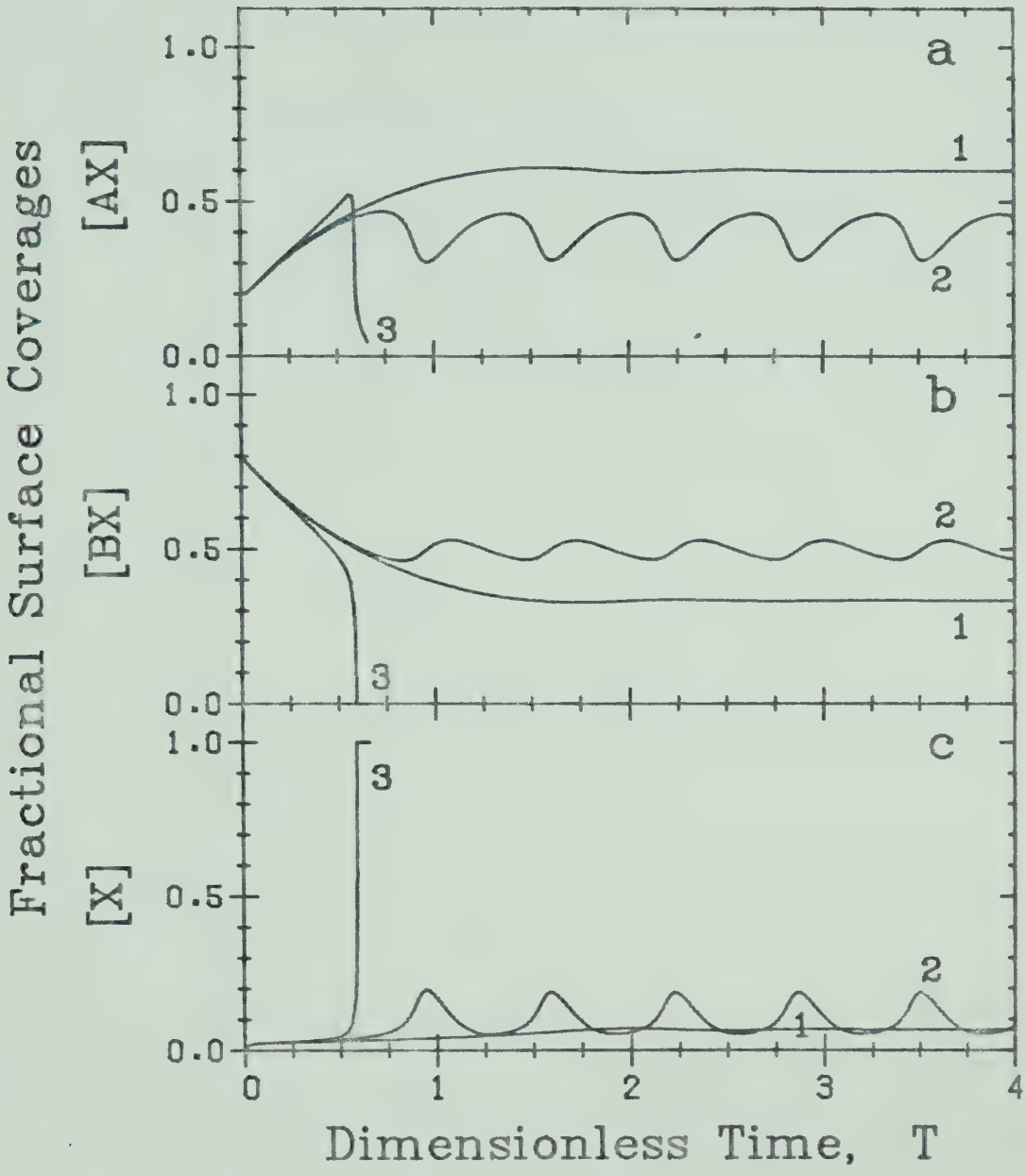

Figure 3.6 Dynamic Differences between Systems #1, #2, and #3 (K_1=48, K_{-1}=2, $K_{2,3}$=1250, K_4=5)

$$K_2[X]^2 = K_{-2}[BXX] \tag{3.15}$$

and the assumption of a negligible concentration of [BXX], which affected the site conservation equation (Eq. 3.9) to give Eq. 3.16,

$$[AX] + [BX] + [X] = 1 \tag{3.16}$$

The previously shown violations of mass conservation could be due to the effects of either, or both, of these assumptions. In the following section, the [BXX] term will not be eliminated from the site conservation equation, and the resulting effect of this on the three systems will be shown.

3.7 Isolation of the Equilibrium Assumption

If [BXX] is not assumed to be negligible, then the normalized site conservation equation is given by:

$$[AX] + [BX] + [X] + 2[BXX] = 1 \tag{3.63}$$

However, if the BXX species is assumed to be at equilibrium with the gas phase, then [BXX] in Eq. 3.63 can be eliminated through the use of Eq. 3.15 to yield:

$$[AX] + [BX] + [X] + 2K_2[X]^2/K_{-2} = 1 \tag{3.64}$$

Equation 3.64 can now be used to eliminate one of [AX], [BX] or [X] from Eqs. 3.21-3.23 to arrive at three new systems, each consisting of two ordinary differential equations.

3.7.1 Elimination of [AX] — System #1A

From Eq. 3.64, the physically realistic ($0 \leq [X] \leq 1$) solution for [X] is given by:

$$[X] = \frac{K_{-2}}{4K_2}\left[-1+\sqrt{1 + \frac{8K_2(1-[AX]-[BX])}{K_{-2}}}\right] \qquad (3.65)$$

Thus, System #1A is given by Eqs. 3.21 and 3.22, where [X] is determined from Eq. 3.65. System #1A is virtually identical to System #1, with the exception that only one simplifying assumption, the equilibrium assumption, is used in System #1A. The removal of the assumption that [BXX] is negligible results in System #1A containing an additional parameter group, K_2/K_{-2}, which does not explicitly occur in System #1. In comparing the behavior of Systems #1 and #1A, it is necessary to specify a value of K_2/K_{-2}. The value of K_2/K_{-2} should be selected such that [BXX] is very small in System #1A, thus the effects of the equilibrium assumption can be isolated.

Shown in Figure 3.7 are the results of integrations of System #1A for several values of K_2/K_{-2}, where the other parameters have been held constant at the values used in Figure 3.6. The initial values $[AX]_0=0.2$, $[BX]_0=0.8$, $[X]_0=0$, and $[BXX]_0=0$ have been used for each integration. These values were chosen to maintain consistency with Figure 3.6. It should be noted that if $[X]_0 \neq 0$ is used, then $[BXX]_0 \neq 0$ is necessary for the initial conditions to be consistent with the equilibrium assumption.

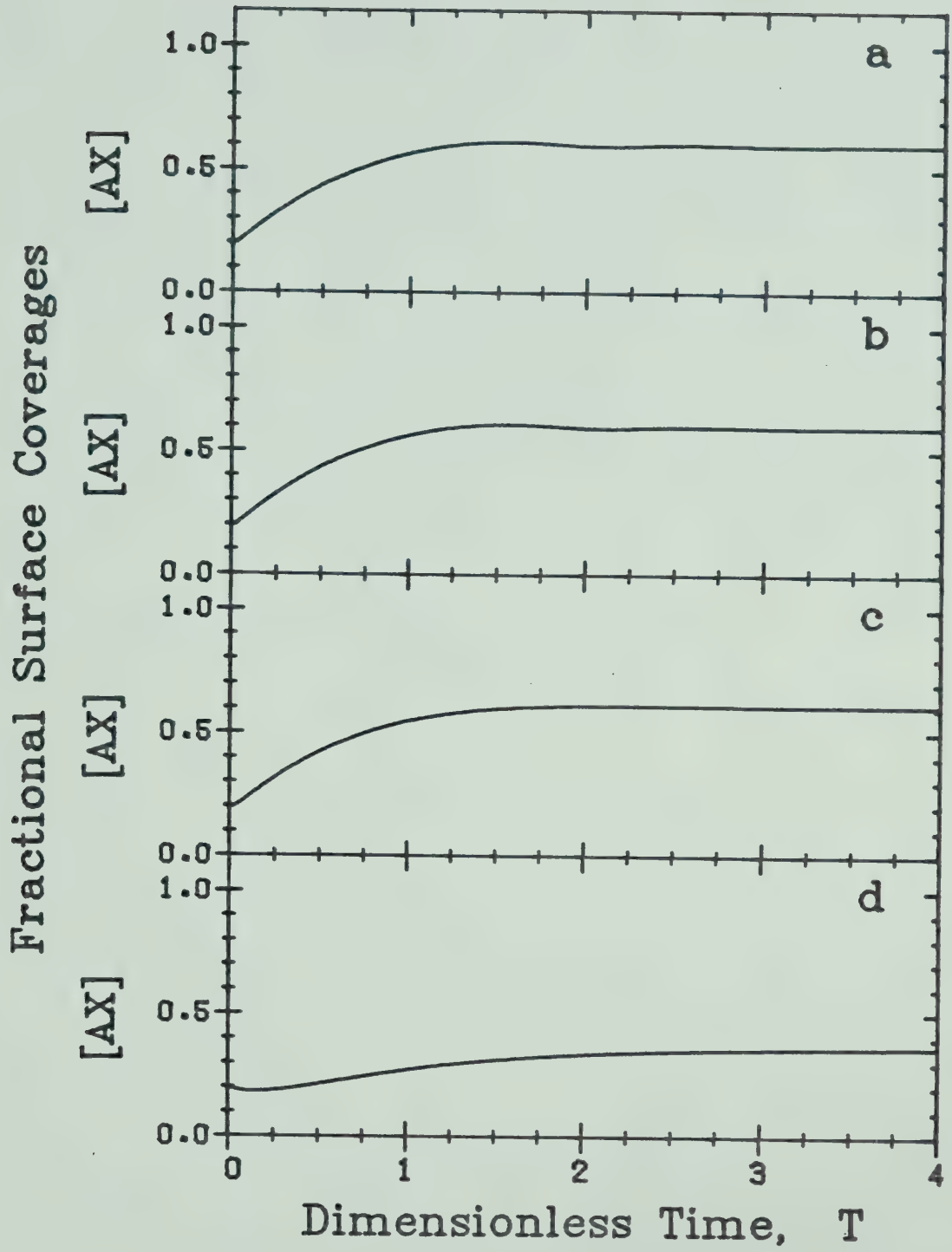

Figure 3.7 System #1A - Effect of K_2/K_{-2} on [AX]
(a) K_2/K_{-2} = 0.0 ; (b) K_2/K_{-2} = 0.10
(c) K_2/K_{-2} = 10. ; (d) K_2/K_{-2} = 10^3
(other parameters as in Figure 3.6)

From Figure 3.7 it is seen that if K_2/K_{-2} is small, then the values of [AX] (also [BX] and [X] which are not shown) from integrations of System #1A are essentially identical to that from System #1 ($K_2/K_{-2} = 0$). This is to be expected, as through the use of Eq. 3.16 it is seen that small values of K_2/K_{-2} will force [BXX] to be small relative to [X]. Hence, the assumption used in System #1, that [BXX] is negligible relative to the other concentrations, will be satisfied when K_2/K_{-2} is small, and under these conditions System #1 and #1A are identical.

3.7.2 Elimination of [AX] — System #2A

From Eq. 3.64, [AX] can be written in terms of [BX] and [X] to give:

$$[AX] = 1 - [BX] - [X] - 2K_2[X]^2/K_{-2} \qquad (3.66)$$

Thus, System #2A is given by Eqs. 3.22 and 3.23, where [AX] is determined from Eq. 3.66. Shown in Figure 3.8 are the results of integrations of System #2A for several values of K_2/K_{-2}, where the other parameters have been held constant at the values used in Figure 3.6, and the initial conditions were the same as those chosen for Figure 3.7. It is seen that when K_2/K_{-2} is small, then the behavior of System #2A is virtually identical to that of System #2. If K_2/K_{-2} is increased from that used in Figure 3.8(b), then the unstable steady-state becomes a stable steady-state as seen in Figure 3.8(c). This occurs due to the surface coverage of the BXX species becoming significant at large values of K_2/K_{-2} .

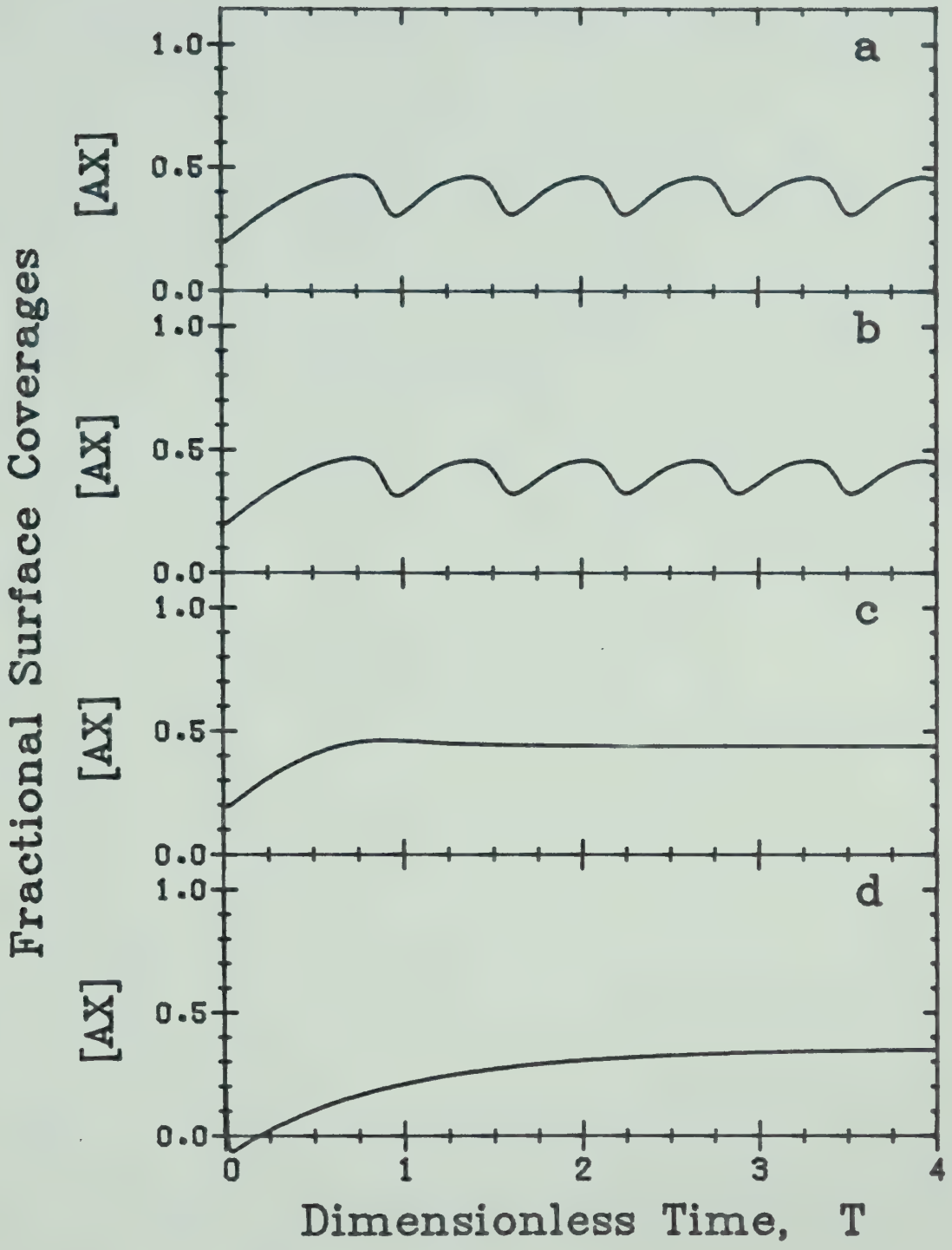

Figure 3.8 System #2A - Effect of K_2/K_{-2} on [AX]
(a) K_2/K_{-2} = 0.0 ; (b) K_2/K_{-2} = 0.10
(c) K_2/K_{-2} = 10. ; (d) K_2/K_{-2} = 10^3
(other parameters as in Figure 3.6)

However, as shown in Figure 3.8(d), if K_2/K_{-2} is further increased some additional interesting, but unexpected, behavior occurs.

In Figure 3.8(d) it is seen that System #2A can display a dynamic violation of mass conservation when K_2/K_{-2} is large, as the concentration of AX decreases from its initial value of 0.20 and passes through negative values before finally reaching its steady-state. Thus, steady-state conformity to the principle of mass conservation does not necessarily imply the same for the system dynamical behavior.

3.7.3 Elimination of [BX] — System #3A

In a manner similar to the above, [BX] in terms of [AX] and [X] is given by:

$$[BX] = 1 - [AX] - [X] - 2K_2[X]^2/K_{-2} \qquad (3.67)$$

Thus, System #3A is given by Eqs. 3.21 and 3.23, where [BX] is determined from Eq. 3.67. Shown in Figure 3.9 are the results of integrations of System #3A for several values of K_2/K_{-2}, where the other parameters and the initial conditions are the same as those used in Figures 3.6 to 3.8. It is seen that removing the assumption that [BXX] is negligible has not improved the performance of System #3A relative to System #3.

For small values of K_2/K_{-2} the behavior of System #3A is identical to that of System #3, in that the violations of mass conservation which occur in System #3 are also found to

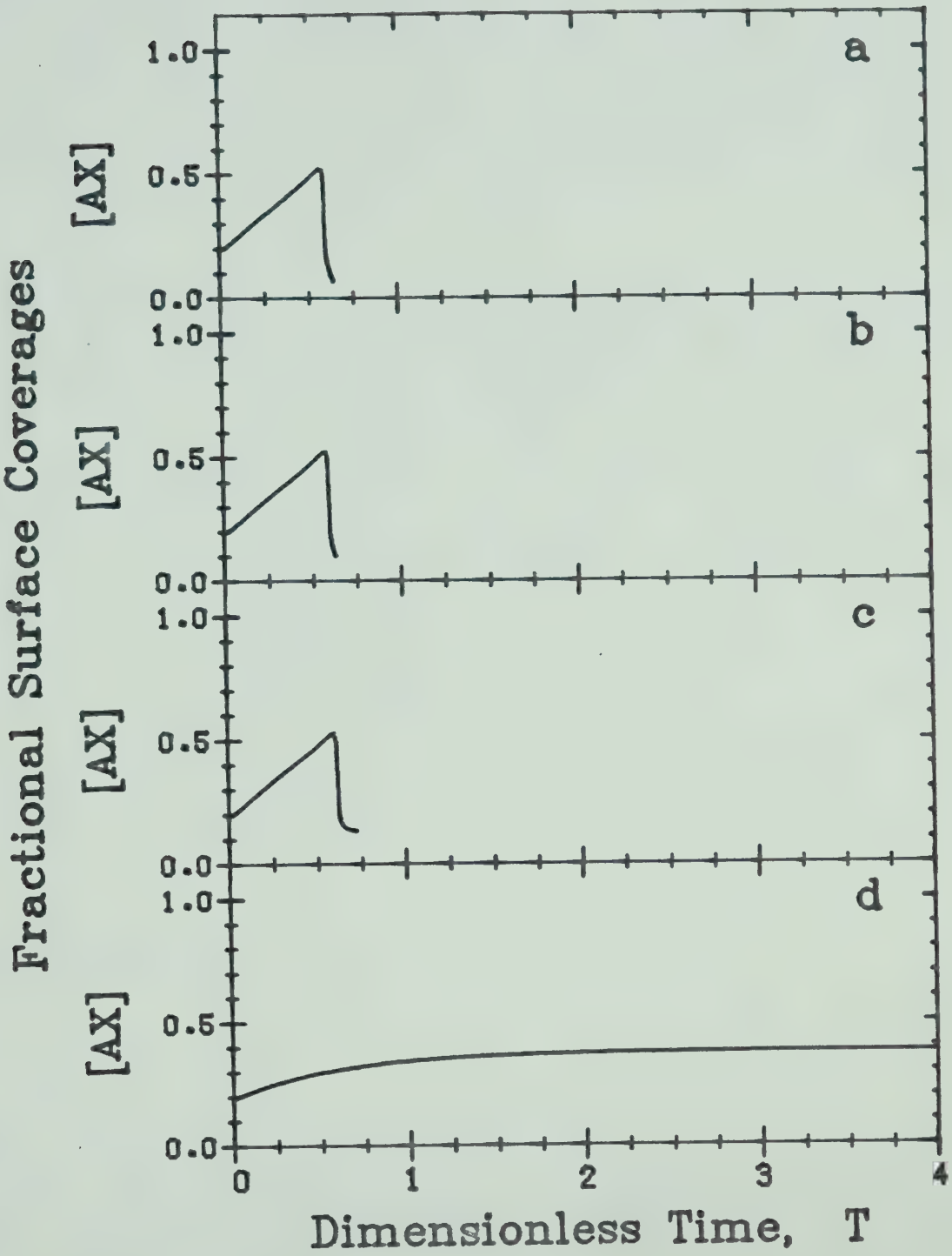

Figure 3.9 System #3A - Effect of K_2/K_{-2} on [AX]
(a) K_2/K_{-2} = 0.0 ; (b) K_2/K_{-2} = 0.10
(c) K_2/K_{-2} = 10. ; (d) K_2/K_{-2} = 10^3
(other parameters as in Figure 3.6)

occur in System #3A. Since only the equilibrium assumption has been used in deriving System #3A, then it can be concluded that these violations of mass conservation are a direct result of the use of the equilibrium assumption.

3.8 Conclusions

The use of the equilibrium assumption in a model of an oscillatory reaction has resulted in three simplified models. Despite the intuitive belief that the predictions of these models should be identical, it has been seen that quantitative and qualitative differences exist between the three models. These differences occur in both the steady-state and the dynamic behavior of the models. In particular, the use of the equilibrium assumption can result in dynamic and steady-state violations of mass conservation.

3.9 Nomenclature

Roman

[A] gas phase concentration of A

[AX] normalized surface phase concentration of A

[B] gas phase concentration of B

[BX] normalized surface concentration of reactive B

[BXX] normalized surface concentration of unreactive B

b constant in the general quartic equation

c constant in the general quartic equation

d	constant in the general quartic equation
e	constant in the general quartic equation
J	Jacobian matrix
k_i	rate constant for the i-th forward reaction
k_{-i}	rate constant for the i-th forward reaction
K_i	dimensionless rate constants for the forward reactions
K_{-i}	dimensionless rate constants for the forward reactions
K_{23}	combined equilibrium and reaction rate constant
P,p	grouping of constants used in the discriminant
Q,q	grouping of constants used in the discriminant
R	grouping of constants used in the discriminant
t	time
T	dimensionless time
x	variable in the general quartic equation
[X]	normalized active site surface concentration
Z	origin shift variable used in the uniqueness analysis

Greek

Δ	discriminant for the general quadratic equation

3.10 References

3.1 Eigenberger, G., Chem. Eng. Sci., 1978 33 1263.

3.2 Eigenberger, G., Fourth Int. Symp. on Proc. Eng., Heidelberg, 1976.

3.3 Gilles, E.D., Eigenberger, G. and Ruppel, W., AIChE J., 1978 24 912.

3.4 Dickson, L.E., A First Course in the Theory of Equations, Wiley, New York, 1922.

3.5 Gavalas, G.R., Nonlinear Differential Equations of Chemically Reacting Systems, Springer-Verlag, New York, 1968.

4. EFFECT OF THE REMOVAL OF THE EQUILIBRIUM ASSUMPTION

4.1 Introduction

In the preceeding chapter, it was seen that the use of the equilibrium assumption in a dynamic model could have unexpected, and unwanted, effects. In particular, it was shown that the manner in which the equilibrium assumption was used could have a dramatic effect on the steady-state and dynamic behavior of the resulting model. These effects could in some situations be manifested through violations of mass conservation. In this chapter the further effects due to the removal of the equilibrium assumption are examined.

4.2 General Model

In the previous chapter it was shown that the use of the mechanism proposed by Eigenberger resulted in a model composed of the following equations:

$$\frac{d[AX]}{dT} = K_1[X] - K_{-1}[AX] - 2K_3[AX]^2[BXX] \qquad (4.1)$$

$$\frac{d[BX]}{dT} = K_4[X] - [BX] \qquad (4.2)$$

$$\frac{d[BXX]}{dT} = K_2[X]^2 - K_{-2}[BXX] - K_3[AX]^2[BXX] \qquad (4.3)$$

where, [X] in Eqs. 4.1-4.3 is determined from the normalized site conservation equation:

$$[X] = 1 - [AX] - [BX] - 2[BXX] \qquad (4.4)$$

Since no simplifying assumptions have been made in deriving Eqs. 4.1-4.3, then the use of the site conservation equation to eliminate [X] is arbitrary, as any one of the four concentrations could be eliminated without incurring the effects described in the previous chapter.

4.3 Stability Analysis

The stability properties of Eqs. 4.1-4.3 are determined from the Jacobian matrix, which for this system is given by:

$$J=\begin{bmatrix} -K_1-K_{-1}-4K_3[AX][BXX] & -K_1 & -2K_1-2K_3[AX]^2 \\ -K_4 & -K_4-1 & -2K_4 \\ -2K_2[X]-2K_3[AX][BXX] & -2K_2[X] & -4K_2[X]-K_{-2}-2K_3[AX]^2 \end{bmatrix} \quad (4.5)$$

The eigenvalues of Eqs. 4.1-4.3 are solutions of the characteristic equation associated with J, which is given by:

$$-\omega^3 + A_1\omega^2 - A_2\omega + A_3 = 0 \quad (4.6)$$

where A_1, A_2 and A_3 are the three invariants of J, i.e.:

$$A_1 = \text{Trace}(J) \quad (4.7)$$

$$A_2 = \text{Minor}(j_{11}) + \text{Minor}(j_{22}) + \text{Minor}(j_{33}) \quad (4.8)$$

$$A_3 = \text{Determinant}(J)$$

and, the terms j_{11}, j_{22} and j_{33} are the elements on the main diagonal of the Jacobian. From Routh's stability criterion [4.1], the necessary and sufficient conditions for a steady-state to be asymptotically stable are that:

Condition #1 $A_1 < 0$ (4.9)

Condition #2 $-A_2 + A_3/A_1 < 0$ (4.10)

Condition #3 $A_3 < 0$ (4.11)

If any of these conditions are violated, then the steady-state will be unstable, as at least one eigenvalue will have a positive real part.

It is seen that Condition #1 is never violated since the Jacobian matrix only contains negative elements. Thus, the stability of Eqs. 4.1-4.3 will be solely dependent on Conditions #2 and #3. While the behavior of A_2 can be readily investigated analytically, no such investigation can be performed for A_3 due to the complexity of the terms in the Jacobian. Thus only a numerical stability analysis can be performed for this system as both Conditions #2 and #3 are dependent on the value of A_3.

A numerical stability investigation, which is not claimed to be exhaustive, has shown that when Condition #3 is violated at a steady-state, then two additional steady-states exist for which Condition #3 is not violated. The stability properties of these additional steady-states, found by examining Condition #2, determine the global stability characteristics of the system. This result is intuitively correct, as a steady-state is locally unbounded if $A_3>0$, as this is the three dimensional analog to a saddle point. In a system obeying conservation balance constraints, an unbounded global solution is not possible,

hence if Condition #3 is violated at a steady-state, then additional steady-states must exist, as a limit cycle cannot surround a unique steady-state which is a saddle point.

In order to compare the general model composed of Eqs. 4.1-4.3, with the simplified model presented by Eigenberger, the parameters K_1, K_{-1}, K_4 and K_{23} will be held constant, where,

$$K_{23} = 2K_2K_3/K_{-2} \tag{4.12}$$

Since these are the only parameters (in modified form) which are present in Eigenberger's simplified model, then any differences in behavior between the general model and the simplified model will be solely due to the effects of the equilibrium assumption. These effects can be determined by examining the behavior of the general model in the K_2-K_{-2} parameter space, as these are the two parameters in the general model which result from the removal of the equilibrium assumption.

A detailed numerical analysis of the stability properties of the general model for the parameters K_1=400, K_{-1}=5.8309, K_{23}=20000, and K_4=5 was performed. These values correspond to Eigenberger's [4.2] parameters k_{13}^{+}=0.02, [AX]g=0.7, k_5^{+}=5 and Tα=20000, for which the simplified model behavior consists of a sustained oscillation about a single, unstable, steady-state, as shown in Figure 4.1. The behavior of the general model in the K_2-K_{-2} parameter space is shown quantitatively in Figure 4.2 and described

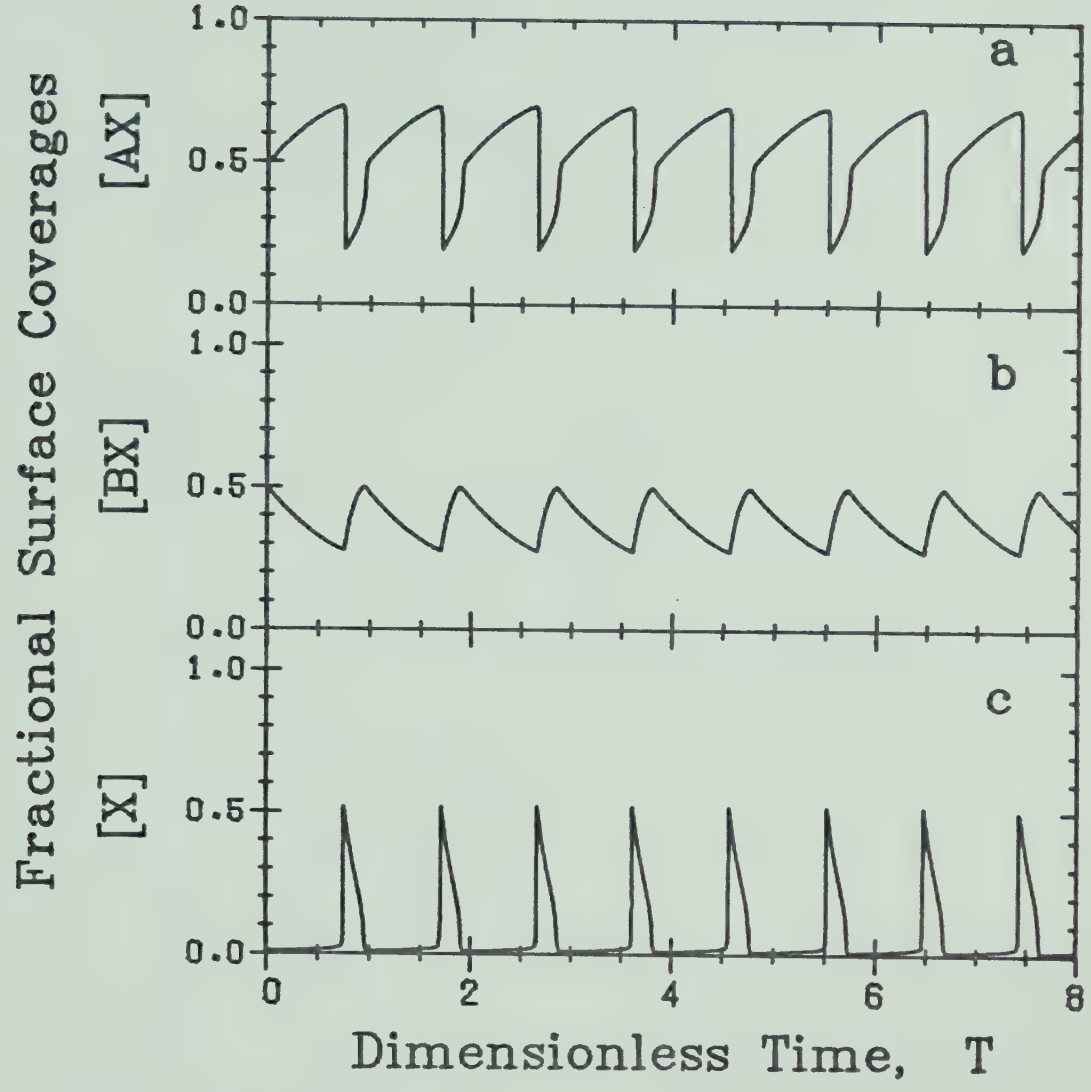

Figure 4.1 Predictions of Eigenberger's Model
(K_1=400, K_{-1}=5.8309, $K_{2,3}$=20000, K_4=5)

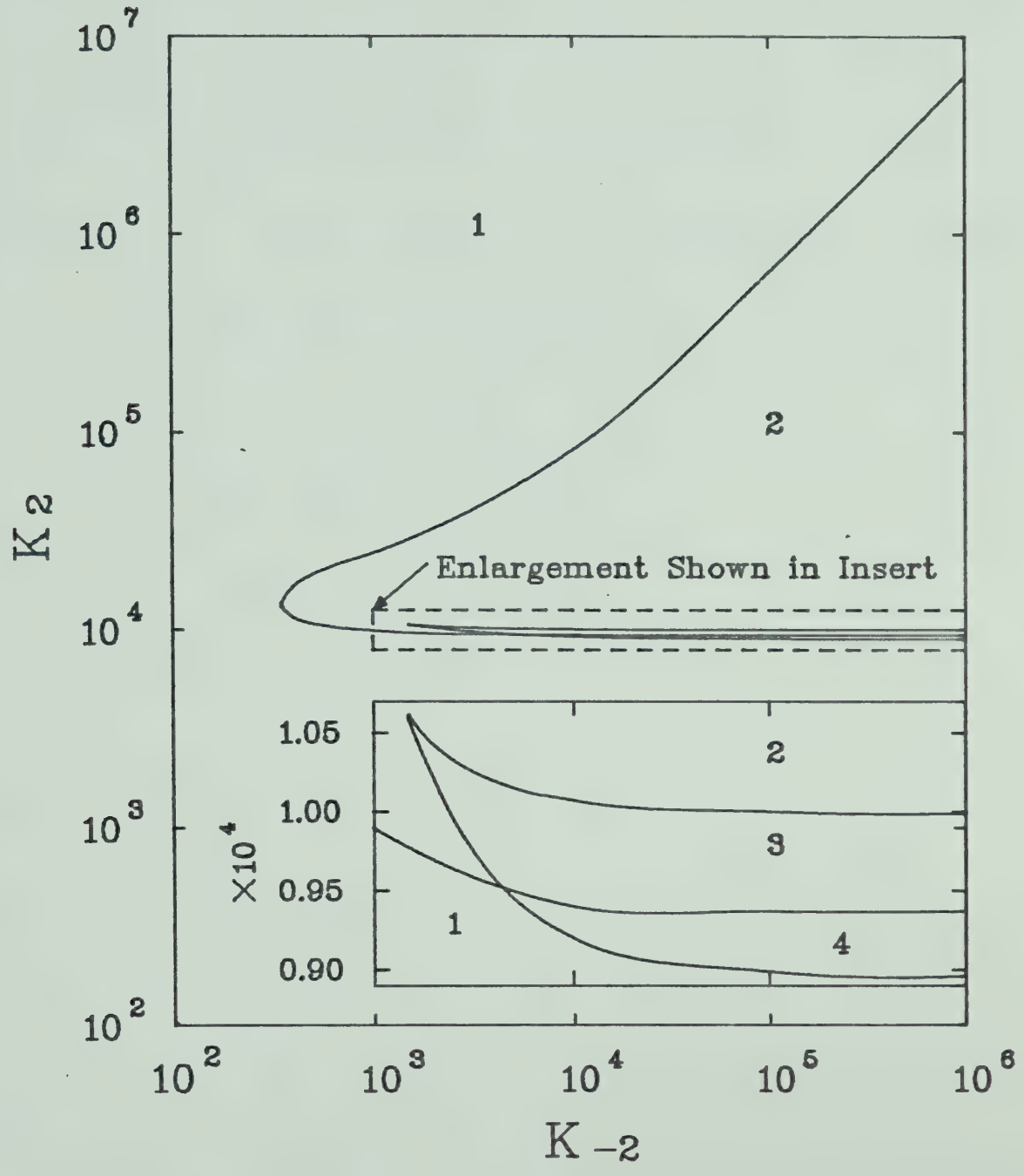

Figure 4.2 Stability Regions for the General Model as a Function of K_2 and K_{-2} (Parameters as in Figure 4.1)

qualitatively in Table 4.1. The computer source code for the program which was used to produce Figure 4.2 is included in Appendix A.

Table 4.1 Types of Solutions to Equations 4.1 - 4.3 (Regions refer to Figure 4.1)

Region	Solution Type	Stability Conditions A_1	$-A_2+A_3/A_1$	A_3
1	one stable steady-state	-	-	-
2	one unstable steady-state (limit cycle)	-	+	-
3	three unstable steady-states (limit cycle surrounds all three steady-states)	-	+	-
		-	+	-
		-	+/-	+
4	one stable, and two unstable steady-states	-	-	-
		-	+	-
		-	+/-	+

In Table 4.1 it is seen that the general model is capable of exhibiting complex behavior not observed in the simplified model (for the previously indicated parameter values). In particular, depending on the values of K_2 and K_{-2}, the general model can have either one or three steady-states with various different types of dynamical behavior. It is important to note that this diversity of behavior is all occurring for the situation in which the simplified model's behavior is fixed at that given in Figure 4.1.

4.4 Numerical Results and Discussion

Numerical integrations of Eqs. 4.1-4.3 with various values of K_2 and K_{-2} were done. Figure 4.3 shows the predicted behavior for values of K_2 and K_{-2} located in region 2 on Figure 4.2, and Figure 4.4 corresponds to K_2 and K_{-2} values located in region 3.

A comparison of Figures 4.3 and 4.4 with Figure 4.1 shows that when solutions of the general model display oscillatory behavior, these oscillations can vary significantly in period and amplitude from those of the simplified model. These differences are important, as one objective of modelling is to obtain a model that quantitatively, or at least semi-quantitatively predicts experimentally observed behavior. Since the experimental data that are most easily obtained are the influences of operating conditions on the period and amplitude of the oscillations, then the first test of the adequacy of a model is whether or not it correctly predicts these effects. Therefore, the frequency and amplitude predictions of a model are very important in testing the validity of the model.

Perhaps as important, Figure 4.2 shows that the general model displays stable behavior and multiple steady-state behavior for large ranges of parameter values over which the simplified model predicts oscillatory behavior. Hence, the general model predicts behavior which is qualitatively and quantitatively different from that displayed by the simplified model for the same parameter values. This

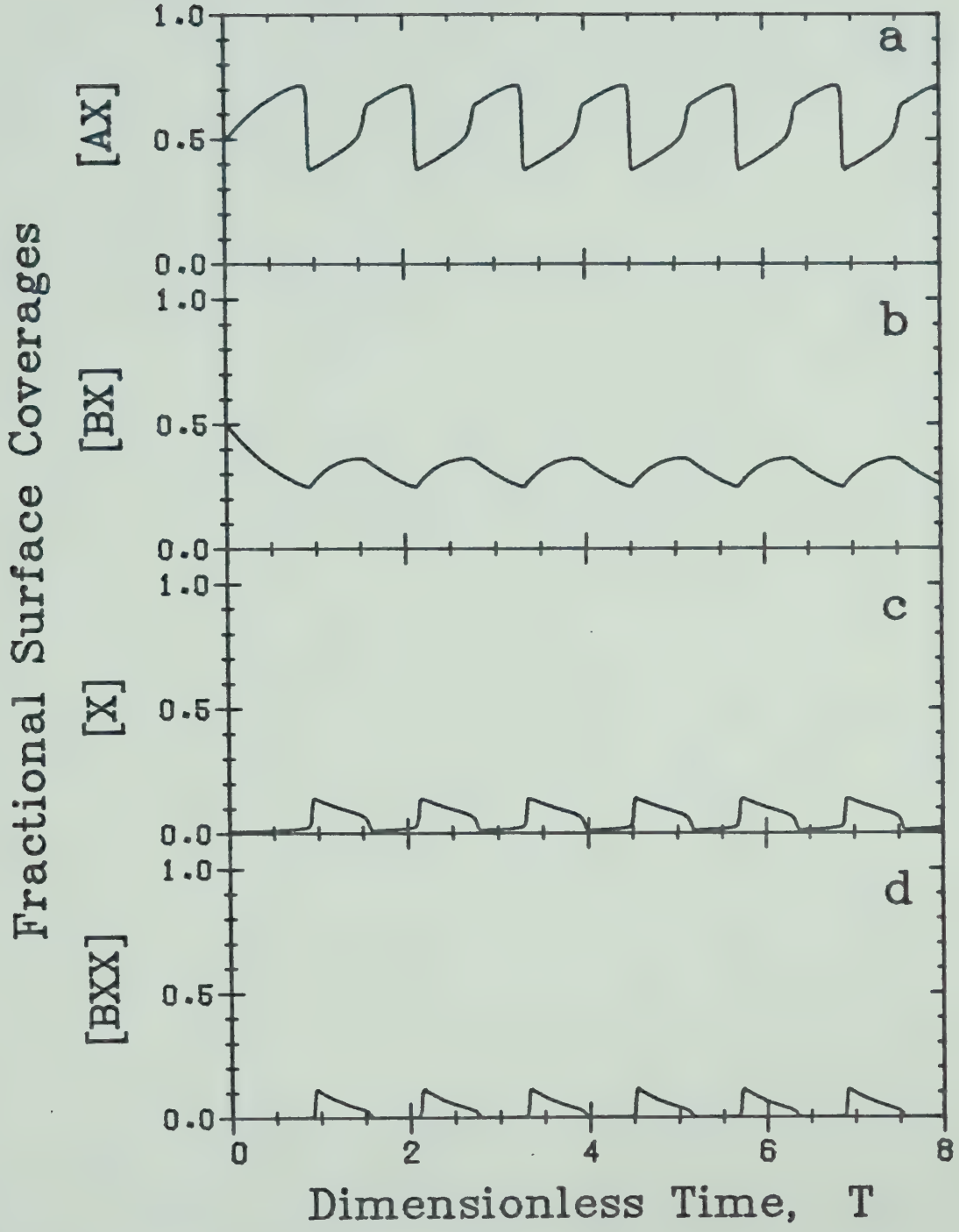

Figure 4.3 Predictions of the General Model
(K_2=6, K_{-2}=10^4, other parameters as in Fig. 4.1)

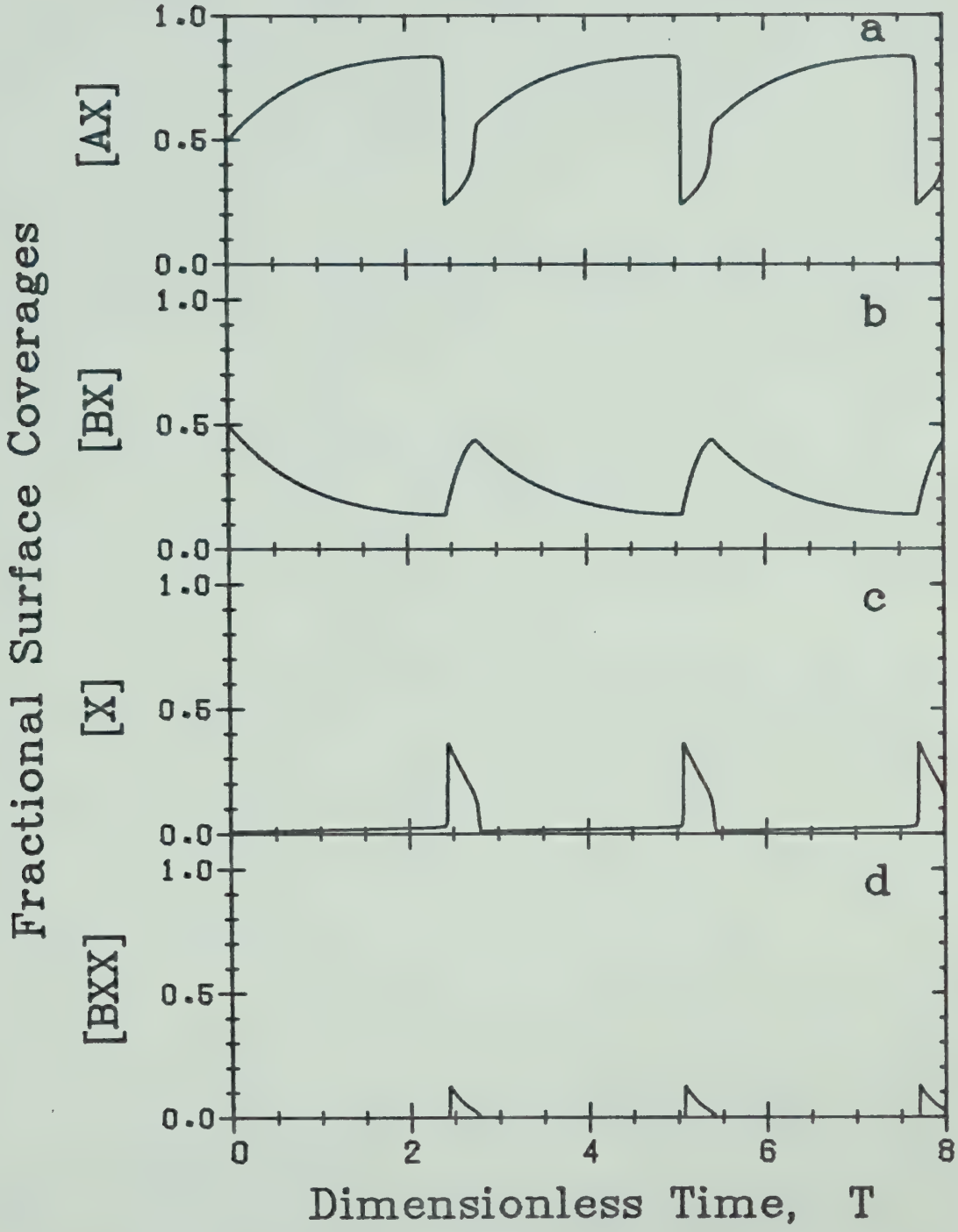

Figure 4.4 Predictions of the General Model
(K_2=1, K_{-2}=10^4, other parameters as in Fig. 4.1)

indicates that assumptions regarding equilibrium behavior of certain reaction steps can greatly alter the predicted behavior of a system.

4.5 Conclusions

It has been demonstrated, contrary to the claim of Pereira and Varama [4.3], that the use of the equilibrium assumption in the construction of a reaction model can qualitatively and quantitatively alter the predicted behavior of the system. This particular simplifying assumption can affect both the number, and the stability, of the steady-states for a reaction model.

Great care must be taken when assumptions are introduced into a model to ensure that these assumptions do not obscure the behavior of the original model.

4.6 Nomenclature

Roman

A_i coefficients of the characteristic equation

[A] gas phase concentration of A

[AX] normalized surface phase concentration of A

[B] gas phase concentration of B

[BX] normalized surface concentration of reactive B

[BXX] normalized surface concentration of unreactive B

j_{ii} element on the main diagonal of the Jacobian matrix

J Jacobian matrix

K_i dimensionless rate constants for the forward reactions

K_{-i} dimensionless rate constants for the reverse reactions

K_{23} combined equilibrium and reaction rate constant

T dimensionless time

[X] normalized active site surface concentration

Greek

ω eigenvalue of the characteristic equation

4.7 References

4.1 Harriott, P., Process Control, McGraw-Hill, New York, 1964.

4.2 Eigenberger, G., Chem. Eng. Sci., 1978 33 1263.

4.3 Pereira, C.J. and Varma, A., Chem. Eng. Sci., 1979 34 1187.

5. CHAOS AND RELATED PHENOMENA

5.1 Introduction

In the preceeding chapter, the behavior of a general model consisting of three ordinary differential equations was compared to that of a simplified model consisting of two ordinary differential equations. It was seen that the steady-state and dynamic behavior of the general model was considerably more complex than that of the simplified model. However, due to the ease of analysis, most of the recent work in examining the stability of chemical reactors has been directed at reactor models which have consisted of two ordinary differential equations. The variables considered in these models have usually been either two reactant concentrations [5.1, 5.2], or one reactant concentration and the reactor temperature [5.3 - 5.5].

One of the implications of examining systems of two ordinary differential equations, such as Eigenberger's simplified model, is that the most complex dynamic behavior that can be obtained is a sustained oscillation of the two variables, which can be represented as a limit cycle in the phase plane. However, recent experimental studies [5.6 - 5.8] have shown that chemical reactors can exhibit chaotic behavior (cycles with high periods, or even aperiodic behavior [5.9]) under certain operating conditions. In order to model such behavior, it is necessary to use a

minimum of three ordinary differential equations, as the Poincaré-Bendixson theorem prohibits the existence of chaotic behavior in systems of two ordinary differential equations. This theorem states that a bounded solution of a two-dimensional dynamical system will converge to either a stable steady-state, or to a stable limit cycle [5.10].

The modelling of chaotic behavior in chemical reaction systems is still in its infancy, as only a few studies [5.8, 5.11, 5.12] have shown that realistic reaction models can display chaotic solutions. In the following it will be shown that chaotic behavior can be exhibited by a very simple chemical reactor model which consists of three ordinary differential equations.

5.2 Model Development

The parallel conversion of two reactants A and B into respective products C and D can be written as:

$$A \longrightarrow C \tag{5.1}$$

$$B \longrightarrow D \tag{5.2}$$

If these reactions are carried out in a nonisothermal, continuous flow, stirred tank reactor, then this chemical system can be modelled by a system of three ordinary differential equations which result from the application of the principles of mass and energy conservation. In deriving the model, the following assumptions will be used:

1. The reactions occur in a continuous flow reactor.

2. The reactor is well mixed so that the temperature and the species concentrations are uniform throughout the reactor.
3. Both reactions are exothermic, and follow first order rate expressions whose temperature dependencies obey the Arrhenius equation.
4. There are no volume changes on reaction.
5. The physical properties of the reaction mixture are temperature invariant.
6. The reaction fluid phase contains the only significant thermal capacitance.
7. The temperature of the reactor wall is held constant at the feed stream inlet temperature.
8. The reactor wall heat transfer coefficient is constant.

Using the above assumptions, reactor mass balances for species A and B, and an overall reactor energy balance, take the form:

$$V \frac{d[A]}{dt'} = Q([A]_o-[A]) - V[A]k_1 e^{-E_1/RT'} \tag{5.3}$$

$$V \frac{d[B]}{dt'} = Q([B]_o-[B]) - V[B]k_2 e^{-E_2/RT'} \tag{5.4}$$

$$V\rho Cp \frac{dT'}{dt'} = Hr_1 V[A]k_1 e^{-E_1/RT'} + Hr_2 V[B]k_2 e^{-E_2/RT'} - Q\rho Cp(T'-T'_o) - SU(T'-T'_o) \tag{5.5}$$

The three balance equations, Eqs. 5.3-5.5, can be written in the following dimensionless form:

$$\frac{dY}{dt} = 1 - Y - YDa_1 e^{\gamma_1 T/(1+T)} \tag{5.6}$$

$$\frac{dZ}{dt} = 1 - Z - ZDa_2 e^{\gamma_2 T/(1+T)} \tag{5.7}$$

$$\frac{dT}{dt} = \alpha(\beta_1 YDa_1 e^{\gamma_1 T/(1+T)} + \beta_2 ZDa_2 e^{\gamma_2 T/(1+T)} - T) \tag{5.8}$$

where,

$$Da_1 = \frac{Vk_1}{Q} e^{-\gamma_1} \tag{5.9a}$$

$$Da_2 = \frac{Vk_2}{Q} e^{-\gamma_2} \tag{5.9b}$$

$$\gamma_1 = \frac{E_1}{RT'_0} \tag{5.9c}$$

$$\gamma_2 = \frac{E_2}{RT'_0} \tag{5.9d}$$

$$\beta_1 = \frac{Q(Hr_1)[A]_0}{T'_0(SU+Q\rho Cp)} \tag{5.9e}$$

$$\beta_2 = \frac{Q(Hr_2)[B]_0}{T'_0(SU+Q\rho Cp)} \tag{5.9f}$$

$$\alpha = 1 + \frac{SU}{Q\rho Cp} \tag{5.9g}$$

$$t = \frac{Qt'}{V} \tag{5.9h}$$

$$T = \frac{T' - T'_0}{T'_0} \tag{5.9i}$$

$$Y = \frac{[A]}{[A]_0} \tag{5.9j}$$

$$Z = \frac{[B]}{[B]_0} \tag{5.9k}$$

An identical set of equations, with different physical interpretations of the parameters, is obtained for two parallel reactions occurring in a nonisothermal, heterogeneously catalyzed system if the surface concentrations are proportional to the gas phase concentrations.

5.3 Stability Analysis

The stability properties of Eqs. 5.6-5.8 are determined from the Jacobian matrix, which for this system of equations is:

$$J=\begin{bmatrix} -1-Da_1 e^{\gamma_1 T/(1+T)} & 0 & -\dfrac{Y\gamma_1 Da_1 e^{\gamma_1 T/(1+T)}}{(T+1)^2} \\ 0 & -1-Da_2 e^{\gamma_2 T/(1+T)} & -\dfrac{Z\gamma_2 Da_2 e^{\gamma_2 T/(1+T)}}{(T+1)^2} \\ \alpha\beta_1 Da_1 e^{\gamma_1 T/(1+T)} & \alpha\beta_2 Da_2 e^{\gamma_2 T/(1+T)} & \dfrac{\alpha Y\gamma_1\beta_1 Da_1 e^{\gamma_1 T/(1+T)}}{(T+1)^2} - \alpha + \dfrac{\alpha Z\gamma_2\beta_2 Da_2 e^{\gamma_2 T/(1+T)}}{(T+1)^2} \end{bmatrix} \tag{5.10}$$

As previously shown, the eigenvalues of Eqs. 5.6-5.8 are solutions of the characteristic equation associated with J, which is given by:

$$-\omega^3 + A_1\omega^2 - A_2\omega + A_3 = 0 \tag{5.11}$$

where A_1, A_2 and A_3 are the three invariants of J. The necessary and sufficient conditions for a steady-state to be

asymptotically stable are that $A_1<0$, $A_3<0$, and $-A_2+A_3/A_1<0$. If any of these three conditions are violated, then the steady-state will be unstable, as at least one eigenvalue will have a positive real part.

A general analytical investigation of when the above stability conditions are violated is not possible due to the complexity of the terms in the Jacobian matrix, and due to the possibility of multiple steady-state solutions of Eqs. 5.6-5.8. A combined analytical and numerical uniqueness analysis [5.13] has shown that, for certain parameter values, as many as five steady-state solutions can exist, each with potentially different stability properties. Certainly a dynamical model which possesses a multitude of coexisting steady-states with a diversity of stability properties could be expected to exhibit complex global behavior. However, we shall show that when the parameter values are restricted so that the steady-state is necessarily unique, both regular and chaotic cycling may still ensue.

5.4 Hopf Bifurcation from a Unique Steady State

Using the techniques outlined by Luss [5.13], it is possible to show that Eqs. 5.6-5.8 will have a unique steady-state over wide ranges of parameter values. In particular, if $Da_2=2.75$, $\beta_1=0.04$, $\gamma_1=\gamma_2=25$, and $\alpha=250$, then a unique steady-state exists for all values of Da_1 and β_2.

For the above parameter values, the stability and character (node, focus, etc.) of the unique steady-state in the Da_1-β_2 parameter space can be determined by calculating the eigenvalues of the characteristic equation. Shown in Figure 5.1 are the regions of equivalent character of the unique staedy-state, where it is seen that the steady-state can be one of four types: (1) an unstable focus (one negative real eigenvalue and two complex conjugate eigenvalues with positive real parts); (2) an unstable node (one negative real eigenvalue and two positive real eigenvalues); (3) a stable focus (one negative real eigenvalue and two complex conjugate eigenvalues with negative real parts); or (4) a stable node (three negative real eigenvalues).

The manner in which a stable steady-state becomes unstable as the parameters are moved from one region to another is shown in Figure 5.2. In this figure, the parameter β_2 is moved from region 1 to region 3, and the effect of this on the time behavior of the dimensionless temperature is illustrated. An examination of the eigenvalues listed in Figure 5.2 reveals that a pair of complex conjugate, purely imaginary eigenvalues occurs at the boundary separating region 1 from region 3. At this boundary, it has been numerically determined that the real parts of the complex conjugate eigenvalues have non-zero derivatives with respect to β_2. Thus, a Hopf bifurcation [5.14] occurs on the boundary separating region 1 from region 3. An examination (not shown here) of the eigenvalues as β_2 is

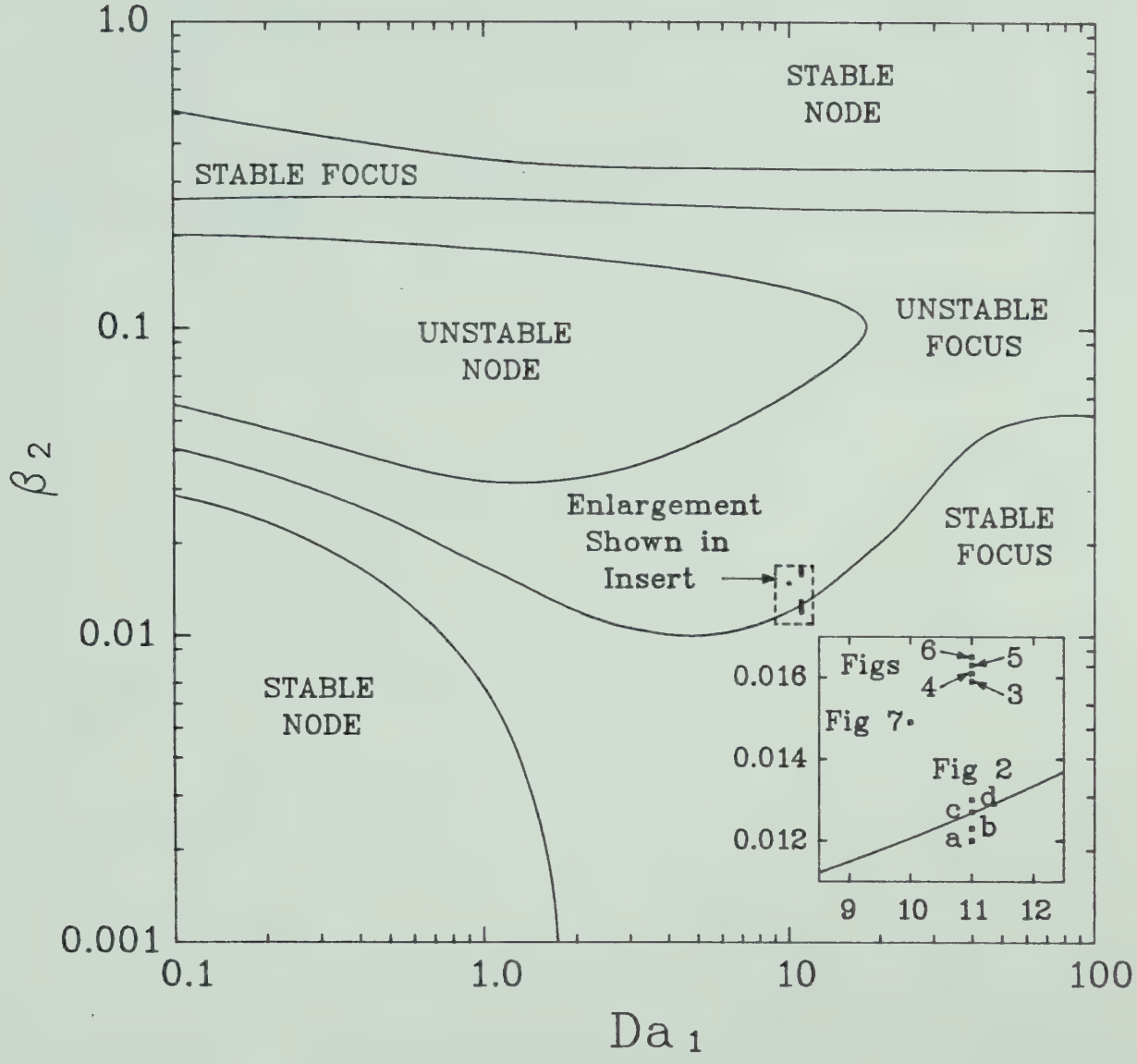

Figure 5.1 Stability Regions as a Function of Da_1 and β_2 (Da_2 = 2.75, β_1 = 0.040, α = 250, $\gamma_1 = \gamma_2$ = 25) Insert shows location of parameters for Figures 5.2 to 5.7

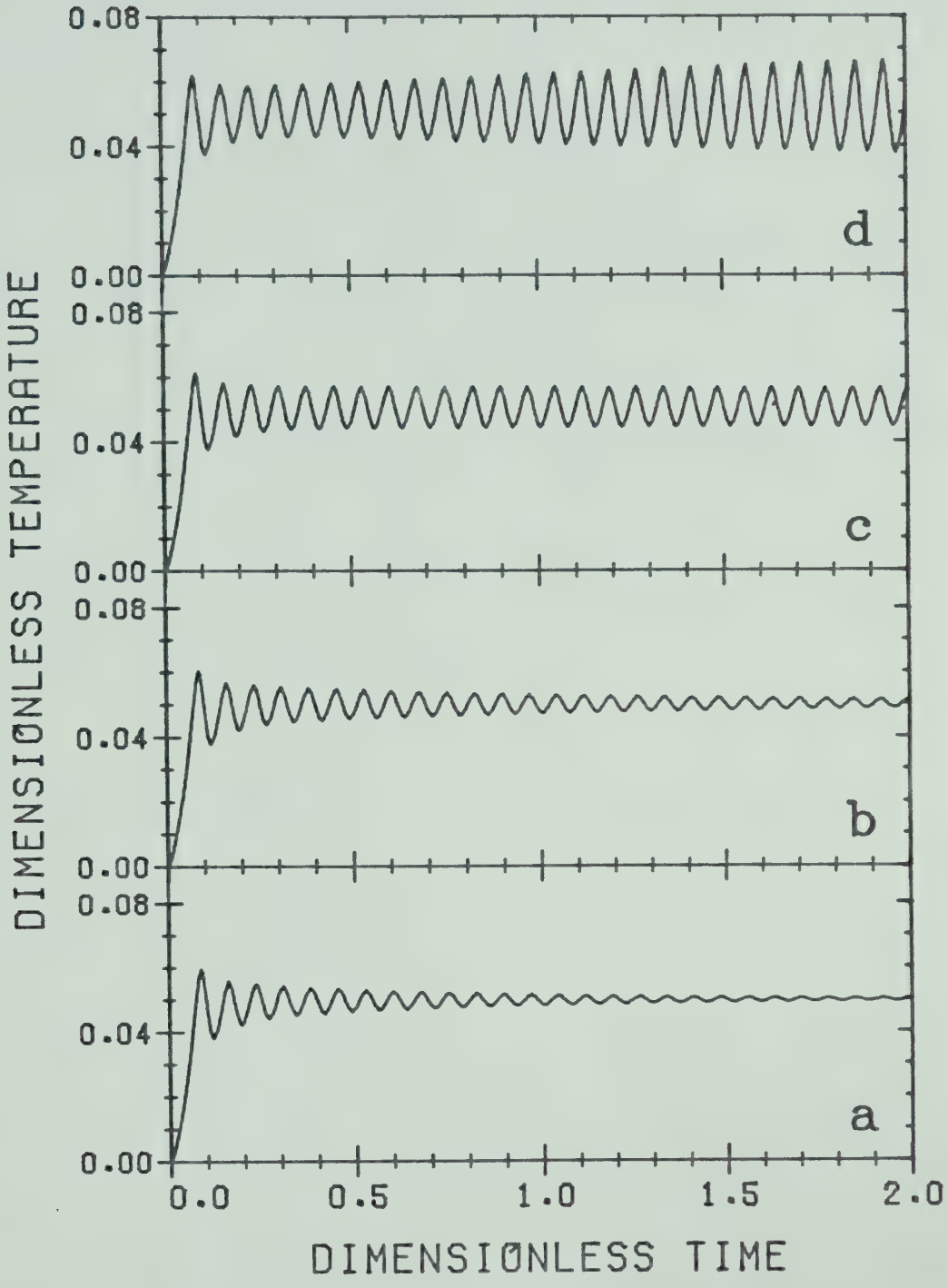

Figure 5.2 Hopf Bifurcation
(a) β_2 = 0.0120 (ω_1 = −11.99 ; ω_2,ω_3 = −1.469 ± 85.52i)
(b) β_2 = 0.0123 (ω_1 = −12.12 ; ω_2,ω_3 = −0.821 ± 85.57i)
(c) β_2 = 0.0127 (ω_1 = −12.30 ; ω_2,ω_3 = 0.042 ± 85.63i)
(d) β_2 = 0.0130 (ω_1 = −12.43 ; ω_2,ω_3 = 0.689 ± 85.67i)
(Da_1 = 11.0, Da_2 = 2.75, β_1 = 0.040, α = 250, γ_1 = γ_2 = 25)

moved from region 2 to region 3 reveals that a Hopf bifurcation also occurs on this boundary.

In all cases, the numerical integration of Eqs. 5.6-5.8 was performed by using Gear's [5.15] method for the integration of stiff systems of ordinary differential equations. For most cases, the results were also checked by using a fourth order Runge-Kutta-Fehlberg [5.16] method, with fifth order error estimation, to integrate Eqs. 5.6-5.8. Hence, two very dissimilar integration methods were used to integrate the system of equations, and similar results were always obtained. The computer source code for these programs is included in Appendix B.

5.5 Complex Oscillations and Chaotic Behavior

From the work of Lorenz [5.17], it is now well known that systems of three or more differential equations can exhibit solutions of arbitrarily high period, as well as aperiodic solutions which are not even asymptotically periodic. This type of behavior is frequently referred to as chaotic behavior. For Eqs. 5.6-5.8, parameter values have been found for which the system can display apparently chaotic behavior. The transition from complex periodic behavior to chaotic behavior, and then back to complex periodic behavior is shown in Figures 5.3 to 5.6.

Each of Figures 5.3 to 5.6 are composed of the following three sections: (a) a plot of the time behavior of

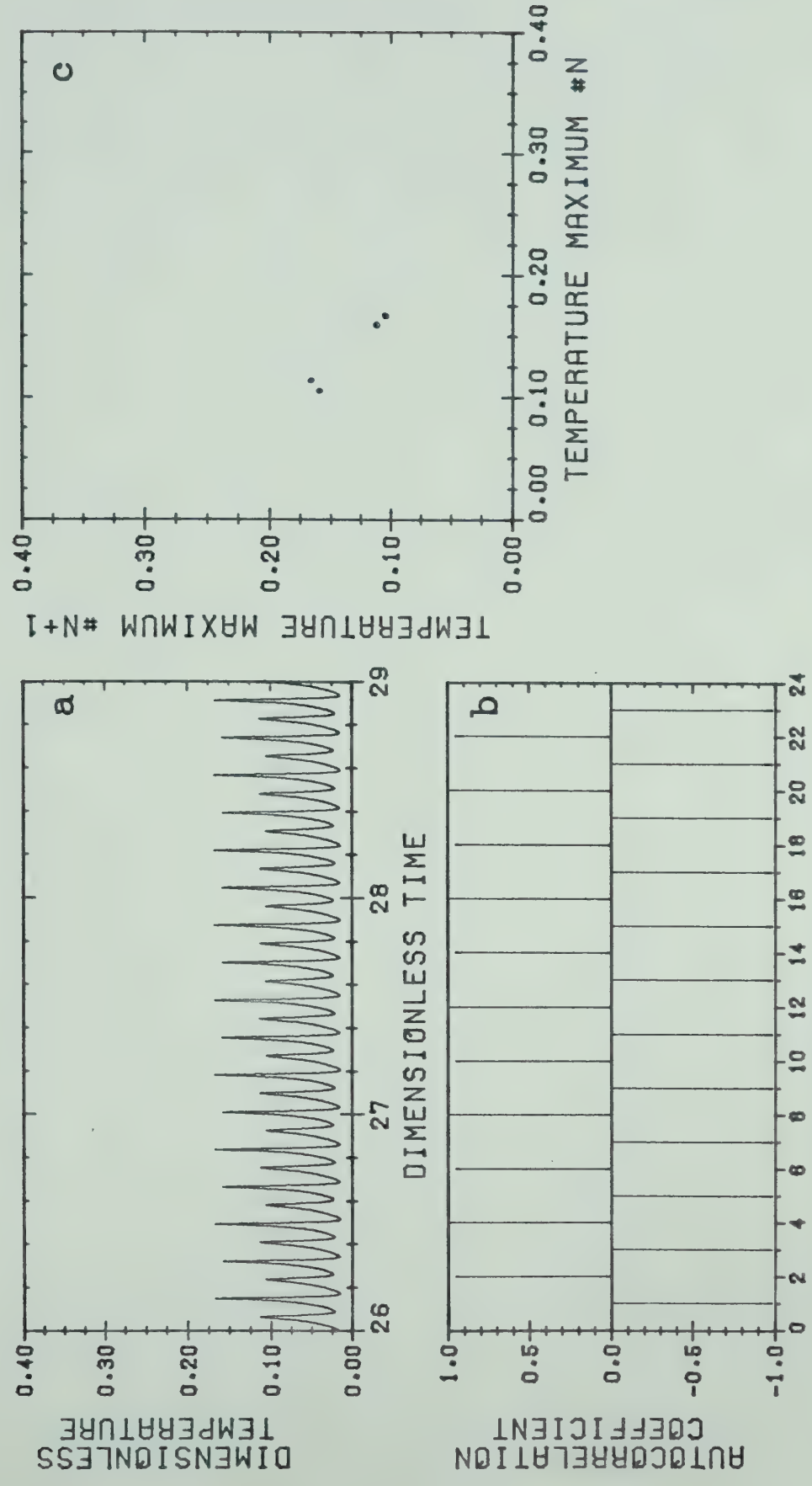

Figure 5.3 Four Maxima per Cycle Oscillation
(β_2 = 0.0159, other parameters as in Figure 5.2)

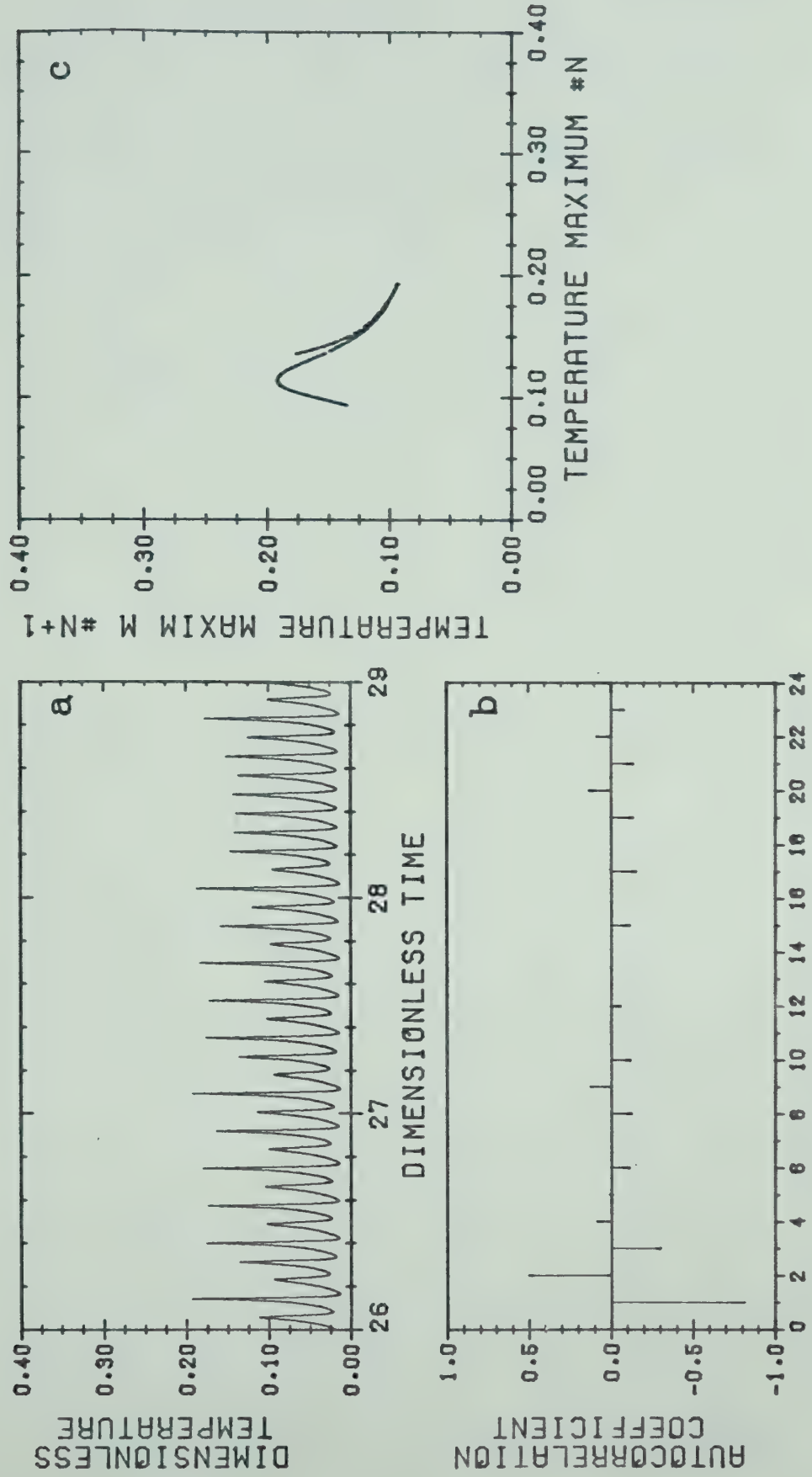

Figure 5.4 Chaotic Oscillation
(β_2 = 0.0161, other parameters as in Figure 5.2)

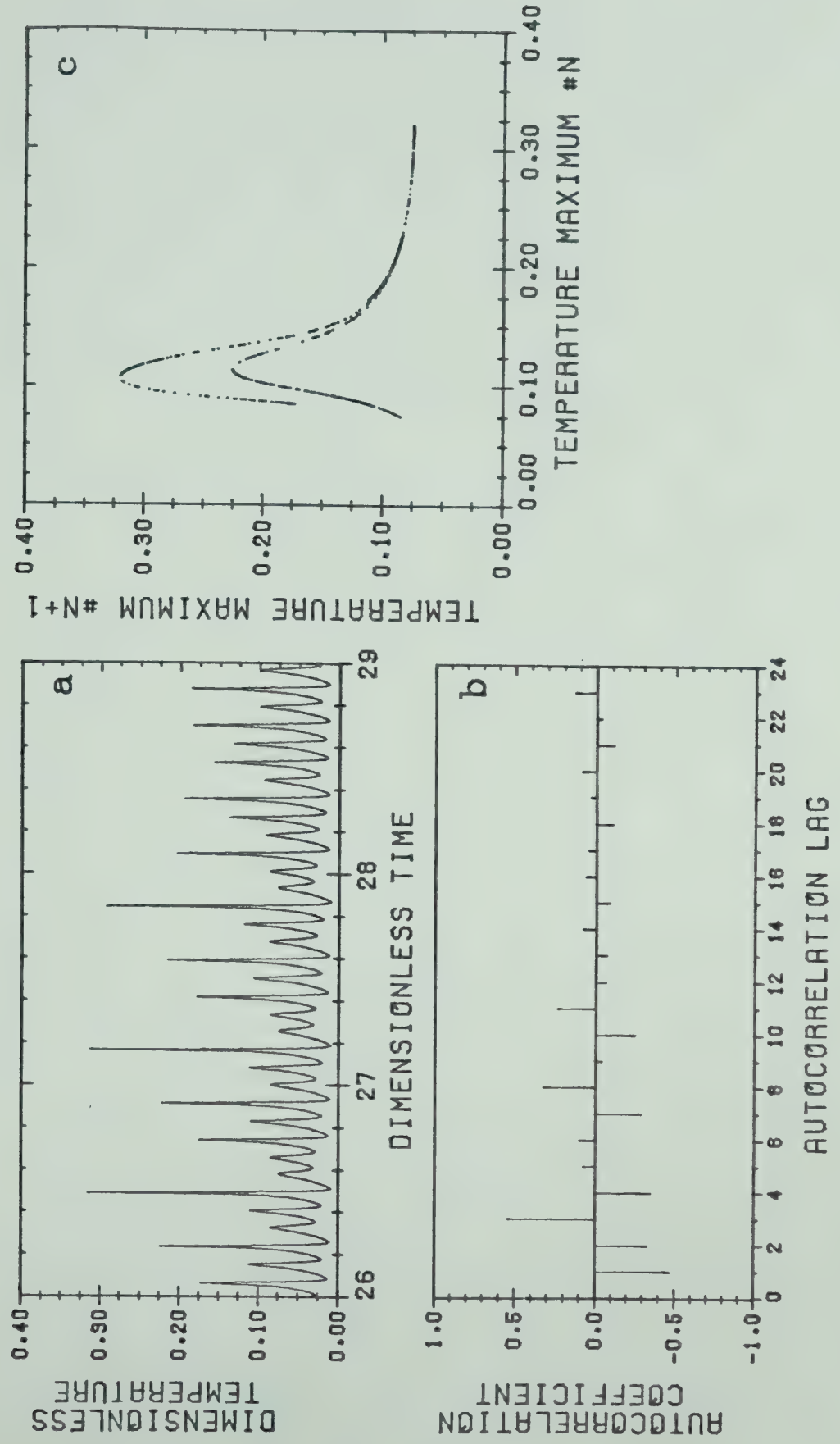

Figure 5.5 Chaotic Oscillation
(β_2 = 0.0163, other parameters as in Figure 5.2)

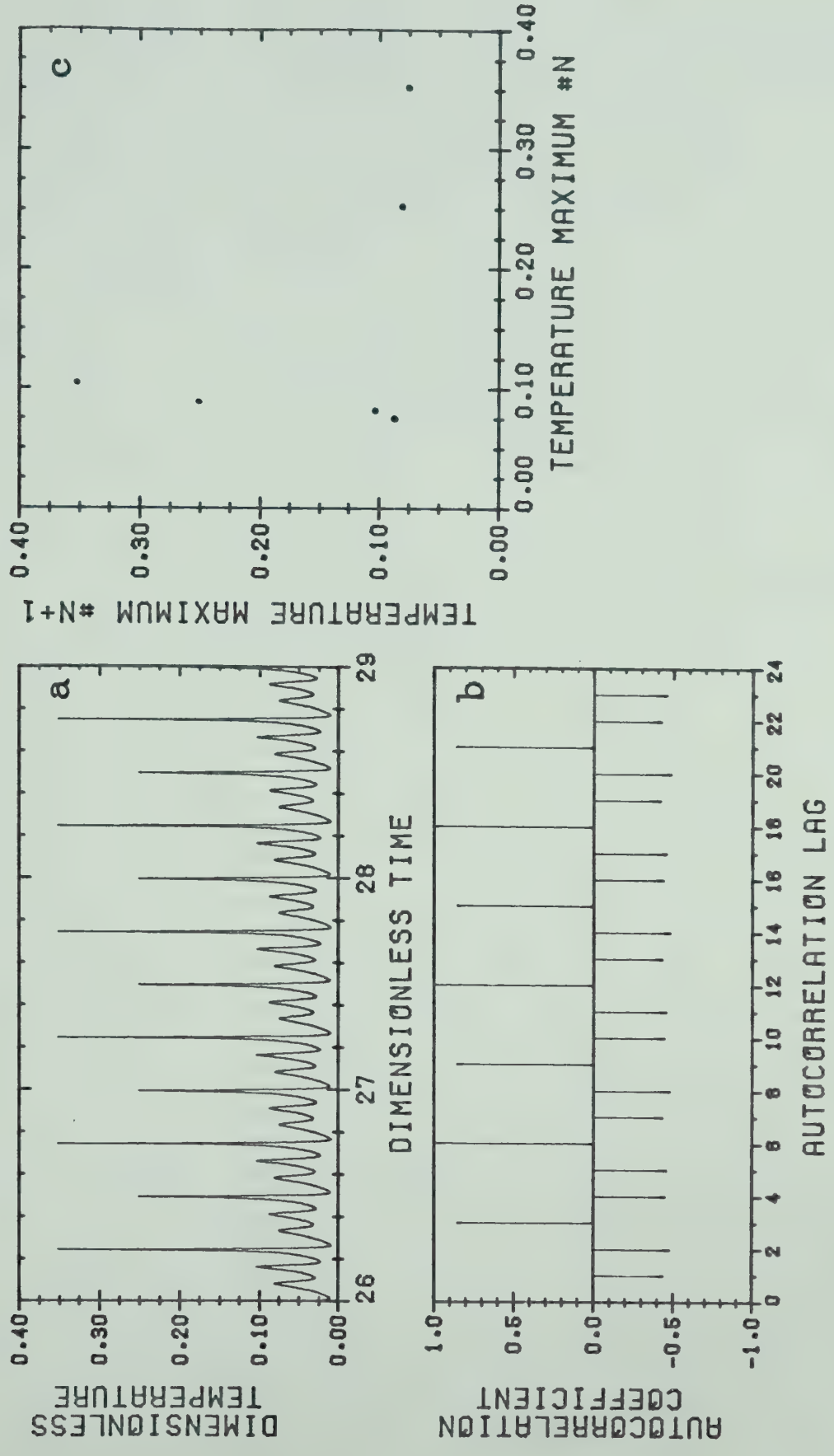

Figure 5.6 Six Maxima per Cycle Oscillation
(β_2 = 0.0165, other parameters as in Figure 5.2)

the dimensionless temperature, (b) an autocorrelation analysis of the temperature maxima, and (c) a next-amplitude plot for the temperature maxima. In the following, each of the groups of (a), (b) and (c) sections for Figures 5.3 to 5.6 will be discussed in turn.

In Figures 5.3(a) to 5.6(a), the variation of dimensionless temperature with time is shown. The behavior for the first 26 units of dimensionless time has been discarded to eliminate the transient effects of the initial conditions. In each case the initial conditions are $T_0=0$, $Y_0=0$, and $Z_0=0$. We see that, as β_2 is increased, the simple oscillation displayed in Figure 5.2 bifurcates into the four maxima per cycle oscillation of Figure 5.3(a). As β_2 is further increased the temperature is shown to behave in a chaotic fashion as in Figures 5.4(a) and 5.5(a). An additional increase in β_2 results in the temperature once again following a stable periodic trajectory, this time with six maxima per cycle, as shown in Figure 5.6(a). Besides stable periodic oscillations of orders four and six, it is possible to have many other numbers of maxima per cycle (2, 3, 6, 8, 9, 16, etc.) depending on the value of β_2. In many systems which display chaotic behavior, it has been found [5.18] that period doubling occurs as the system behavior changes from a stable periodic to a chaotic solution. In general, for the system of Eqs. 5.6-5.8, period doubling does not occur, although it has been observed for some sets of parameter values.

In Figures 5.3(b) to 5.6(b) the results of an autocorrelation analysis on the temperature maxima are shown. The autocorrelation analysis was performed by first reducing the complete time series of temperatures obtained from the integration program, into a vector of temperature maxima, Tm(i), where i varies from 1 to N, and N is the number of temperature maxima in the time series. The autocorrelation coefficient for L lag units (correlation between Tm(i) and Tm(i+L)) was then calculated from:

$$AC(L) = \frac{1}{N-L} \sum_{i=1}^{N-L} \frac{(Tm(i)-\overline{Tm})(Tm(i+L)-\overline{Tm})}{Var(Tm)} \qquad (5.12)$$

where,

$$\overline{Tm} = \frac{1}{N} \sum_{i=1}^{N} Tm(i) \qquad (5.13)$$

$$Var(Tm) = \frac{1}{N} \sum_{i=1}^{N} (Tm(i)-\overline{Tm})^2 \qquad (5.14)$$

It is important to realize that the temperature maxima are considered to be equally separated by one lag unit when they are stored in the vector which only contains the temperature maxima, even though the maxima were perhaps separated by varying amounts of dimensionless time in the original unreduced time series.

In Figure 5.3(b) the autocorrelation analysis clearly indicates that an oscillation with four maxima per cycle occurs because the autocorrelation coefficient is equal to 1.0 at a value of four lag units and at all multiples of four lag units. The large value of the autocorrelation coefficient at a value of two lag units indicates that the four maxima per cycle oscillation is very close to being a two maxima per cycle oscillation. This type of behavior is also shown in Figure 5.6(b) where the six maxima per cycle oscillation is clearly shown by the autocorrelation coefficient having a value of 1.0 at six lag units and at all multiples of six lag units.

For the chaotic behavior displayed in Figures 5.4(a) and 5.5(a), it is seen that the corresponding autocorrelation coefficients given in Figures 5.4(b) and 5.5(b) are never equal to one, and in fact they approach zero at large lag values. While only twenty-four lag units are shown in Figures 5.4(b) and 5.5(b), the autocorrelation coefficients have been calculated for several hundred lag units, and no long periods of oscillation were detected. This particular form of autocorrelation analysis, as detailed above, has been found to be a very useful, and computationally efficient, method of detecting chaotic behavior in the solution of Eqs. 5.6-5.8.

In Figures 5.3(c) to 5.6(c) are shown the next-amplitude plots, in which successive dimensionless temperature maxima Tm(i+1) are plotted against Tm(i). If a

stable periodic solution exists, this will be shown on a next-amplitude plot by the existence of a finite number of points which correspond to the number of maxima per cycle in the periodic oscillation. For example, Figure 5.3(c) has only four points on it, and this corresponds to an oscillation with four maxima per cycle. Similarily, the six maxima per cycle oscillation in Figure 5.6(a) generates a next-amplitude plot containing exactly six points, as shown in Figure 5.6(c).

The next-amplitude plots become more complex for the case of chaotic oscillations. Lorenz, in a series of papers (cf. references in [10]) modelled turbulent fluid flow through a simplified set of equations. From these he numerically solved for X(n), the maximum kinetic energy of successive waves. He plotted X(n+1) versus X(n), and found that a continuous cusp-shaped curve y=F(x) (with a single maximum value at the cusp) approximated this data. However, as can be seen in Figures 5.4(c) and 5.5(c), the chaotic behavior of Eqs. 5.6-5.8 does not generate a single curve, rather, at least two curves are visually apparent. This is not to imply that the relationship between Tm(i) and Tm(i+1) is non-unique, but rather, as Tm(i) varies there are an infinite number of switchings between the curves. The curves must be discontinuous because the next-amplitude map is single valued, i.e. a vertical line which crosses through a point on one curve necessarily crosses through no point on the other curve. Figures 5.3(c) to 5.6(c) do not represent

the full extent of possible forms of the next-amplitude plots, as even more complex forms can exist depending on the choice of parameters.

5.6 Chaos and Fractal Curves

Shown in Figure 5.7(c) is a next-amplitude plot in which three curves are distinctly observable. The chaotic oscillation of the dimensionless temperature which generated this next-amplitude plot is shown in Figure 5.7(a), and the autocorrelation analysis is given in Figure 5.7(b).

Sections of the curves shown on Figure 5.7(c) were expanded to more closely examine their structure. Shown in Figure 5.8 are successive magnifications of the regions enclosed in the dashed rectangular boxes. Figure 5.8(b) shows quite distinctly that the "single" curve in the dashed box of Figure 5.8(a) is actually composed of at least three curves. In Figures 5.8(c) and 5.8(d) it is seen that upon additional magnification, these curves expand into even more curves. It is reasonable to expect that "curves" on the next-amplitude plot shown in Figure 5.7 are actually composed of an infinite number of curves, and in fact these are fractal curves in the sense of being self-similar [5.19]. Specifically, the transverse structure across the roughly parallel curve segments is essentially that of a Cantor set, while on the curves the points appear to distribute themselves densely.

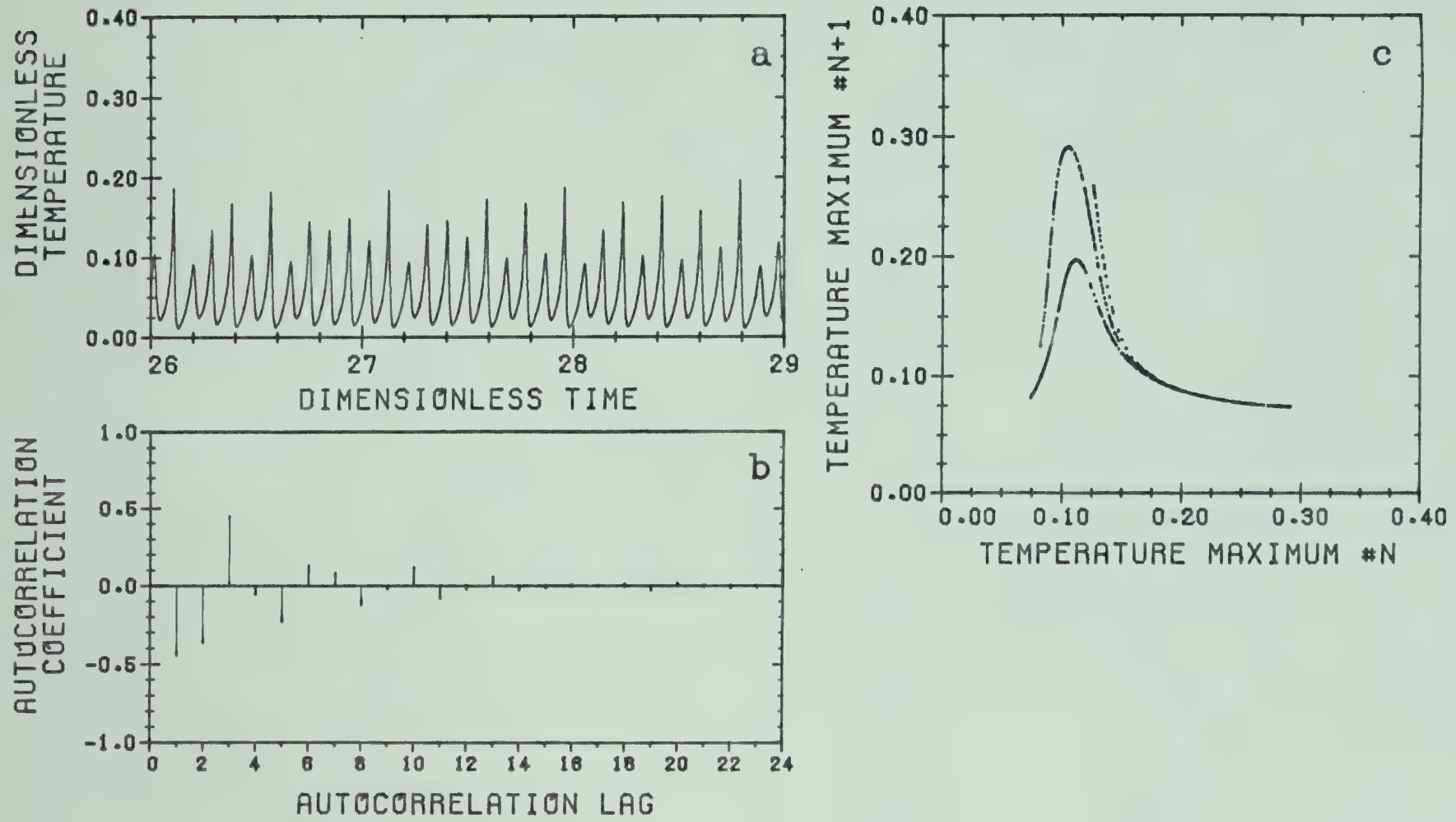

Figure 5.7 Chaotic Oscillation With Emergence of a Third Curve on the Next-Amplitude Plot (Da_1 =10.0, Da_2 = 2.75, β_1 =0.040, β_2 = 0.0149, α = 250, $\gamma_1 = \gamma_2$ = 25)

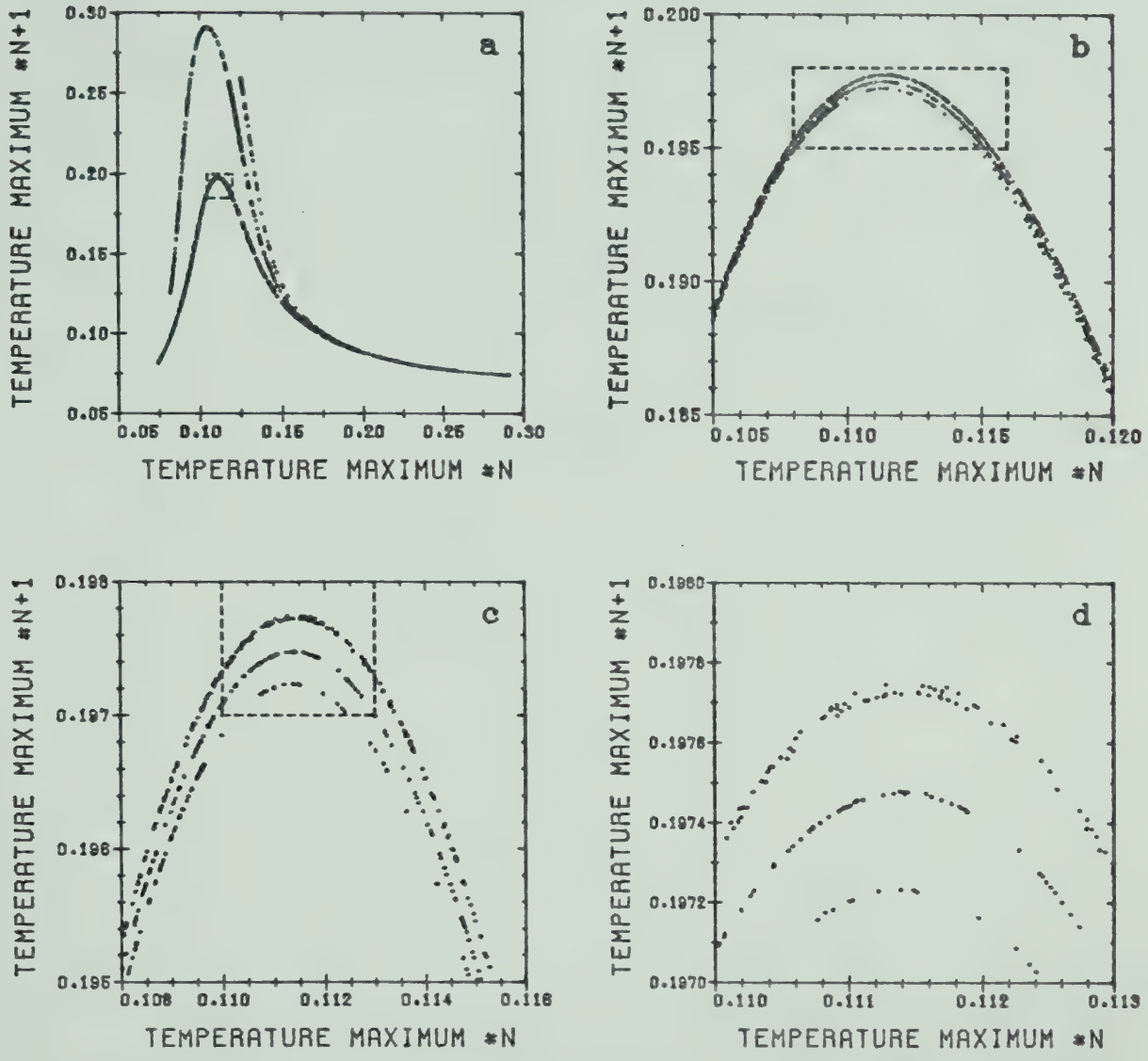

Figure 5.8 Fractal Curves in the Next-Amplitude Plot
(a) Next-amplitude plot from Figure 5.7(c)
(b) 278:1 expansion of region in dashed box in (a)
(c) 9.4:1 expansion of region in dashed box in (b)
(d) 8:1 expansion of region in dashed box in (c)

Such a topological structure has been encountered in a number of examples of second-order recurrences which approximate certain three-dimensional dynamical systems that have been used to describe turbulent flow. These recurrences take the form of the Poincaré return map to the flow, i.e. the map which describes the flow on some transverse planar section. A well-known example is the Hénon return map to the Lorenz equations [5.20].

It should be mentioned that the production of Figure 5.8 was not a trivial task, as the approximately 150 points shown in Figure 5.8(d) were obtained by integrating Eqs. 5.6-5.8 so that approximately 15000 temperature maxima were recorded. This integration required slightly more than ten days of CPU time on a dedicated Hewlett-Packard 1000 21MXE minicomputer.

5.7 Trajectories in T-Y-Z Space

While the manner in which the variables T, Y and Z change with time is of interest, the forms which they create in three dimensional T-Y-Z space are of even more interest, as these will delimit the shape of the attractor which the trajectories are following. For the chaotic oscillation shown in Figure 5.7, the T-Y, T-Z and Z-Y views of the system trajectory are shown on Figures 5.9(a)-(c) respectively. From these two-dimensional views, the complete shape of the three-dimensional trajectory can be

constructed.

Several positions have been labelled in Figure 5.9(b) in an attempt to describe the three-dimensional shape of the attractor. If a trajectory starts near position 1 on the front (out of the paper) of the lower band, it will travel from right to left and pass through position 2 such that it is now located on the back (behind the paper) of the upper band at position 3. From there, the trajectory passes under the right-most part of the attractor such that it arrives at position 4 which is on the back of the lower band. The trajectory passes along the inside of the "circular-well" (clearly shown in Figure 5.9(a)) in a clockwise fashion until it reaches position 5, which is on the front side of the upper band. From position 5, the trajectory travels over the top of the right-most part of the attractor, ultimately arriving at position 6, which like position 1, is located on the front of the lower band. The trajectory will now repeat itself in a similar way.

This motion is identical to that which would result from following a Möbius-band, hence this attractor should be known as a "Möbius-band attractor". In some respects, this attractor is similar to an idealized attractor described by Rössler [5.21]. Besides this particular shape, many other forms of the attractor have been observed for other parameter values.

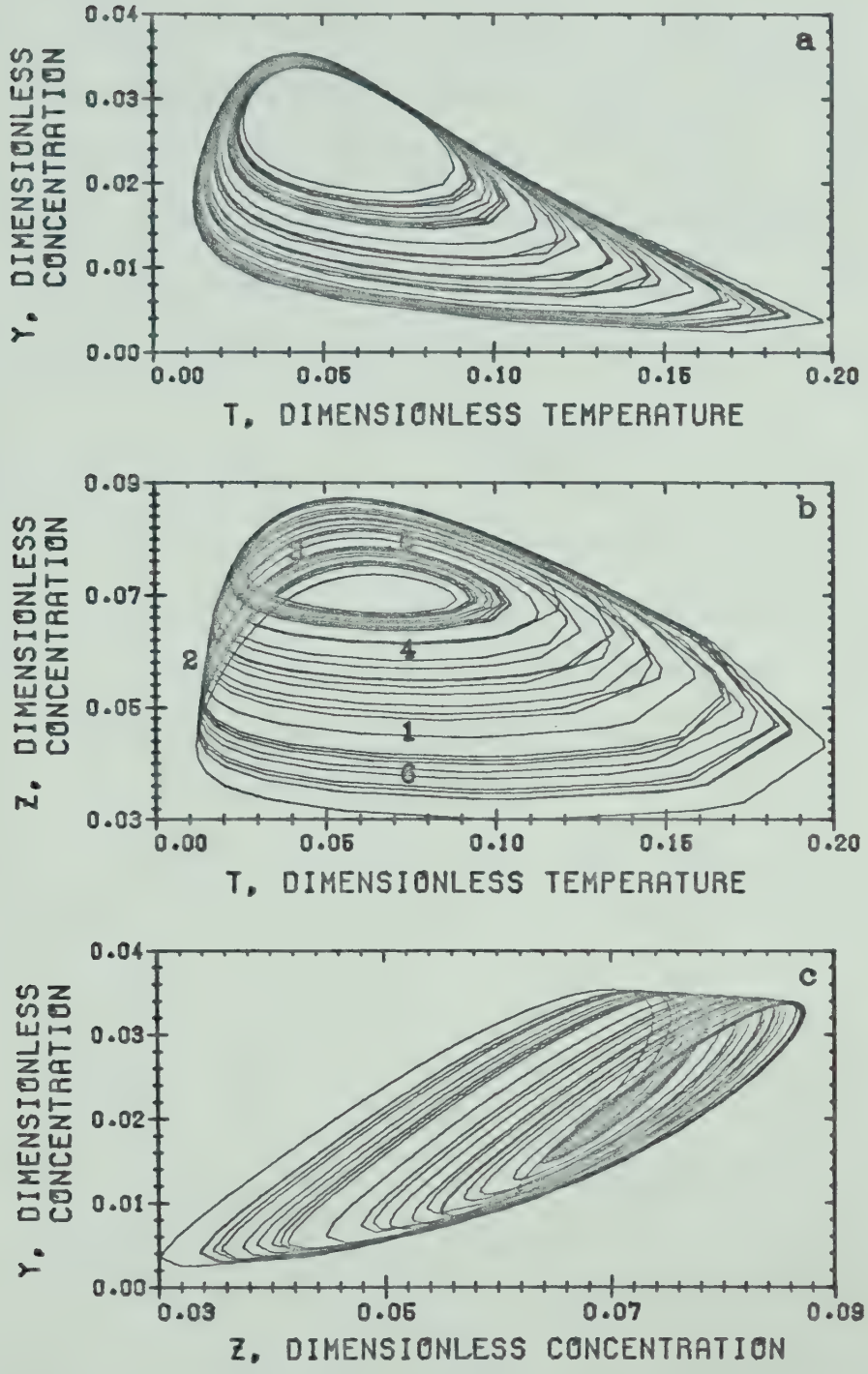

Figure 5.9 Two-Dimensional Views of the Three-Dimensional Attractor (all parameters as in Figure 5.7)
(a) T-Y view (clockwise motion when viewed from above)
(b) T-Z view (Möbius-band structure is displayed)
(c) Z-Y view (motion is clockwise)

5.8 Conclusions

It has been shown that a very simple chemical reactor model consisting of three ordinary differential equations can display complex periodic and chaotic behavior. This behavior has been analyzed by examining autocorrelation coefficients, next-amplitude plots, and state-space trajectories.

Through the use of the autocorrelation analysis it has been shown that the chaotic behavior does not contain any high order oscillations. When only the temperature maxima are used, the autocorrelation analysis is a very useful, and computationally efficient, method of examining complex periodic and chaotic behavior.

The next-amplitude plots have been found to be composed of very complex structures, which upon close examination appear to be fractal curves.

A detailed inspection of the state-space trajectories during a chaotic oscillation has shown that the trajectories follow a Möbius-band attractor. Other more complex forms of the attractor have also been found.

5.9 Nomenclature

Roman

A_i constants in the characteristic equation

$[A]$ concentration of A in the reactor

$[A]_o$ concentration of A in the reactor feed

$[B]$ concentration of B in the reactor

$[B]_o$ concentration of B in the reactor feed

Cp heat capacity

Da_i Damköhler numbers for the two reactions

E_i/R activation energies for the two reactions

Hr_i heats of reaction for the two reactions

J Jacobian matrix

$j_{i,i}$ elements on the main diagonal of the Jacobian matrix

k_i rate constants for the two reactions

L number of lags for autocorrelation analysis

Q reactor volumetric feed rate

S area for heat transfer

t dimensionless time

t' time

T dimensionless temperature

T' reactor temperature

T'_o temperature of the reactor feed

Tm dimensionless temperature maximum

$\overline{Tm}$ average of the dimensionless temperature maxima

U reactor heat transfer coefficient

V reactor volume

Y dimensionless concentration of species A

Z dimensionless concentration of species B

Greek

α dimensionless heat transfer coefficient

β_i dimensionless heat of reaction

γ_i dimensionless activation energies

ρ density

ω eigenvalue of the Jacobian matrix

5.10 References

5.1 Eigenberger, G., Chem. Eng. Sci., 1978 33 1263.

5.2 Ivanov, E.A., Chumakov, G.A., Slinko, M.G., Bruns, D.D. and Luss, D., Chem. Eng. Sci., 1980 35 795.

5.3 Uppal, A., Ray, W.H. and Poore, A.B., Chem. Eng. Sci., 1974 29 967.

5.4 Uppal, A., Ray, W.H. and Poore, A.B., Chem. Eng. Sci., 1976 31 205.

5.5 Vaganov, D.A., Samoilenko, N.G. and Abramov, V.G., Chem. Eng. Sci., 1978 33 1133.

5.6 Kurtanjek, Z., Sheintuch, M. and Luss, D., J. Catal., 1980 66 11.

5.7 Sheintuch, M., AIChE J., 1981 27 20.

5.8 Renola, G.T., Ph.D. Thesis, University of Illinois 1977.

5.9 Li, T.-Y. and Yorke, J.A., Amer. Math. Monthly 1975 82 985.

5.10 Rosen, R., Dynamical System Theory in Biology,

Wiley-Interscience, New Yory 1970.

5.11 Kahlert, C., Rössler, O.E. and Varma, A., Preprint - Workshop on Modelling Chemical Reaction Systems, Heidleberg, 1980.

5.12 Lynch, D.T., Rogers, T.D. and Wanke, S.E., accepted Intl. J. Math. Model.

5.13 Pikios, C.A. and Luss, D., Chem. Eng. Sci., 1979 34 919.

5.14 Hassard, B.D., Kazarinoff, N.D. and Wan, Y-H., Theory and Applications of Hopf Bifurcation, London Mathematical Society Lecture Note Series 41, Cambridge University Press, Cambridge, 1981.

5.15 Gear, C.W., Numerical Initial Value Problems in Ordinary Differential Equations, Prentice-Hall, Englewood Cliffs, New Jersey, 1971.

5.16 Shampine, L.F. and Allen, R.C., Numerical Computing - An Introduction, W.B. Saunders Company, Toronto, 1973.

5.17 Lorenz, E.N., J. Atmos. Sci., 1963 20 130.

5.18 Lubkin, G.B., Phys. Today, March 1981 34 17.

5.19 Mandelbrot, B.B., Fractals - Form, Chance, and Dimension, W.H. Freeman, San Francisco, 1977.

5.20 Hénon, M., Comm. Math. Phys., 1976 50 69.

5.21 Rössler, O.E., Bull. Math. Biol., 1977 39 275.

6. DESCRIPTION OF THE EXPERIMENTAL APPARATUS

In the preceeding chapters several topics have been investigated which are of general interest in the modelling of oscillatory behavior in chemical and catalytic reactors. However, no attempt has been made to exhaustively investigate the large number of recent models which have been proposed as explanations for oscillatory behavior. It appears that the devising of mechanisms for explaining oscillatory behavior is only limited by the imagination of those who model. In order to determine which mechanisms are physically realistic, it is necessary to perform model validation through comparison with actual experimental observations. To this end, a reactor for studying the dynamics of chemical reactions over supported metal catalysts was constructed. This reactor and associated equipment are described in this chapter.

6.1 General Description of the Equipment

As initially conceived, the experimental apparatus was to consist of a recycle reactor system which could be used to study the oxidation of carbon monoxide on a supported platinum catalyst, as this was one of the reactions for which there were reports of experimental observations of oscillatory behavior. Since previous experimental work upon

which to base a design was not available, it was necessary to adhere to several very general considerations in the design and construction of the apparatus.

It was desired that the apparatus be capable of being used for general investigations of gas phase reactions on supported metal catalysts, i.e. it was not to be constructed specifically for the oxidation of carbon monoxide on one particular catalyst. In particular, temperature measurement and control over a wide range of operating conditions was to be possible, and similarily, the gas metering and delivery system was to be capable of accurately providing gas mixtures over a wide range of compositions and flow rates. Also, due to the dynamic nature of the phenomena which were to be studied, continuous product analysis was essential. A general description of the apparatus which was constructed is given in Figure 6.1, and in the following, each of the major sections of the apparatus will be described in detail.

6.2 Feed Metering and Mixing

Shown in Figure 6.2 is a detailed schematic of the feed metering and mixing section of the apparatus. As can be seen, provision was made for using various gases (O_2, CO, N_2, He, etc.) for the purposes of reaction or dilution. With one exception, all these gases were supplied from high pressure cylinders obtained from Union Carbide Limited through a local distributor, Consumer's Welding Supplies

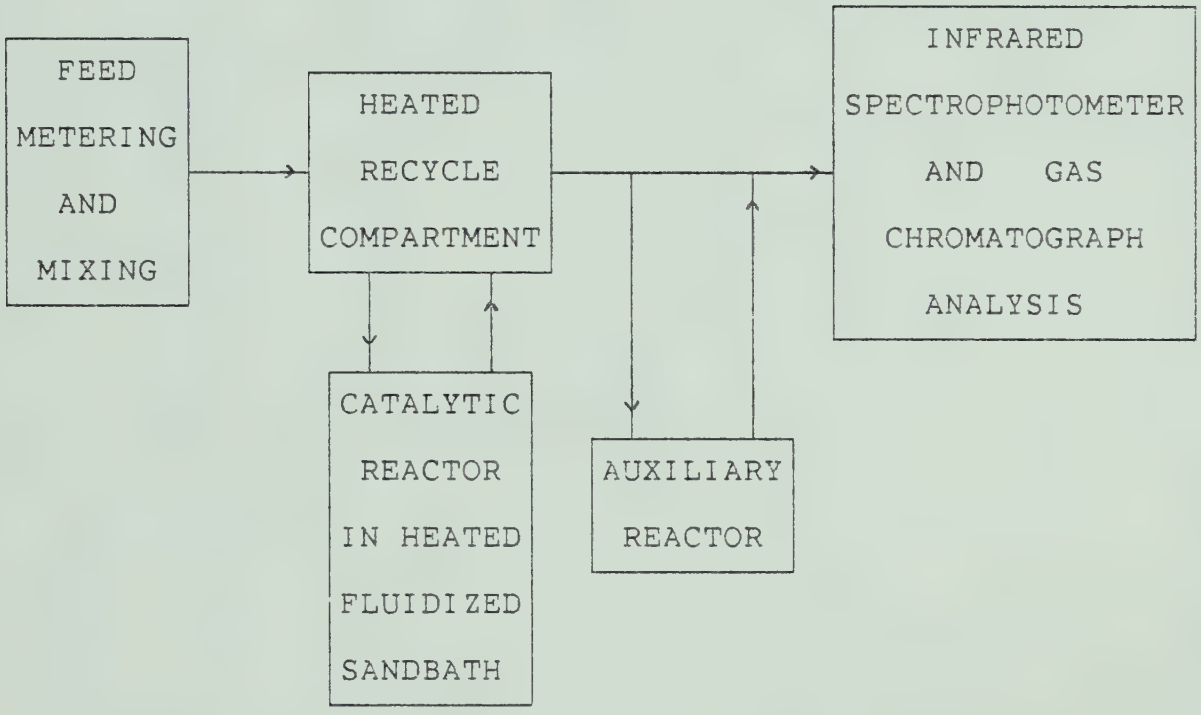

Figure 6.1 General Description of the Experimental Apparatus

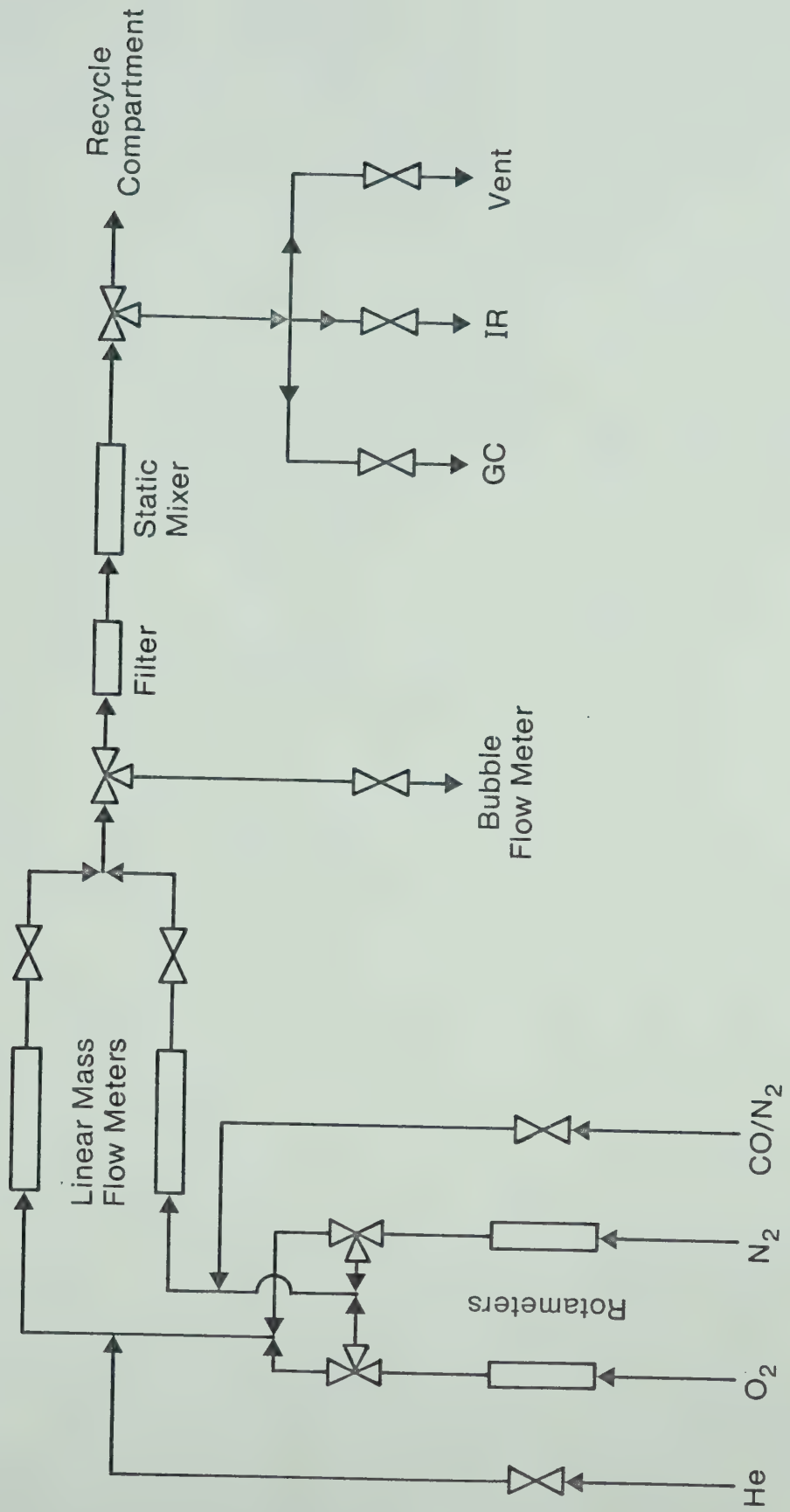

Figure 6.2 Feed Metering and Mixing Schematic

Limited. The oxygen and nitrogen were very dry grade (99.6% and 99.99% min. purity, respectively), the helium was prepurified grade (99.995% min. purity), and the carbon monoxide was C.P. grade (99.5% min. purity). The outlet pressures from the gas cylinders were controlled through the use of several Matheson model 8H two stage regulators. The sole exception to the above was a cylinder of ultra high purity oxygen (99.99% min. purity) obtained from the Matheson Company, the pressure of which was controlled via a Matheson model 19 high purity, single stage, regulator.

The flow rates of the various gases were measured by two Matheson rotameters (#600 and #610 tubes) and by two Matheson linear mass flowmeters, model 8116-0153 (Ser. #1768) 0-5000 SCCM, and model ALL-100 (Ser. #1002) 0-100 SCCM. The voltages generated by the two mass flowmeters were continuously recorded by a two pen Hewlett-Packard model 7100B-14-21-25 (Ser. #844A04091) chart recorder. The flow rates of the gases were adjusted by using metering valves located at the exhaust end of the rotameters, and by two Whitey model 21 fine metering valves located on the downstream side of the linear mass flowmeters. The pressure in each rotameter was constant at the outlet pressure of the cylinder regulator which supplied the gas since all the valves were located downstream of the rotameters.

The flowmeters and rotameters were calibrated for a number of gases at two different pressures, and these calibrations are included in Appendix C. The linear mass

flowmeters were found to be insensitive to pressure over the range of the calibrations and the high range mass flowmeter (0-5000 SCCM) was only calibrated for a small range of flow rates since a 50 cm^3 bubble flowmeter was used for the calibrations.

From Figure 6.2 it is seen that if the gases were not sent to the bubble flowmeter, then they were instead passed through a particulate filter (particles seven microns in diameter or greater were removed) and a static gas mixer. The gas mixer consisted of stainless steel baffles placed inside a 20 cm piece of 1.9 cm diameter stainless steel tubing. From the mixer, a three way ball valve was used to direct the gas either to the recycle compartment, and on to the reactor, or to the gas chromatograph and the infrared spectrophotometer for analysis or calibration. In the construction of the feed metering and mixing apparatus, brass tubing and valves were used upstream of the rotameters and flowmeters, and stainless steel valves and tubing were used on the downstream side.

6.3 Heated Recycle Compartment

Shown in Figure 6.3 is a detailed schematic of the heated recycle compartment. The primary purpose of the recycle compartment was to provide feed to the reactor at approximately the reaction temperature. The temperature in this compartment was measured with an iron - constantan

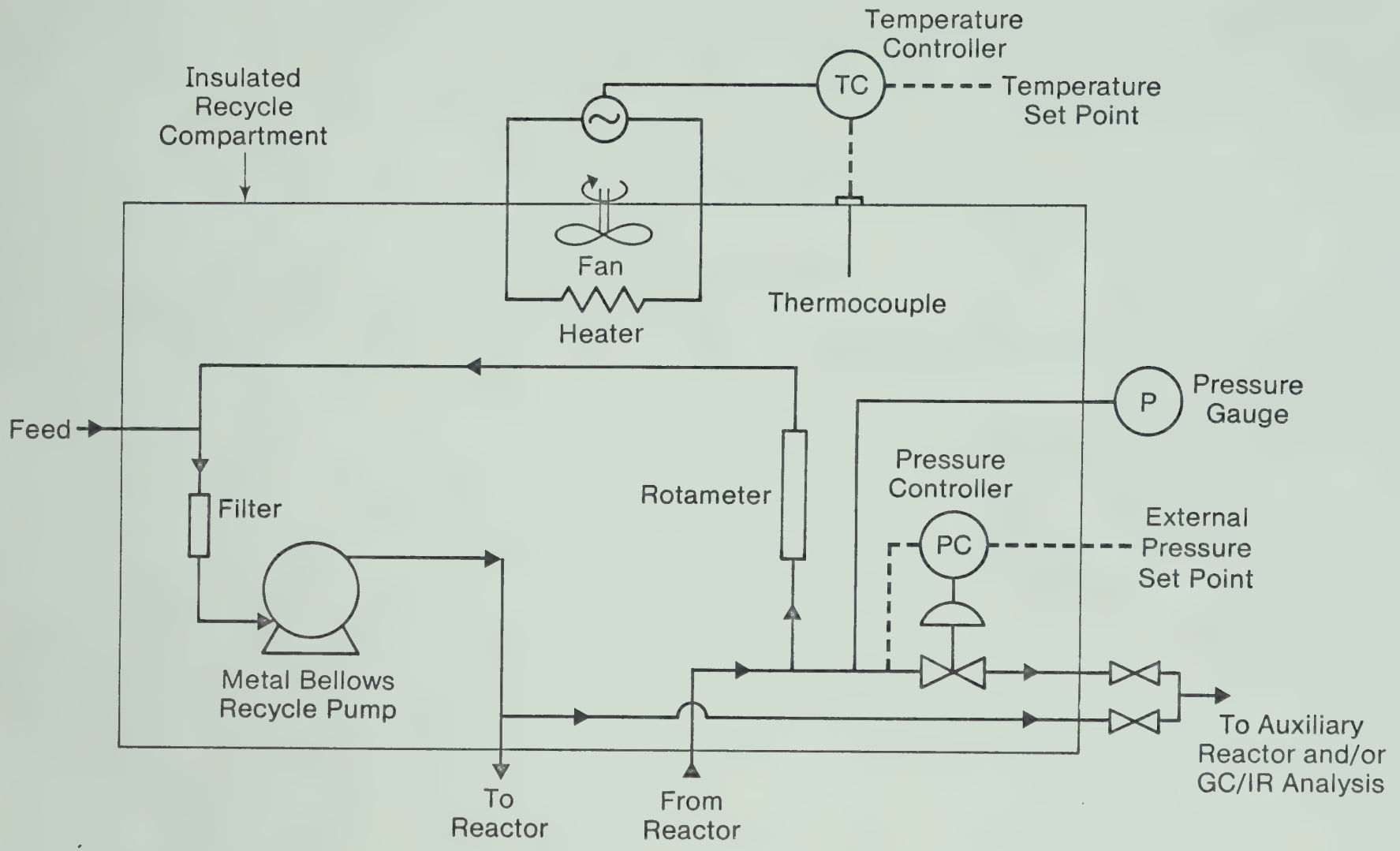

Figure 6.3 Heated Recycle Compartment Schematic

thermocouple (type J), controlled with a Honeywell model R7161J (Ser. #1015-1) temperature controller, and recorded on a Honeywell model 687378-1 (Ser. #68-06-07) Electronik 16 multipoint. A thirty-three ohm resistance coil with a radiation shield was used as the load for the temperature controller, and the heated air was circulated by a Universal Electric Co. model 80-041 (Ser. #6A54775R) motor with a squirrel cage fan. Heat losses from the recycle compartment were minimized by placing fiberglass insulation on the inside walls of the compartment.

Located in the recycle compartment were the necessary pieces of equipment for recycling the reactor product stream and controlling the flow of the effluent stream. Stainless steel was used throughout as the material of construction.

The recycle was accomplished with a Metal Bellows Corporation model MB-118HT (Ser. #1622) metal bellows pump. The metal bellows pump was driven with a variable speed one horsepower Reliance VSD motor, model B56G3104 (Ser. #27F85W05-AZ). This motor was manually controllable over the range 30 to 2000 RPM by means of an associated electronic speed controller. A gas filter capable of removing particulate matter with diameters of seven microns or greater was placed on the suction side of the recycle pump in order to protect the metal bellows. As indicated in Figure 6.3, the flow rate of the recycle stream was monitored with a rotameter (Matheson #605 tube), and the pressure in the recycle line was measured with an Ashcroft

(30 inches Hg vacuum - 30 psig) pressure gauge.

The flow of the effluent stream was controlled with a Moore constant differential flow controller, model 63SUI (Ser. #PC-5402). This flow controller was used to manipulate the effluent flow rate such that the pressure in the recycle line (and in the reactor) was kept equal to an externally applied pressure. This external pressure (set point for the flow controller) was provided by a Moore Nulmatic model 40-100 (Ser. #PC-7170) pressure regulator which was connected to a low pressure air line.

While a gas analysis was normally performed on the reactor effluent stream, it was also possible, as shown in Figure 6.3, to sample the stream (recycle plus new feed) entering the reactor. However, sampling this stream was difficult as it was not under the control of the flow controller. This line was primarily used to sample the reactor effluent when the reactor was run as an integral bed reactor. For integral bed operation, the recycle pump was turned off, and the flow direction was opposite to that indicated in Figure 6.3.

6.4 Catalytic Reactor in Heated Fluidized Sandbath

A schematic of the fluidized sandbath, and catalytic reactor in which the catalyst particles were placed, is shown in Figure 6.4. The temperature of the inlet feed to the reactor was controlled by a Thermo Electric 400 model

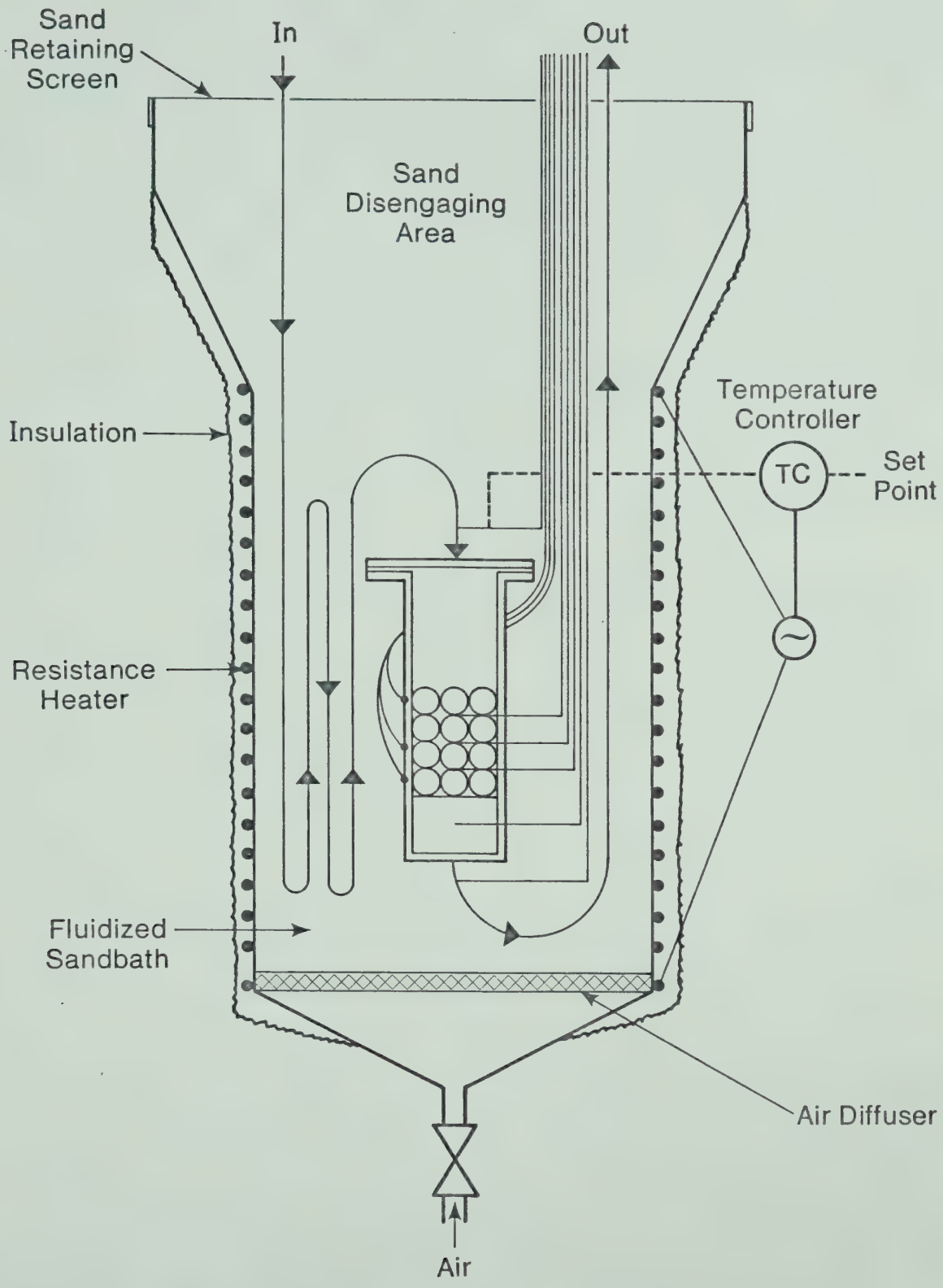

Figure 6.4 Reactor in Sandbath

3242200 (Ser. #56486-118) temperature controller which was used to heat the sandbath walls. These walls were wrapped with resistance wire which presented a fourteen ohm load to the temperature controller and the resistance wire was covered with insulation to minimize heat losses. The heat released at the sandbath walls was transferred to the reactor by the fluidized sandbath. The sand (alundum) was fluidized by passing air through a sintered metal plate at the bottom of the bed of sand and a fine mesh screen was clamped to the top of the sandbath to prevent excessive losses of sand.

The details of the reactor construction are shown in Figure 6.5 where the placements of the catalyst bed and the various thermocouples are shown. Stainless steel was used throughout as the material of construction. With one exception, all of the thermocouples, including those welded to the reactor wall, were type J (iron - constantan). The sole exception was a type T (copper - constantan) thermocouple located in the tubing at the end of the reactor preheat section. This location was the control point for the temperature controller which required a type T thermocouple, hence the different type. The voltages produced by the thermocouples were recorded by the previously mentioned Honeywell multipoint, and in addition, the voltages of the control thermocouple and the thermocouple located immediately below the catalyst bed were continuously recorded using a two pen Varian model A-25 (Ser. #49044924)

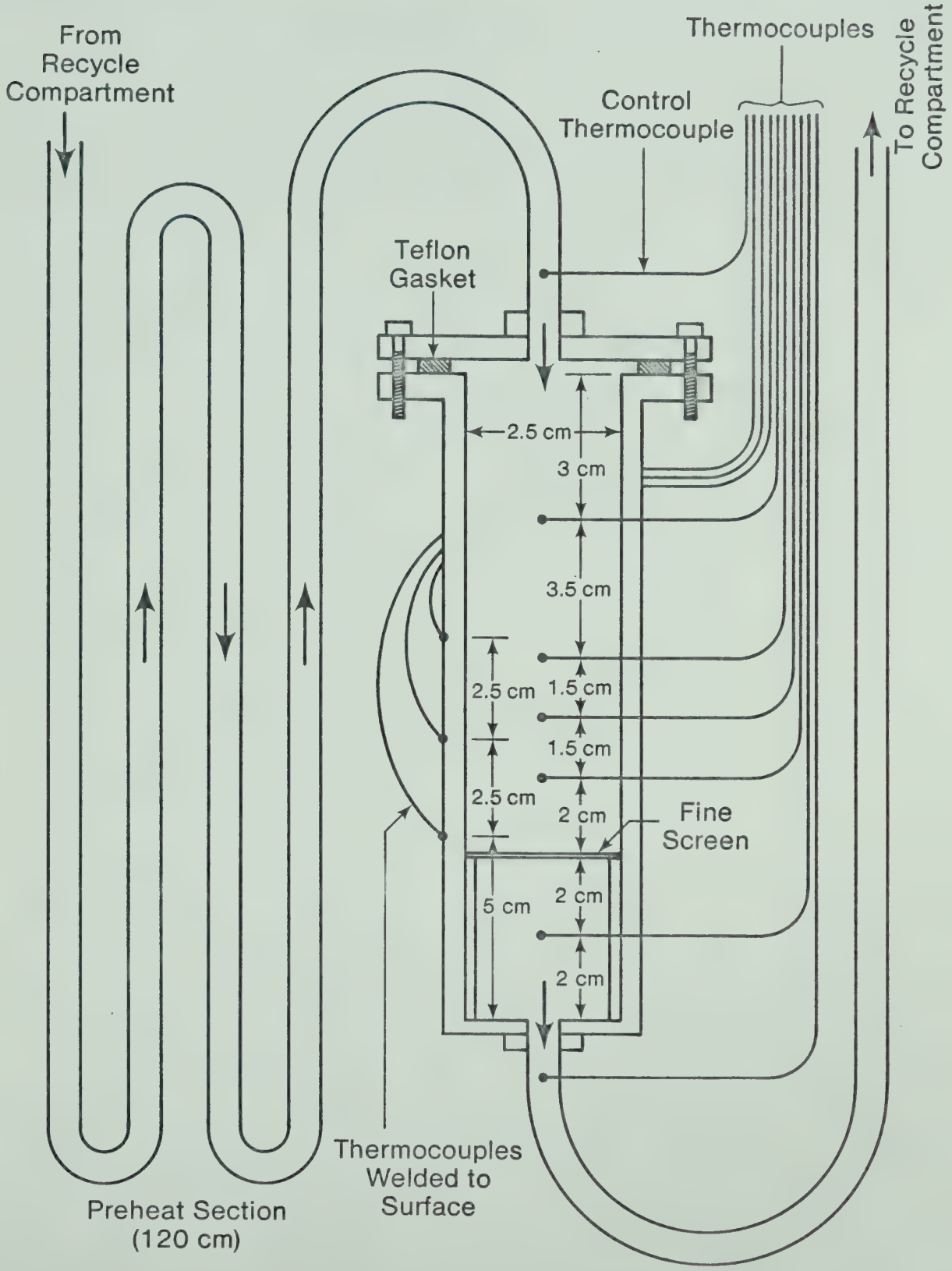

Figure 6.5 Reactor Detail

chart recorder.

The total volume of the empty reactor, the recycle pump (operating at 1800 RPM), and the associated tubing was determined to be in the range 245 to 260 cm^3. This range of volumes was determined by observing the effluent carbon monoxide concentrations from a step input of carbon monoxide in the feed to the empty (no catalyst) reactor. The volume of the reactor was then calculated by assuming that the reactor and tubing could be approximately described as a first order system with a time delay. Due to the size of the reactor, a maximum of approximately thirty grams of supported (Al_2O_3) catalyst could be used. This catalyst was supported by a fine screen at the bottom, and retained by a ball of glass wool at the top. The flow direction in the reactor was downwards when operated as a recycle reactor, and upwards when operated as an integral bed reactor.

6.5 Auxiliary Reactor

The auxiliary reactor, shown schematically in Figure 6.6, was designed and constructed in order to improve the accuracy of the measurement of the concentration of carbon monoxide in the reactor effluent. This was achieved by completely converting all of the carbon monoxide to carbon dioxide. The concentration of carbon monoxide was then determined by taking the difference between the carbon dioxide concentrations in the effluents from the auxiliary

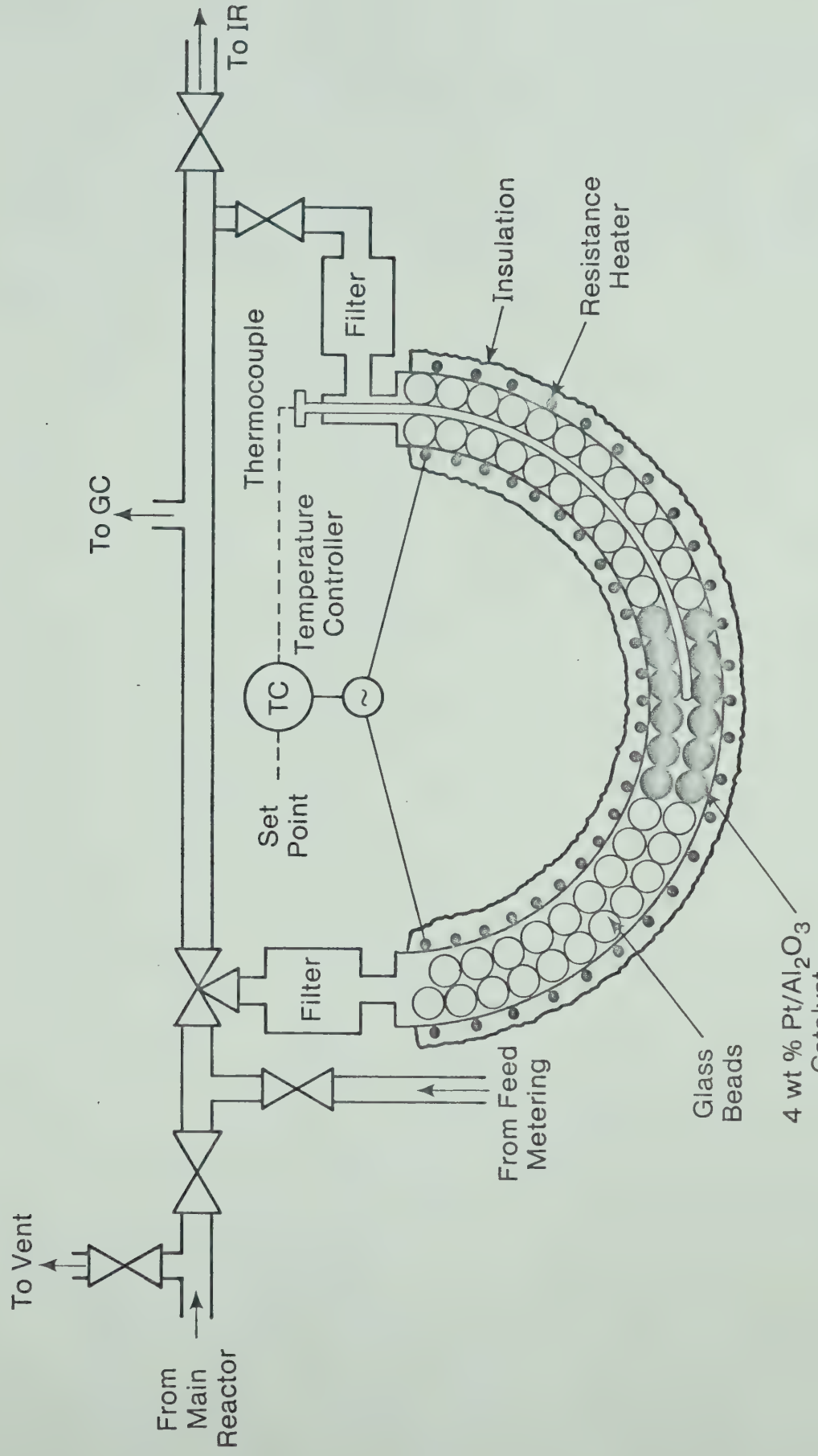

Figure 6.6 Auxiliary Reactor

reactor and the main reactor. This resulted in an improvement in the accuracy of the measurement of the carbon dioxide concentration due to the infrared spectrophotometer being an order of magnitude more sensitive to carbon dioxide than to carbon monoxide (as will be shown in the next section).

The construction details of the auxiliary reactor are quite straightforward, as the reactor was made from a 25 cm piece of 1.2 cm diameter stainless steel tubing. Approximately ten grams of 4 wt% Pt/Al_2O_3 catalyst was placed in the reactor, and the remaining volume was filled with glass beads. Due to the elimination of most of the dead volume through the use of the glass beads, it was found that the auxiliary reactor was also of use in determining some of the features of the dynamic behavior of the main reactor. Further details with respect to this are provided in the following chapter. Two gas filters capable of removing particulates with diameters of seven microns or greater were placed at either end of the reactor to prevent the contamination of the connecting tubing with fine catalyst particles. The gas from the main reactor was routed to the auxiliary reactor by opening one block valve and by switching one three way valve. All valves, filters and tubing were constructed of stainless steel.

The temperature in the auxiliary reactor was measured by a type J thermocouple placed in the catalyst bed. This temperature was controlled by a Honeywell model R7161J (Ser.

#1007-1) temperature controller, and it was recorded by using the Honeywell multipoint. The load for the temperature controller consisted of forty-one ohms of high resistance wire which was tightly wound around asbestos insulating tape on the reactor. For safety purposes, a thick layer of insulation was placed over the resistance wire.

6.6 Gas Composition Analysis

The analysis of the compositions of the various streams was accomplished by using both a gas chromatograph (GC) and an infrared spectrophotometer (IR). The arrangement of valves and tubing (stainless steel throughout) connecting the GC and the IR to the rest of the apparatus was such that any gas stream could be completely or partially vented, or could be sent to the GC and/or the IR. In the experimental work that was performed, the IR was used as the main tool for collecting dynamic information due to the continuous nature of its output, and the GC was used primarily for determining the overall compositions on a discrete basis. The use of the GC was necessary since several of the components in the reactant and product streams (O_2, N_2 and He) are infrared inactive.

6.6.1 Gas Chromatograph

As part of the experimental equipment, a Hewlett-Packard model 5734A (Ser. #1825A01203) gas chromatograph was used. This GC contained both a flame ionization detector and a thermal conductivity (TC) detector. In this work only the TC detector was used.

The gas sampling was performed through the use of a gas sampling valve which contained two sample loops (0.5 cm^3 per loop). The sample loops were arranged such that one loop was continuously purged with sample when the other loop was used to inject a sample. Thus, there was a continuous flow of sample through the sampling valve.

The output from the GC was recorded and integrated by a Hewlett-Packard model 3380A (Ser. #1324A01206) electronic integrator. This integrator was very user oriented, as with the push of one button it would automatically (under the control of the various switch settings) record and integrate the GC signal, produce a printed analysis of the signal, and stop itself. Hence, it required very little user attention.

It was desired that the GC operation should be as user oriented as the integrator operation. To achieve this some rather stringent constraints were placed on the use of the GC. The GC column was to be designed such that the five components, CO, CO_2, O_2, N_2, and H_2O, could be resolved into distinct peaks with a total analysis time of less than ten minutes. Further, no bypass valves, or other devices requiring user attention, were to be included in the column

design.

Satisfying these constraints was not a trivial task, as an examination of the gas chromatography literature quickly revealed that it is extremely difficult to easily separate this mixture into its individual components. By a trial and error procedure it was determined that the parallel-series column arrangement shown in Figure 6.7 would satisfy the stated constraints. From this figure it is seen that a sample entering the column arrangement was equally split between the two parallel branches. The split ratio could be varied by adjusting the two needle valves located inside the GC oven, but it was found that an equal split gave the best results.

Samples which passed through the Porapak T - Spherocarb branch of the column arrangement were resolved into three very distinct peaks, namely, a composite peak composed of O_2, N_2 and CO, a distinct CO_2 peak, and a slightly tailing H_2O peak. A typical chromatogram for a sample passing through this side of the arrangement is shown in Figure 6.8(a).

Samples which passed through the 5A molecular sieve branch of the column were also resolved into three distinct peaks, namely, an O_2 peak, a N_2 peak, and a CO peak. A typical chromatogram for a sample passing through the 5A molecular sieve column is shown in Figure 6.8(b). No peaks for H_2O or CO_2 emerge from this column, as these two components are very strongly adsorbed by 5A molecular sieves

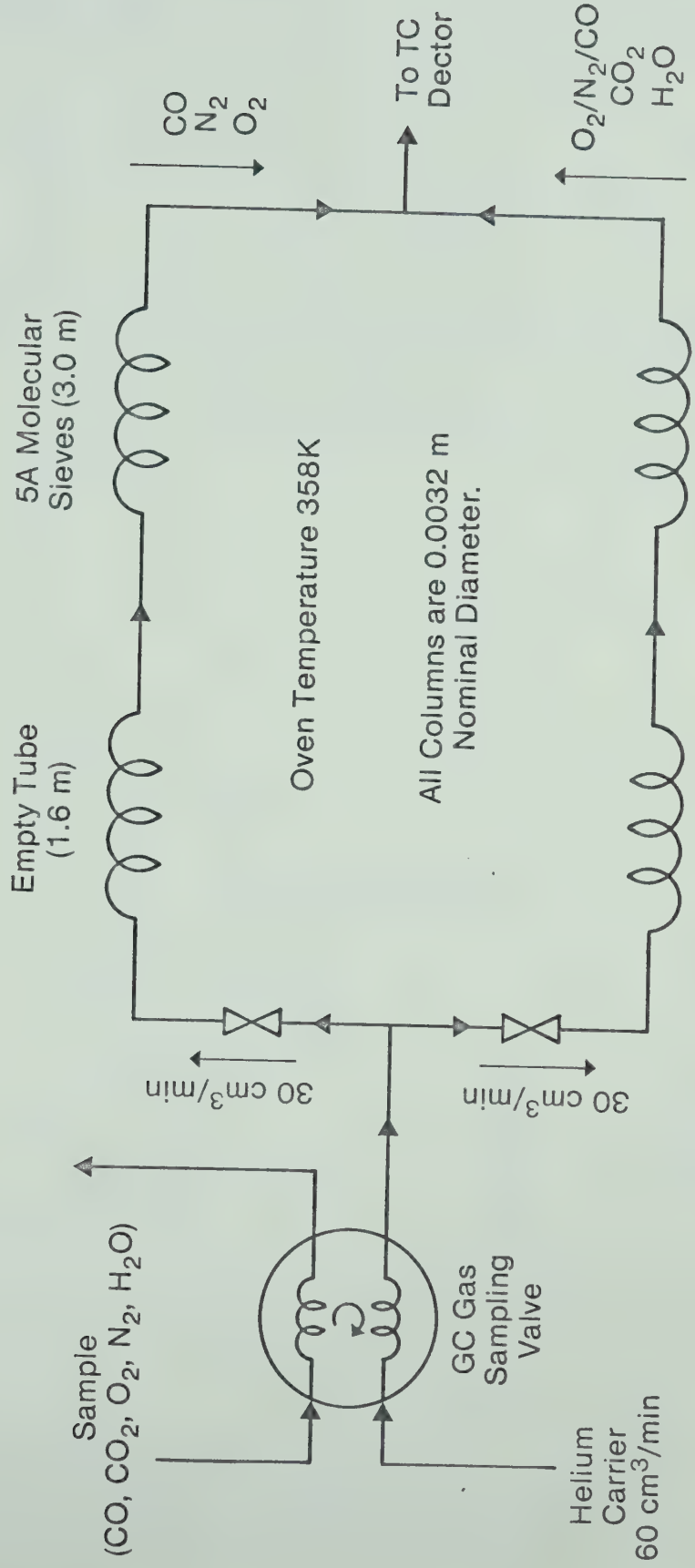

Figure 6.7 Gas Chromatograph Column Arrangement

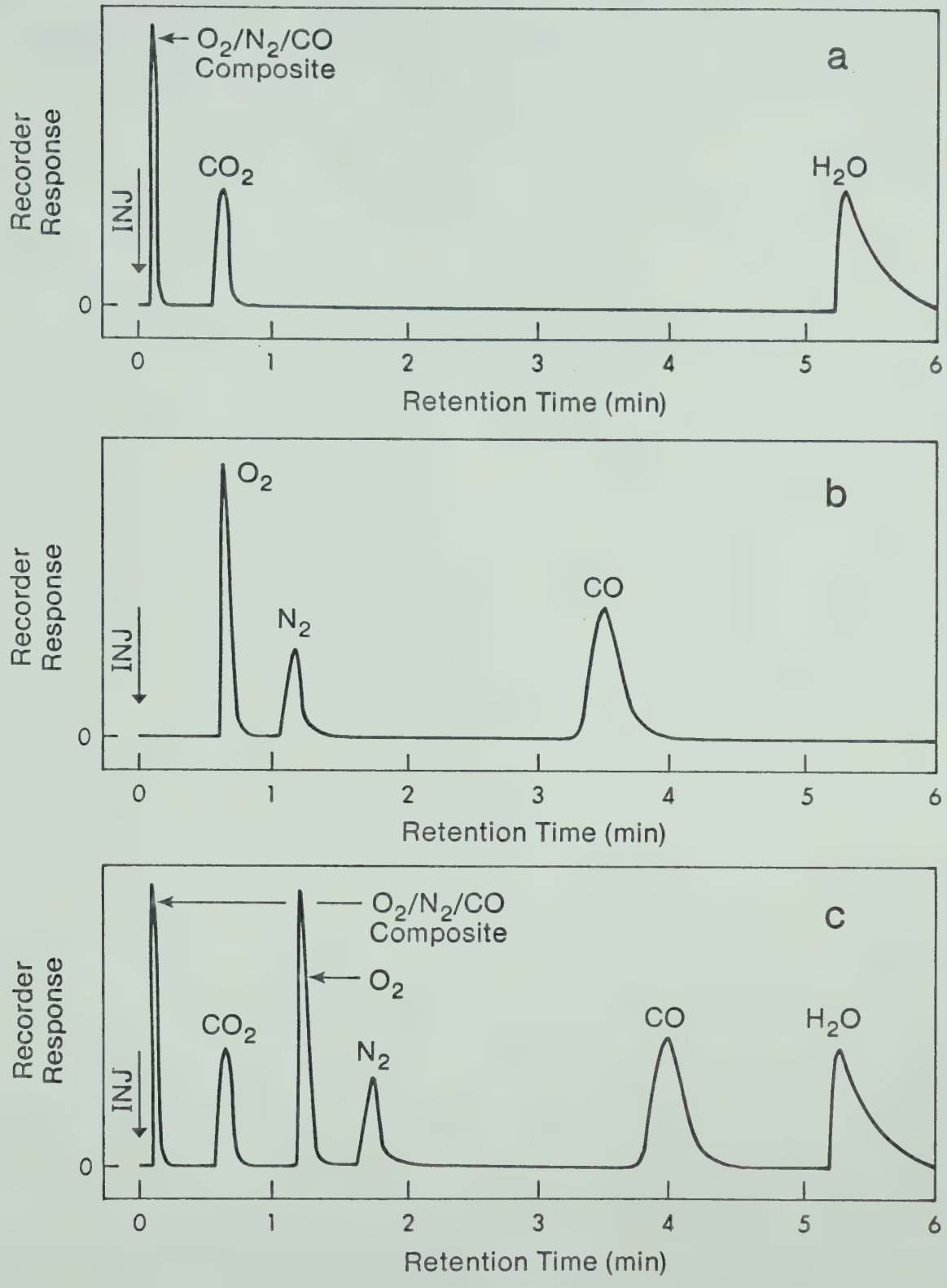

Figure 6.8 Typical GC Chromatograms
(a) Porapak T – Spherocarb Columns
(b) 5A Molecular Sieve Column
(c) Total Column Arrangement as in Figure 6.7

at 353 K (the oven temperature). These components were purged from the column on a regular basis by raising the column temperature to 450 K for several hours with helium flowing through the columns. A comparison of the (a) and (b) parts of Figure 6.8 shows that some overlapping of the peaks would occur if the exit streams from the two columns were mixed before the TC detector. To eliminate this overlapping of peaks, a carefully selected length of empty tubing was placed in front of the 5A molecular sieve column. This empty column provided a time delay of approximately 30 seconds which enabled the three peaks from the 5A molecular sieve column to emerge in the 'window' between the CO_2 and the H_2O peaks from the other branch of the arrangement. A typical chromatogram of a sample passing through the total column arrangement is shown in Figure 6.8(c).

Once the column arrangement was finalized, the GC was calibrated using various mixtures prepared by the previously calibrated flow metering and mixing equipment. These calibrations are included in Appendix D along with a procedure for determining the overall sample composition from a knowledge of the component response factors and the percentage area under each curve in Figure 6.8(c).

6.6.2 Infrared Spectrophotometer

The investigation of the dynamic behavior of the concentrations of CO_2 and CO from the reactor was performed through the use of a Pye Unicam model SP3-200 (Ser. #291036)

ratio recording infrared spectrophotometer. A Pye Unicam model SP3-050 (Ser. #299184) data processor was used in conjunction with the IR to perform specialized operations such as accurate placement of the monochrometer for constant wavenumber scanning and conversion of transmittance to absorbance.

In order to continuously analyze a sample stream, it was necessary to construct a continuous flow sample cell for the IR. Two cells were constructed, the first of which was found to be unsatisfactory due to it having a very low signal to noise ratio. This was caused by a short cell pathlength and low IR transmission through the cell due to incorrect cell geometry. These factors necessitated the construction of a second sample cell, shown in Figure 6.9, which had a pathlength twice that of the first cell, and was constructed such that it conformed almost exactly to the IR beam geometry. These improvements resulted in satisfactory performance of the IR as the signal to noise ratio was increased by approximately an order of magnitude over that obtainable with the first cell. In the construction of these cells, stainless steel was used throughout, with sodium chloride windows in the first cell, and calcium fluoride windows in the second cell.

A further large increase in the signal to noise ratio was achieved by purging the IR sample chamber with air from which the atmospheric CO_2 and H_2O had been removed. These gases were removed by passing low pressure air through a bed

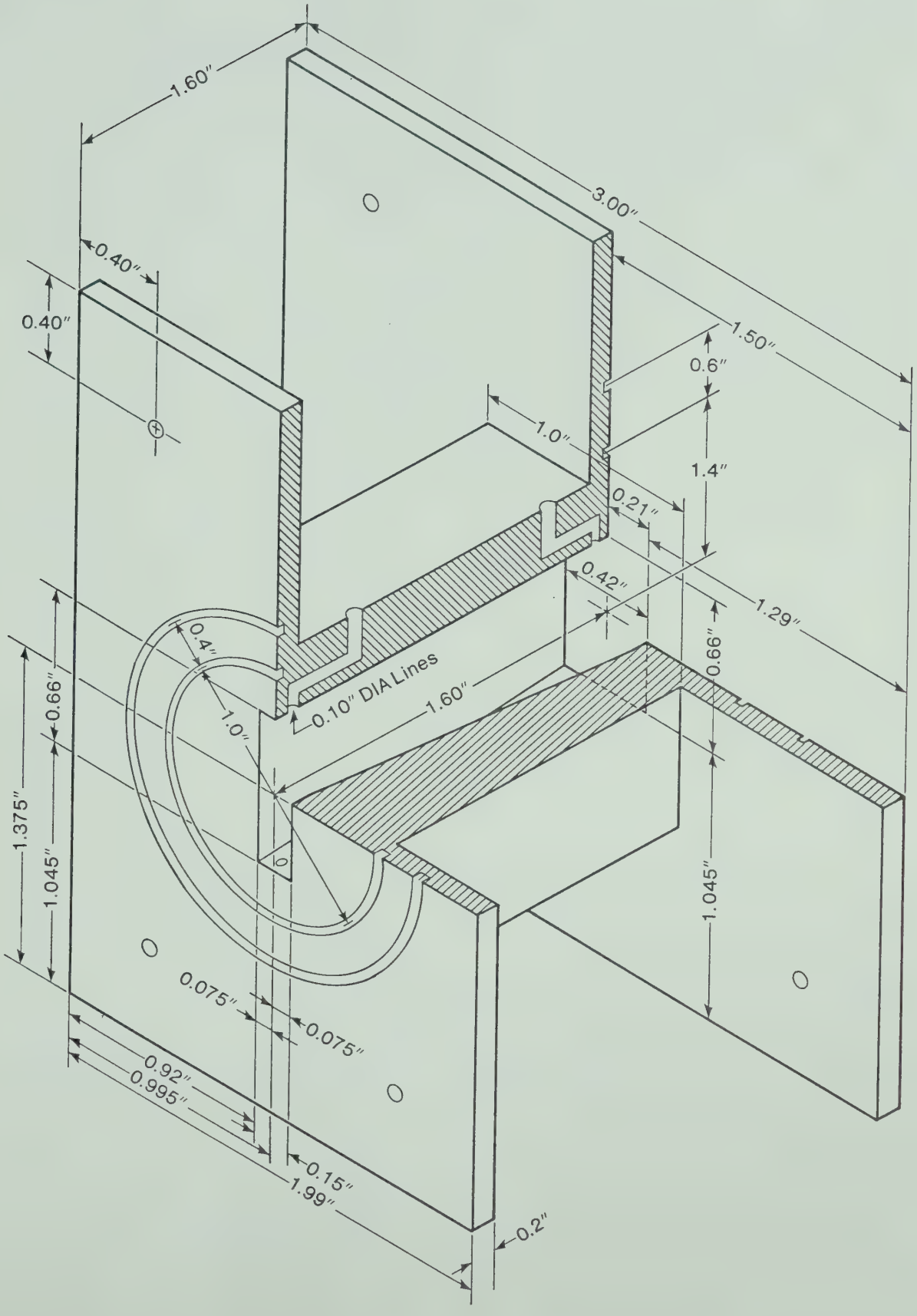

Figure 6.9 Infrared Spectrophotometer Sample Cell

of Ascarite (A.H. Thomas Co.) to remove the CO_2, and a bed of indicating drierite to remove the atmospheric H_2O.

Calibration curves for the IR, shown in Figure 6.10, were made by feeding the sample cell with gas mixtures which were prepared using the feed metering and mixing equipment. From these curves it is seen that the IR is approximately ten times as sensitive to CO_2 as it is to CO. In preparing these curves the CO absorbance was always measured at 2172 cm^{-1}, and the CO_2 absorbance was always measured at 2355 cm^{-1}. At these wavenumbers CO and CO_2 strongly absorb infrared radiation without interfering with each other. It is seen that the calibration curves are not linear and thus do not conform to Beer's Law predictions.

In calibrating the IR, as in normal operation, the temperature of the gases entering the sample cell was always very close to the ambient temperature in the laboratory. This was achieved by passing the gases through the inner tube of a small double pipe heat exchanger which had cooling water at ambient temperature flowing between the two tubes. This heat exchanger was primarily built as a precautionary measure to prevent hot gases from the auxiliary reactor (500 K) from entering the IR sample cell.

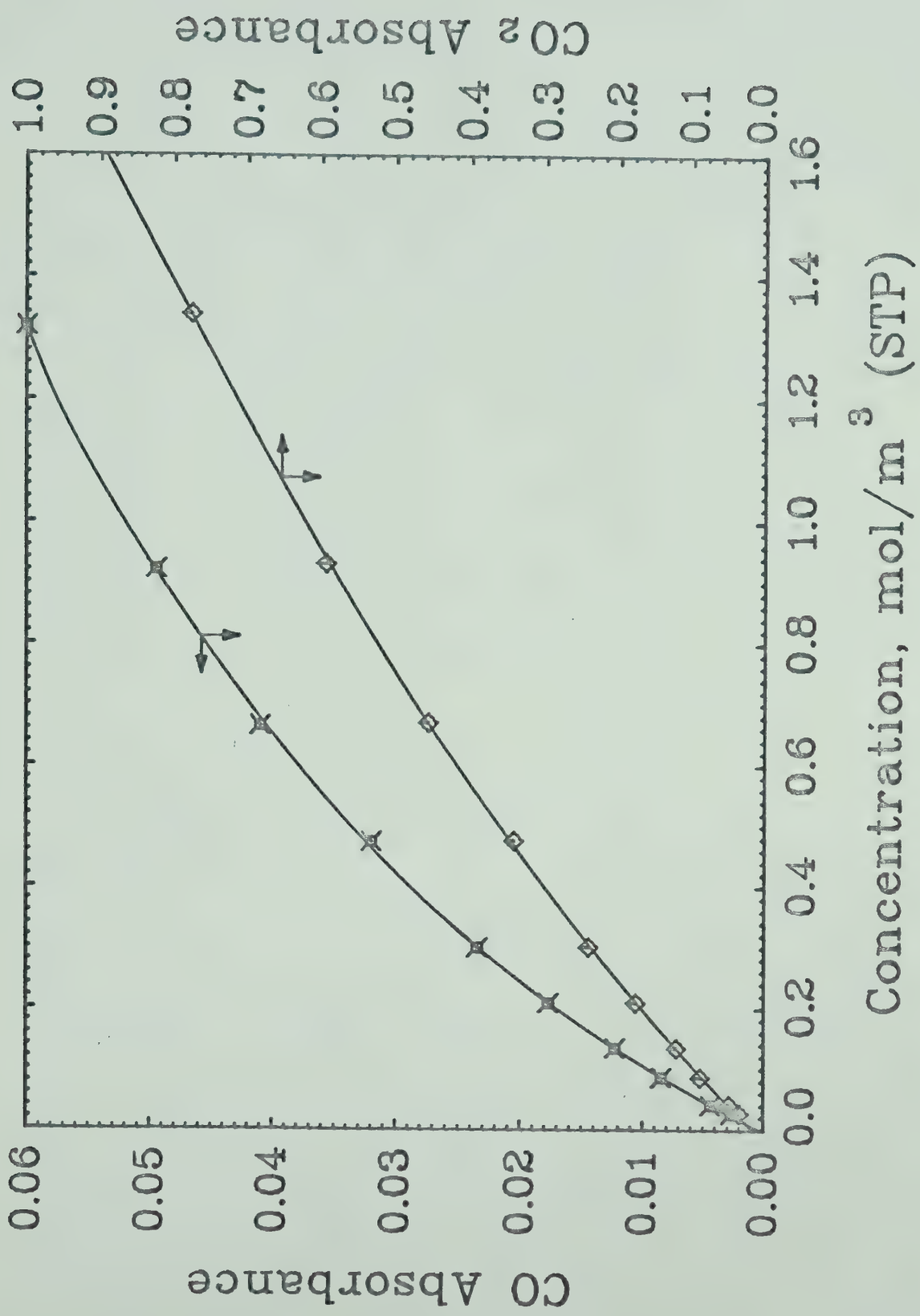

Figure 6.10 IR Calibration Curves for CO and CO_2

7. OSCILLATORY BEHAVIOR IN THE OXIDATION OF CARBON MONOXIDE

Once the equipment described in the preceding chapter was constructed, it was decided to investigate the existence of oscillatory behavior in the oxidation of carbon monoxide over supported metal catalysts. It was expected that this reaction could display oscillatory behavior due to the previous observations reported in the literature. These previously reported observations are summarized in a literature review, and following the literature review the remainder of the chapter is devoted to a description of experimental observations of oscillatory behavior for CO oxidation over supported metal catalysts using the equipment described in the preceeding chapter.

7.1 Literature Review

Presented in this section is a short review of the published literature concerning experimental observations of oscillatory behavior in the oxidation of carbon monoxide. The review is restricted to this rather narrow area as any comprehensive treatment of the various investigations concerning the catalytic oxidation of carbon monoxide would fill several volumes, with another volume necessary to reconcile the many contradictory observations which have been made. In the following literature review, the references have been cited in approximately their chronological order of publication so that some appreciation may be

gained of the sequencial developments in the field.

It appears that Beusch et al. [7.1, 7.2] were the first to observe oscillations in the catalytic oxidation of carbon monoxide. Their observations were made using a single pellet of 0.3% Pt/Al_2O_3 suspended in a differential reactor (no recycle). Oscillations in the carbon dioxide concentration were observed in the temperature range 453 - 523 K, and typically these oscillations were accompanied by small (~ 2 K) temperature oscillations. They speculated that several states of chemisorbed carbon monoxide participated in the reaction. This hypothesis was further refined by Hugo and Jakubith [7.3] who observed carbon dioxide oscillations in the temperature range 384 - 423 K when using a platinum mesh catalyst in a recycle reactor. They proposed that the oscillations were the result of a shift between bridged and linear forms of chemisorbed carbon monoxide.

In the two preceeding works, observations of oscillations were made by analyzing gas phase compositions, thus oscillations on the catalyst surface could only be inferred. The existence of surface oscillations was first estabilished by Dauchot and Van Cakenberghe [7.4] who showed that concentration and temperature oscillations could occur on catalyst surfaces. This was done through the use of resistivity measurements for platinum wires, and work function measurements for thin platinum films. Their conjecture was that the oscillations were caused by differences in the rates of adsorption of oxygen and carbon monoxide, with large surface

thermal effects resulting from the adsorption and reaction processes.

Each of the preceeding works had in common the use of a platinum catalyst and the rejection of the classical transport phenomena explanation for the oscillatory behavior. Both of these links were broken in work by Eckert et al. [7.5] in which concentration and temperature oscillations (~3 K) were reported for carbon monoxide oxidation in a recycle reactor in which a CuO/Al_2O_3 (1:1) catalyst was used. The recycle rate and the reaction temperature (430 K) were deliberately set such that transport limitations were encountered, and this was used as the explanation for the oscillatory behavior.

However, the earlier view that oscillatory behavior could occur in the absence of transport limitations was reinforced by McCarthy et al. [7.6] who showed that oscillatory behavior could occur in a gradientless, spinning basket, continuous stirred tank reactor. A 0.035% Pt/Al_2O_3 catalyst was used and the oscillations were observed at reaction rates near the maximum of the 'abnormal' reaction rate curve for carbon monoxide oxidation. It was believed that these oscillations were due to nonunique surface reaction rate control. In subsequent work by Varghese et al. [7.7] using the same rector and catalyst in the temperature range 370 - 430 K, it was found that two qualitatively different types of oscillations could occur depending on whether 'pure' or 'impure' oxygen was used. When oxygen

with trace amounts of hydrocarbon impurities was used, large multipeak and chaotic relaxation oscillations were observed. However, if very pure oxygen was used only small symmetrical oscillations occurred. The existence of the relaxation oscillations was attributed to periodic build-up and elimination of the hydrocarbon impurities on the catalyst surface. No explanation was attempted concerning the small symmetrical oscillations, but the existence of localized temperature excursions could not be ruled out as a possible cause.

In parallel with the above work, oscillatory behavior resulting from the simultaneous oxidation of hydrocarbons (1-butene) and carbon monoxide was explicitly studied by Cutlip and Kenney [7.8] using a 0.5% Pt/Al_2O_3 catalyst in a gradientless recycle reactor. They failed to observe any oscillatory behavior when only carbon monoxide was oxidized, but sustained oscillations and multipeak behavior were encountered in the temperature range 423 - 438 K when the simultaneous oxidation of 1-butene and carbon monoxide was carried out. They believed that the oscillations were the result of a periodic build-up and burn-off of the 1-butene on the catalyst surface.

The belief that multipeak and chaotic phenomena were the result of the interaction of two reactions (hydrocarbon and CO oxidations) was challenged by Sheintuch and Schmitz [7.9], Plichta and Schmitz [7.10] and Sheintuch [7.11] in investigations of carbon monoxide oxidation on a platinum

foil in a gradientless stirred tank reactor. They found that single and multipeak behavior, multiple limit cycles, and chaos could occur in the temperature range 423 - 544 K. It was their belief that intrinsic chaotic behavior exists for this reaction. However, this assertion must be tempered with the observation that the activity of the platinum was not very reproducible.

The existence of complex dynamic phenomena has also been reported by Rathousky et al. [7.12] in an investigation of carbon monoxide oxidation on a Pt/Al_2O_3 catalyst in a recycle reactor over the temperature range 433 - 473 K. They present experimental results which indicate that long periods of time (>9 hours) are necessary to determine the character of some types of complex dynamic behavior.

In summarizing the experimental work which has just been described about all that can be said is that oscillations do exist, and these oscillations may be simple or complex in nature. No concensus has yet been reached concerning the underlying mechanism which causes the oscillations, and in fact very little work aimed at elucidating this mechanism has been performed since most of the reported experimental work has been of a descriptive (as opposed to mechanistic) nature. However, despite the abundance of descriptive studies, a thorough experimental examination of the effects of various operating conditions on oscillatory behavior has yet to appear in the literature.

In the following sections of this chapter, a detailed investigation of the effects of various reactor operating conditions on oscillatory behavior is presented. Whenever possible, comments are made regarding the underlying mechanism responsible for the oscillatory behavior.

7.2 Preliminary Experimental Work

At the time that the experimental work was started it was not possible to state a priori whether or not a particular catalyst could display oscillatory behavior. Hence, a certain amount of preliminary work with several catalysts was necessary in order to determine both the reaction characteristics of the catalysts as well as the operating characteristics of the apparatus.

The first catalyst which was examined was a supported platinum on alumina catalyst obtained from Englehard Industries Limited. This catalyst, which contained 0.3 weight percent platinum, was obtained in the form of cylindrical alumina pellets which were one-eighth of an inch in diameter and length. Several beds of this catalyst were placed in the reactor and used for preliminary investigations into the nature of the catalytic oxidation of carbon monoxide. In each case the catalyst pellets were pretreated in flowing dry air at 625 K in a tube furnace for approximately twelve hours before being placed in the reactor. Also, the weight of the bed placed in the reactor was kept constant at twenty

grams. If less than twenty grams of catalyst pellets were used, then the remainder of the bed was composed of inert alumina cylinders which were similar in size and shape to the catalyst pellets. Unfortunately, the use of this catalyst did not lead to any observations of oscillatory behavior. Instead it was found that this catalyst displayed other interesting types of behavior. In particular, at low temperatures (363 - 373 K) this catalyst displayed multiple steady-state behavior in that for a given set of operating conditions it was found that two stable steady-states always existed. These steady-states represented the extremes which were possible, i.e. total conversion, or virtually no conversion of the carbon monoxide. The high conversion steady-state could be reached by initially purging the reactor with pure oxygen before introducing any carbon monoxide in the feed stream, and conversely the low conversion steady-state could be reached by initially purging the reactor with pure carbon monoxide (or an 11% CO in N_2 mixture) before introducing any oxygen in the feed. Also, it was sometimes possible to drive the system from a high conversion steady-state to a low conversion steady-state by making an abrupt increase in the carbon monoxide concentration in the feed. However, the reverse was not true as a low conversion steady-state could not be driven to a high conversion steady-state by making an abrupt decrease in the feed stream carbon monoxide concentration.

It was with regard to these transitions from high to low conversion steady-states that a further interesting property of this catalyst was observed. It was found that the previously mentioned transition from a high to a low conversion steady-state did not occur if the carbon monoxide concentration was increased incrementally rather than abruptly. In fact, if the carbon monoxide concentration was increased incrementally it was possible to feed very large amounts of carbon monoxide to the reactor and still stay at the high conversion steady-state. However, as the molar flow of carbon monoxide became large the reactor ceased to behave isothermally, as small (2 - 5 K) temperature gradients developed over the length of the catalyst bed.

This type of behavior (total conversion of large amounts of CO with a temperature gradient along the bed) persisted even when only very small amounts of catalyst (less than one gram) were placed in the reactor. It was believed that this behavior was the result of catalyst surface temperatures which were much higher than the bulk temperature. If a finite amount of time was required for these surface temperatures to adjust to feed concentration changes, then this hypothesis also explains why the very high reaction rates could only be reached by incrementally increasing the feed carbon monoxide concentration.

After investigating the behavior of this catalyst at many different operating conditions it became apparent that

oscillatory behavior was not going to be displayed, and that it would be necessary to use a different catalyst.

The second catalyst which was used in these preliminary screening tests was a General Motors converter catalyst (type #78925, package #6498995). This catalyst, which contained approximately 0.04% platinum and 0.04% palladium supported on alumina, was obtained in the form of spherical pellets approximately one-eight of an inch in diameter. This catalyst was primarily chosen because it had a lower metal loading than the first catalyst. By using a catalyst with a low metal loading it was hoped that isothermal reactor operation could be maintained, and that some of the problems encountered with the first catalyst could be avoided.

After investigating the behavior of this Pt-Pd catalyst at many sets of operating conditions, it was found that oscillatory behavior could occur, and shown in Figure 7.1 are some typical oscillations of the carbon dioxide concentration as recorded by using the IR at 2355 cm^{-1}. Shown in Figure 7.1(a) is a very long period oscillation which occurred when five grams of catalyst (diluted to twenty grams) were placed in the reactor. This oscillation was very regular as it was reproducible over a period of several hours. It was found that the period and amplitude were quite sensitive to the concentration of CO in the feed, and it was possible to obtain oscillations with periods in excess of one hour.

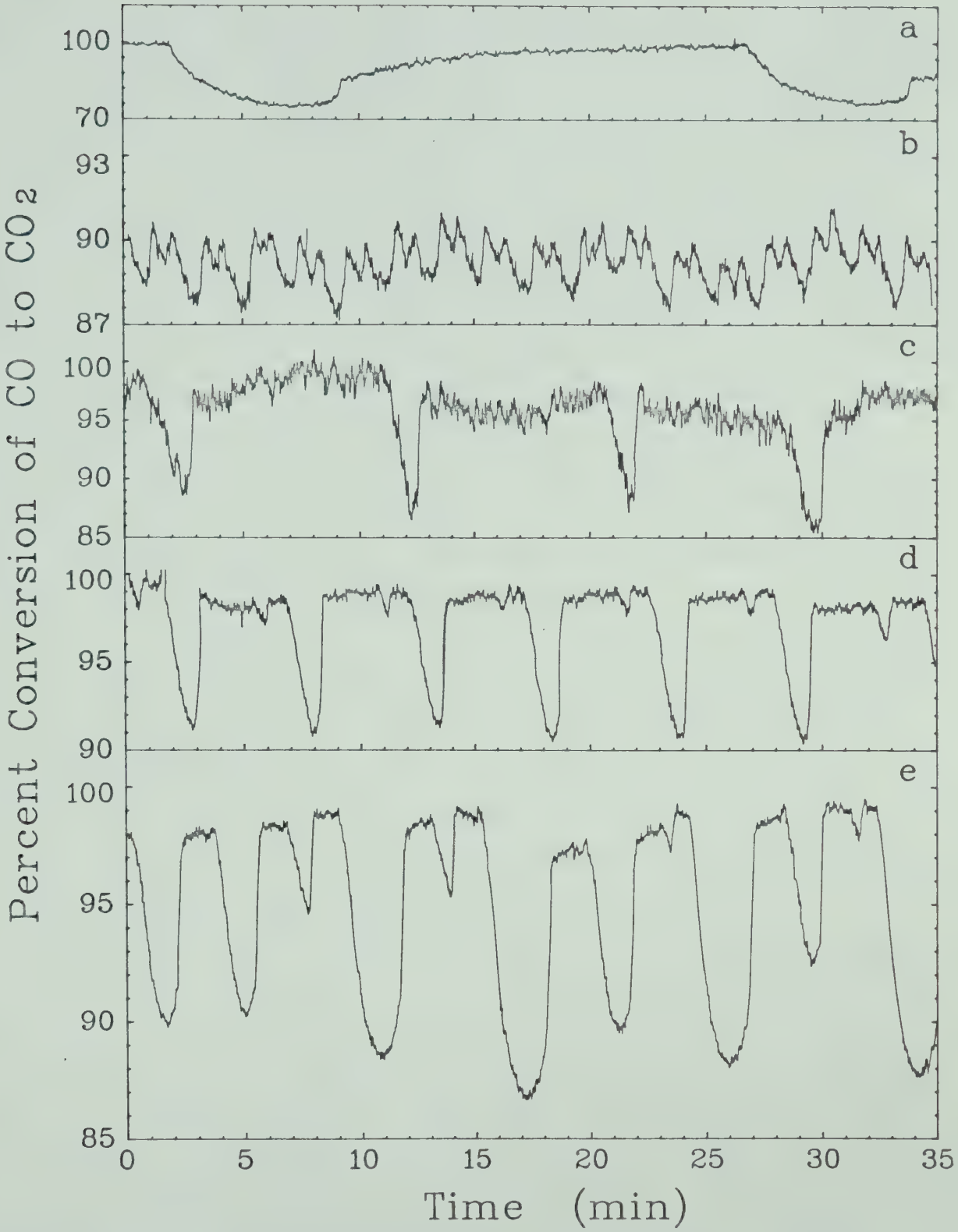

Figure 7.1 Preliminary Observations — GM Pt-Pd Catalyst
(a) T = 413 K, Q_o = 121 SCCM, 0.79% CO, 92.81% O_2, 6.40% N_2
(b) T = 413 K, Q_o = 129 SCCM, 0.61% CO, 94.46% O_2, 4.93% N_2
(c) T = 403 K, Q_o = 117 SCCM, 0.68% CO, 93.82% O_2, 5.50% N_2
(d) T = 403 K, Q_o = 116 SCCM, 0.55% CO, 95.00% O_2, 4.45% N_2
(e) T = 403 K, Q_o = 118 SCCM, 0.64% CO, 94.18% O_2, 5.18% N_2

Since studying the parametric sensitivity of an oscillatory phenomena with a period of an hour would be extremely time consuming, the operating conditions and the amount of catalyst in the reactor were varied in an attempt to obtain oscillations with shorter periods. Shown in Figures 7.1(b) and (c) are oscillations which occurred when twenty grams of the catalyst was placed in the reactor (no dilution). These oscillations were recorded using the first IR sample cell which had a low signal to noise ratio as mentioned in the previous chapter. The increase in the signal to noise ratio which was achieved through the design of the second IR sample cell is shown in Figure 7.1(d).

It is seen that what appears to be a single peak oscillation in Figure 7.1(c) could in fact have been a two peak per cycle oscillation as shown in Figure 7.1(d), as the small peaks which are readily observable using the second IR sample cell would have been completely obscured by the noisy signal which was obtained from the first IR cell.

Shown in Figure 7.1(e) is another interesting phenomena which was observed during the preliminary work with the twenty gram bed of Pt-Pd catalyst. While an oscillation was definitely occurring, it is seen that the behavior was not periodic as there was no regular cycle which repeated itself. This type of behavior was found to occur over a fairly large range of operating conditions.

Once it had been established that oscillatory behavior definitely occurred when this Pt-Pd catalyst was used, it

was decided to determine if oscillatory behavior could be observed if a different catalyst was used. To this end a number of supported platinum catalysts were prepared. These catalysts contained 0.05 weight percent platinum supported on one-eighth inch alumina spheres. Two different batches of this catalyst were prepared, and although both batches displayed oscillatory behavior, they did so under different reaction conditions due to large differences in activity between the two batches.

The first batch of 0.05% Pt/Al_2O_3 catalyst was not homogeneous as large dark spots, indicating high metal loadings, were visually apparent on many of the catalyst particles. While this catalyst displayed oscillatory behavior, as shown in Figure 7.2(a), the nonhomogeneous nature of the catalyst resulted in a very erratic conversion of CO, with a resulting high noise level in the IR signal. Also, it was suspected that local hot-spots existed on the catalyst particles during reaction conditions due to the high reaction rates in the regions of high metal loadings.

Some of these problems were alleviated when a second batch of 0.05% Pt/Al_2O_3 catalyst was prepared using a rotary drier instead of manual stirring during the evaporation step in the catalyst preparation. These catalyst particles were visually very homogeneous, and it was found that the noise level in the IR signal was much reduced when this second batch of catalyst was used instead of the first batch. Also, the second batch of catalyst had a much higher

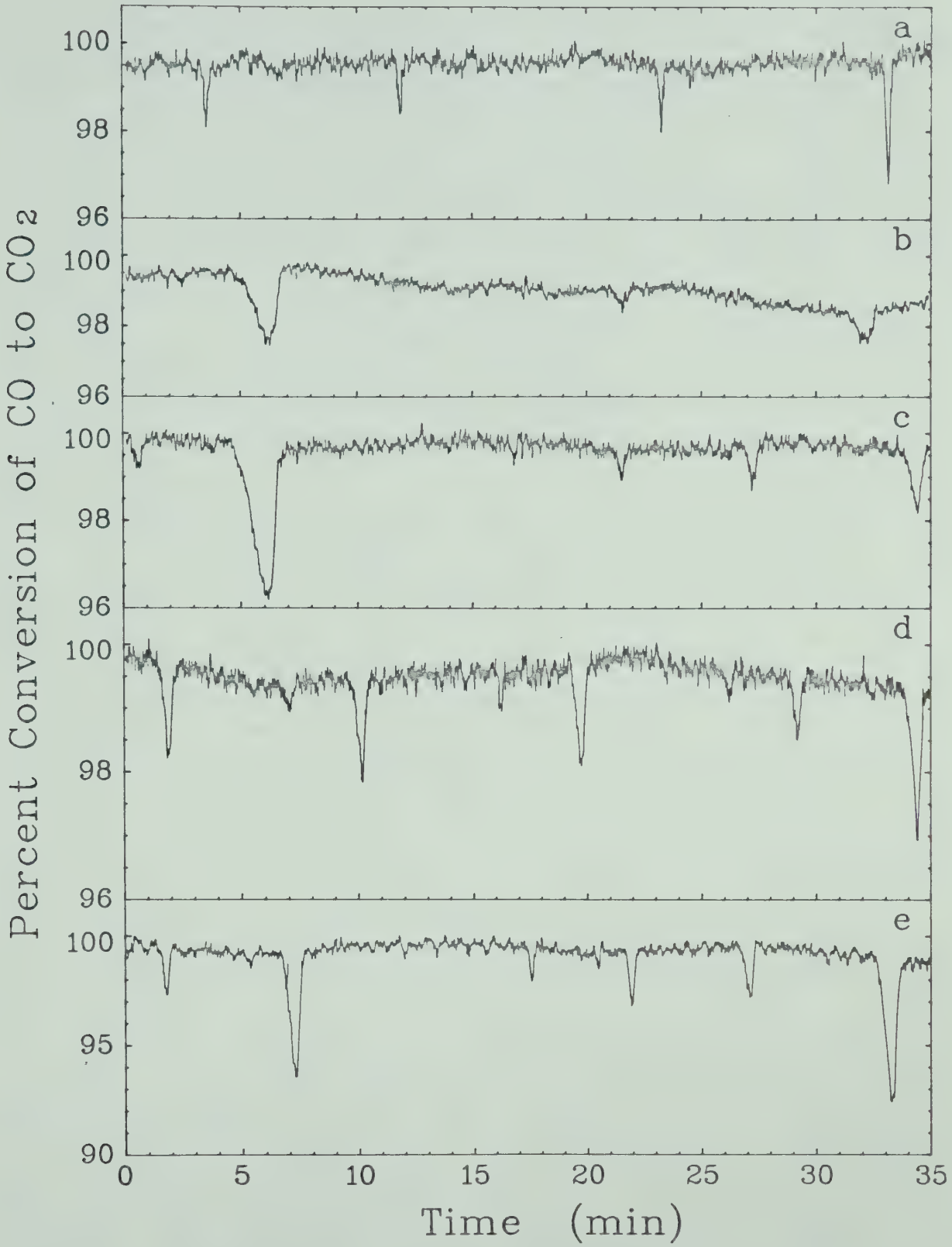

Figure 7.2 Preliminary Observations — 0.05% Pt Catalysts
(a) T = 367 K, Q_o = 257 SCCM, 1.93% CO, 82.45% O_2, 15.62% N_2
(b) T = 318 K, Q_o = 114 SCCM, 0.88% CO, 92.00% O_2, 7.12% N_2
(c) T = 329 K, Q_o = 120 SCCM, 1.38% CO, 87.45% O_2, 11.17% N_2
(d) T = 339 K, Q_o = 129 SCCM, 2.01% CO, 81.73% O_2, 16.26% N_2
(e) T = 339 K, Q_o = 333 SCCM, 0.94% CO, 91.45% O_2, 7.61% N_2

activity than either the first batch, or the Pt-Pd converter catalyst, as it displayed oscillatory behavior at very low temperatures at which the other catalysts were virtually inactive. Shown in Figures 7.2(b) to (d) are oscillations which were observed when twenty grams of the second batch of 0.05% Pt/Al_2O_3 catalyst were used in the reactor at 318 K, 329 K and 339 K, respectively. It was found that the relatively high noise level apparent in Figure 7.2(d) could be reduced by increasing the volumetric flow rate, as shown in Figure 7.2(e).

The oscillations shown in Figure 7.2 are typical of those observed for the two batches of 0.05% Pt/Al_2O_3 catalyst, as it was rare that a periodic single peak per cycle oscillation would develop. Rather, a very irregular oscillation would usually occur, and typically this oscillation would not continue for more than a few hours. Usually within a few hours (sometimes a few minutes) of the start of the oscillation, a large CO maximum (CO_2 minimun) would occur which would drive the system to a low conversion steady-state.

Thus, in the preliminary work it has been shown that oscillatory behavior can occur for several different catalysts. Of the catalysts used, the Pt-Pd converter catalyst gave the 'best' results in the sense that besides chaotic behavior, a periodic oscillation with a low noise level could be observed. The existence of a periodic, low noise, oscillation was desired so that the effects of changes in

operating conditions on the period and amplitude (or the existence) of the oscillatory behavior could be examined.

7.3 Effects of Operating Conditions

In this section are presented the results of a detailed examination of the effects of various operating conditions on the existence and behavior of oscillations observed for the oxidation of carbon monoxide carried out on the Pt-Pd converter catalyst described in the previous section. All of the observations presented in this section were obtained using twenty grams of the GM convertor catalyst, and in all cases the carbon monoxide was obtained from a specially prepared mixture of 11% carbon monoxide in nitrogen.

The oxygen which was used was normally Linde very dry grade, but this was replaced by Matheson ultra high purity oxygen on a number of occasions, and no noticable effect on the oscillatory behavior was observed. Also, it was determined that the reactor, recycle pump and associated tubing were catalytically inert by observing that no carbon dioxide was produced when carbon monoxide - oxygen mixtures were admitted to the reactor system at 425 K with the catalyst bed removed from the reactor. Unless otherwise stated, the reactor pressure was always set at one psig so that the absolute reactor pressure was very close to one standard atmosphere (compensation for Edmonton's elevation).

7.3.1 CO_2, CO and Combined Oscillations

Shown in Figures 7.3(a) and (b) are typical oscillations of CO_2 and CO, respectively, at 393 K. These oscillations were both self-starting and self-sustaining in that no external perturbations were necessary in order to have the oscillations start, and once started the oscillations continued indefinitely. The oscillations shown in Figures 7.3(a) and (b) were not recorded simultaneously since the IR spectrophotometer can only monitor one frequency at a time. The slight mismatch in the oscillations is due to the sequential nature of the recordings.

The oscillation in carbon dioxide concentration shown in Figure 7.3(a) can be broken down into three regions which continually repeat themselves, namely, a slow increase to a maximum, a more rapid decrease to a minimum, and a fast (virtually instantaneous) increase to a local maximum with a small amount of overshoot. These three regions had counterparts in the carbon monoxide oscillations shown in Figure 7.3(b) which were; a region of virtually zero CO concentration, a slow rise to a maximum, and a rapid decrease to zero concentration, respectively.

Shown in Figure 7.3(c) are the oscillations which resulted from passing the effluent from the main reactor through the auxiliary reactor such that all the carbon monoxide was totally converted to carbon dioxide. The approximately straight tracing in the rightmost part of Figure 7.3(c) is the result of bypassing the feed stream

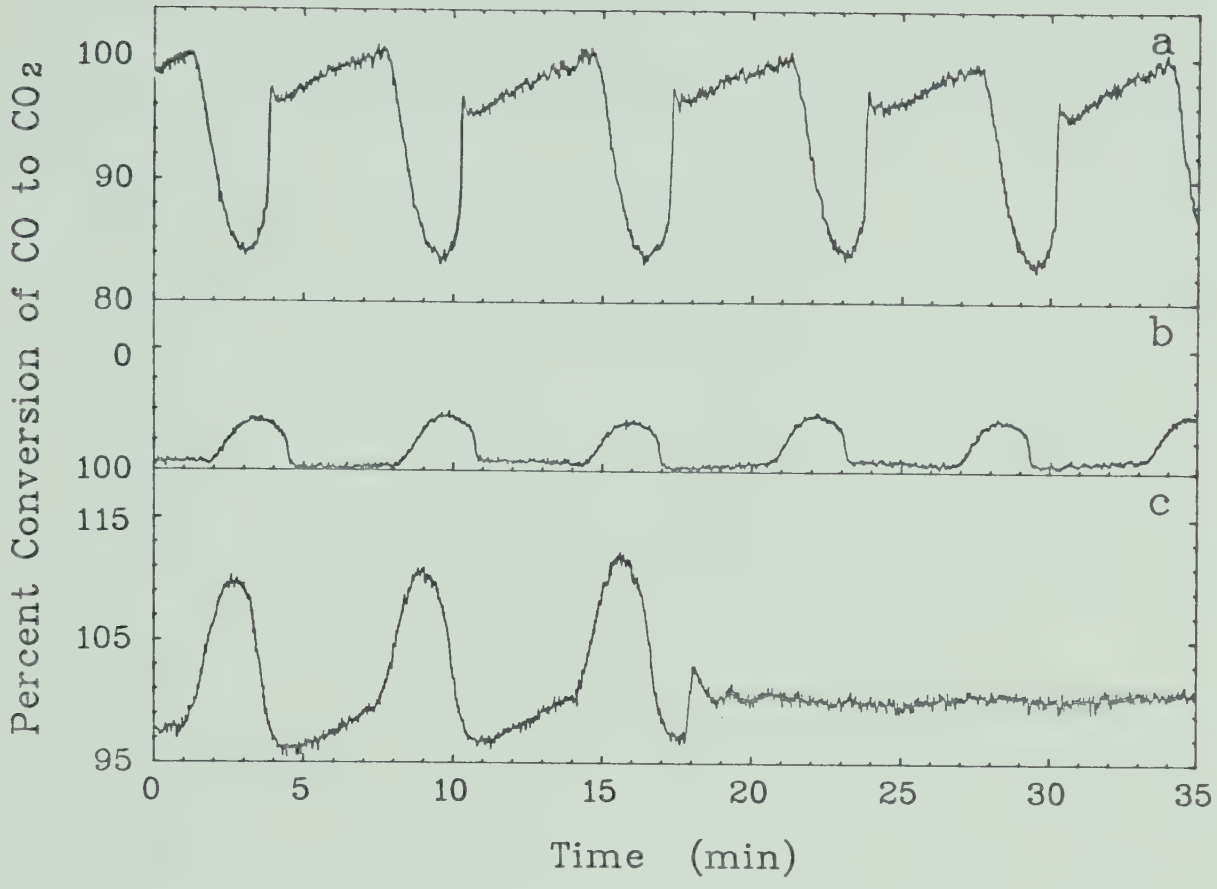

Figure 7.3 Simple Oscillatory Behavior
(a) Periodic Carbon Dioxide Oscillations
(b) Corresponding Carbon Monoxide Oscillations
(c) Effluent From Auxiliary Reactor
($T = 393$ K, $Q_0 = 154$ SCCM, 0.32% CO, 97.09% O_2, 2.59% N_2)

around the reactor such that it passed directly through the auxiliary reactor, thus this tracing represents the 100% conversion line. From a comparison of Figures 7.3(a) to (c) it is seen that there is no phase lead or lag between the CO and CO_2 concentration oscillations, as the oscillations in Figure 7.3(c) appear to be a direct combination of those in Figures 7.3(a) and (b) once the differences in IR sensitivity to CO and CO_2 are taken into account. If there was any phase lead or lag between the CO and CO_2 oscillations, it would show up in the form of local maxima, minima, and/or extra points of inflection in Figure 7.3(c). This absence of phase differences between the CO and CO_2 oscillations can be used as an indication that the oscillations are occurring in the absence of mass transport limitations.

A detailed examination of the dynamic behavior of CO_2, CO, and CO_2 plus CO shown in Figure 7.3 yields valuable insight into the phenomena occurring during oscillations. The oscillation at about 11 to 17 min in Figure 7.3 will be used as an illustration. (It should be kept in mind that the slight mismatch in oscillations between parts (a), (b) and (c) of the figure are due to the previously mentioned sequential recording of the outputs.) Observations for the above oscillation, which are similar to those for other oscillations, are summarized in Table 7.1.

The observations in Table 7.1 are explained by the following sequence of events: In Region 1, CO accumulates on the catalyst surface and a gradual increase in CO_2 rate of

Table 7.1 Description of Oscillation Shown in Figure 7.3

Region	Time (min)	Behavior of Bulk CO_2, CO and CO plus CO_2 Concentrations
1	11 to 14.5	(a). gradual increase in CO_2 conc. (b). no CO in product (c). combined CO plus CO_2 in product less than CO in feed
2	14.5 to 16.5	(a). fairly rapid increase in CO_2 conc. (b). fairly rapid increase in CO conc. (c). combined CO plus CO_2 in product exceeds amount of CO in feed
3	16.5 to 17	(a). very rapid increase in CO_2 conc. (b). very rapid decrease in CO conc. to zero (c). combined CO plus CO_2 in product decreases from greater than to less than amount of CO in feed

formation occurs; in Region 2, desorption of CO and decreased rates of CO_2 formation take place; and in Region 3, rapid accumulation of CO on the surface of the catalyst and rapid increase in CO_2 production occurs. Significant oscillation in the temperature of the metal crystallites appear to be the only reasonable explanation for these phenomena. The increase in CO accumulation and CO_2 formation in Region 1 results in an increase in surface (or metal crystallite) temperature. This increase has to be very rapid at the end of Region 1, which results in the CO desorption in Region 2. The cooling effects of CO desorption tend to balance the heating effects of CO reaction until the surface is completely depleted of CO. Once the

surface is depleted, the temperature drops rapidly with subsequent rapid adsorption of CO and increased CO_2 production in Region 3. The mechanism by which communication between different metal crystallites in the catalyst pellets occurs is not clear. Changes in bulk CO concentration and/or slight variations in bulk phase temperatures may be responsible.

7.3.2 Recycle Ratio

Shown in Figure 7.4 are the effects of recycle ratio on a carbon dioxide oscillation. It is seen in Figure 7.4(a) that if the reactor is operated as an integral bed reactor (no recycle) that oscillatory behavior can occur. Upon close examination the oscillations from the integral bed reactor are seen to be not simple in nature, but rather each cycle is composed of two distinct peaks. This observation is reinforced in Figure 7.4(b) where it is seen that the positive feedback effect which results from increasing the recycle ratio from 0:1 to 3:1 has resulted in the doublet nature of the oscillation becoming emphasized. However, as the recycle ratio is further increased in Figures 7.4(c) to (f), it is seen that a new form of oscillation similar to that shown in Figure 7.3 emerges. The oscillation shown in Figure 7.4(f) did not change upon further increases in the recycle ratio and hence this oscillation represents that which occurs in a well mixed reactor in the absence of transport limitations.

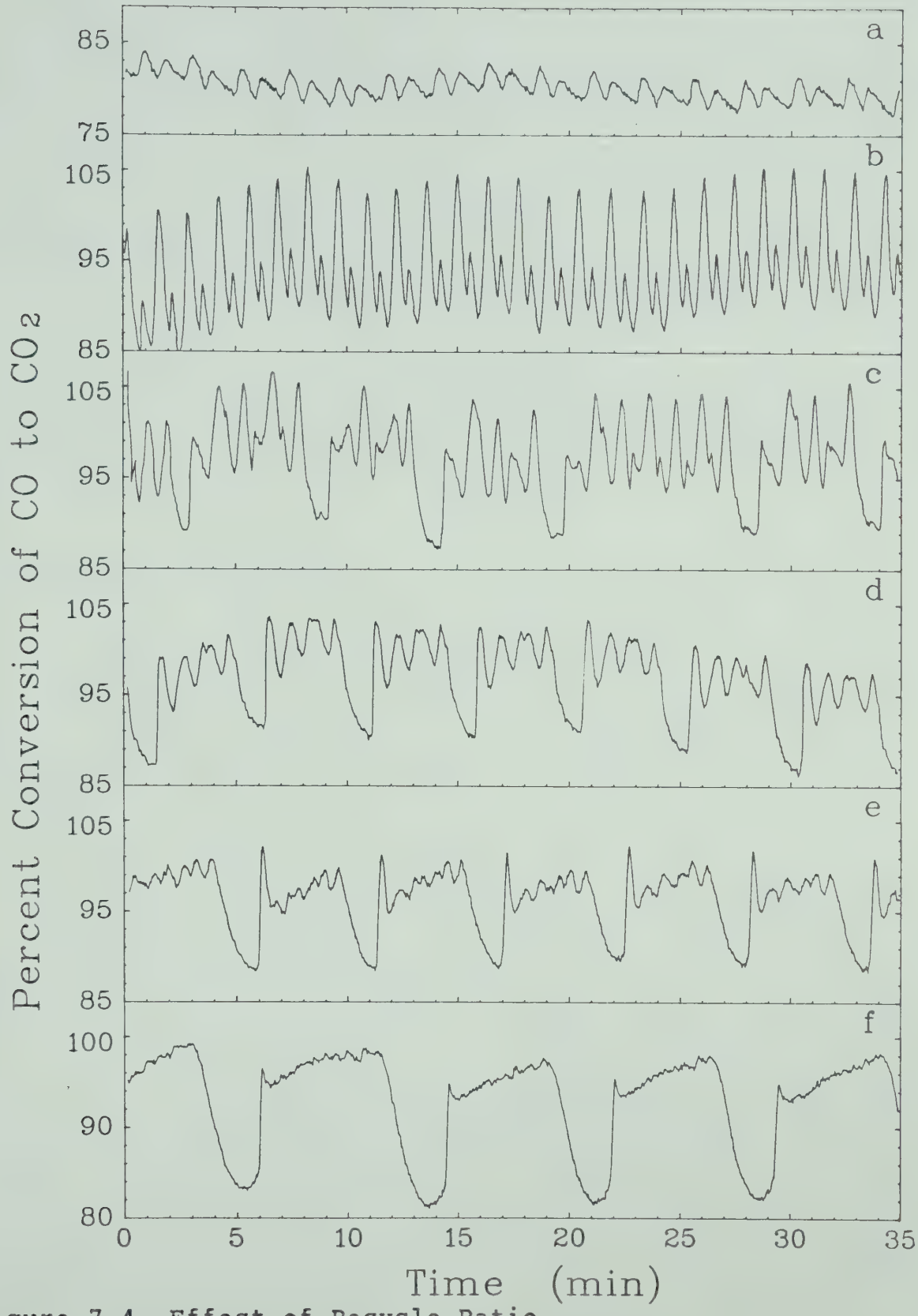

Figure 7.4 Effect of Recycle Ratio
(a) No Recycle (b) Recycle Ratio = 3.0
(c) Recycle Ratio = 3.7 (d) Recycle Ratio = 5.1
(e) Recycle Ratio = 6.9 (f) Recycle Ratio = 30
(T = 393 K, Q_o = 143 SCCM, 0.29% CO, 97.36% O_2, 2.35% N_2)

It is believed that the oscillations shown in Figure 7.4(a) were caused by transport resistances between the bulk phase and the catalyst surface, whereas the oscillations in Figure 7.4(f) occurred in the absence of transport resistances, and thus were possibly related to the underlying mechanism of the reaction. Since it was desired to examine oscillations in the absence of heat and mass transfer limitations, the recycle pump was always run at 1800 RPM which corresponded to a recycle ratio of between 100:1 and 200:1.

7.3.3 Bulk Temperature

Shown in Figure 7.5 are the effects of bulk temperature on the oxidation of carbon monoxide. It is seen that as the bulk temperature was increased, the system moved from an intermediate conversion steady-state shown in Figure 7.5(a), to a periodic single peak per cycle oscillation as shown in Figure 7.5(b). Upon further increases in the bulk temperature it is seen in Figure 7.5(c) that the frequency and amplitude of the oscillations decreased, and that the oscillations were no longer periodic, as shown in Figures 7.5(d) and (e). As the bulk temperature was further increased, the frequency and amplitude of the oscillations became very small as shown in Figure 7.5(f), and finally the system passed to a high conversion steady-state as seen in Figure 7.5(g).

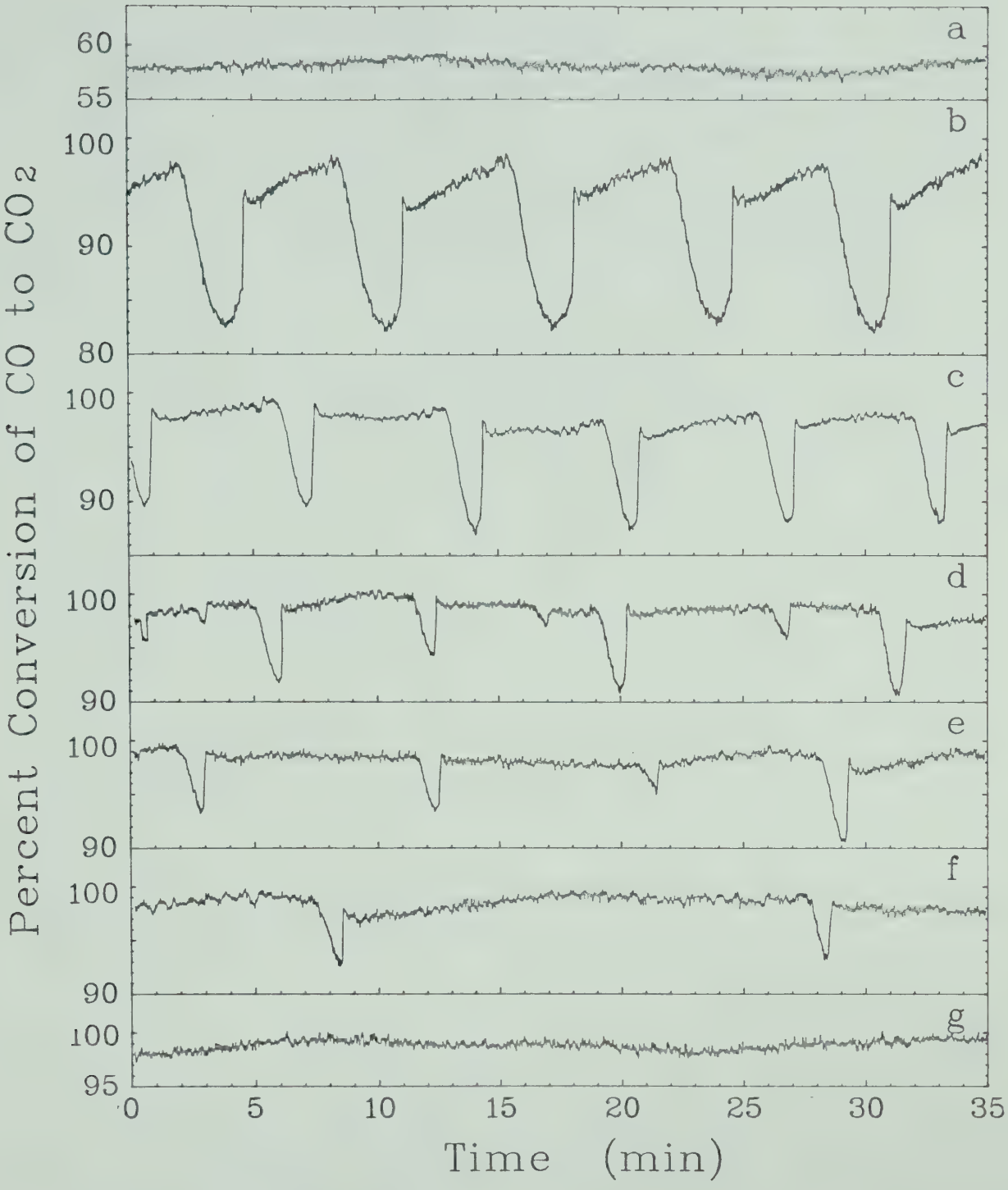

Figure 7.5 Effect of Bulk Temperature
(a) T = 388 K (b) T = 393 K (c) T = 398 K (d) T = 403 K
(e) T = 408 K (f) T = 413 K (g) T = 423 K
(Q_o = 149 SCCM, 0.33% CO, 97.00% O_2, 2.67% N_2)

7.3.4 Concentration of CO in the Feed

Shown in Figure 7.6 are the effects of varying the concentration of carbon monoxide in the feed to the reactor. It is seen that decreases in the feed concentration of CO resulted in the system behaving quite similarily to that shown in Figure 7.5 for increases in the bulk temperature. In particular, as the feed CO was decreased, the system passed from an intermediate conversion steady-state to a periodic single peak per cycle oscillation. Upon further decreases in the feed CO concentration, it is seen that the frequency and amplitude of the oscillations decreased, and ultimately the system passed to a high conversion steady-state at a very low concentration of CO in the feed stream.

It is interesting to note that there was also a qualitative change in the shape of the oscillations as the feed CO concentration was lowered (or the bulk temperature increased), as the slow increase to a maximum after the rapid increase in CO_2 concentration which is clearly shown in Figure 7.6(b) is virtually eliminated in Figures 7.6(d) and (e). It is believed that this slow increase in the CO_2 concentration is the result of a surface capacitance effect. Hence, it would be expected that this effect would be more prominant at high concentrations of CO in the feed, as this should correspond to high surface concentrations of carbon monoxide. Similarily, low bulk temperatures should imply large CO surface concentrations.

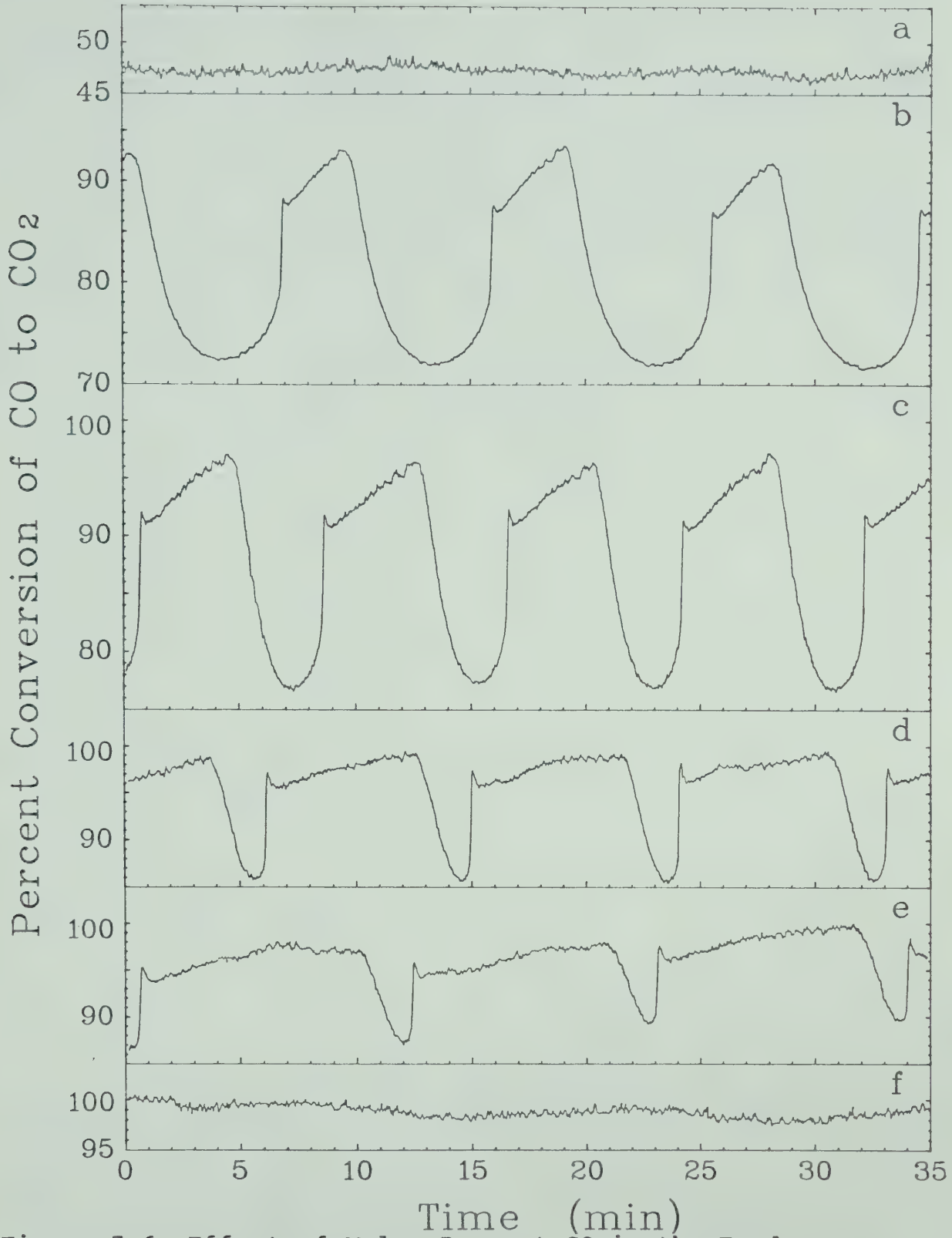

Figure 7.6 Effect of Molar Percent CO in the Feed
(a) T = 393 K, Q_o = 146 SCCM, 0.78% CO, 92.91% O_2, 6.31% N_2
(b) T = 393 K, Q_o = 146 SCCM, 0.76% CO, 93.09% O_2, 6.15% N_2
(c) T = 393 K, Q_o = 146 SCCM, 0.69% CO, 93.73% O_2, 5.58% N_2
(d) T = 393 K, Q_o = 146 SCCM, 0.53% CO, 95.18% O_2, 4.29% N_2
(e) T = 393 K, Q_o = 146 SCCM, 0.42% CO, 96.18% O_2, 3.40% N_2
(f) T = 393 K, Q_o = 146 SCCM, 0.11% CO, 99.00% O_2, 0.89% N_2

7.3.5 Volumetric Feed Rate - CO/O_2 Constant

Shown in Figure 7.7 are the effects of changes in the volumetric feed rate on the behavior of the system. In examining these effects the bulk temperature and the ratio of CO to O_2 were held constant. It is seen that decreases in the volumetric feed rate resulted in qualitatively identical behavior to that shown in the preceeding section for decreases in the feed CO concentration. As shown in Figure 7.7, the system passed from an intermediate conversion steady-state to a large amplitude periodic oscillation when the volumetric feed rate was decreased. Upon further decreases in the volumetric feed rate, the frequency and amplitude of the oscillations decreased, and it is believed that ultimately a high conversion steady-state would have been reached. This was not attempted as it would have necessitated going to very low feed rates with a resulting large increase in the noise in the IR signal due to poor mixing in the IR sample cell.

7.3.6 Volumetric Feed Rate - Molar CO Flow Constant

In Figure 7.8 are shown the effects of variations in volumetric feed rate to the reactor with the molar flow of carbon monoxide held constant. It is seen that as the volumetric feed rate was increased that the system passed from an intermediate conversion steady-state to a periodic single peak per cycle oscillation. However, as the feed rate was further increased, a comparison of Figures 7.8(b) and (c)

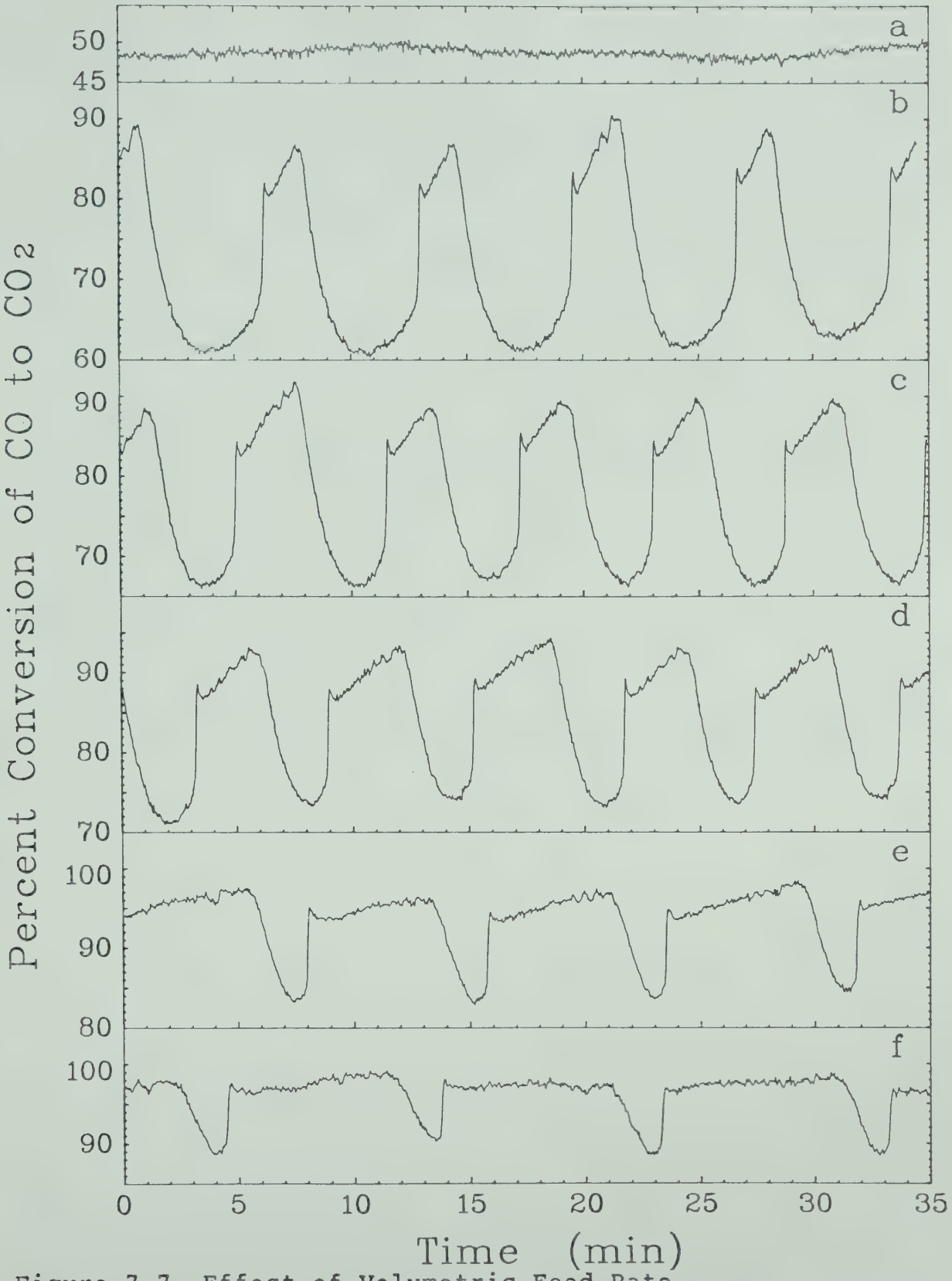

Figure 7.7 Effect of Volumetric Feed Rate
(Constant CO/O_2 in the Feed)
(a) Q_o = 322 SCCM (b) Q_o = 267 SCCM (c) Q_o = 222 SCCM
(d) Q_o = 189 SCCM (e) Q_o = 131 SCCM (f) Q_o = 105 SCCM
(T = 393 K, 0.23% CO, 97.91% O_2, 1.86% N_2)

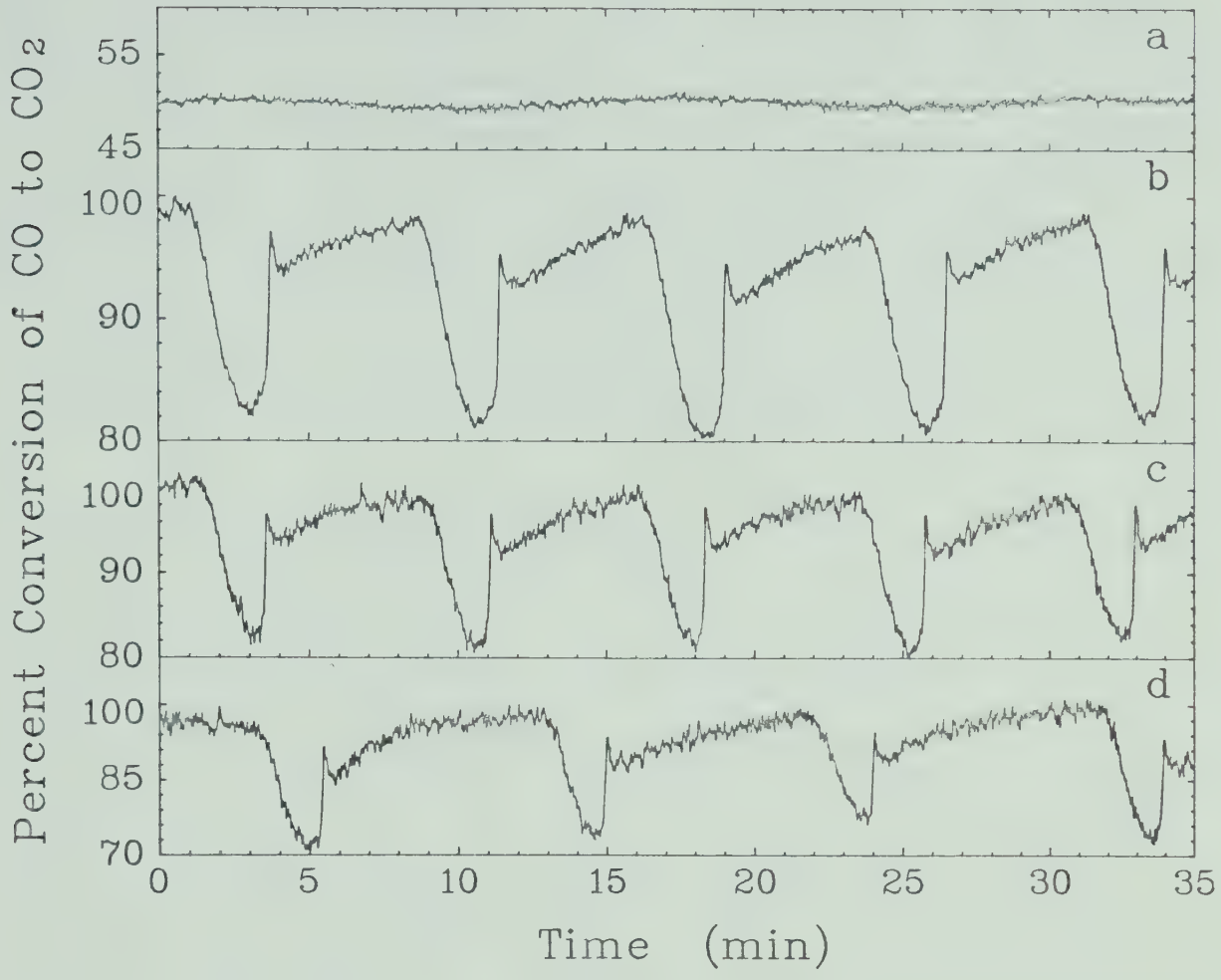

Figure 7.8 Effect of Volumetric Feed Rate
(Constant CO Molar Flow in the Feed)
(a) T = 393 K, Q_o = 115 SCCM, 0.41% CO, 96.27% O_2, 3.32% N_2
(b) T = 393 K, Q_o = 250 SCCM, 0.19% CO, 98.27% O_2, 1.54% N_2
(c) T = 393 K, Q_o = 400 SCCM, 0.12% CO, 98.91% O_2, 0.97% N_2
(d) T = 393 K, Q_o = 600 SCCM, 0.08% CO, 99.27% O_2, 0.65% N_2

shows that the frequency and amplitude of the oscillations were virtually unchanged. A further increase in the volumetric feed rate resulted in a decrease in the frequency and an increase in the amplitude (using the conversion scale) of the oscillations as seen in Figure 7.8(d). Further increases in the volumetric feed rate were not made, as further dilution of the carbon monoxide and carbon dioxide resulted in very weak, noisy, signals from the IR.

7.3.7 Nitrogen and Helium Diluents

Shown in Figure 7.9 are the effects on the carbon monoxide oscillations due to the partial replacement of oxygen with nitrogen and helium. The oscillations preceeding point A in Figure 7.9 were typical of those which occurred when the reactor feed was composed of carbon monoxide and oxygen (with a small amount of nitrogen from the CO/N_2 mixture). At point A, nitrogen was used to replace approximately 25% of the oxygen in the feed and it is seen that this had a definite effect on the oscillations. A comparison of the oscillations before and after the introduction of the nitrogen shows that the widths of the oscillatory maxima were increased due to an elongation of the regions between the maxima and the abrupt transitions to 100% conversion.

At point B in Figure 7.9, the nitrogen which was introduced at point A, was replaced by an equal flow of helium. It is seen that replacing the nitrogen with helium had only

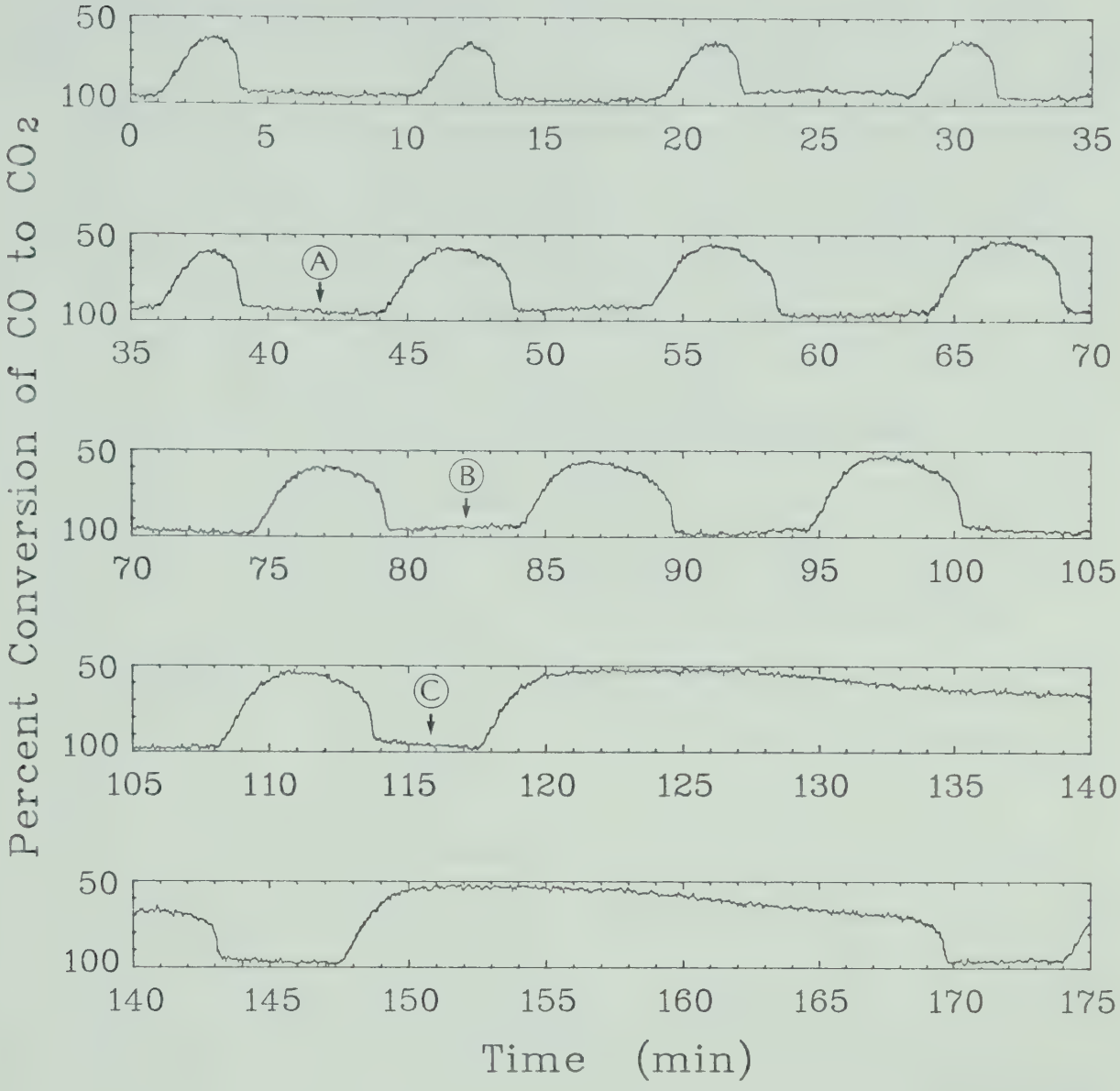

Figure 7.9 Effect of Nitrogen and Helium Diluents on CO Oscillations (T = 393 K, Q_0 = 155 SCCM)
Before A — 0.33% CO, 97.00% O_2, 2.67% N_2
After A — 0.33% CO, 70.15% O_2, 29.53% N_2
After B — 0.33% CO, 70.15% O_2, 2.67% N_2, 26.85% He
After C — 0.33% CO, 50.09% O_2, 2.67% N_2, 46.89% He

a minor effect on the carbon monoxide oscillations, as the small differences before and after point B can be attributed to inaccuracies in the flow system by which nitrogen and helium were used to replace oxygen. Thus, it appears that the changes in the oscillations which result from replacing oxygen with nitrogen or helium are solely due to a dilution effect, as equal dilutions with nitrogen and helium had equal effects on the carbon monoxide oscillations.

These observations seem to rule out heat transfer from the metal crystallites to the gas phase being important to the existence of oscillatory behavior, as otherwise the large difference in thermal conductivity between nitrogen and helium would be expected to have a more pronounced effect than was observed.

At point C in Figure 7.9, a further 25% of the oxygen feed was replaced with helium, and it is seen that this had a very dramatic effect on the oscillations, as the regions between the maxima and the abrupt transitions to 100% conversion became very elongated. It is worth noting that these were the only parts of the oscillations which are seriously affected by the replacement of oxygen with helium, as the abrupt transitions to 100% conversion, the flat region at 100% conversion, and the slow rise to a maximun were all only slightly changed from those originally (0 - 40 minutes in Figure 7.9) observed. This seems to indicate that the oxygen concentration is only of importance during that one part of the oscillatory cycle, and that other

factors (surface temperature, CO concentration, etc.) are important during the other parts of the cycle.

7.3.8 Reactor Pressure

As described in the previous chapter, the reactor pressure could be varied by changing the external set point pressure applied to the reactor pressure controller. Shown in Figure 7.10 are the effects of varying the reactor pressure from 1 to 16 psig (1 to 2 atmospheres absolute). It is seen that the amplitude of the oscillations continually decreased as the pressure was increased, but that the frequency of the oscillations passed through a minimum.

This type of effect in which the frequency passed through a minimum when an operating parameter was changed had not been previously encountered, and hence these observations were carefully checked and they were found to be reproducible. As the pressure is increased, it appears that competing processes occur which affect the surface concentrations of oxygen and carbon monoxide due to changes in the bulk phase concentrations. However, the manner in which these processes produce the effects shown in Figure 7.10 is not presently understood.

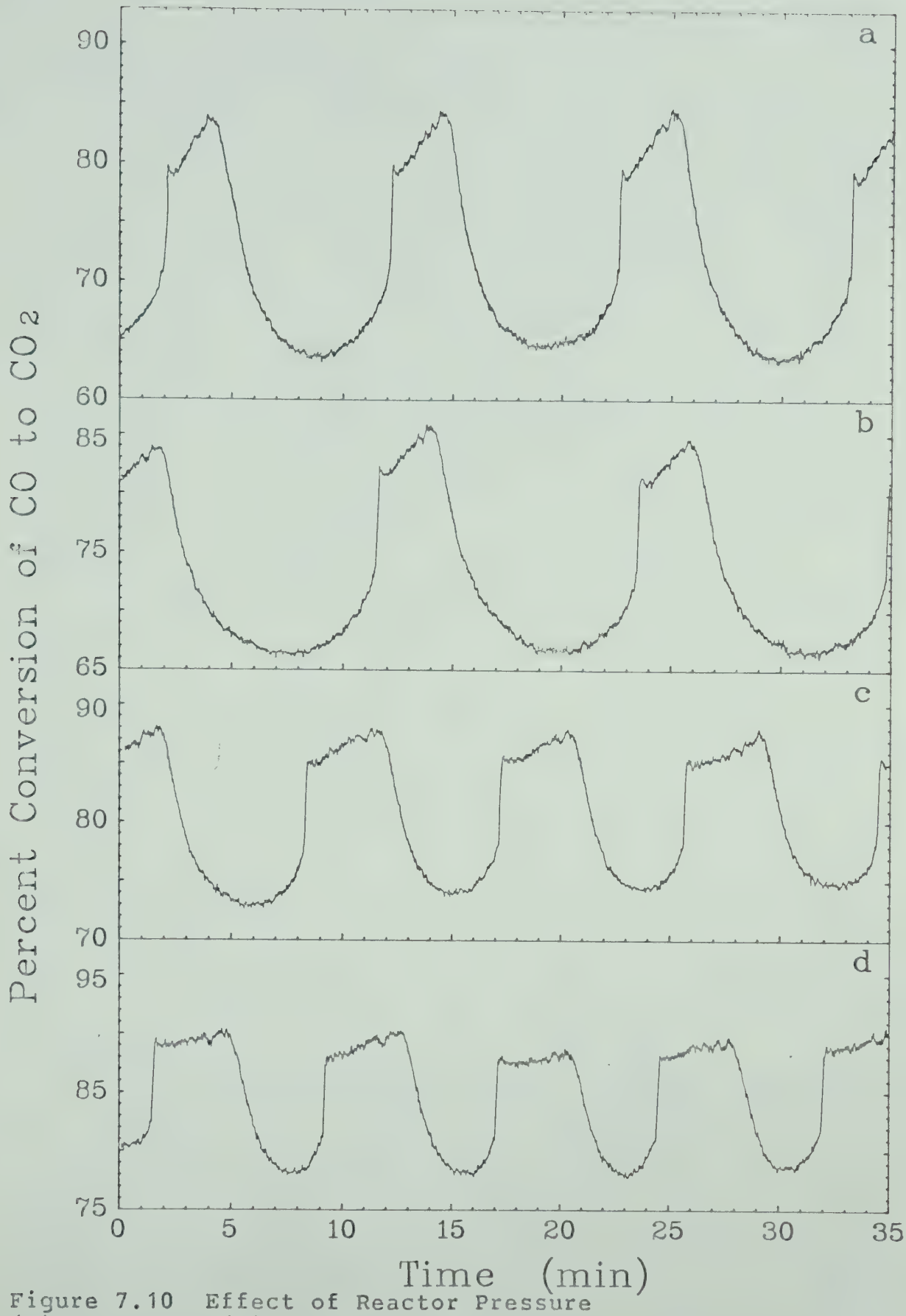

Figure 7.10 Effect of Reactor Pressure
(a) 1 PSIG (b) 6 PSIG (c) 11 PSIG (d) 16 PSIG
(T = 393 K, Q_o = 151 SCCM, 0.34% CO, 96.91% O_2, 2.75% N_2)

7.4 Qualitative Effects of Temperature

In most of the preceeding sections, the reaction temperature was held constant at 393 K to facilitate comparions between the effects of the various operating conditions which were varied. However, it has been found that interesting changes occurred in the oscillatory behavior when it was examined at temperatures other than 393 K. Some of these qualitative changes which occurred when the bulk temperature was varied are shown in Figure 7.11, where it is seen that two qualitatively different types of oscillations could occur depending on the reaction temperature.

It is believed that different mechanisms are responsible for the different types of oscillations shown in Figure 7.11(a) (373 K) and 7.11(e) (423 K). However, the mechanisms are obviously not mutually exclusive as shown by the coexistence of both types of oscillations in Figure 7.11(d) (413 K). As was stated when the effect of the recycle ratio was examined, it is believed that the small fast oscillations are the result of transport resistances, while the large relaxation oscillations are probably related to the underlying mechanism of the reaction.

Further evidence that transport resistances are significant at 423 K can be inferred from the steady-state behavior of the reaction. At temperatures less than 413 K no high conversion steady-state was ever observed which was significantly different from 100% conversion, i.e. no points could ever be obtained on the reaction rate curve in the

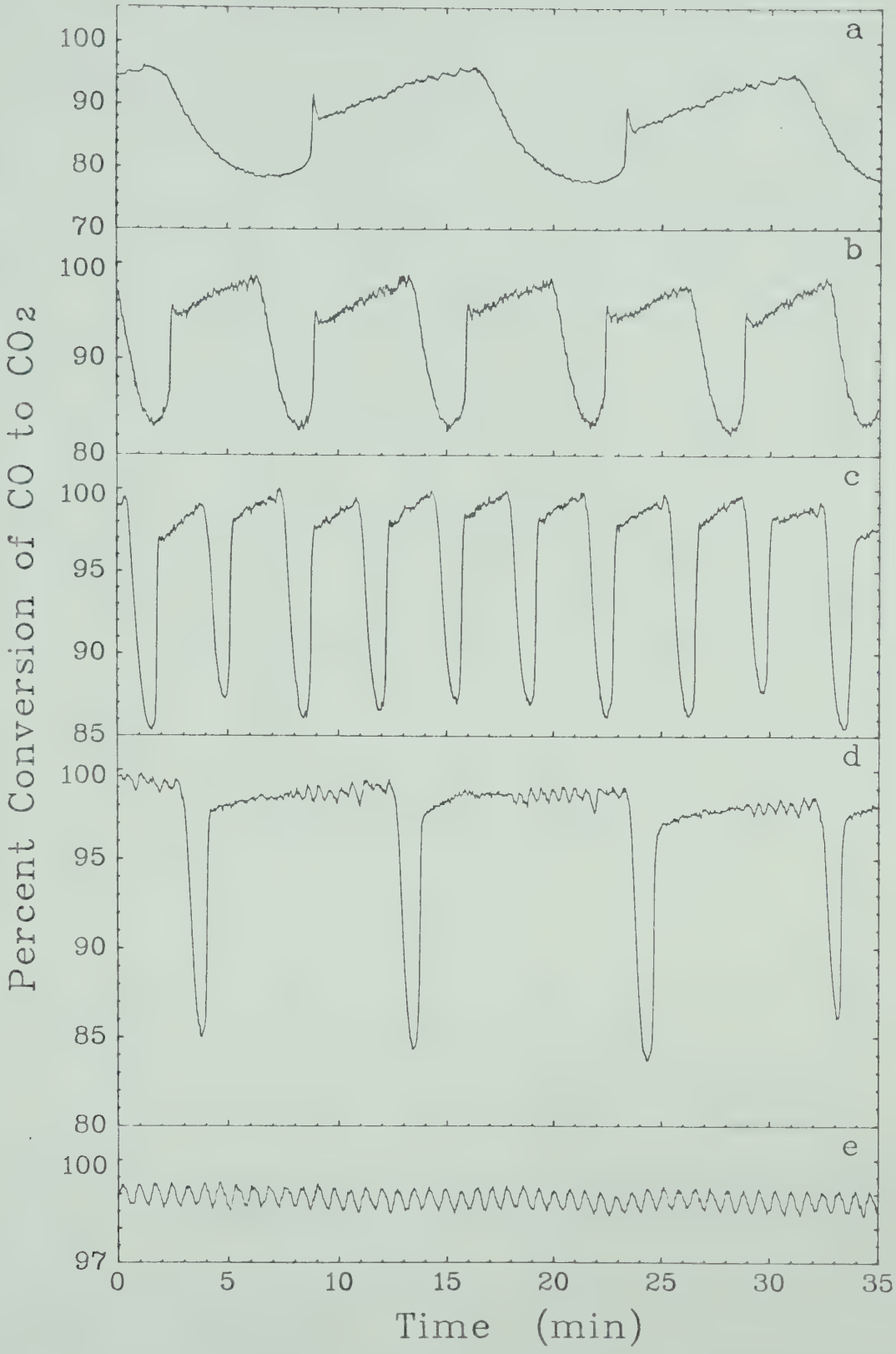

Figure 7.11 Qualitative Effects of Temperature
(a) T = 373 K, Q_o = 227 SCCM, 0.087% CO, 99.18% O_2, 0.73% N_2
(b) T = 393 K, Q_o = 154 SCCM, 0.32% CO, 97.09% O_2, 2.59% N_2
(c) T = 413 K, Q_o = 157 SCCM, 0.71% CO, 93.55% O_2, 5.74% N_2
(d) T = 423 K, Q_o = 164 SCCM, 1.09% CO, 90.08% O_2, 8.83% N_2
(e) T = 433 K, Q_o = 171 SCCM, 1.46% CO, 86.73% O_2, 11.81% N_2

region where the reaction rate increased with increasing carbon monoxide concentration, as the CO concentration was never significantly different from zero when the system was at a high conversion steady-state. Thus at temperatures less than 413 K the reaction rate was not limited by any transport constraints, and the reaction rate controlling step was one of the kinetic steps in the reaction.

However, at temperatures above 413 K high conversion steady-states at less than 100% conversion could be obtained, as at these steady-states it was possible to measure finite amounts of carbon monoxide in the reactor effluent. Since these high conversion steady-states were normally obtained under conditions of high CO concentration in the feed stream, it was suspected that what was being measured was a transport resistance curve, and not a reaction rate curve.

7.5 Chaos and Nitrogen Dilution at 423 K

In the preceeding section it was shown that as the temperature increased the large relaxation oscillations disappeared and only the transport related oscillations remained. Since increased rate of reaction is the main result of increased temperature, it was suspected that the relaxation oscillations could be observed at high temperatures if the reaction rate was somehow decreased. This decrease in the reaction rate was most easily accomplished

by replacing oxygen with nitrogen in the reaction gas mixture at 423 K, and the effects of this at various nitrogen to oxygen ratios are shown in Figure 7.12.

It is seen, as the nitrogen to oxygen ratio was increased, that the occurrence of relaxation oscillations could be initiated. Further increases in the nitrogen to oxygen ratio resulted in the frequency and amplitude of the relaxation oscillations increasing until they completely obscured the transport related oscillations. Also, it is seen that the oscillatory behavior was not regular and periodic, as in the preceeding sections, but rather was very irregular, and perhaps should be called chaotic.

As shown in Chapter 5, when two nonlinear oscillators are operating simultaneously, interesting phenomena such as chaos can occur. Thus, the chaotic behavior which was observed for this catalytic system is attributed to the interaction of the mechanistic and the transport related oscillations.

7.6 Reproducibility of Oscillations

Changes in the catalyst activity can be a major problem when examining catalytic reactions, for if the activity changes then experimental observations are not reproducible and very little information can be obtained about the true mechanism of the reaction. Fortunately, in this study, it was found that the catalyst activity was very constant.

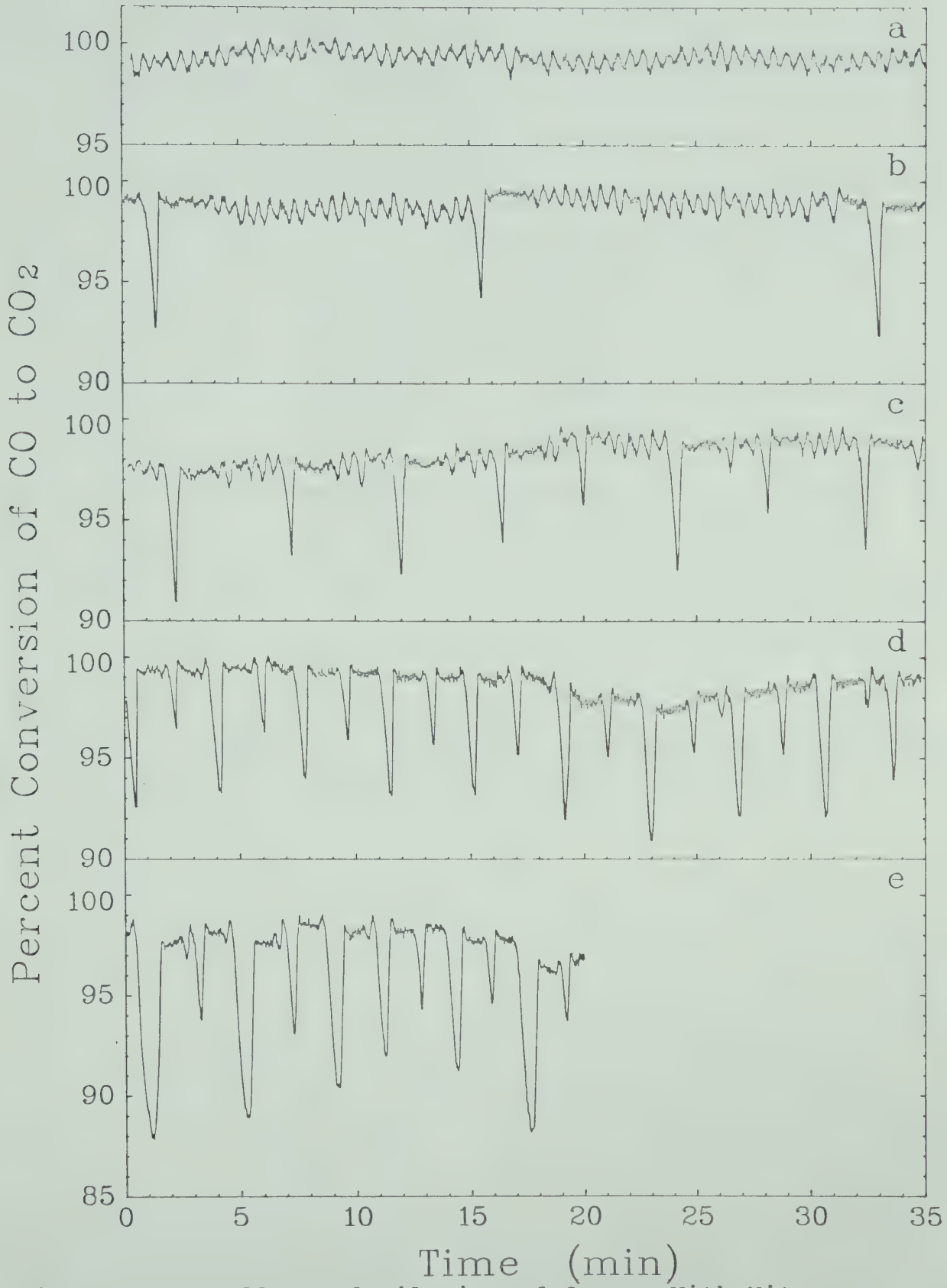

Figure 7.12 Effect of Dilution of Oxygen With Nitrogen
(a) N_2/O_2 = 0.06 (b) N_2/O_2 = 1.3 (c) N_2/O_2 = 1.9
(d) N_2/O_2 = 2.8 (e) N_2/O_2 = 3.6
(T = 433 K, Q_o = 170 SCCM, 0.66% CO)

This is shown in Figure 7.13, where it is seen that the oscillatory behavior was very reproducible over a period of approximately 250 hours of use of the catalyst.

In Figure 7.13, the oscillations shown in the (a) section were obtained at the beginning of the preceeding investigation of the effects of operating conditions on oscillatory behavior, and the oscillations in the (b) and (c) sections were obtained in the middle (after ~150 hours of operation), and at the end (after ~250 hours of operation) of this investigation, respectively. While these oscillations were very reproducible, it was found that changes in catalyst activity could occur under certain types of reaction conditions. Fortunately these particular reaction conditions were not encountered during the investigation of the effects of operating conditions, but rather were encountered while performing subsequent work at higher temperatures.

These changes in activity are well illustrated in Figure 7.14 where the effect of severe reaction conditions at 473 K on the catalyst activity were investigated. It is seen that interesting transient phenomena occurred after each increase in the CO feed concentration at points A, B and C, and it appears that a sustained oscillation was occurring between points C and D. At point D the feed CO concentration was further increased, and as can be seen, an abrupt transition to a low conversion steady-state occurred. After the system moved to the low conversion steady-state,

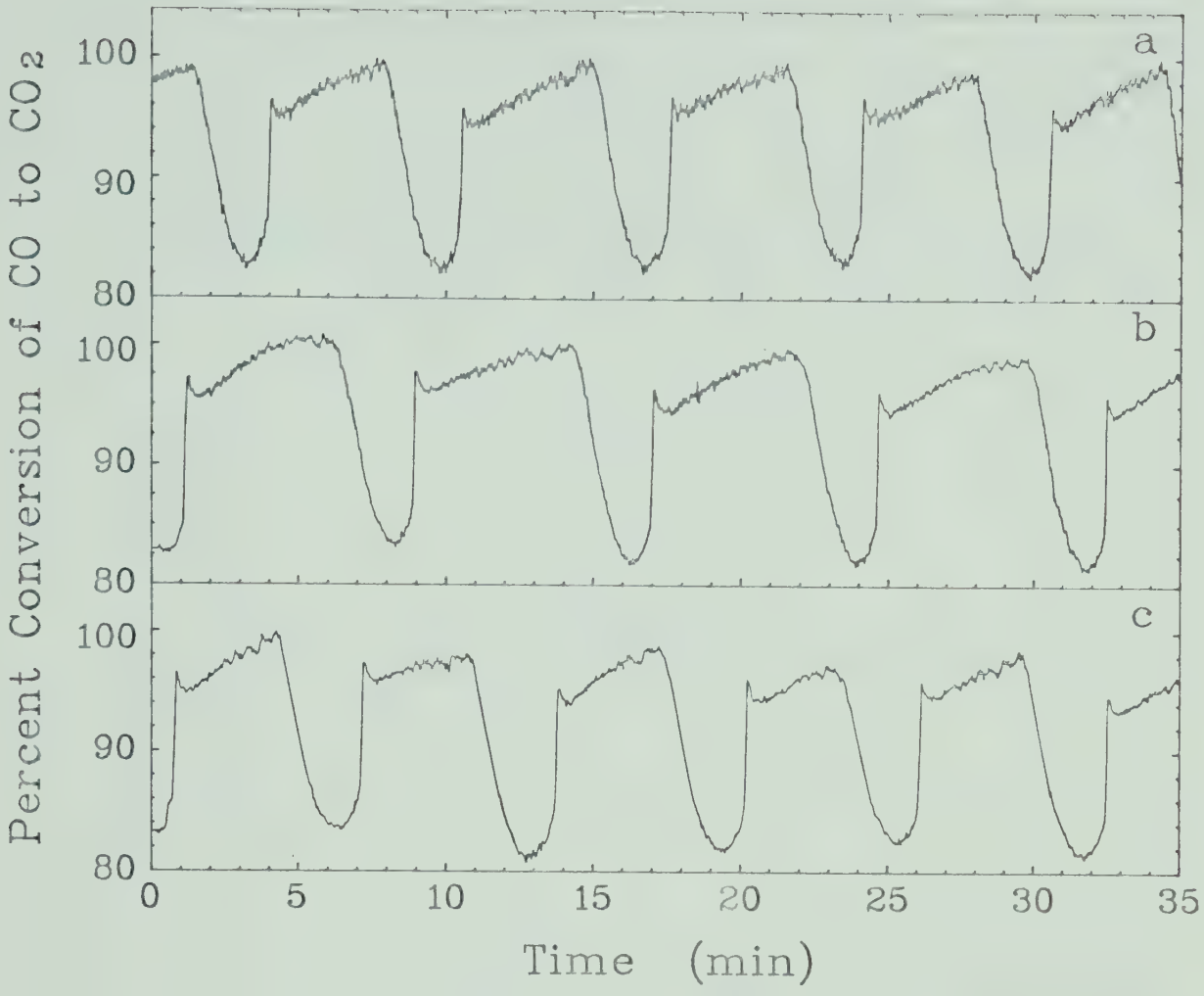

Figure 7.13 Reproducibility of the Oscillatory Behavior
(a) T = 393 K, Q_o = 154 SCCM, 0.32% CO, 97.09% O_2, 2.59% N_2
(b) T = 393 K, Q_o = 154 SCCM, 0.30% CO, 97.27% O_2, 2.43% N_2
(c) T = 393 K, Q_o = 151 SCCM, 0.30% CO, 97.27% O_2, 2.43% N_2

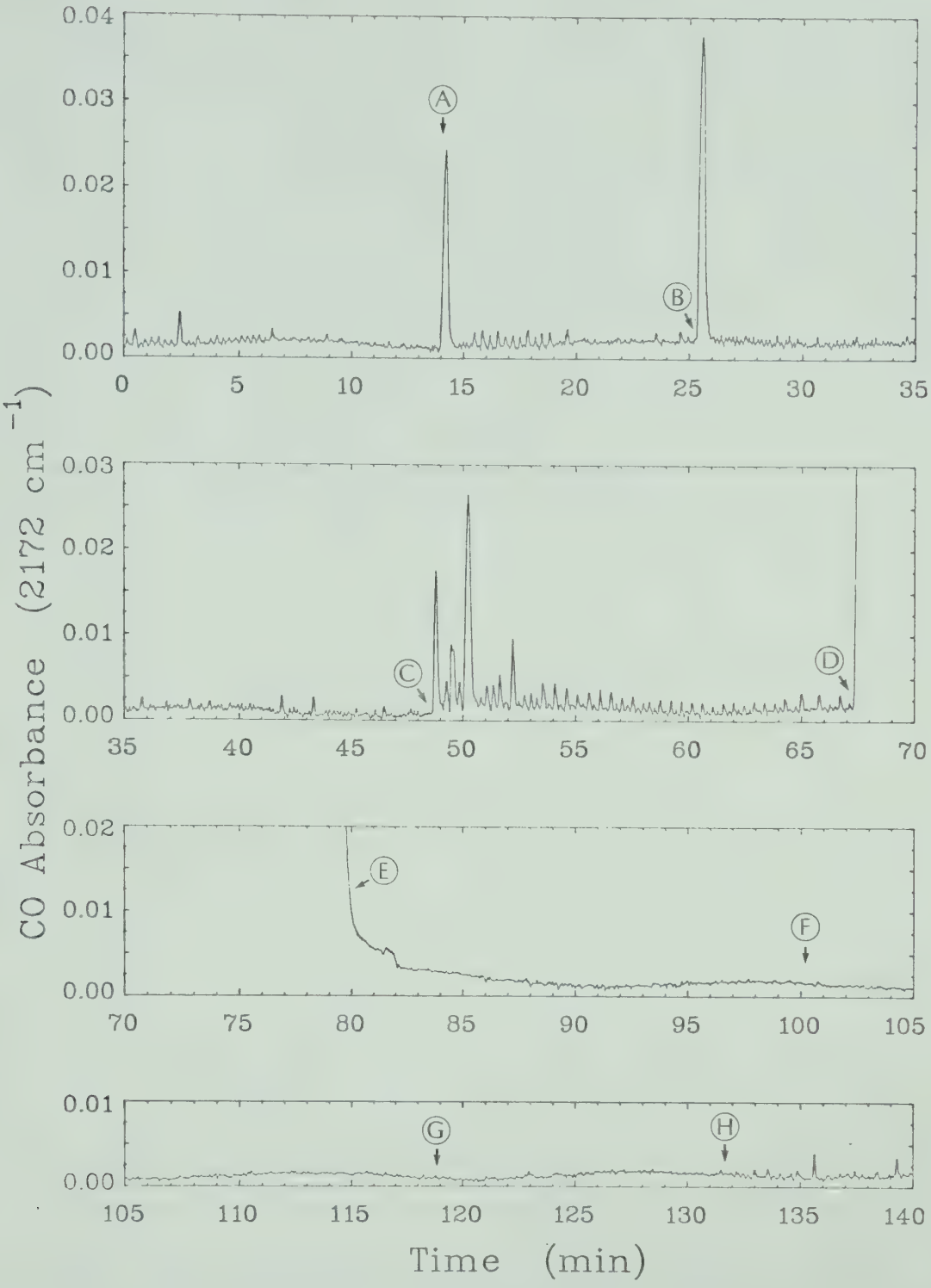

Figure 7.14 Catalyst Activity Changes at 473 K
Before A — Q_o = 246 SCCM, 7.6% CO, 30.9% O_2, 61.5% N_2
After A — Q_o = 291 SCCM, 8.1% CO, 26.1% O_2, 65.8% N_2
After B — Q_o = 361 SCCM, 8.7% CO, 21.1% O_2, 70.2% N_2
After C — Q_o = 320 SCCM, 9.8% CO, 10.9% O_2, 79.3% N_2
At D — Q_o = 307 SCCM, 10.2% CO, 7.2% O_2, 82.6% N_2
Between D and E — Q_o = 76 SCCM, 0% CO, 100% O_2, 0% N_2
After E — Same as before A; After F — Same as after A
After G — Same as after B ; After H — Same as after C

the feed CO was stopped, and the reactor was purged with oxygen.

Purging with oxygen resulted in the carbon monoxide concentration in the reactor being decreased to the point where the oxidation reaction once again started to proceed with an appreciable rate. In fact, the rate of the reaction became so large that the CO concentration in the reactor decreased to a low level virtually instantaneously. At point E, the reactor feed conditions were reset to those which existed before point A, and changes in the reactor feed conditions at points F, G and H were made which were similar to those previously made at points A, B and C, respectively.

A comparison of the system behavior after the similar operating condition changes were made at points A and F, B and G, or C and H shows that significant changes occurred in the catalyst activity. It is apparent that the catalyst activity was much higher after point E, than it was before point D. It is believed that the increase in activity probably occurred due to some restructuring of the catalyst surface which occurred when the system was moved from the low to the high conversion steady-state by purging with oxygen. This restructuring was possibly caused by extremely high surface temperatures which occurred when the reaction rate became very large as the CO concentration in the reactor went from a high to a low level virtually instantaneously.

To verify that the catalyst activity had indeed changed, the reactor temperature was reduced to 393 K, and the feed conditions were set at values similar to those which resulted in the oscillations shown in Figure 7.13. It was found that oscillatory behavior no longer occurred as the system went to a total conversion steady-state due to the increased activity of the catalyst. Thus, the oscillations shown in Figure 7.13 could no longer be reproduced after subjecting the catalyst to the severe reaction conditions at 473 K.

These observations of changes in the catalyst activity were of some concern, as they seemed to throw into doubt the reproducible nature of the oscillatory behavior. An attempt was made to determine why the catalyst behavior had originally been so reproducible. From an examination of the records of the preliminary work with this catalyst, it was determined that the catalyst temperature had never been raised above 433 K under reaction conditions (625 K during pretreatment). Also it was determined that at 423 K the catalyst had several times been subjected to the previously mentioned severe reaction conditions, i.e. at 423 K the reaction several times underwent abrupt transitions from low to high conversion steady-states due to the reactor being purged with oxygen after it had filled with carbon monoxide. These abrupt transitions from low to high conversion steady-states had occurred early in the life of the catalyst, and it appears that due to them the catalyst

activity was stabilized, and thus remained very constant during the subsequent experimental work, the majority of which was performed at temperatures below 423 K.

In order to determine the effects of both the severe reaction conditions and the initial pretreatment, it was decided to examine the behavior of a new twenty gram batch of the Pt-Pd converter catalyst under various operating conditions. Before being placed in the reactor, the batch of catalyst was pretreated at 625 K in flowing dry air for approximately twelve hours. Thus, this catalyst was subjected to the same pretreatment as the previous batches of catalyst.

After being placed in the reactor, the catalyst was subjected to reaction conditions at 393 K which were similar to those under which the oscillations shown in Figure 7.13 were obtained. It was found that the catalyst was very inactive and that only a single very low conversion steady-state existed. The reactor temperature was then raised to 423 K, and it was found that the catalyst displayed oscillatory behavior which was qualitatively similar to that shown in Figure 7.13 for the previous batch of catalyst at 393 K. The reaction was then driven to a low conversion steady-state by flooding the reactor with carbon monoxide, and following this the reactor was purged with oxygen. This type of treatment was very similar to that which the first batch of catalyst had been subjected early in its life.

Once the oxygen purge was started it was observed that the carbon monoxide concentration initially decreased solely due to the mixing effect, but that upon reaching a certain point it abruptly decreased virtually instantaneously to zero concentration. This abrupt transition was similar in many repects to that shown in Figure 7.14, and it was found that the catalyst activity had increased following the abrupt transition. Upon setting the operating conditions back to those in effect before the reactor was flooded with CO, it was found that while oscillatory behavior still occurred, it was qualitatively different in that the period, amplitude and shape of the peaks had changed.

The reactor was then subjected to the above process several times, and it was found that each abrupt transition had a smaller and smaller effect on the activity of the catalyst. Finally it was observed that the catalyst activity became constant and that it was no longer affected by further abrupt transitions from low to high conversion steady-states. Following this, the reactor temperature was lowered to 393 K, and it was found that when the feed conditions were set at those given in Figure 7.13 that oscillatory behavior occurred which was qualitatively similar to that shown in Figure 7.13.

The above similarity of the oscillatory behavior was taken as an indication that the activity of the second batch of Pt-Pd catalyst was now similar to that of the first batch. Thus, this form of 'reaction pretreatment' appears

to stabilize the catalyst activity as long as the catalyst bulk temperature is kept below that at which the 'reaction pretreatment' was performed.

7.7 Conclusions

From the experimental observations presented in the preceeding sections of this chapter, a number of comments can be made regarding the mechanistic details of oscillatory behavior.

1. Two qualitatively different types of oscillations can occur during carbon monoxide oxidation. At low temperatures, relaxation oscillations which are related to the kinetic mechanism of the reaction predominate, while at high temperatures, small symmetrical oscillations caused by transport limitations occur.
2. Chaotic behavior can occur when both types of oscillations are occurring simultaneously due to the coupling of the two nonlinear oscillators.
3. Since oscillations were observed at temperatures as low as 318 K, it appears that the reversible formation of surface oxides of platinum and/or the migration of oxygen into the bulk platinum must be ruled out as a possible cause of the relaxation oscillations.
4. The presence of hydrocarbon impurities in the feed stream are eliminated as a cause of oscillatory behavior due to the existence of oscillations when ultra high

purity oxygen was used as the feed gas. Also, no water peaks were ever detected chromatographically, thus ruling out any significant accumulation and oxidation of hydrocarbons on the catalyst surface.

5. Catalyst activity can be greatly increased by subjecting the catalyst to severe reaction conditions. It appears that this increase in the activity is a result of surface restructuring caused by high metal surface temperatures during periods of large instantaneous reaction rates.
6. Since high instantaneous reaction rates occur whenever the carbon monoxide concentration oscillates from a high to a low level, then significant changes in temperature of the metal surface must occur whenever an oscillation occurs. However, if the catalyst has been 'reaction pretreated' at a temperature which is higher than that at which the oscillations are occurring, then no changes in catalyst activity will occur due to the temperature variations during the oscillations.
7. It is believed that the oscillatory behavior observed at low temperatures is caused by an interplay between the rates of adsorption of carbon monoxide and oxygen, with thermal effects being produced by the large instantaneous releases of energy during periods of abrupt transition from high to low concentrations of carbon monoxide.

7.8 References

7.1 Beusch, H., Fieguth, P. and Wicke, E., Chemical Reaction Engineering, First Intl. Symp. on Chem. React. Eng. Wash. 1970, Adv. Chem. Ser. 109, p.615, ACS, Washington, 1972.

7.2 Beusch, H., Fieguth, P. and Wicke, E., Chem. Ing. Techn., 1972 44 445.

7.3 Hugo, P. and Jakubith, M., Chem. Ing. Techn., 1972 44 383.

7.4 Dauchot, J.P. and Van Cakenberghe, J., Nature Phys. Sci., Nov. 26, 1973 246 61.

7.5 Eckert, E., Hlavacek, V. and Marek, M., Chem. Eng. Commun., 1973 1 95.

7.6 McCarthy, E., Zahradnik, J., Kuczynski, G.C. and Carberry, J.J., J. Catal., 1975 39 29.

7.7 Varghese, P., Carberry, J.J. and Wolf, E.E., J. Catal., 1978 55 76.

7.8 Cutlip, M.B. and Kenney, C.N., Chemical Reaction Engineering - Houston, ACS Symp. Ser. 65, p.475, ACS, Washington, 1978.

7.9 Sheintuch, M. and Schmitz, R.A., Chemical Reaction Engineering - Houston, ACS Symp. Ser. 65, p.487, ACS, Washington, 1978.

7.10 Plichta, R.T. and Schmitz, R.A., Chem. Eng. Commun., 1979 3 387.

7.11 Sheintuch, M., AIChE J., 1981 27 20.

7.12 Rathousky, J., Kira, E. and Hlavacek, V., Chem. Eng. Sci., 1981 36 776.

8. A MODEL FOR OSCILLATORY BEHAVIOR FOR CO OXIDATION

In the preceeding chapters reference has often been made to the many models which purport to explain oscillatory behavior, eg. [8.1 - 8.6]. Unfortunately, the predictions of these models have rarely been validated through detailed comparison with experimental data. In addition, many of these models contain simplifying assumptions, thus rendering their predictions suspect when viewed in the light of the development in Chapters 2 to 4. In this chapter, a model for the catalytic oxidation of carbon monoxide will be developed which is free of those simplifying assumptions which cause violations of mass conservation, and some initial results from this model are compared to the experimental observations contained in the preceeding chapter.

8.1 Model Development

In the previous chapter it was stated that variations in the catalyst surface temperature were believed to play an important role in the observed oscillatory behavior. In particular, the interaction of these temperature variations with the rates of reaction and adsorption of oxygen and carbon monoxide was considered to be a key step in the reaction mechanism. Significant temperature rises during adsorption and reaction have been reported for supported

metal catalysts [8.7 - 8.9], and Dagonnier and co-workers [8.4, 8.5] have proposed a model that considers variations in surface temperature to explain oscillatory behavior. Their three ordinary differential equation model does not consider variations in bulk phase concentrations which, as has been shown in Chapter 7, are very significant, hence a more complete model for the catalytic oxidation of CO over a supported metal catalyst was developed. This new model is based on the following assumptions:

1. The experimental recycle reactor is assumed to behave as an ideal continuous stirred tank reactor.
2. The feed to the reactor only contains O_2, CO and inerts, i.e. no CO_2 is present in the reactor feed.
3. The reactor pressure is constant.
4. The temperature of the bulk gas phase is constant and the feed stream enters at the reactor temperature.
5. The temperature of the catalyst support is identical to the bulk gas phase temperature.
6. The temperature of the supported metal crystallites can vary and all heat transfer from the metal is approximated by a single convection term.
7. The physical properties of the metal catalyst are temperature invariant.
8. The temperature of all metal crystallites is the same.
9. The temperature of the metal catalyst is uniform throughout each crystallite.

10. Neither the adsorption of CO nor O_2 are activated.
11. Oxygen dissociates upon adsorption on the surface. Each oxygen (O_2) molecule thus requires two surface sites for adsorption.
12. Carbon monoxide adsorbs in the linear form on the catalyst surface and thus each carbon monoxide molecule occupies a single surface site.
13. The conversion of carbon monoxide to carbon dioxide proceeds only through the surface reaction of carbon monoxide and oxygen surface species, i.e. solely Langmuir-Hinshelwood kinetics [8.10 - 8.12].
14. The reaction is considered to be facile (structure insensitive).
15. The surface area for adsorption is the same as the surface area for heat transfer.
16. The inerts and the CO_2 do not adsorb on the metal surface.
17. The surface sites are conserved.
18. Neither the reaction activation energy nor the heats of adsorption or desorption are affected by the surface coverage.

From the above assumptions, the kinetics of the reaction mechanism can be depicted as follows (S is a surface site):

$$CO(g) + S \underset{k_{-1}}{\overset{k_1}{\rightleftharpoons}} COS \qquad (8.1)$$

$$O_2(g) + 2S \underset{k_{-2}}{\overset{k_2}{\rightleftharpoons}} 2OS \qquad (8.2)$$

$$COS + OS \xrightarrow{k_3} CO_2(g) + 2S \qquad (8.3)$$

For this mechanism the use of the preceeding assumptions leads to the development of a model which consists of six ordinary differential equations, namely: three gas phase mass balances for CO, O_2 and CO_2; two surface phase species balances for COS and OS; and one overall energy balance for the metal catalyst. These six equations are written as follows:

Balances on gas phase CO, O_2 and CO_2

$$V \frac{d[CO]}{dt'} = Q_o[CO]_o - Q[CO] - Ak_1[CO][S] + Ak_{-1}[COS] \qquad (8.4)$$

$$V \frac{d[O_2]}{dt'} = Q_o[O_2]_o - Q[O_2] - Ak_2[O_2][S]^2 + Ak_{-2}[OS]^2 \qquad (8.5)$$

$$V \frac{d[CO_2]}{dt'} = - Q[CO_2] + Ak_3[COS][OS] \qquad (8.6)$$

Balances on surface phase COS and OS

$$AL \frac{d[OS]}{dt'} = 2Ak_2[O_2][S]^2 - 2Ak_{-2}[OS]^2 - Ak_3[COS][OS] \qquad (8.7)$$

$$AL \frac{d[COS]}{dt'} = Ak_1[CO][S] - Ak_{-1}[COS] - Ak_3[COS][OS] \qquad (8.8)$$

Energy balance on the metal catalyst

$$mCp \frac{dT'}{dt'} = A\{Hr_1(k_1[CO][S] - k_{-1}[COS]) + Hr_2(k_2[O_2][S]^2 - k_{-2}[OS]^2) + Hr_3k_3[COS][OS]\} - UA(T'-T'_o) \qquad (8.9)$$

where: $$[S] = 1 - [COS] - [OS] \quad (8.10)$$

$$k_{-1} = k^{\circ}_{-1}EXP(-E_1/RT') \quad (8.11)$$

$$k_{-2} = k^{\circ}_{-2}EXP(-E_2/RT') \quad (8.12)$$

$$k_3 = k^{\circ}_3EXP(-E_3/RT') \quad (8.13)$$

$$Q = Q_o + A(RT'_o/P_o)\{-k_1[CO][S] + k_{-1}[COS] - k_2[O_2][S]^2 + k_{-2}[OS]^2 + k_3[COS][OS]\} \quad (8.14)$$

These equations can be written in dimensionless form by defining the following dimensionless groups:

$$X = [CO]/[CO]_o \quad (8.15)$$

$$Y = [O_2]/[O_2]_o \quad (8.16)$$

$$Z = [CO_2]/[CO]_o \quad (8.17)$$

$$T = (T'-T'_o)/T'_o \quad (8.18)$$

$$t = t'Q_o/V \quad (8.19)$$

$$\alpha_1 = V[CO]_o/AL \quad (8.20)$$

$$\alpha_2 = 2V[O_2]_o/AL \quad (8.21)$$

$$\alpha_3 = UAV/mCpQ_o \quad (8.22)$$

$$\beta_1 = Hr_1[CO]_oQ_o/UAT'_o \quad (8.23)$$

$$\beta_2 = Hr_2[O_2]_oQ_o/UAT'_o \quad (8.24)$$

$$\beta_3 = Hr_3[CO]_oQ_o/UAT'_o \quad (8.25)$$

$$\gamma_1 = E_1/RT'_o \quad (8.26)$$

$$\gamma_2 = E_2/RT'_o \quad (8.27)$$

$$\gamma_3 = E_3/RT'_o \quad (8.28)$$

$$K_1 = Ak_1/Q_o \quad (8.29)$$

$$K_2 = Ak_2/Q_o \quad (8.30)$$

$$K_3 = Ak^{\circ}_3EXP(-\gamma_3)/Q_o[CO]_o \quad (8.31)$$

$$K_{-1} = Ak^{\circ}_{-1}EXP(-\gamma_1)/Q_o[CO]_o \quad (8.32)$$

$$K_{-2} = Ak^{\circ}_{-2}EXP(-\gamma_2)/Q_o[O_2]_o \tag{8.33}$$

$$F = 1 + (RT^{\prime}_o/P_o)\{-K_1[CO]_oX[S] + K_{-1}EXP(\gamma_1T/(1+T))[CO]_o[COS] - K_2[O_2]_oY[S]^2 + K_{-2}EXP(\gamma_2T/(1+T))[O_2]_o[OS]^2 + K_3EXP(\gamma_3T/(1+T))[CO]_o[COS][OS]\} \tag{8.34}$$

Inserting the dimensionless groups into Eqs. 8.4-8.9 gives:

$$\frac{dX}{dt} = 1 - FX - K_1X[S] + K_{-1}EXP(\gamma_1T/(1+T))[COS] \tag{8.35}$$

$$\frac{dY}{dt} = 1 - FY - K_2X[S]^2 + K_{-2}EXP(\gamma_2T/(1+T))[OS]^2 \tag{8.36}$$

$$\frac{dZ}{dt} = - FZ + K_3EXP(\gamma_3T/(1+T))[COS][OS] \tag{8.37}$$

$$\frac{d[OS]}{dt} = \alpha_2(K_2Y[S]^2 + K_{-2}EXP(\gamma_2T/(1+T))[OS]^2) - \alpha_1K_3EXP(\gamma_3T/(1+T))[COS][OS] \tag{8.38}$$

$$\frac{d[COS]}{dt} = \alpha_1(K_1X[S] + K_{-1}EXP(\gamma_1T/(1+T))[COS]) - \alpha_1K_3EXP(\gamma_3T/(1+T))[COS][OS] \tag{8.39}$$

$$\frac{dT}{dt} = \alpha_3\beta_1(K_1X[S] - K_{-1}EXP(\gamma_1T/(1+T))[COS]) + \alpha_3\beta_2(K_2Y[S]^2 - K_{-2}EXP(\gamma_2T/(1+T))[OS]^2) + \alpha_3\beta_3K_3EXP(\gamma_3T/(1+T))[COS][OS] - \alpha_3T \tag{8.40}$$

8.2 Stability and Uniqueness

An analytical investigation of the regions of stability and uniqueness for Eqs. 8.35-8.40 is obviously impossible due to the complexity of the system. Instead a numerical investigation was performed so that for any given set of parameters, the number and stability of the steady-states could be determined (see Appendix E for computer programs).

It was found, over large ranges of parameter values, that both steady-state multiplicity and instability were possible. Indeed, for some sets of parameter values as many as five steady-states were found to coexist, with varying numbers of the steady-states being stable or unstable depending on the parameter values.

When large numbers of steady-states coexisted, the behavior of the system for a given set of initial conditions could only be determined by numerical integration (computer programs in Appendix E). From these integrations it has been found that this model can display complex dynamic and steady-state behavior such as steady-state hysteresis, simple periodic solutions, coexistence of stable limit cycles with stable steady-states, and multipeak oscillatory behavior. Also of interest was the finding that, for all the parameter values investigated, this model always possessed a stable low conversion steady-state (surface almost completely covered with CO).

8.3 Numerical Integration Results

In this section, selected results of numerical integrations of Eqs. 8.35-8.40 for several sets of parameter values are presented. The results are of a preliminary nature and should not be considered as an exhaustive delimiting of the behavior of the model.

Shown in Figures 8.1(a) and (b) are the results of numerical integrations of Eqs. 8.35-8.40 for a set of parameter values for which five steady-states (four of which are unstable) existed. It is seen that the oscillations are qualitatively and quantitatively similar to the experimental results shown in Figure 7.3, as not only are the oscillations similar with respect to period and amplitude, but even the shapes of the oscillations agree in many respects. The major qualitative difference between the experimental and model oscillations occurs in the region of the carbon dioxide maximum. Experimentally the carbon dioxide concentration continued to slowly increase after the virtually instantaneous increase from the minimum, whereas the carbon dioxide concentration shown in Figure 8.1 decreases slowly after the instantaneous increase. However, the other regions of the experimental and model oscillations are in substantial agreement.

The similarities between the model and experimental results are further emphasized in Figures 8.1(c) and (d) where the amplitude of the oscillations have been scaled so that the experimental order of magnitude difference in IR sensitivity between CO and CO_2 is duplicated in the model results.

If it is assumed that the mechanism postulated in deriving Eqs. 8.35-8.40 is an accurate representation of the physical reality, then the model can be used to determine the behavior of variables (temperature, concentration, etc.)

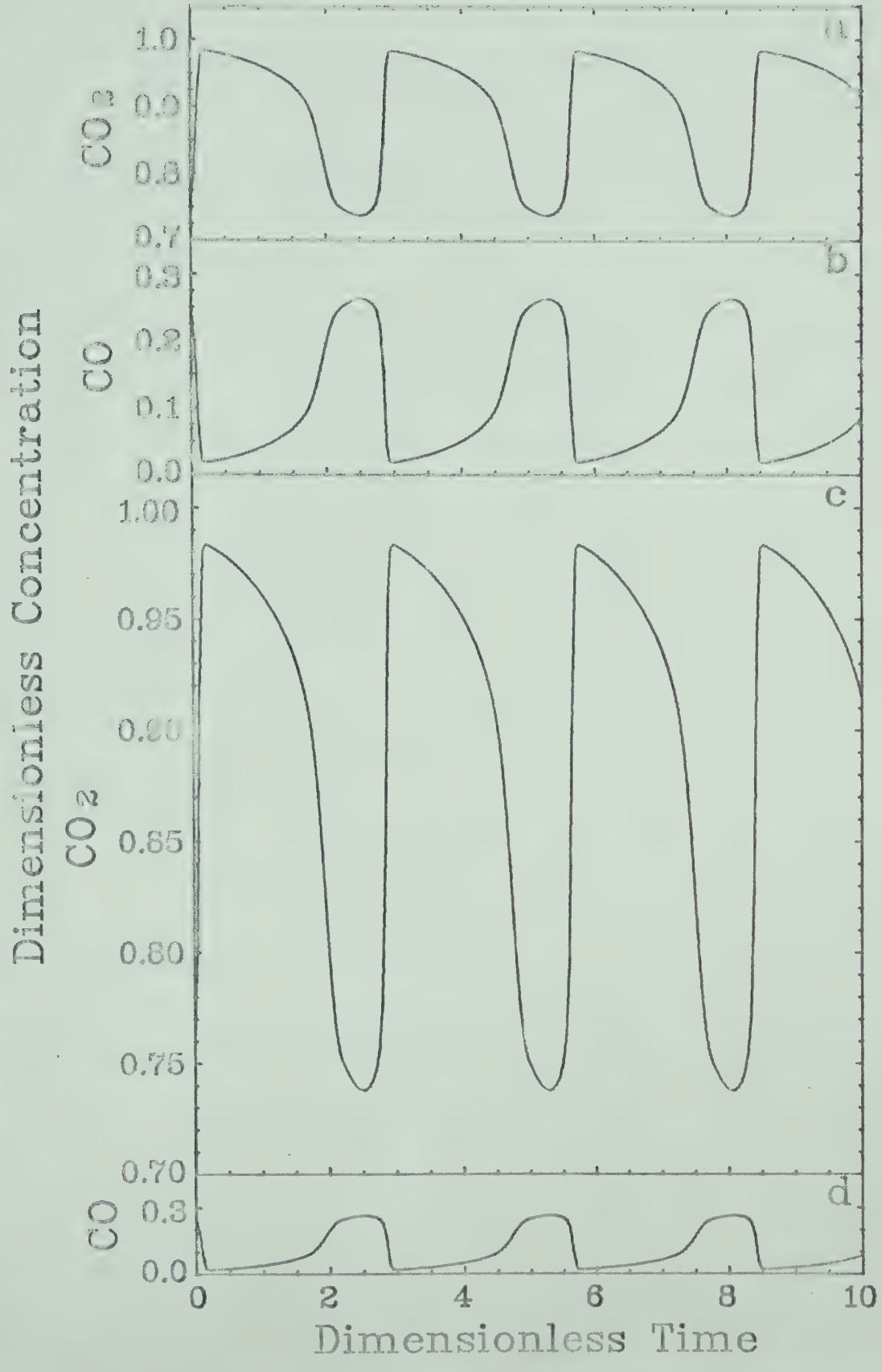

Figure 8.1 Oscillations Similar to Experimental Observations (parameters given in Table 8.1)

Table 8.1 Parameter Values for Figures 8.1 and 8.2

PARAMETER	FIGURE			
	1(a)-(b)	2(a)	2(b)	2(c)
K_1	1316	834	1000	5000
K_{-1}	$7.27*10^{-3}$	$5.11*10^{-4}$	10^{-8}	0.1
K_2	132	92.6	10	0.5
K_{-2}	$3.10*10^{-14}$	$2.18*10^{-14}$	10^{-4}	10^{-14}
K_3	0.765	0.539	0.500	1.000
α_1	0.245	0.245	0.100	0.050
α_2	233	233	50	50
α_3	4.70	4.73	5.00	20.0
β_1	0.284	0.269	0.040	0.080
β_2	259	245	5	5
β_3	0.118	0.112	0.050	0.060
γ_1	35.6	35.6	40.0	40.0
γ_2	71.2	71.2	60.0	60.0
γ_3	25.4	25.4	30.0	30.0

which were not measured experimentally. For example, the model predicts that the gas phase CO and CO_2 oscillations shown in Figure 8.1 are accompanied by catalyst temperature oscillations of 520 K to 700 K (180 K amplitude), and carbon monoxide surface coverage oscillations over the range 10^{-3} to 10^{-5} (complete coverage = 1). It is in the determination of this type of information for variables which are difficult (or impossible) to measure experimentally that a model can be particularly useful.

The model predicts considerably different behavior than that shown in Figure 8.1 for other parameter values. Shown in Figure 8.2 are carbon monoxide oscillations for three different sets of parameter values. These oscillations illustrate the extremes which are possible, as either slow oscillations with a relatively broad maximum, or fast oscillations with sharp peaks are possible. A comparison of these oscillations with the experimental data shows that the oscillations in Figures 8.2(a) and (b) are similar to those shown in Figure 7.9.

Besides the single peak oscillations shown in Figures 8.1 and 8.2, this model can predict complex multipeak behavior as shown in Figure 8.3, where it is seen that two or three maxima per cycle behavior can occur. While the doublet nature of the CO_2 oscillation is barely evident in Figure 8.3(a), it is very pronounced in Figure 8.3(b). It is interesting to note that the CO_2 oscillations shown in Figure 8.3(b) are qualitatively very similar to that shown

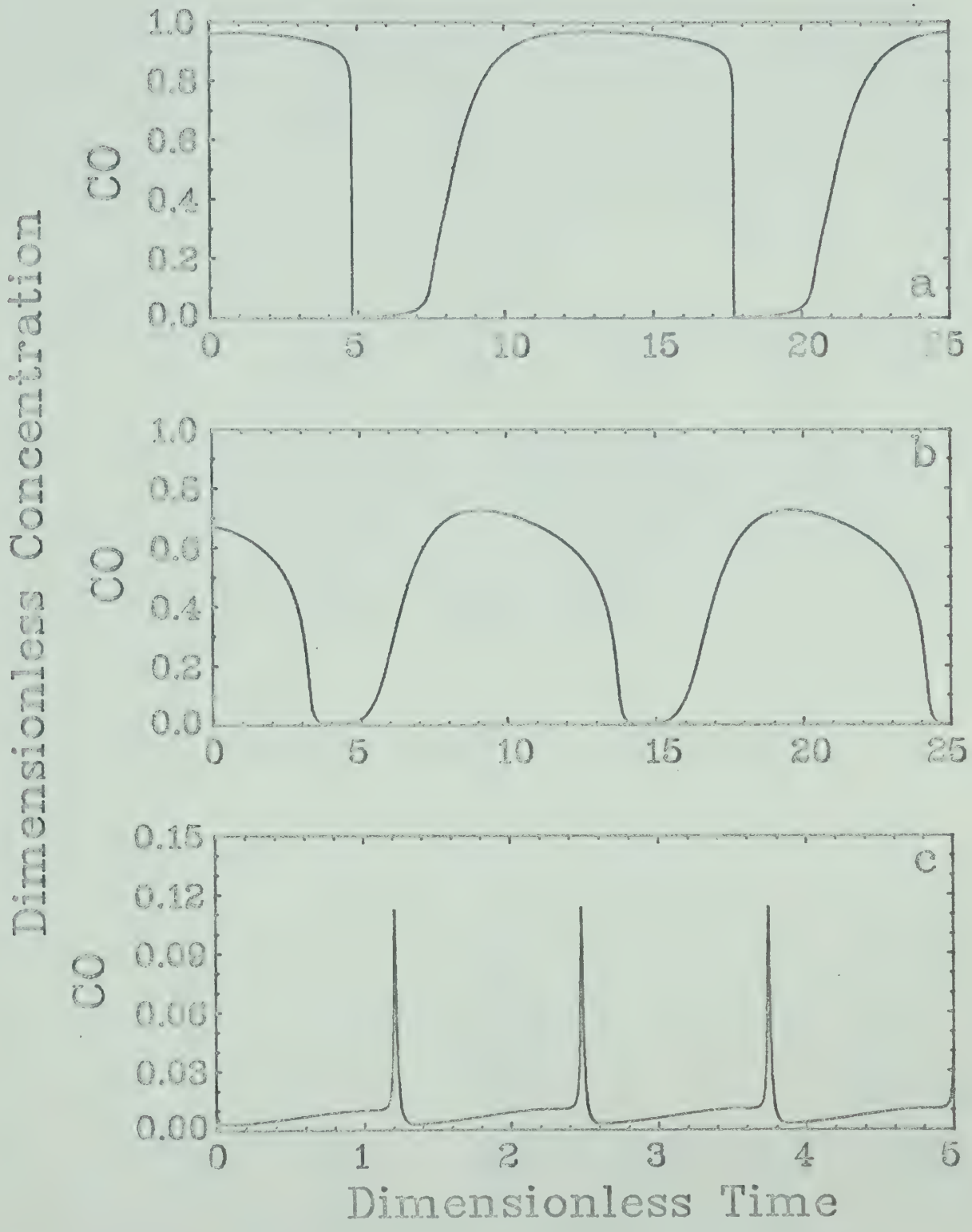

Figure 8.2 Extreme Forms of the CO Oscillations
(parameters given in Table 8.1)

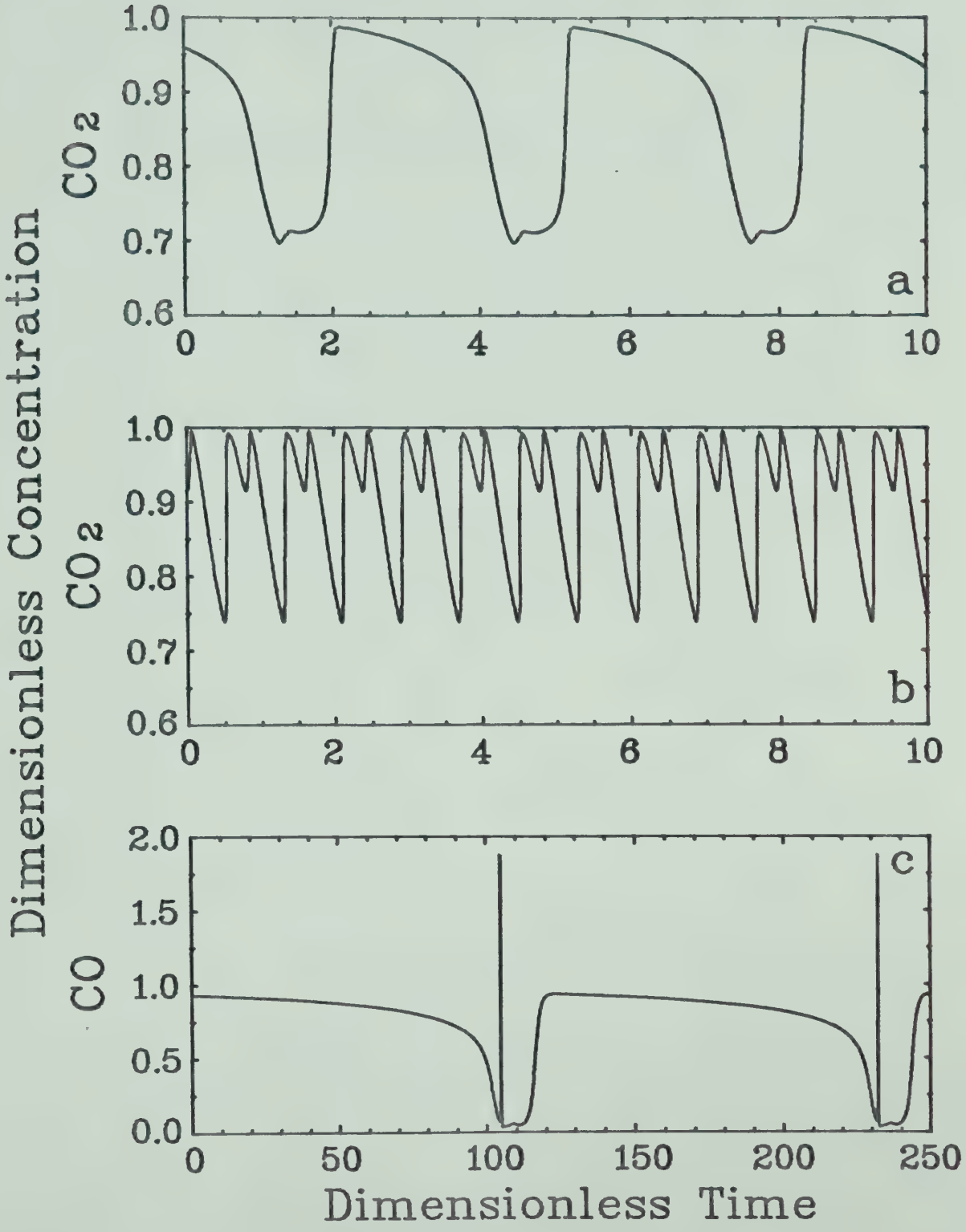

Figure 8.3 Multipeak Oscillations
(parameters given in Table 8.2)

Table 8.2 Parameter Values for Figure 8.3

PARAMETER	FIGURE		
	3(a)	3(b)	3(c)
K_1	834	10^4	914
K_{-1}	$5.11*10^{-3}$	$1.00*10^{-3}$	$6.19*10^{-2}$
K_2	92.6	500	0.914
K_{-2}	$2.18*10^{-14}$	$1.00*10^{-14}$	$2.08*10^{-14}$
K_3	0.539	10.0	0.815
α_1	0.245	0.100	$9.98*10^{-3}$
α_2	233	50	12.1
α_3	4.41	20.0	1.31
β_1	0.288	0.100	0.0833
β_2	262	5	96.5
β_3	0.120	0.040	0.0347
γ_1	35.6	40.0	35.6
γ_2	71.2	60.0	71.2
γ_3	25.4	30.0	25.4

in Figure 7.1(b). However, the complex three maxima per cycle oscillation shown in Figure 8.3(c) does not correspond to anything which was observed experimentally. These oscillations (three maxima per cycle) were produced by adjusting the parameters so that the model predicted large CO surface coverages, with correspondingly large amounts of CO desorbed from the surface during the high temperature parts of the oscillations.

8.4 Conclusions

The oscillations shown in Figures 8.1 to 8.3 are the results from a preliminary investigation of the model composed of Eqs. 8.35-8.40 . The initial results of the model predictions are very promising since this model is able to reproduce some of the fine structure of the experimentally observed oscillations. However, considerably more model testing and experimental verification is required before definite conclusions about the validity of the model can be made. Nevertheless it can be definitely concluded that oscillatory behavior does not require multiple reaction mechanisms, heats of adsorption and activation energies that are functions of surface coverage, or the presence of unreactive adsorbed species.

8.5 Nomenclature

Roman

A	surface area of metal
Cp	heat capacity of the catalytic metal
[CO]	gas phase concentration of CO
$[CO_2]$	gas phase concentration of CO_2
[COS]	normalized surface phase concentration of adsorbed CO
E_i/R	activation energies
F	ratio of inlet to exit volumetric flow rates
Hr_i	energy released upon adsorption or reaction
k_i^o	pre-exponential factors for the i-th reaction
k_i	rate constants for the i-th forward reaction
k_{-i}	rate constants for the i-th reverse reaction
K_i	dimensionless rate constants for the forward reactions
K_{-i}	dimensionless rate constants for the reverse reactions
L	surface capacity (active sites per unit area)
m	mass of catalytic metal
$[O_2]$	gas phase concentration of oxygen
[OS]	normalized surface concentration of adsorbed oxygen
P	pressure
Q	volumetric flow rate
[S]	normalized concentration of active sites
t	dimensionless time
t'	time
T	dimensionless temperature
T'	metal crystallite temperature

T_0' temperature of the reactor feed

U reactor heat transfer coefficient

V reactor volume

X dimensionless concentration of carbon monoxide

Y dimensionless concentration of oxygen

Z dimensionless concentration of carbon dioxide

Greek

$\alpha_{1,2}$ dimensionless ratios of gas to surface capacitance

α_3 dimensionless heat transfer coefficient

β_i dimensionless heats of reaction and adsorption

γ_i dimensionless activation energies

Subscript

$_0$ feed conditions

8.6 References

8.1 Sheintuch, M. and Schmitz, R.A., Catal. Rev. Sci. Eng., 1977 15 107.

8.2 Vayenas, C.G., Georgakis, C., Michaels, J. and Tormo, J., J. Catal., 1981 67 348.

8.3 Herz, R.K. and Marin, P., J. Catal., 1980 65 281.

8.4 Dagonnier, R., Dumont, M. and Nuyts, J., J. Catal., 1980 66 130.

8.5 Dagonnier, R. and Nuyts, J., J. Chem. Phys., 1976 65 2061.

8.6 McCarthy, E., Zahradnik, J., Kuczynski, G.C. and Carberry, J.J., J. Catal., 1975 39 29.

8.7 Cusumano, J.A. and Low, M.J.D., J. Catal., 1970 17 98.

8.8 Mills, G.A., Weller, S. and Cornelius, E.B., Second Intl. Cong. for Catal., Paris 1960, p. 2221, Editions Technip, Paris, 1961.

8.9 Jech, C., Second Intl. Cong. for Catal., Paris 1960, p. 2285, Editions Technip, Paris, 1961.

8.10 Engel, T. and Ertl, G., Adv. Catal., 1979 28 1.

8.11 Matsushima, T., J. Catal., 1978 55 337.

8.12 Matsushima, T., Sur. Sci., 1979 79 63.

9. RECOMMENDATIONS

Conclusions have been presented at the end of each chapter and will not be repeated here, but in the course of pursuing the research described in this thesis many additional areas of possible research have been encountered. While limitations of time, equipment and/or interest have resulted in these research areas not being fully pursued, it is realized that others may wish to do so. Listed below are recommendations for future experimental and theoretical work that will further the understanding of heterogeneous catalytic reactions.

1. Further investigations into the effects of simplifying assumptions are definitely needed. Of particular usefulness would be the development of criteria for determining a priori when specific simplifying assumptions are justified.
2. General techniques should be developed for the determination of regions of steady-state uniqueness for systems of equations which obey conservation laws. Presently the regions of uniqueness can only be determined by various ad hoc procedures.
3. The phenomenon of chaotic solutions for models of chemical systems needs further investigation. A systematic method of determining the regions (or even

the existence) of chaotic behavior in systems of equations would be a major achievement. At present, parameter values which give rise to chaotic behavior can only be found by "chance", i.e. through the numerical integration of equations for many sets of parameter values.

4. During the numerical examination of oscillatory and chaotic behavior, it was found that the computer algorithms used to perform the integrations (Gear's and Runge-Kutta-Fehlberg) were inefficient. The development of specialized algorithms for integrating equations with oscillatory and chaotic solutions would be very useful.
5. Additional reaction systems should be investigated to determine if oscillatory behavior over supported metal catalysts is restricted to oxidation reactions.
6. Experimental measurements of surface concentration and temperature oscillations would be useful in further elucidating the reaction mechanism. For CO oxidation, in situ IR measurements could be used to determine the relationship between gas phase and surface phase concentration oscillations.
7. The experimental data on the effects of operating conditions should be used to validate (or invalidate) the predictions of the many models which predict oscillatory behavior.
8. Futher development and testing of the proposed six ODE model is warranted due to the initial promising results.

Appendix A Computer Programs for Chapters 3 and 4

This appendix contains the source code of the program which was used to integrate the various systems of equations encountered in Chapters 3 and 4. This program was run on a Hewlett-Packard model 1000 21MX E-series computer, hence the code contains certain statements which are not part of standard FORTRAN. These statements were necessary to perform the various file handling operations on the HP-1000. Also included in this appendix is the source code for the program which calculated the number and the stability of the steady-states for the three ordinary differential equation model derived in Chapter 4. Since this program uses subroutines from the IMSL library, it had to be run on the main university computer system (MTS - Amdahl), as the IMSL subroutines are only available on that system.

```
C
C  PROGRAM IS USED TO INTEGRATE THE VARIOUS VERSIONS OF
C  EIGENBERGER'S MODEL. SUBROUTINES F1, F2 AND F3 ARE USED
C  TO INTEGRATE SYSTEMS 1, 3 AND 2 (CHAP. 3) RESPECTIVELY.
C  SUBROUTINES F4, F5 AND F6 ARE USED FOR INTEGRATING
C  SYSTEMS 1A, 3A AND 2A REPECTIVELY, AND SUBROUTINE F7 IS
C  USED IN THE INTEGRATION OF THE FULL MODEL (CHAPTER 4)
C
FTN4
      PROGRAM EIGEN(,800), VERSIONS OF EIGENBERGER'S MODEL
      EXTERNAL F1,F2,F3,F4,F5,F6,F7
      DIMENSION IDCB(144),NAME(3),YY(5),IBUF(100),NAMEI(3)
     *,SPARAM(6),IDCBI(144)
      DOUBLE PRECISION Y(4),A,H,HMX,AER,RER,DA,YP(4)
     *,PARAM(6),DDA,HH,HHMX,ASV,YSV(4),DABS,DSQRT
      COMMON PARAM
      CALL DTACH
      LUNW=LOGLU(ISIS)
      LUNR=LUNW
      CALL IFMTE(LUNW)
      WRITE(LUNW,800)
800   FORMAT(" ENTER NAME OF INPUT FILE, AND LU FOR OUTPUT")
      READ(LUNR,290) NAMEI,LUNO
290   FORMAT(3A2,1X,I2)
      CALL OPEN(IDCBI,IERR,NAMEI,0,1)
      CALL READF(IDCBI,IERR,IBUF)
      CALL CODE
      READ(IBUF,*) A,DA,AER,RER
      CALL READF(IDCBI,IERR,IBUF)
      CALL CODE
      READ(IBUF,*) N,NF,NP,NINT,IPLOT
      NOV=5
      NIV=4
      CALL READF(IDCBI,IERR,IBUF)
      CALL CODE
      READ(IBUF,*) (Y(I),I=1,NIV)
      CALL READF(IDCBI,IERR,IBUF)
      CALL CODE
      READ(IBUF,*) (PARAM(I),I=1,NP)
      WRITE(LUNO,901)
      CALL DFILE(IDCBI,IDCB,NAME)
      CALL CODE
      WRITE(IBUF,350) NINT
350   FORMAT(3I4)
      CALL WRITF(IDCB,IERR,IBUF,2)
      CALL CODE
      WRITE(IBUF,350) N,NF,NP
      CALL WRITF(IDCB,IERR,IBUF,6)
      DO 10 I=1,NP
 10   SPARAM(I)=SNGL(PARAM(I))
      CALL CODE
      WRITE(IBUF,361) (SPARAM(I),I=1,NP)
361   FORMAT(6E12.5)
      CALL WRITF(IDCB,IERR,IBUF,6*NP)
```

```
      DDA=DA
      HH=DDA/4.0D0
      HHMX=DDA/2.0D0
      YY(1)=SNGL(A)
      DO 12 I=1,NIV
12    YY(I+1)=SNGL(Y(I))
      CALL CODE
      WRITE(IBUF,361) (YY(I),I=1,NOV)
      CALL WRITF(IDCB,IERR,IBUF,6*NOV)
      NPINT=1
      ICOUNT=0
      DO 30 II=1,NINT
      IDUM=1
22    CONTINUE
      DO 26 KK=1,IDUM
      ASV=A
      DO 14 I=1,NIV
14    YSV(I)=Y(I)
      GO TO (710,720,730,740,750,760,770) NF
710   CALL RKF(A,Y,N,F1,DDA,HH,HHMX,AER,RER,IFLAG)
      Y(4)=0.0D0
      Y(3)=1.D0-Y(1)-Y(2)
      GO TO 790
720   CALL RKF(A,Y,N,F2,DDA,HH,HHMX,AER,RER,IFLAG)
      Y(4)=0.0D0
      Y(2)=1.D0-Y(1)-Y(3)
      GO TO 790
730   CALL RKF(A,Y,N,F3,DDA,HH,HHMX,AER,RER,IFLAG)
      Y(4)=0.0D0
      Y(1)=1.D0-Y(2)-Y(3)
      GO TO 790
740   CALL RKF(A,Y,N,F4,DDA,HH,HHMX,AER,RER,IFLAG)
      Y(3)=1.D0-Y(1)-Y(2)
      IF(PARAM(5).LE.1.0D-10) GO TO 745
      Y(3)=(-1.D0+DSQRT(1.D0+8.D0*PARAM(5)*(1.D0-Y(1)
     *-Y(2))))/(4.D0*PARAM(5))
745   Y(4)=PARAM(5)*Y(3)*Y(3)
      GO TO 790
750   CALL RKF(A,Y,N,F5,DDA,HH,HHMX,AER,RER,IFLAG)
      Y(2)=1.D0-Y(1)-Y(3)-2.D0*PARAM(5)*Y(3)*Y(3)
      Y(4)=PARAM(5)*Y(3)*Y(3)
      GO TO 790
760   CALL RKF(A,Y,N,F6,DDA,HH,HHMX,AER,RER,IFLAG)
      Y(1)=1.D0-Y(2)-Y(3)-2.D0*PARAM(5)*Y(3)*Y(3)
      Y(4)=PARAM(5)*Y(3)*Y(3)
      GO TO 790
770   CALL RKF(A,Y,N,F7,DDA,HH,HHMX,AER,RER,IFLAG)
      Y(3)=1.D0-Y(1)-Y(2)-2.D0*Y(4)
790   IF(IFLAG.NE.1) GO TO 100
      YY(1)=SNGL(A)
      DO 25 JJ=1,NIV
25    YY(JJ+1)=SNGL(Y(JJ))
      IF(KK.EQ.IDUM) GO TO 26
      CALL CODE
```

```
      WRITE(IBUF,361) (YY(I),I=1,NOV)
      CALL WRITF(IDCB,IERR,IBUF,6*NOV)
      WRITE(LUNO,905) (YY(I),I=1,NOV)
      NPINT=NPINT+1
26    CONTINUE
      IF(IDUM.NE.1) GO TO 27
      IF(DABS((YSV(1)-Y(1))/Y(1)).LT.0.10D0) GO TO 27
      A=ASV
      DO 16 I=1,NIV
 16   Y(I)=YSV(I)
      IDUM=10
      DDA=DA/10.0D0
      HH=DDA/4.0D0
      HHMX=DDA/2.0D0
      GO TO 22
27    CONTINUE
      ICOUNT=ICOUNT+1
      DDA=DA
      HH=DDA/4.0D0
      HHMX=DDA/2.0D0
      IF(ICOUNT/IPLOT*IPLOT.NE.ICOUNT) GO TO 30
      CALL CODE
      WRITE(IBUF,361) (YY(I),I=1,NOV)
      CALL WRITF(IDCB,IERR,IBUF,6*NOV)
      WRITE(LUNO,905) (YY(JJ),JJ=1,NOV)
      NPINT=NPINT+1
900   FORMAT(5X,"TIME",11X,"AX",14X,"BX",13X," X ")
901   FORMAT(5X,"TIME",11X,"AX",14X,"BX",14X,"X",14X,"XBX")
905   FORMAT(" ",E10.4,1X,8(E15.6,1X))
30    CONTINUE
      WRITE(LUNO,910) NPINT
910   FORMAT(" "," # OF POINTS =",I5)
      CALL CLOSE(IDCB)
      CALL OPEN(IDCB,IERR,NAME,2,1)
      CALL RWNDF(IDCB)
      CALL CODE
      WRITE(IBUF,350) NPINT
      CALL WRITF(IDCB,IERR,IBUF,2)
      CALL CLOSE(IDCB)
      STOP
100   CONTINUE
      WRITE(LUNO,915) IFLAG,A,(Y(II),II=1,N)
915   FORMAT(" ",I3,8(D15.6,1X))
      CALL CLOSE(IDCB)
      CALL OPEN(IDCB,IERR,NAME,2,1)
      CALL RWNDF(IDCB)
      CALL CODE
      WRITE(IBUF,350) NPINT
      CALL WRITF(IDCB,IERR,IBUF,2)
      CALL CLOSE(IDCB)
      STOP
      END
      SUBROUTINE F1(T,Y,YP),DAX/DT, DBX/DT (ALL ASSUMPTIONS)
      DOUBLE PRECISION Y(3),YP(3),T
```

```
      DOUBLE PRECISION AX,BX,DAX,DBX,D,E,F,H,G,GR
      COMMON D,E,F,H,G,GR
      AX=Y(1)
      BX=Y(2)
      DAX=D*(1.D0-AX-BX)-E*AX-F*AX*AX*(1.D0-AX-BX)**2
      DBX=H*(1.D0-BX-AX)-BX
      YP(1)=DAX
      YP(2)=DBX
      YP(3)=0.0D0
      RETURN
      END
      SUBROUTINE F2(T,Y,YP), DAX/DT, DX/DT (ALL ASSUMPTIONS)
      DOUBLE PRECISION Y(3),YP(3),T
      DOUBLE PRECISION AX,X,BX,DX,DBX,D,E,F,H,G,GR
      COMMON D,E,F,H,G,GR
      AX=Y(1)
      X=Y(3)
      DAX=D*X-E*AX-F*AX*AX*X*X
      DX=-D*X+E*AX-H*X+1.D0-X-AX+2.D0*F*AX*AX*X*X
      YP(1)=DAX
      YP(2)=0.0D0
      YP(3)=DX
      RETURN
      END
      SUBROUTINE F3(T,Y,YP),DBX/DT, DX/DT (ALL ASSUMPTIONS)
      DOUBLE PRECISION Y(3),YP(3),T
      DOUBLE PRECISION X,BX,DX,DBX,D,E,F,H,G,GR
      COMMON D,E,F,H,G,GR
      X=Y(3)
      BX=Y(2)
      DBX=H*X-BX
      DX=-D*X+E*(1.D0-X-BX)-H*X+BX+2.D0*F*(1.D0-X-BX)**2*X*X
      YP(3)=DX
      YP(2)=DBX
      YP(1)=0.0D0
      RETURN
      END
      SUBROUTINE F4(T,Y,YP),DAX/DT, DBX/DT EQUIL. ASSUMPTION
      DOUBLE PRECISION Y(3),YP(3),T
      DOUBLE PRECISION AX,X,BX,DAX,DX,DBX,D,E,F,H,G,GR,DSQRT
      COMMON D,E,F,H,G,GR
      AX=Y(1)
      BX=Y(2)
      X=1.D0-AX-BX
      IF(G.LE.1.D-10) GO TO 10
      X=(-1.D0+DSQRT(1.D0+8.D0*G*(1.D0-AX-BX)))/(4.D0*G)
10    DAX=D*X-E*AX-F*AX*AX*X*X
      DBX=H*X-BX
      YP(1)=DAX
      YP(2)=DBX
      YP(3)=0.0D0
      RETURN
      END
      SUBROUTINE F5(T,Y,YP),DAX/DT, DX/DT  EQUIL. ASSUMPTION
```

```
      DOUBLE PRECISION Y(3),YP(3),T
      DOUBLE PRECISION AX,BX,X,DAX,DBX,DX,D,E,F,H,G,GR
      COMMON D,E,F,H,G,GR
      AX=Y(1)
      X=Y(3)
      BX=1.D0-AX-X-2.D0*G*X*X
      DAX=D*X-E*AX-F*AX*AX*X*X
      DX=-D*X+E*Y-H*X+BX+2.D0*F*AX*AX*X*X
      YP(1)=DAX
      YP(2)=0.0D0
      YP(3)=DX
      RETURN
      END
      SUBROUTINE F6(T,Y,YP),DBX/DT, DX/DT  EQUIL. ASSUMPTION
      DOUBLE PRECISION Y(3),YP(3),T
      DOUBLE PRECISION AX,X,BX,DX,DBX,D,E,F,H,G,GR
      COMMON D,E,F,H,G,GR
      X=Y(3)
      BX=Y(2)
      AX=1-BX-X-2.D0*G*X*X
      DBX=H*X-BX
      DX=-D*X+E*AX-H*X+BX+2.D0*F*AX*AX*X*X
      YP(3)=DX
      YP(2)=DBX
      YP(1)=0.0D0
      RETURN
      END
      SUBROUTINE F7(T,Y,YP), DX/DT, DBX/DT, AND DBXX/DT
      DOUBLE PRECISION Y(4),YP(4),T
      DOUBLE PRECISION AX,BX,XBX,X,DAX,DBX,DXBX
      DOUBLE PRECISION D,E,F,H,G,GR
      COMMON D,E,F,H,G,GR
      AX=Y(1)
      BX=Y(2)
      XBX=Y(4)
      X=1.D0-AX-BX-2.D0*XBX
      DAX=D*X-E*AX-F*AX*AX*XBX/G
      DBX=H*X-BX
      DXBX=G*GR*X*X-GR*XBX-F*AX*AX*XBX/(2.D0*G)
      YP(1)=DAX
      YP(2)=DBX
      YP(4)=DXBX
      YP(3)=0.0D0
      RETURN
      END
      SUBROUTINE DFILE(IDCBI,IDCB,NAME),OUTPUT FILE CREATION
      DIMENSION IDCB(144),NAME(3),ISIZE(2),IDCBI(144)
      CALL READF(IDCBI,IERR,NAME)
      CALL CLOSE(IDCBI)
      ISIZE(1)=48
      ITYPE=3
      ISECU=1
      ICR=135
      CALL OPEN(IDCB,IERR,NAME,0,1)
```

```
      CALL CLOSE(IDCB)
      CALL PURGE(IDCB,IERR,NAME,1)
      CALL CREAT(IDCB,IERR,NAME,ISIZE,ITYPE,ISECU,ICR)
      CALL OPEN(IDCB,IERR,NAME,0,ISECU)
      RETURN
      END
      SUBROUTINE RKF(A,Y,N,F,DA,H,HMX,ABSER,RELER,IFLAG,
     *,NPINT,IDCB), VARIABLE STEP INTEGRATION OF ODE'S
C
C  THIS CODE INTEGRATES A SYSTEM OF FIRST ORDER ORDINARY
C  DIFFERENTIAL EQUATIONS BY RUNGE-KUTTA-FEHLBERG METHOD
C  WITH AUTOMATIC ESTIMATION OF LOCAL ERROR AND STEP SIZE
C  ADJUSTMENT - SHAMPINE AND ALLEN (REF. 5.16)
C
      DOUBLE PRECISION Y(N),YTEMP(20),TEMP(20),R(20)
      DOUBLE PRECISION K1(20),K2(20),K3(20),K4(20),K5(20)
     *,K6(20),U,RELER,ABSER,HMX,A,B,DA,HMAX,H,HKEEP,ARG
     *,RATIO,DABS,DMAX1,DMIN1,DSIGN,DSQRT,TR
      REAL DOUT(20)
      INTEGER IBUF(100),IDCB(144)
      U=1.0D-11
      IF(RELER.LT.0.0D0.OR.ABSER.LT.0.0D0) GO TO 18
      IF(RELER+ABSER.EQ.0.0D0) GO TO 18
      IF(HMX.LE.0.0D0) GO TO 18
      B=A+DA
      IF(DABS(DA).LE.13.D0*U*DMAX1(DABS(A),DABS(B)))GO TO 19
      HMAX=DMIN1(HMX,DABS(DA))
      IF(DABS(H).LE.13.0D0*U*DABS(A)) H=HMAX
      IADJS=0
3     H=DSIGN(DMIN1(DABS(H),HMAX),DA)
      IF(DABS(B-A).GT.1.25D0*DABS(H)) GO TO 4
      HKEEP=H
      IADJS=1
      H=B-A
4     CALL F(A,Y,K1)
5     CONTINUE
      DO 6 I=1,N
6     YTEMP(I)=Y(I)+0.25D0*H*K1(I)
      ARG=A+0.25D0*H
      CALL F(ARG,YTEMP,K2)
      DO 7 I=1,N
7     YTEMP(I)=Y(I)+H*(K1(I)*3.D0/32.D0+K2(I)*(9.D0/32.D0))
      ARG=A+H*(3.D0/8.D0)
      CALL F(ARG,YTEMP,K3)
      DO 8 I=1,N
8     YTEMP(I)=Y(I)+H*(K1(I)*(1932.D0/2197.D0)
     *-K2(I)*(7200.D0/2197.D0)+K3(I)*(7296.D0/2197.D0))
      ARG=A+H*(12.D0/13.D0)
      CALL F(ARG,YTEMP,K4)
      DO 9 I=1,N
9     YTEMP(I)=Y(I)+H*(K1(I)*(439.D0/216.D0)-8.D0*K2(I)
     *+K3(I)*(3680.D0/513.D0)-K4(I)*(845.D0/4104.D0))
      ARG=A+H
      CALL F(ARG,YTEMP,K5)
```

```
      DO 10 I=1,N
10    YTEMP(I)=Y(I)+H*(-K1(I)*(8.D0/27.D0)+2.D0*K2(I)
     *-K3(I)*(3544.D0/2565.D0)+K4(I)*(1859.D0/4104.D0)
     *-K5(I)*(11.D0/40.D0))
      ARG=A+0.5D0*H
      CALL F(ARG,YTEMP,K6)
      DO 11 I=1,N
      TEMP(I)=K1(I)*(25.D0/216.D0)+K3(I)*(1408.D0/2565.D0)
     *+K4(I)*(2197.D0/4104.D0)-0.2D0*K5(I)
11    YTEMP(I)=Y(I)+H*TEMP(I)
      DO 12 I=1,N
12    R(I)=K1(I)/360.D0-K3(I)*(128.D0/4275.D0)-K4(I)
     **(2197.D0/75240.D0)+K5(I)/50.D0+K6(I)*(2.D0/55.D0)
      RATIO=0.0D0
      DO 13 I=1,N
      TR=DABS(R(I))/(RELER*DABS(YTEMP(I))+ABSER)
13    RATIO=DMAX1(RATIO,TR)
      IF(RATIO.GT.1.D0) GO TO 15
      DO 40 I=1,N
      IF(K1(I)*K5(I).GT.0.0D0) GO TO 40
      IF(K5(I).EQ.0.0D0) GO TO 40
      DOUT(1)=SNGL(A)
      DO 35 JJ=1,N
35    DOUT(JJ+1)=SNGL(Y(JJ))
      M=N+1
      IF(N.EQ.2) M=N+2
      CALL CODE
      WRITE(IBUF,900) (DOUT(JJ),JJ=1,M)
900   FORMAT(11E12.5)
      CALL WRITF(IDCB,IERR,IBUF,6*M)
      NPINT=NPINT+1
      GO TO 45
40    CONTINUE
45    CONTINUE
      DO 14 I=1,N
14    Y(I)=YTEMP(I)
      A=A+H
      IF(IADJS.EQ.1) GO TO 16
      RATIO=DMAX1(RATIO,6.5536D-04)
15    RATIO=DMIN1(RATIO,4096.D0)
      H=0.8D0*H/DSQRT(DSQRT(RATIO))
      IF(DABS(H).LE.13.D0*U*DABS(A)) GO TO 19
      IF(RATIO.LE.1.D0) GO TO 3
      IADJS=0
      GO TO 5
16    IFLAG=1
      H=HKEEP
      RETURN
18    IFLAG=3
      RETURN
19    IFLAG=4
      RETURN
      END
```

```
C
C  THIS PROGRAM IS USED TO DETERMINE THE NUMBER AND
C  STABILITY OF THE STEADY-STATES FOR THE GENERAL
C  THREE ODE MODEL DERIVED FROM EIGENBERGERS MECHANISM
C
      EXTERNAL F
      DOUBLE PRECISION Y(1),WA(3),PAR(6),EPS,DSQRT,F
      DOUBLE PRECISION AX,BX,XBX,X,DAX,DBX,DXBX
      DOUBLE PRECISION FAC1,FAC2,FAC3
      DOUBLE PRECISION RJ(3,3),WK(3)
      COMPLEX*16 W(3),Z(3,3)
     READ(5,790) NRUN
 790  FORMAT(I2)
      DO 100 KK=1,NRUN
       READ(5,795) ITMAX,NSIG,EPS
 795   FORMAT(2I3,D10.5)
       WRITE(6,794)
 794   FORMAT('1',/////)
       WRITE(6,796) ITMAX,NSIG,EPS
 796   FORMAT(T10,' MAX # ITERATIONS = ',I3,/,T10,' # SIG '
     *,'DIGITS =',I4,/,T10,' MAX FUNCT. VALUE = ',D13.6,//)
       READ(5,800) (PAR(I),I=1,6)
 800   FORMAT(6D10.5)
       WRITE(6,900) PAR
 900    FORMAT(' ',T10,' K13*    = ',D13.6,/,
     * T10,' K5*     = ',D13.6,/,T10,' TALHPA = ',D13.6,/,
     * T10,' AXG     = ',D13.6,/,
     * T10,' K2*     = ',D13.6,/,T10,' K25*    = ',D13.6,/)
       READ(5,810) Y(1)
 810   FORMAT(2D10.5)
       WRITE(6,905) Y
 905   FORMAT(' ',T10,' INITIAL VALUE OF XBX  = ',D13.6,5X)
       N=1
       CALL ZSYSTM(F,EPS,NSIG,N,Y,ITMAX,WA,PAR,IER)
       WRITE(6,910) ITMAX,IER
 910   FORMAT(T11,'# OF ITERATIONS =',I5,5X,' IER = ',I4,//)
       XBX=Y(1)
       FAC1=2.D0*PAR(1)*PAR(5)/(1.D0+PAR(2))
       FAC2=(PAR(1)**2)*PAR(5)/(2.0D0*(PAR(4)**3))
       FAC3=8.0D0*FAC1*(1.D0-2.D0*XBX)*XBX
       AX=(-FAC2-FAC1+DSQRT((FAC1+FAC2)**2+FAC3))/(4.D0*XBX)
       BX=(1.D0-AX-2.D0*XBX)*PAR(2)/(1.D0+PAR(2))
       X=(1.D0-AX-BX-2.D0*XBX)
       DAX=PAR(3)*PAR(1)*X-PAR(3)*PAR(1)**2*AX/(4.D0*
     *PAR(4)**3)-PAR(3)*AX*AX*XBX/PAR(5)
       DBX=PAR(2)*X-BX
       DXBX=PAR(5)*PAR(6)*X*X-PAR(6)*XBX-PAR(3)*AX*AX*XBX/
     *(2.D0*PAR(5))
       WRITE(6,950) AX,BX,XBX,X
 950   FORMAT(' ',T10,' AX   = ',D13.6,/,T10,' BX   = ',D13.6,
     * /,T10,' XBX  = ',D13.6,/,T10,' X    = ',D13.6,//)
       WRITE(6,960) DAX,DBX,DXBX
 960   FORMAT(T10,' DAX  = ',D13.6,/,T10,' DBX  = ',D13.6,
     * /,T10,' DXBX = ',D13.6,//)
```

```
      RJ(1,1)=-PAR(3)*(PAR(1)+PAR(1)**2/(4.D0*PAR(4)**3)
     **+2.D0*AX*XBX/PAR(5))
      RJ(1,2)=-PAR(3)*PAR(1)
      RJ(1,3)=-PAR(3)*(2.D0*PAR(1)+AX*AX/PAR(5))
      RJ(2,1)=-PAR(2)
      RJ(2,2)=-PAR(2)-1.D0
      RJ(2,3)=-2.D0*PAR(2)
      RJ(3,1)=-2.D0*PAR(5)*PAR(6)*X-PAR(3)*AX*XBX/PAR(5)
      RJ(3,2)=-2.D0*PAR(5)*PAR(6)*X
      RJ(3,3)=-4.D0*PAR(5)*PAR(6)*X-PAR(6)-PAR(3)*AX*AX/
     *(2.D0*PAR(5))
      CALL EIGRF(RJ,3,3,0,W,Z,3,WK,IER)
      WRITE(6,970) (JJ,W(JJ),JJ=1,3)
970   FORMAT(T11,'EIGENVALUE #',I1,'=',D13.6,'+',D13.6,'i')
100   CONTINUE
      STOP
      END
      FUNCTION F(Y,K,PAR)
      DOUBLE PRECISION F,Y(1),PAR(1),DSQRT
      DOUBLE PRECISION X,AX,BX,XBX,FAC1,FAC2,FAC3
      IF(Y(1).LE.0.0D0) Y(1)=1.0D-12
      XBX=Y(1)
      FAC1=2.0D0*PAR(1)*PAR(5)/(1.D0+PAR(2))
      FAC2=PAR(1)**2*PAR(5)/(2.0D0*PAR(4)**3)
      FAC3=8.D0*FAC1*(1.D0-2.D0*XBX)*XBX
      AX=(-FAC2-FAC1+DSQRT((FAC2+FAC1)**2+FAC3))/(4.D0*XBX)
      BX=(1.D0-AX-2.D0*XBX)*PAR(2)/(1.D0+PAR(2))
      X=1.D0-AX-BX-2.D0*XBX
      F=PAR(5)*PAR(6)*X*X-PAR(6)*XBX-PAR(3)*AX*AX*XBX/
     *(2.D0*PAR(5))
      RETURN
      END
```

Appendix B Computer Programs for Chapter 5

This appendix contains the source code of the computer programs which were used in Chapter 5. The first program, DIM3, was used to integrate the system of three ordinary differential equations using the RKF and Gear's methods. The second program, AUTOC, was used to calculate the autocorrelation coefficients. Both of these programs were run on the HP-1000 minicomputer, hence the deviations from standard FORTRAN. Also included in this appendix is the source code for the program which was used to determine the regions of uniqueness and instability for the three ordinary differential equation model presented in Chapter 5. This program was run on the main university computer system (MTS - Amdahl) due to its usage of the IMSL subroutines.

```
C
C  THIS PROGRAM IS USED TO INTEGRATE THE SYSTEM OF THREE
C  ORDINARY DIFFERENTIAL EQUATIONS PRESENTED IN CHAPTER 5.
C  THE INTEGRATION CAN BE PERFORMED USING EITHER GEAR'S
C  METHOD OR THE RKF METHOD.
C
FTN4,X
      BLOCK DATA NAME, NAMED BLOCK DATA AREAS
      DOUBLE PRECISION DA1,DA2,B1,B2,GAM1,GAM2,ALPHA,DA
      COMMON /PARAM/ DA1,DA2,B1,B2,GAM1,GAM2,ALPHA
      COMMON /CT/NPINT,IPINT,NDLAY,IMAX,IBUF(100),IDCBO(144)
      END
      PROGRAM DIM3(,31005), THREE ODE MODEL (CHAOS)
      EXTERNAL F2,F3,PDERV
      DIMENSION NAMEO(3),X(4),NAMEI(3),IDCBI(144)
     *,IBUFA(50,IRBUF(33)
      DOUBLE PRECISION Y(3),A,H,HMX,AER,RER,DA
      DOUBLE PRECISION DA1,DA2,B1,B2,GAM1,GAM2,ALPHA
      DOUBLE PRECISION TPT,YCO,ZHC,G(8,3)
      DOUBLE PRECISION GSAVE(39),GMAX(3),GERR(3),GPW(18)
      COMMON /PARAM/ DA1,DA2,B1,B2,GAM1,GAM2,ALPHA
      COMMON /CT/NPINT,IPINT,NDLAY,IMAX,IBUF(100),IDCBO(144)
      EQUIVALENCE (NAMEI(1),IRBUF(2)),(ICRI,IRBUF(6))
      EQUIVALENCE (ICRO,IRBUF(10)),(LUNO,IRBUF(14))
      CALL DTACH
      LUNW=LOGLU(ISIS)
      LUNR=LUNW
      CALL IFMTE(LUNW)
      CALL GETST(IBUFA,-17,ILOG)
      CALL PARSE(IBUFA,ILOG,IRBUF)
      IF(ILOG.GT.0) GO TO 600
      WRITE(LUNW,800)
800   FORMAT(" NAME OF INPUT DATA FILE ")
      READ(LUNR,290) NAMEI
290   FORMAT(3A2,1X,I2)
      WRITE(LUNW,801)
801   FORMAT("ENTER INPUT CRN, OUTPUT CRN, AND OUTPUT LUN")
      READ(LUNR,*) ICRI,ICRO,LUNO
600   CALL OPEN(IDCBI,IERR,NAMEI,0,1,ICRI)
      CALL READF(IDCBI,IERR,IBUF)
      CALL CODE
      READ(IBUF,*) N,INTG
      CALL READF(IDCBI,IERR,IBUF)
      CALL CODE
      READ(IBUF,*) A,DA,H,HMX,AER,RER
      CALL READF(IDCBI,IERR,IBUF)
      CALL CODE
      READ(IBUF,*) TPT,YCO,ZHC
      CALL READF(IDCBI,IERR,IBUF)
      CALL CODE
      READ(IBUF,*) DA1,B1,GAM1,ALPHA
      IF(N.EQ.2) GO TO 1
      CALL READF(IDCBI,IERR,IBUF)
      CALL CODE
```

```
      READ(IBUF,*) DA2,B2,GAM2
 1    CONTINUE
      CALL READF(IDCBI,IERR,IBUF)
      CALL CODE
      READ(IBUF,*) NINT,IPLOT,NDLAY
      WRITE(LUNO,330) A,DA,H,HMX,AER,RER
      WRITE(LUNO,330) TPT,YCO,DA1,B1,GAM1,ALPHA
      IF(N.EQ.3) WRITE(LUNO,330) ZHC,DA2,B2,GAM2
330   FORMAT(12(1PD13.5))
      WRITE(LUNO,345) NINT,IPLOT,N,INTG,NDLAY
345   FORMAT(6(5X,I4))
      Y(1)=TPT
      Y(2)=YCO
      Y(3)=ZHC
      X(1)=SNGL(A)
      X(2)=SNGL(Y(1))
      X(3)=SNGL(Y(2))
      X(4)=SNGL(Y(3))
      CALL DFILE(IDCBI,ICRI,IDCBO,NAMEO,ICRO)
      CALL CODE
      WRITE(IBUF,350)NINT
350   FORMAT(I6)
      CALL WRITF(IDCBO,IERR,IBUF,3)
      SDA1=SNGL(DA1)
      SDA2=SNGL(DA2)
      SB1=SNGL(B1)
      SB2=SNGL(B2)
      SGAM1=SNGL(GAM1)
      SGAM2=SNGL(GAM2)
      SALPHA=SNGL(ALPHA)
      CALL CODE
      WRITE(IBUF,360) SDA1,SB1,SGAM1,SALPHA
360   FORMAT(12(1PE13.5))
      CALL  WRITF(IDCBO,IERR,IBUF,26)
      IF(N.EQ.2) GO TO 2
      CALL CODE
      WRITE(IBUF,360) SDA2,SB2,SGAM2
      CALL WRITF(IDCBO,IERR,IBUF,20)
 2    CALL CODE
      WRITE(IBUF,360) A,DA,H,HMX,AER,RER
      CALL WRITF(IDCBO,IERR,IBUF,40)
      IF(NDLAY.GT.0) GO TO 5
      CALL CODE
      WRITE(IBUF,360) (X(I),I=1,4)
      CALL WRITF(IDCBO,IERR,IBUF,26)
 5    NPINT=1
      IF(NDLAY.GT.0) NPINT=0
      DO 7 I=1,N
      GMAX(I)=0.01D0
 7    G(1,I)=Y(I)
      JS=0
      DO 10 IPINT=1,NINT
      IF(N.EQ.2.AND.INTG.EQ.0)
     *CALL RKF(A,Y,N,F2,DA,H,HMX,AER,RER,IFLAG)
```

```
      IF(N.EQ.3.AND.INTG.EQ.0)
     *CALL RKF(A,Y,N,F3,DA,H,HMX,AER,RER,IFLAG)
      IF(INTG.EQ.1)CALL SGEAR(N,A,DA,G,GSAVE,H,HMX
     *,RER,1,GMAX,GERR,IFLAG,JS,6,GPW,PDERV)
      IF(INTG.EQ.0) GO TO 9
      DO 8 I=1,N
8     Y(I)=G(1,I)
9     IF(IFLAG.NE.1) GO TO 100
      IF(IPINT.LT.NDLAY) GO TO 10
      X(1)=SNGL(A)
      X(2)=SNGL(Y(1))
      X(3)=SNGL(Y(2))
      X(4)=SNGL(Y(3))
      IF(IPINT/IPLOT*IPLOT.NE.IPINT) GO TO 10
      IF(IMAX.EQ.1) GO TO 10
      CALL CODE
      WRITE(IBUF,360) (X(I),I=1,4)
      CALL WRITF(IDCBO,IERR,IBUF,26)
      WRITE(LUNO,330) A,Y(1),Y(2),Y(3)
      NPINT=NPINT+1
10    CONTINUE
      WRITE(LUNO,910) NPINT
910   FORMAT(" "," # OF POINTS =",I5)
      CALL CLOSE(IDCBO)
      CALL OPEN(IDCBO,IERR,NAMEO,2,1,ICRO)
      CALL RWNDF(IDCBO)
      CALL CODE
      WRITE(IBUF,350) NPINT
      CALL WRITF(IDCBO,IERR,IBUF,3)
      CALL CLOSE(IDCBO)
      STOP
100   CONTINUE
      WRITE(LUNO,915) IFLAG,A,Y(1),Y(2),Y(3)
915   FORMAT(" ",I3,4(D15.6,1X))
      CALL CLOSE(IDCBO)
      CALL OPEN(IDCBO,IERR,NAMEO,2,1,ICRO)
      CALL RWNDF(IDCBO)
      CALL CODE
      WRITE(IBUF,350) NPINT
      CALL WRITF(IDCBO,IERR,IBUF,3)
      CALL CLOSE(IDCBO)
      STOP
      END
      SUBROUTINE F2(T,Y,YP)
      DOUBLE PRECISION Y(2),YP(2),T,DEXP,DSQRT,DABS,DA
      DOUBLE PRECISION DA1,DA2,B1,B2,GAM1,GAM2,ALPHA
      DOUBLE PRECISION TPT,YCO,DTPT,DYCO
      COMMON /PARAM/DA1,DA2,B1,B2,GAM1,GAM2,ALPHA
      TPT=Y(1)
      YCO=Y(2)
      DTPT=ALPHA*DA1*B1*YCO*DEXP(GAM1*TPT/(1.D0+TPT))
     *-ALPHA*TPT
      DYCO=(1.D0-YCO)-DA1*YCO*DEXP(GAM1*TPT/(1.D0+TPT))
      YP(1)=DTPT
```

```
      YP(2)=DYCO
      RETURN
      END
      SUBROUTINE F3(T,Y,YP)
      DOUBLE PRECISION Y(1),YP(1),T,DEXP,DSQRT,DABS,DA
      DOUBLE PRECISION DA1,DA2,B1,B2,GAM1,GAM2,ALPHA
      DOUBLE PRECISION TPT,YCO,ZHC,DTPT,DYCO,DZHC
      COMMON /PARAM/DA1,DA2,B1,B2,GAM1,GAM2,ALPHA
      TPT=Y(1)
      YCO=Y(2)
      ZHC=Y(3)
      DTPT=ALPHA*(DA1*B1*YCO*DEXP(GAM1*TPT/(1.D0+TPT))+
     *DA2*B2*ZHC*DEXP(GAM2*TPT/(1.D0+TPT))-TPT)
      DYCO=1.D0-YCO*(1.D0+DA1*DEXP(GAM1*TPT/(1.D0+TPT)))
      DZHC=1.D0-ZHC*(1.D0+DA2*DEXP(GAM2*TPT/(1.D0+TPT)))
      YP(1)=DTPT
      YP(2)=DYCO
      YP(3)=DZHC
      RETURN
      END
      SUBROUTINE PDERV(T,Y,YP,PW,M,IND)
      DOUBLE PRECISION Y(8,M),YP(M),PW(M,M),T,DEXP,DSQRT
      DOUBLE PRECISION DA1,DA2,B1,B2,GAM1,GAM2,ALPHA
      DOUBLE PRECISION TPT,YCO,ZHC,DTPT,DYCO,DZHC,DABS,DA
      COMMON /PARAM/ DA1,DA2,B1,B2,GAM1,GAM2,ALPHA
      TPT=Y(1,1)
      YCO=Y(1,2)
      ZHC=Y(1,3)
      IF(IND.EQ.1) GO TO 100
      DTPT=ALPHA*(DA1*B1*YCO*DEXP(GAM1*TPT/(1.D0+TPT))+
     *DA2*B2*ZHC*DEXP(GAM2*TPT/(1.D0+TPT))-TPT)
      DYCO=1.D0-YCO*(1.D0+DA1*DEXP(GAM1*TPT/(TPT+1.D0)))
      DZHC=1.D0-ZHC*(1.D0+DA2*DEXP(GAM2*TPT/(TPT+1.D0)))
      YP(1)=DTPT
      YP(2)=DYCO
      YP(3)=DZHC
      RETURN
100   CONTINUE
      PW(2,1)=-DA1*YCO*GAM1*DEXP(GAM1*TPT/(1.D0+TPT))/
     *((1.D0+TPT)**2)
      PW(2,2)=-1.D0-DA1*DEXP(GAM1*TPT/(TPT+1.D0))
      PW(2,3)=0.0D0
      PW(3,1)=-DA2*ZHC*GAM2*DEXP(GAM2*TPT/(TPT+1.D0))/
     *((TPT+1.D0)**2)
      PW(3,2)=0.0D0
      PW(3,3)=-1.0D0-DA2*DEXP(GAM2*TPT/(TPT+1.D0))
      PW(1,1)=ALPHA*(-B1*PW(2,1)-B2*PW(3,1)-1.D0)
      PW(1,2)=ALPHA*DA1*B1*DEXP(GAM1*TPT/(1.D0+TPT))
      PW(1,3)=ALPHA*DA2*B2*DEXP(GAM2*TPT/(1.D0+TPT))
      RETURN
      END
      SUBROUTINE DFILE(IDCBI,ICRI,IDCBO,NAMEO,ICRO)
      DIMENSION IDCBO(144),NAMEO(3),ISIZE(2),IDCBI(144)
      CALL READF(IDCBI,IERR,NAMEO)
```

```
      CALL CLOSE(IDCBI)
      ISIZE(1)=48
      ITYPE=3
      ISECU=1
      CALL OPEN(IDCBO,IERR,NAMEO,0,1,ICRO)
      CALL CLOSE(IDCBO)
      CALL PURGE(IDCBO,IERR,NAMEO,1,ICRO)
      CALL CREAT(IDCBO,IERR,NAMEO,ISIZE,ITYPE,ISECU,ICRO)
      CALL OPEN(IDCBO,IERR,NAMEO,0,ISECU,ICRO)
      RETURN
      END
      SUBROUTINE RKF(A,Y,N,F,DA,H,HMX,ABSER,RELER,IFLAG)
     *,VARIABLE STEP INTEGRATION OF ODE'S, DTL 11/06/79
C
C  THIS CODE INTEGRATES A SYSTEM OF FIRST ORDER ORDINARY
C  DIFFERENTIAL EQUATIONS BY RUNGE-KUTTA-FEHLBERG METHOD
C  WITH AUTOMATIC ESTIMATION OF LOCAL ERROR AND STEP SIZE
C  ADJUSTMENT -- SHAMPINE AND ALLEN (REF 5.16)
C
      DOUBLE PRECISION Y(N),YTEMP(20),TEMP(20),R(20)
      DOUBLE PRECISION K1(20),K2(20),K3(20),K4(20),K5(20)
     *,K(20),U,RELER,ABSER,HMX,A,B,DA,HMAX,H,HKEEP,ARG,RATIO
     *,DABS,DMAX1,DMIN1,DSIGN,DSQRT,TR,ASV,HMIMA
      REAL DOUT(20)
      COMMON /CT/NPINT,IPINT,NDLAY,IMAX,IBUF(100),IDCBO(144)
      U=1.0D-16
      IMAX=0
      IF(RELER.LT.0.0D0.OR.ABSER.LT.0.0D0) GO TO 18
      IF(RELER+ABSER.EQ.0.0D0) GO TO 18
      IF(HMX.LE.0.0D0) GO TO 18
      B=A+DA
      ASV=A
      IF(DABS(DA).LE.13.D0*U*DMAX1(DABS(A),DABS(B)))GO TO 19
      HMAX=DMIN1(HMX,DABS(DA))
      IF(DABS(H).LE.13.0D0*U*DABS(A)) H=HMAX
      IADJS=0
3     H=DSIGN(DMIN1(DABS(H),HMAX),DA)
      IF(DABS(B-A).GT.(1.25D0+10.D0*U)*DABS(H)) GO TO 4
      HKEEP=H
      IADJS=1
      H=B-A
4     CALL F(A,Y,K1)
5     CONTINUE
      DO 6 I=1,N
6     YTEMP(I)=Y(I)+0.25D0*H*K1(I)
      ARG=A+0.25D0*H
      CALL F(ARG,YTEMP,K2)
      DO 7 I=1,N
7     YTEMP(I)=Y(I)+H*(K1(I)*3.D0/32.D0+K2(I)*(9.D0/32.D0))
      ARG=A+H*(3.D0/8.D0)
      CALL F(ARG,YTEMP,K3)
      DO 8 I=1,N
8     YTEMP(I)=Y(I)+H*(K1(I)*(1932.D0/2197.D0)-K2(I)
     **(7200.D0/2197.D0)+K3(I)*(7296.D0/2197.D0))
```

```
      ARG=A+H*(12.D0/13.D0)
      CALL F(ARG,YTEMP,K4)
      DO 9 I=1,N
9     YTEMP(I)=Y(I)+H*(K1(I)*(439.D0/216.D0)-8.D0*K2(I)
     *+K3(I)*(3680.D0/513.D0)-K4(I)*(845.D0/4104.D0))
      ARG=A+H
      CALL F(ARG,YTEMP,K5)
      DO 10 I=1,N
10    YTEMP(I)=Y(I)+H*(-K1(I)*(8.D0/27.D0)+2.D0*K2(I)
     *-K3(I)*(3544.D0/2565.D0)+K4(I)*(1859.D0/4104.D0)
     *-K5(I)*(11.D0/40.D0))
      ARG=A+0.5D0*H
      CALL F(ARG,YTEMP,K6)
      DO 11 I=1,N
      TEMP(I)=K1(I)*(25.D0/216.D0)+K3(I)*(1408.D0/2565.D0)
     *+K4(I)*(2197.D0/4104.D0)-0.2D0*K5(I)
11    YTEMP(I)=Y(I)+H*TEMP(I)
      DO 12 I=1,N
12    R(I)=K1(I)/360.D0-K3(I)*(128.D0/4275.D0)-K4(I)
     **(2197.D0/75240.D0)+K5(I)/50.D0+K6(I)*(2.D0/55.D0)
      RATIO=0.0D0
      DO 13 I=1,N
      TR=DABS(R(I))/(RELER*DABS(YTEMP(I))+ABSER)
13    RATIO=DMAX1(RATIO,TR)
      IF(RATIO.GT.1.D0) GO TO 15
      IF(IPINT.LE.NDLAY) GO TO 45
      DO 40 I=1,N
      IF(K1(I)*K5(I).GT.0.0D0) GO TO 40
      IF(K1(I).EQ.0.0D0) GO TO 40
      IF((IPINT/IPLOT*IPLOT.EQ.IPINT).AND.
     *(B-A.LT.1.D-04)) IMAX=1
      IF((IPINT/IPLOT*IPLOT.EQ.IPINT).AND.
     *(A-ASV.LT.0.0001D0))IMAX=2
C     *.OR.(A-ASV.LT.0.0001D0))) IMAX=1
      IF(IMAX.EQ.2) CALL POSNT(IDCBO,IERR,-1,0)
      IF(IMAX.EQ.2) NPINT=NPINT-1
      DOUT(1)=SNGL(A)
      HMIMA=H*DABS(K1(I)/(K1(I)-K5(I)))
      DO 35 JJ=1,N
35    DOUT(JJ+1)=SNGL(Y(JJ))+SNGL(HMIMA*K1(JJ))
      M=N+1
      IF(N.EQ.2) M=N+2
      CALL CODE
      WRITE(IBUF,900) (DOUT(JJ),JJ=1,M)
900   FORMAT(11(1PE13.5))
      CALL WRITF(IDCBO,IERR,IBUF,6*M+2)
      NPINT=NPINT+1
      GO TO 45
40    CONTINUE
45    CONTINUE
      DO 14 I=1,N
14    Y(I)=YTEMP(I)
      A=A+H
      IF(IADJS.EQ.1) GO TO 16
```

```
      RATIO=DMAX1(RATIO,6.5536D-04)
15    RATIO=DMIN1(RATIO,4096.D0)
      H=0.8D0*H/DSQRT(DSQRT(RATIO))
      IF(DABS(H).LE.13.D0*U*DABS(DA)) GO TO 19
      IF(RATIO.LE.1.D0) GO TO 3
      IADJS=0
      GO TO 5
16    IFLAG=1
      H=HKEEP
      RETURN
18    IFLAG=3
      RETURN
19    IFLAG=4
      RETURN
      END
      SUBROUTINE SGEAR(N,T,DT,Y,SAVE,H,HMX,EPS,MF,YMAX
     *,ERROR,KFLAG,JSTART,MAXDER,PW,PDERV)
C
C
C     INTEGRATION OF STIFF AND NON-STIFF SETS OF N ODE'S
C     'NUMERICAL INITIAL VALUE PROBLEMS IN ORDINARY
C     DIFFERENTIAL EQUATIONS', BY C. W. GEAR (REF 5.15)
C
C
C     DESCRIPTION OF VARIABLES IN CALL LIST
C N ... # OF FIRST ORDER ODE'S
C T ... THE INDEPENDENT VARIABLE
C DT .. CODE WILL ATTEMPT TO INTEGRATE FROM T TO T+DT
C     (PROBABLY USING SEVERAL STEPS DEPENDING ON H AND HMX)
C Y ... AN 8 BY N ARRAY CONTAINING THE DEPENDENT VARIABLES
C    AND THEIR SCALED DERIVATIVES. Y(1,I) I=1,N CONTAINS THE
C    VALUES OF Y AT T. ONLY Y(1,I) IS PROVIDED BY THE
C    CALLING PROGRAM ON THE FIRST ENTRY. Y(J+1,I) CONTAINS
C    THE J-TH DERIVATIVE SCALED BY H**J/J! .
C SAVE ... WORK AREA OF SIZE 13 BY N
C H ... THE STEP SIZE TO BE ATTEMPTED ON THE NEXT STEP.
C       A SMALL VALUE OF H SHOULD BE USED ON THE FIRST CALL.
C HMAX ... THE MAXIMUM ALLOWABLE STEP SIZE.
C EPS ... THE EUCLIDEAN OF THE SINGLE STEP ERROR ESTIMATES
C       DIVIDED BY YMAX(I) MUST BE LESS THAN EPS. TO ACHIEVE
C       THIS, THE ORDER AND/OR THE STEP SIZE IS ALTERED.
C  MF ... THE METHOD INDICATOR.
C         0 - AN ADAMS PREDICTOR CORRECTOR IS USED.
C         1 - A MULTI-STEP METHOD FOR STIFF SYSTEMS IS USED.
C           THE JACOBIAN MATRIX MUST BE SUPPLIED BY PDERV
C         2 - SAME AS 1, EXCEPT NUMERICAL DIFFERENCING USED
C             TO GENERATE THE JACOBIAN.
C YMAX ... VECTOR OF N VALUES WHICH CONTAIN THE MAXIMUM OF
C           EACH Y FOUND SO FAR. NORMALLY SET TO 1 ON ENTRY.
C ERROR ... VECTOR OF N VALUES OF SINGLE STEP ERRORS FOR Y'S
C KFLAG ... A COMPLETION CODE
C           1 - THE STEP WAS SUCCESFUL
C          -1 - STEP TAKEN WITH H=HMIN, BUT EPS NOT MET
C          -2 - THE MAXIMUM ORDER SPECIFIED WAS TOO LARGE.
```

```
C          -3 - CORRECTOR CONVERGENGE COULD NOT BE ACHIEVED
C          -4 - THE REQUESTED ERROR IS TOO SMALL
C JSTART ... AN INPUT INDICATOR
C             -1 - REPEAT THE LAST STEP WITH A NEW H
C              0 - PERFORM THE FIRST STEP (INITIALIZATION)
C             +1 - TAKE A NEW STEP CONTINUING FROM THE LAST
C           AT EXIT, JSTART IS SET TO NQ, THE CURRENT ORDER
C           OF THE METHOD. NQ IS ALSO THE ORDER OF THE
C           MAXIMUM DERIVATIVE AVAILABLE.
C MAXDER ... THE MAXIMUM DERIVATIVE THAT SHOULD BE USED IN
C             THE MEHOD. THIS RESTRICTS THE ORDER, AS ORDER
C             IS EQUAL TO THE HIGHEST DERIVATIVE USED.
C             IF MF=0, MAXDER < 8 IS NECESSARY.
C             IF MF=1 OR 2, MAXDER < 7 IS NECESSARY.
C PW ... WORK AREA OF SIZE 2*N**2
C PDERV ... EXTERNAL SUBROUTINE PDERV(T,Y,DY,PW,M,IND)
C           THE NAME OF THIS SUBROUTINE WUST BE PLACED IN
C           AN EXTERNAL STATEMENT IN THE MAIN PROGRAM.
C           IF IND = 0, THEN PDERV IS USED TO CALCULATE THE
C           VALUES OF THE DERIVATIVES OF THE DEPENDENT
C           VARIABLES (STORED IN Y(1,I),I=1,N)) WITH RESPECT
C           TO THE INDEPENDENT VARIABLE T. THESE DERIVATIVES
C           ARE PLACED IN THE ARRAY DY(I).
C           IF MF = 1, THEN IF IND = 1 , PDERV IS USED TO
C           DETERMINE THE ELEMENTS IN THE JACOBIAN MATRIX.
C           PW(I,J) SHOULD BE ASSIGNED THE VALUE OF THE
C           PARTIAL DERIVATIVE OF THE I-TH EQUATION WITH
C           RESPECT TO THE J-TH DEPENDENT VARIABLE.
C           PW SHOULD BE DIMENSIONED PW(M,M) OR PW(M,1)
C
      DOUBLE PRECISION Y(8,1),YMAX(1),SAVE(10,1),ERROR(1)
     *,PERTST(7,2,3),PW(1),A(8)
     *,BND,D,DBLE,DMIN1,DMAX1,DABS,E,EDWN,ENQ1,ENQ2,
     *,ENQ3,EPS,ERROR,EUP,H,HMAX,HMIN,HNEW,HOLD,
     *,PEPSH,PR1,PR2,PR3,R,R1,RACUM,T,TOLD,HMX,B,TSV,U,DT,S
      REAL DOUT(20)
      COMMON /CT/NPINT,IPINT,NDLAY,IMAX,IBUF(100),IDCBO(144)
      DATA PERTST /2.D0,4.5D0,7.3333D0,10.42D0,13.7D0
     *,17.15D0,1.D0,2.D0,12.D0,24.D0,37.89D0,53.33D0,70.08D0
     *,87.97D0,3.D0,6.D0,9.167D0,12.5D0,15.98D0,1.D0,1.D0,
     *,12.D0,24.D0,37.89D0,53.33D0,70.08D0,87.97D0,1.D0,
     *,1.D0,1.D0,0.5D0,0.1667D0,0.04133D0,0.008267D0,1.D0,
     *,1.D0,1.D0,2.D0,1.D0,0.3157D0,.07407D0,.0139D0/
      DATA A(2) /-1.0D0/
      U=1.D-16
      IMAX=0
      B=T+DT
      TSV=T
      HMAX=DMIN1(HMX,DABS(DT))
      HMIN=DMAX1(U*T,DMIN1(U,U*HMAX))
      IADJS=0
50    H=DMAX1(H,13.0D0*U*DABS(T))
      IF(DABS(B-T).GT.(1.D0+10.D0*U)*DABS(H))GO TO 70
      IADJS=1
```

```
      H=B-T
70    CONTINUE
      IRET=1
      KFLAG=1
      IF(JSTART.LE.0) GO TO 140
100   DO 110 I=1,N
      DO 110 J=1,K
110   SAVE(J,I)=Y(J,I)
      HOLD=HNEW
      IF(H.EQ.HOLD) GO TO 130
120   RACUM=H/HOLD
      IRET1=1
      GO TO 750
130   NQOLD=NQ
      TOLD=T
      RACUM=1.D0
      IF(JSTART.GT.0) GO TO 250
      GO TO 170
140   IF(JSTART.EQ.-1) GO TO 160
      NQ=1
      N3=N
      N1=N*10
      N2=N1+1
      N4=N**2
      N5=N1+N
      N6=N5+1
      N7=12*N
      DO 145 JJ=1,N
145   SAVE(N7+JJ,1)=0.0D0
      CALL PDERV(T,Y,SAVE(N2,1),PW,N3,0)
      DO 150 I=1,N
150   Y(2,I)=SAVE(N1+I,1)*H
      HNEW=H
      K=2
      GO TO 100
160   IF(NQ.EQ.NQOLD) JSTART=1
      T=TOLD
      NQ=NQOLD
      K=NQ+1
      GO TO 120
170   IF(MF.EQ.0) GO TO 180
      IF(NQ.GT.6) GO TO 190
      GO TO (221,222,223,224,225,226),NQ
180   IF(NQ.GT.7) GO TO 190
      GO TO(211,212,213,214,215,216,217),NQ
190   KFLAG=-2
      RETURN
211   A(1)=-1.D0
      GO TO 230
212   A(1)=-1.D0/2.D0
      A(3)=-1.D0/2.D0
      GO TO 230
213   A(1)=-5.D0/12.D0
      A(3)=-3.D0/4.D0
```

```
      A(4)=-1.D0/6.D0
      GO TO 230
214   A(1)=-3.D0/8.D0
      A(3)=-11.D0/12.D0
      A(4)=-1.D0/3.D0
      A(5)=-1.D0/24.D0
      GO TO 230
215   A(1)=-251.D0/720.D0
      A(3)=-25.D0/24.D0
      A(4)=-35.D0/72.D0
      A(5)=-5.D0/48.D0
      A(6)=-1.0D0/120.0D0
      GO TO 230
216   A(1)=-95.D0/288.D0
      A(3)=-137.D0/120.D0
      A(4)=-5.D0/8.D0
      A(5)=-17.D0/96.D0
      A(6)=-1.D0/40.D0
      A(7)=-1.D0/720.D0
      GO TO 230
217   A(1)=-19087.D0/60480.D0
      A(3)=-49.D0/40.D0
      A(4)=-203.D0/270.D0
      A(5)=-49.D0/192.D0
      A(6)=-7.D0/144.D0
      A(7)=-7.D0/1440.D0
      A(8)=-1.D0/5040.D0
      GO TO 230
221   A(1)=-1.D0
      GO TO 230
222   A(1)=-2.D0/3.D0
      A(3)=-1.D0/3.D0
      GO TO 230
223   A(1)=-6.D0/11.D0
      A(3)=-6.D0/11.D0
      A(4)=-1.D0/11.D0
      GO TO 230
224   A(1)=-12.D0/25.D0
      A(3)=-7.D0/10.D0
      A(4)=-1.D0/5.D0
      A(5)=-1.D0/50.D0
      GO TO 230
225   A(1)=-120.D0/274.D0
      A(3)=-225.D0/274.D0
      A(4)=-85.D0/274.D0
      A(5)=-15.D0/274.D0
      A(6)=-1.D0/274.D0
      GO TO 230
226   A(1)=-180.D0/441.D0
      A(3)=-58.D0/63.D0
      A(4)=-15.D0/36.D0
      A(5)=-25.D0/252.D0
      A(6)=-3.D0/252.D0
      A(7)=-1.D0/1764.D0
```

```
230   K=NQ+1
      IDOUB=K
      MTYP=(4-MF)/2
      ENQ1=0.5D0/DBLE(FLOAT(NQ))
      ENQ2=0.5D0/DBLE(FLOAT(NQ+1))
      ENQ3=0.5D0/DBLE(FLOAT(NQ+2))
      PEPSH=EPS
      EUP=(PERTST(NQ,MTYP,2)*PEPSH)**2
      E=(PERTST(NQ,MTYP,1)*PEPSH)**2
      EDWN=(PERTST(NQ,MTYP,3)*PEPSH)**2
      IF(EDWN.EQ.0.0D0) GO TO 780
      BND=EPS*ENQ3/DBLE(FLOAT(N))
240   IWEVAL=MF
      GO TO(250,680),IRET
250   T=T+H
      DO 260 J=2,K
      DO 260 J1=J,K
      J2=K-J1+J-1
      DO 260 I=1,N
260   Y(J2,I)=Y(J2,I)+Y(J2+1,I)
      DO 270 I=1,N
270   ERROR(I)=0.0D0
      DO 430 L=1,3
      CALL PDERV(T,Y,SAVE(N2,1),PW,N3,0)
      IF(IWEVAL.LT.1) GO TO 350
      IF(MF.EQ.2) GO TO 310
      CALL PDERV(T,Y,SAVE(N2,1),PW,N3,1)
      R=A(1)*H
      DO 280 I=1,N4
280   PW(I)=PW(I)*R
290   DO 300 I=1,N
300   PW(I*(N3+1)-N3)=1.D0+PW(I*(N3+1)-N3)
      IWEVAL=-1
      CALL MXINV(PW,N,N3,2*N3,J1)
      IF(J1.GT.0) GO TO 350
      GO TO 440
310   DO 320 I=1,N
320   SAVE(9,I)=Y(1,I)
      DO 340 J=1,N
      R=EPS*DMAX1(EPS,DABS(SAVE(9,J)))
      Y(1,J)=Y(1,J)+R
      D=A(1)*H/R
      CALL PDERV(T,Y,SAVE(N6,1),PW,N3,0)
      DO 330 I=1,N
330   PW(I+(J-1)*N3)=(SAVE(N5+I,1)-SAVE(N1+I,1))*D
340   Y(1,J)=SAVE(9,J)
      GO TO 290
350   IF(MF.NE.0) GO TO 370
      DO 360 I=1,N
360   SAVE(9,I)=Y(2,I)-SAVE(N1+I,1)*H
      GO TO 410
370   DO 380 I=1,N
380   SAVE(N5+I,1)=Y(2,I)-SAVE(N1+I,1)*H
      DO 400 I=1,N
```

```
      D=0.0D0
      DO 390 J=1,N
390   D=D+PW(I+(J-1)*N3)*SAVE(N5+J,1)
400   SAVE(9,I)=D
410   NT=N
      DO 420 I=1,N
      Y(1,I)=Y(1,I)+A(1)*SAVE(9,I)
      Y(2,I)=Y(2,I)-SAVE(9,I)
      ERROR(I)=ERROR(I)+SAVE(9,I)
      IF(DABS(SAVE(9,I)).LE.(BND*YMAX(I))) NT=NT-1
420   CONTINUE
      IF(NT.LE.0) GO TO 490
430   CONTINUE
      IADJS=0
440   T=TOLD
      IF((H.LE.(HMIN*1.00001D0)).AND.
     *((IWEVAL-MTYP).LT.-1)) GO TO 460
      IF((MF.EQ.0).OR.(IWEVAL.NE.0)) RACUM=RACUM*0.25D0
      IWEVAL=MF
      IRET1=2
      GO TO 750
460   KFLAG=-3
470   DO 480 I=1,N
      DO 480 J=1,K
480   Y(J,I)=SAVE(J,I)
      H=HOLD
      NQ=NQOLD
      JSTART=NQ
      RETURN
490   D=0.0D0
      DO 500 I=1,N
500   D=D+(ERROR(I)/YMAX(I))**2
      IWEVAL=0
      IF(D.GT.E) GO TO 540
      IF(K.LT.3) GO TO 520
      DO 510 J=3,K
      DO 510 I=1,N
510   Y(J,I)=Y(J,I)+A(J)*ERROR(I)
520   KFLAG=1
      HNEW=H
      IF(IDOUB.LE.1) GO TO 550
      IDOUB=IDOUB-1
      IF(IDOUB.GT.1) GO TO 700
      DO 530 I=1,N
530   SAVE(10,I)=ERROR(I)
      GO TO 700
540   KFLAG=KFLAG-2
      IADJS=0
      IF(H.LE.(HMIN*1.00001D0)) GO TO 740
      T=TOLD
      IF(KFLAG.LE.-5) GO TO 720
550   PR2=(D/E)**ENQ2*1.2D0
      PR3=1.D+20
      IF((NQ.GE.MAXDER).OR.(KFLAG.LE.-1)) GO TO 570
```

```
      D=0.0D0
      DO 560 I=1,N
560   D=D+((ERROR(I)-SAVE(10,I))/YMAX(I))**2
      PR3=(D/EUP)**ENQ3*1.4D0
570   PR1=1.D+20
      IF(NQ.LE.1) GO TO 590
      D=0.0D0
      DO 580 I=1,N
580   D=D+(Y(K,I)/YMAX(I))**2
      PR1=(D/EDWN)**ENQ1*1.3D0
590   CONTINUE
      IF(PR2.LE.PR3) GO TO 650
      IF(PR3.LT.PR1) GO TO 660
600   R=1.D0/DMAX1(PR1,1.D-04)
      NEWQ=NQ-1
610   IDOUB=10
      IF((KFLAG.EQ.1).AND.(R.LT.(1.1D0))) GO TO 700
      IF(NEWQ.LE.NQ) GO TO 630
      DO 620 I=1,N
620   Y(NEWQ+1,I)=ERROR(I)*A(K)/DBLE(FLOAT(K))
630   K=NEWQ+1
      IF(KFLAG.EQ.1) GO TO 670
      RACUM=RACUM*R
      IRET1=3
      GO TO 750
640   IF(NEWQ.EQ.NQ) GO TO 250
      NQ=NEWQ
      GO TO 170
650   IF(PR2.GT.PR1) GO TO 600
      NEWQ=NQ
      R=1.D0/DMAX1(PR2,1.D-04)
      GO TO 610
660   R=1.D0/DMAX1(PR3,1.D-04)
      NEWQ=NQ+1
      GO TO 610
670   IRET=2
      R=DMIN1(R,HMAX/DABS(H))
      H=H*R
      HNEW=H
      IF(NQ.EQ.NEWQ) GO TO 680
      NQ=NEWQ
      GO TO 170
680   R1=1.D0
      DO 690 J=2,K
      R1=R1*R
      DO 690 I=1,N
690   Y(J,I)=Y(J,I)*R1
      IDOUB=K
700   DO 710 I=1,N
710   YMAX(I)=DMAX1(YMAX(I),DABS(Y(1,I)))
      JSTART=NQ
      IF(IPINT.LE.NDLAY) GO TO 714
      DO 712 JJ=1,N
      IF((SAVE(N7+JJ,1)*Y(2,JJ).GT.0.0D0).OR.
```

```
     *(SAVE(N7+JJ,1).EQ.0.0D0)) GO TO 712
      IF((IPINT/IPLOT*IPLOT.EQ.IPINT).AND.
     *((B-T).LT.0.0001D0)) IMAX=1
      IF((IPINT/IPLOT*IPLOT.EQ.IPINT).AND.
     *((T-TSV).LT.0.0001D0)) IMAX=2
      IF(IMAX.EQ.2) CALL POSNT(IDCBO,IERR,-1,0)
      IF(IMAX.EQ.2) NPINT=NPINT-1
      DOUT(1)=SNGL(T)
      DO 713 KK=1,N
713   DOUT(KK+1)=0.0
      S=-DABS(Y(2,JJ)/(Y(2,JJ)-SAVE(N7+JJ,1)))
      NQQ1=NQ+1
      DO 715 KK=1,N
      DO 711 J=1,NQQ1
 711  DOUT(KK+1)=DOUT(KK+1)+SNGL(Y(J,KK)*S**(J-1))
C     DOUT(KK+1)=SNGL(Y(1,KK)+S*H*Y(2,KK))
715   CONTINUE
      M=N+1
      IF(N.EQ.2) M=N+2
      CALL CODE
      WRITE(IBUF,900) (DOUT(KK),KK=1,M)
900   FORMAT(11(1PE13.5))
      CALL WRITF(IDCBO,IERR,IBUF,6*M+2)
      NPINT=NPINT+1
      GO TO 714
712   CONTINUE
714   DO 716 JJ=1,N
716   SAVE(N7+JJ,1)=Y(2,JJ)
      IF(IADJS.EQ.0) GO TO 50
      RETURN
720   IF(NQ.EQ.1) GO TO 780
      CALL PDERV(T,Y,SAVE(N2,1),PW,N3,0)
      R=H/HOLD
      DO 730 I=1,N
      Y(1,I)=SAVE(1,I)
      SAVE(2,I)=HOLD*SAVE(N1+I,1)
730   Y(2,I)=SAVE(2,I)*R
      NQ=1
      KFLAG=1
      GO TO 170
740   KFLAG=-1
      HNEW=H
      JSTART=NQ
      RETURN
750   RACUM=DMAX1(DABS(HMIN/HOLD),RACUM)
      RACUM=DMIN1(RACUM,DABS(HMAX/HOLD))
      R1=1.D0
      DO 760 J=2,K
      R1=R1*RACUM
      DO 760 I=1,N
760   Y(J,I)=SAVE(J,I)*R1
      H=HOLD*RACUM
      DO 770 I=1,N
770   Y(1,I)=SAVE(1,I)
```

```
      IDOUB=K
      GO TO (130,250,640),IRET1
780   KFLAG=-4
      IF(DABS(B-T).GT.(1.D0+10.D0*U)*DABS(H)) GO TO 470
      T=B
      GO TO 710
C     GO TO 470
      END
C DECK MXINV
C
.....................................................
C
C       SUBROUTINE MXINV
C
C       PURPOSE
C          INVERSION OF A REAL SQUARE MATRIX.
C
C       USAGE
C          CALL MXINV(A,N,M,M2,IER)
C
C       DESCRIPTION OF PARAMETERS
C A     -  MATRIX TO BE INVERTED.
C N     -  A MATRIX DIMENSION (UPPER LEFT CORNER)
C M     -  ROW DIMENSION OF A IN CALLING PROGRAM
C M2    -  2*M # OF COLUMNS IN A MATRIX IN CALLING PROGRAM
C IER   -  ERROR FLAG.
C          =1, NORMAL RETURN.
C          =-1, MATRIX A IS ALGORITHMICALLY SINGULAR.
C
C   MATRIX A IS DESTROYED, AND IS REPLACED BY ITS INVERSE
C
C       SUBROUTINES AND FUNCTION SUBPROGRAMS REQUIRED
C          DABS(FORTRAN)
C
C       REFERENCE
C          MATRIXALGEBRA OG ALGEBRAISKE LIGNINGER.
C          VILLADSEN,J.
C          1968, POLYTEKNISK FORLAG, COPENHAGEN, DENMARK.
C
.....................................................
C
      SUBROUTINE MXINV(A, N, M, M2, IER)
      DOUBLE PRECISION A(M,M2), DET, OPSTO, DABS
      INTEGER I, IER, IP1, J, K, N, NP1, NT2
      NT2 = N * 2
      DET = 1.D0
      NP1 = N + 1
      DO 40 I = 1, N
        DO 40 J = NP1, NT2
          A(I,J) = 0.D0
          IF (I - J + N) 40, 30, 40
   30     A(I,J) = 1.D0
   40 CONTINUE
      DO 140 I = 1, N
```

```
      IP1 = I + 1
      OPSTO = DABS(A(I,I))
      K = I
      DO 60 J = I, N
        IF (DABS(A(J,I)) - OPSTO) 60, 60, 50
 50     K = J
        OPSTO = DABS(A(J,I))
 60   CONTINUE
      IF (K - I) 70, 90, 70
 70   DET = -DET
      DO 80 J = I, NT2
        OPSTO = A(I,J)
        A(I,J) = A(K,J)
 80   A(K,J) = OPSTO
 90   IF (A(I,I)) 100, 180, 100
100   OPSTO = 1.D0/ A(I,I)
      DET = DET / OPSTO
      DO 110 J = I, NT2
110   A(I,J) = A(I,J) * OPSTO
      DO 140 J = 1, N
        IF (I - J) 120, 140, 120
120     OPSTO = A(J,I)
        DO 130 K = IP1, NT2
130     A(J,K) = A(J,K) - OPSTO * A(I,K)
140 CONTINUE
150 DO 170 I = 1, N
      DO 160 J = 1, N
        NJ = N + J
160   A(I,J) = A(I,NJ)
170 CONTINUE
    IER=1
    RETURN
180 IER = -1
    RETURN
    END
```

```
C
C  THIS PROGRAM IS USED TO CALCULATE THE AUTOCORRELATION
C  COEFFICIENTS FOR A SERIES OF TEMPERATURE MAXIMA.
C  THE AUTOCORRELATION COEFFICIENTS CAN BE CALCULATED
C  BASED ON EITHER THE AMPLITUDE OR THE FREQUENCY OF
C  THE TEMPERATURE MAXIMA.
C
FTN4,X
      PROGRAM AUTOC(,30500), CALCULATION OF AUTOCORRELATIONS
      DIMENSION IDCBI(144),NAMEI(3),T(10000),AC(50),Z(4)
      DIMENSION IBUF(100),NAMEO(3),IDCBO(144),ZS(4)
      DOUBLE PRECISION T1BAR,TKBAR,VART1,VARTK,VAR
     *,DBLE,AUTCV
      LUNW=LOGLU(ISIS)
      LUNR=LUNW
      CALL IFMTE(LUNW)
      CALL IER0E(LUNW)
      WRITE(LUNW,800)
800   FORMAT(" ENTER INPUT DATA FILE NAME, AND ICRI")
      READ(LUNW,805) NAMEI,ICRI
805   FORMAT(3A2,1X,I3)
      WRITE(LUNW,801)
801   FORMAT(" ENTER OUTPUT FILE NAME, AND ICRO")
      READ(LUNW,805) NAMEO,ICRO
      CALL DFILE(IDCBO,NAMEO,ICRO)
      CALL OPEN(IDCBI,IERR,NAMEI,0,1,ICRI)
      CALL READF(IDCBI,IERR,IBUF,4)
      CALL CODE
      READ(IBUF,*) NINT
      WRITE(LUNW,704) NINT
704   FORMAT(" NINT = ",I5)
      WRITE(LUNW,705)
705   FORMAT(" ENTER NINT, AND K (# OF AUTOCORRELATIONS)  ")
      READ(LUNW,*) NINT,K
      WRITE(LUNW,706)
706   FORMAT("ENTER TYPE OF A-C, 1=TIME(FREQ), 2=TEMP(AMP)")
      READ(LUNR,*) ITYPE
      KP1=K+1
      CALL CODE
      WRITE(IBUF,910) KP1
      CALL WRITF(IDCBO,IERR,IBUF,3)
910   FORMAT(I6)
      CALL READF(IDCBI,IERR,IBUF,26)
      CALL WRITF(IDCBO,IERR,IBUF,26)
      CALL READF(IDCBI,IERR,IBUF,20)
      CALL WRITF(IDCBO,IERR,IBUF,20)
      CALL READF(IDCBI,IERR,IBUF,39)
      CALL WRITF(IDCBO,IERR,IBUF,39)
      IF(ITYPE.EQ.2) GO TO 10
      DO  5 I=1,NINT
      CALL READF(IDCBI,IERR,IBUF,26)
      CALL CODE
      READ(IBUF,*) (Z(II),II=1,4)
 5    T(I)=Z(2)-Z(1)
```

```
      GO TO 20
10    DO 15 I=1,NINT
      CALL READF(IDCBI,IERR,IBUF,26)
      CALL CODE
      READ(IBUF,*) (Z(II),II=1,4)
15    T(I)=Z(3)
20    CALL CLOSE(IDCBI)
      DO 60 IK=1,K
      NSUM=NINT-IK
      T1BAR=0.0D0
      TKBAR=0.0D0
      DO 30 ISUM=1,NSUM
      T1BAR=T1BAR+DBLE(T(ISUM))/DBLE(FLOAT(NSUM))
 30   TKBAR=TKBAR+DBLE(T(ISUM+IK))/DBLE(FLOAT(NSUM))
      VART1=0.0D0
      VARTK=0.0D0
      DO 40 ISUM=1,NSUM
      VART1=VART1+((DBLE(T(ISUM))-T1BAR)**2)/
     *DBLE(FLOAT(NSUM))
  40  VARTK=VARTK+((DBLE(T(ISUM+IK))-TKBAR)**2)/
     *DBLE(FLOAT(NSUM))
      VAR=(VART1+VARTK)/2.0D0
      AUTCV=0.0D0
      DO 50 ISUM=1,NSUM
50    AUTCV=AUTCV+(DBLE(T(ISUM))-T1BAR)*(DBLE(T(ISUM+IK))
     *-TKBAR)/DBLE(FLOAT(NSUM))
60    AC(IK)=SNGL(AUTCV/VAR)
      ACO=1.
      IO=0
      CALL CODE
      WRITE(IBUF,920) IO,ACO
      CALL WRITF(IDCBO,IERR,IBUF,9)
      WRITE(LUNW,920) IO,ACO
920   FORMAT(I4,1X,1PE13.5)
      DO 80 IK=1,K
      CALL CODE
      WRITE(IBUF,920) IK,AC(IK)
      CALL WRITF(IDCBO,IERR,IBUF,9)
 80   WRITE(LUNW,920) IK,AC(IK)
900   FORMAT(6(1PE13.5))
      CALL CODE
      WRITE(IBUF,900) T1BAR,TKBAR,VART1,VARTK
      CALL WRITF(IDCBO,IERR,IBUF,26)
      WRITE(LUNW,900) T1BAR,TKBAR,VART1,VARTK
      CALL LOCF(IDCBO,IERR,IREC,IRB,IOFF,JSEC)
      ITRUN=(JSEC/2)-(IRB+1)
      CALL CLOSE(IDCBO,IERR,ITRUN)
      STOP
      END
      SUBROUTINE DFILE(IDCBO,NAMEO,ICRO)
      DIMENSION IDCBO(144),NAMEO(3),ISIZE(2)
      ISIZE(1)=-1
      ITYPE=3
      ISECU=1
```

```
CALL OPEN(IDCBO,IERR,NAMEO,0,1,ICRO)
CALL CLOSE(IDCBO)
CALL PURGE(IDCBO,IERR,NAMEO,1,ICRO)
CALL CREAT(IDCBO,IERR,NAMEO,ISIZE,ITYPE,ISECU,ICRO)
CALL OPEN(IDCBO,IERR,NAMEO,0,ISECU,ICRO)
RETURN
END
```

```
      IMPLICIT REAL*8(A-H,O-Z)
C
C   PROGRAM USED FOR MULTIPLICITY AND STABILITY ANALYSIS
C   FOR 3 ODE SYSTEM FOR BETA2 VARYING WITH OTHER PARAMETERS
C   HELD CONSTANT.
C
      EXTERNAL FT
      DIMENSION EVAL(2,3),BB(3),YSS(5),TSS(5),ZSS(5)
      COMPLEX*16 W(3)
      EQUIVALENCE (W(1),EVAL(1,1))
      COMMON /BLK1/ DA1,DA2,B1,B2,GAM1,GAM2,ALPHA
      READ(5,900) DA1,DA2,B1,GAM1,GAM2,ALPHA
 900  FORMAT(6D10.5)
      READ(5,905) NDATA
 905  FORMAT(I2)
      INR=7
      MM=NDATA-(NDATA/7)*7
      NOALL=NDATA/7+1
      IF(NDATA.EQ.(NDATA/7)*7) NOALL=NDATA/7
      DO 200 IOALL=1,NOALL
      IF((IOALL.EQ.NOALL).AND.(NDATA.NE.(NDATA/7)*7)) INR=MM
      WRITE(6,805)
 805  FORMAT('1',//////)
      WRITE(6,810) DA1,DA2,B1,ALPHA,GAM1,GAM2
 810  FORMAT(T20,'DA1  = ',1PD11.4,T51,'DA2  = ',D11.4,/,
     *T20,'B1   = ',D11.4,T51,'ALPHA= ',D11.4,/,
     *T20,'GAM1 = ',D11.4,T51,'GAM2 = ',D11.4,////)
      DO 100 IDAT=1,INR
      READ(5,900) B2
      DO 20 IJ=1,5
  20  TSS(IJ)=((B1+B2)/5.0D0)*DFLOAT(IJ-1)+(B1+B2)*0.01D0
      EPS=1.0D-05
      EPS2=1.0D-04
      ETA=0.10D0
      NSIG=5
      N=5
      ITMAX=50
      IER=0
      CALL UERSET(2,LEVOLD)
      CALL ZREAL1(FT,EPS,EPS2,ETA,NSIG,N,TSS,ITMAX,IER)
      NSS=0
      DO 30 IJ=1,5
      IF((TSS(IJ).LT.0.0).OR.(TSS(IJ).GT.(B1+B2)))GO TO 30
      NSS=NSS+1
      TSS(NSS)=TSS(IJ)
      FAC1=DEXP(GAM1*TSS(NSS)/(1.D0+TSS(NSS)))
      FAC2=DEXP(GAM2*TSS(NSS)/(1.D0+TSS(NSS)))
      YSS(NSS)=1.D0/(1.D0+DA1*FAC1)
      ZSS(NSS)=1.D0/(1.D0+DA2*FAC2)
      CALL EVALUE(W,BB,TSS(NSS),YSS(NSS),ZSS(NSS))
      WRITE(6,820) B2,TSS(NSS),YSS(NSS),ZSS(NSS)
 820  FORMAT(' ',T10,'B2  =',1PD11.4,T29,'T =',D11.4,T46,
     *'Y =',D11.4,T63,'Z =',D11.4)
      BB(2)=BB(2)+BB(3)/BB(1)
```

```
      WRITE(6,825) (BB(I),I=1,3)
  825 FORMAT(T10,'TRACE =',1PD11.4,T32,'-SM + DET / TR =',
     *D11.4,T61,'DET =',D11.4)
      WRITE(6,830) (EVAL(1,J),J=1,3)
  830 FORMAT(T10,'EIGENVALUES: REAL',T30,1PD11.4,T45,D11.4,
     *T60,D11.4)
      WRITE(6,835) (EVAL(2,J),J=1,3)
  835 FORMAT(T23,'IMAG',T30,1PD11.4,T45,D11.4,T60,D11.4,//)
   30 CONTINUE
  100 CONTINUE
  200 CONTINUE
      STOP
      END
      DOUBLE PRECISION FUNCTION FT(T)
      IMPLICIT REAL*8(A-H,O-Z)
      COMMON /BLK1/ DA1,DA2,B1,B2,GAM1,GAM2
      T2=T
      IF(T.LE.0.0D0) T2=1.0D-10
      IF(T.GE.B1+B2) T2=B1+B2-1.0D-10
      T3=DEXP(-GAM1*T2/(1.0D0+T2))
      T4=DEXP(-GAM2*T2/(1.0D0+T2))
      FT=DA1*B1/(T3+DA1)+DA2*B2/(T4+DA2)-T2
      RETURN
      END
      SUBROUTINE EVALUE(W,BB,T,Y,Z)
      IMPLICIT REAL*8(A-H,O-Z)
      DIMENSION RJ(3,3),WK(3),BB(3)
      COMPLEX*16 W(3),ZZ(3,3)
      COMMON /BLK1/DA1,DA2,B1,B2,GAM1,GAM2,ALPHA
      IER=0
      RJ(1,1)=-1.D0-DA1*DEXP(GAM1*T/(T+1.D0))
      RJ(1,2)=0.0D0
      RJ(1,3)=-DA1*DEXP(GAM1*T/(T+1.D0))*Y*GAM1/(T+1.D0)**2
      RJ(2,1)=0.0D0
      RJ(2,2)=-1.0D0-DA2*DEXP(GAM2*T/(T+1.D0))
      RJ(2,3)=-DA2*DEXP(GAM2*T/(T+1.D0))*Z*GAM2/(T+1.D0)**2
      RJ(3,1)=ALPHA*DA1*B1*DEXP(GAM1*T/(T+1.D0))
      RJ(3,2)=ALPHA*DA2*B2*DEXP(GAM2*T/(T+1.D0))
      RJ(3,3)=ALPHA*(-B1*RJ(1,3)-B2*RJ(2,3)-1.D0)
      TRACE=RJ(1,1)+RJ(2,2)+RJ(3,3)
      SMINOR=RJ(1,1)*RJ(2,2)-RJ(2,1)*RJ(1,2)+RJ(2,2)*RJ(3,3)
     *-RJ(3,2)*RJ(2,3)+RJ(1,1)*RJ(3,3)-RJ(3,1)*RJ(1,3)
      DET=RJ(1,1)*RJ(2,2)*RJ(3,3)-RJ(3,1)*RJ(2,2)*RJ(1,3)
     *+RJ(1,2)*RJ(2,3)*RJ(3,1)-RJ(2,1)*RJ(1,2)*RJ(3,3)
     *+RJ(1,3)*RJ(3,2)*RJ(2,1)-RJ(1,1)*RJ(2,3)*RJ(3,2)
      BB(1)=TRACE
      BB(2)=-1.D0*SMINOR
      BB(3)=DET
      CALL EIGRF(RJ,3,3,0,W,ZZ,3,WK,IER)
      IF(IER.LT.32) RETURN
      WRITE(6,810) IER
  810 FORMAT(//,T20,'IER FROM EIGRF = ',I4)
      RETURN
      END
```

Appendix C Rotameter and Flowmeter Calibrations

Shown in Figures C.1 to C.5 are calibration curves for the two rotameters and the two linear mass flowmeters. The rotameters and mass flowmeters were calibrated at both 20 psig and at 30 psig. However, unlike the rotameters, the mass flowmeters are not affected by changes in pressure. Thus the calibration curves in Figures C.4 to C.5 are valid over a wide range of pressures (1 psia to 250 psia). In all cases the flow rates are given at the standard conditions of zero degrees Celsius and one atmosphere.

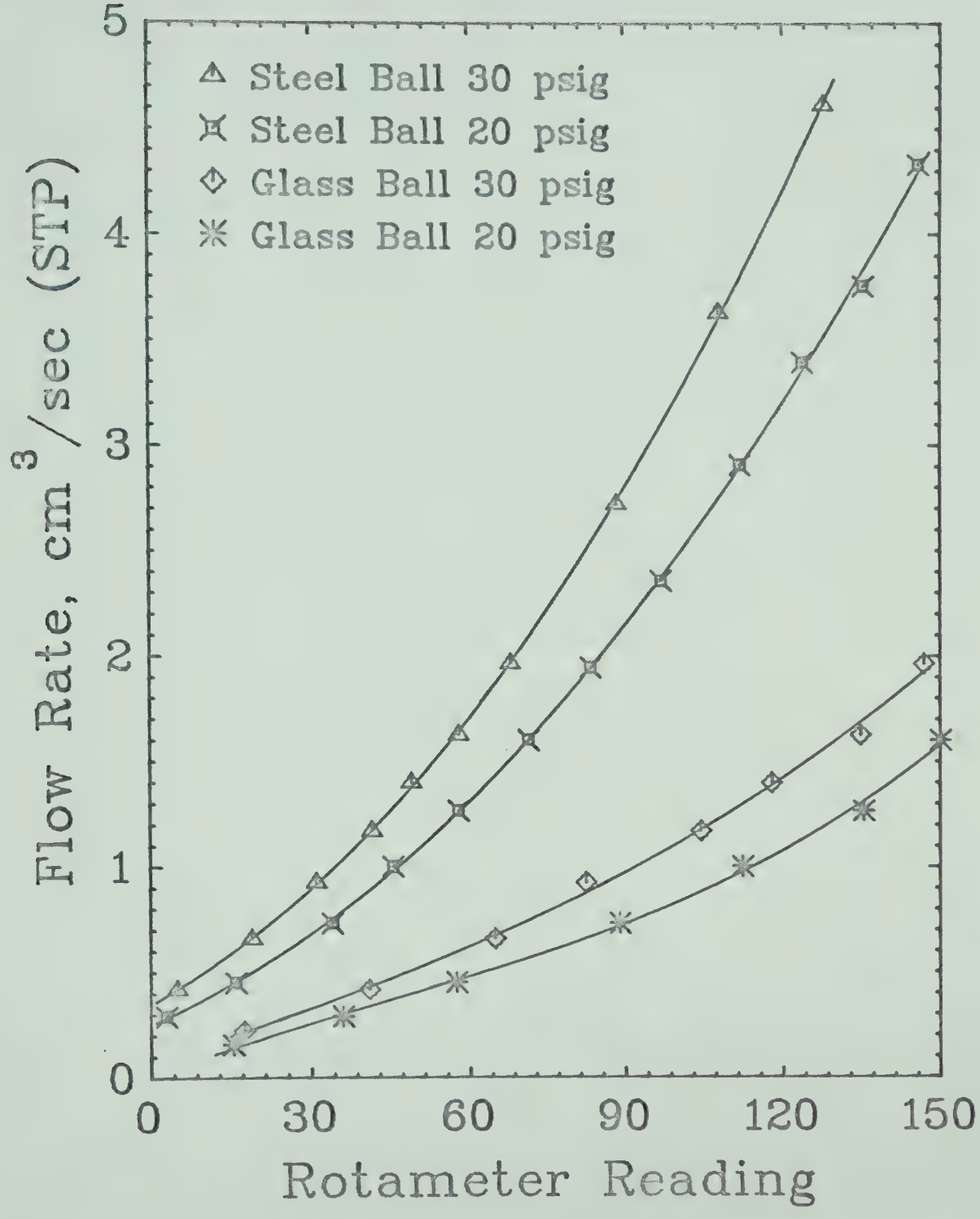

Figure C.1 Rotameter Calibration Curves for Oxygen (Matheson #600 tube)

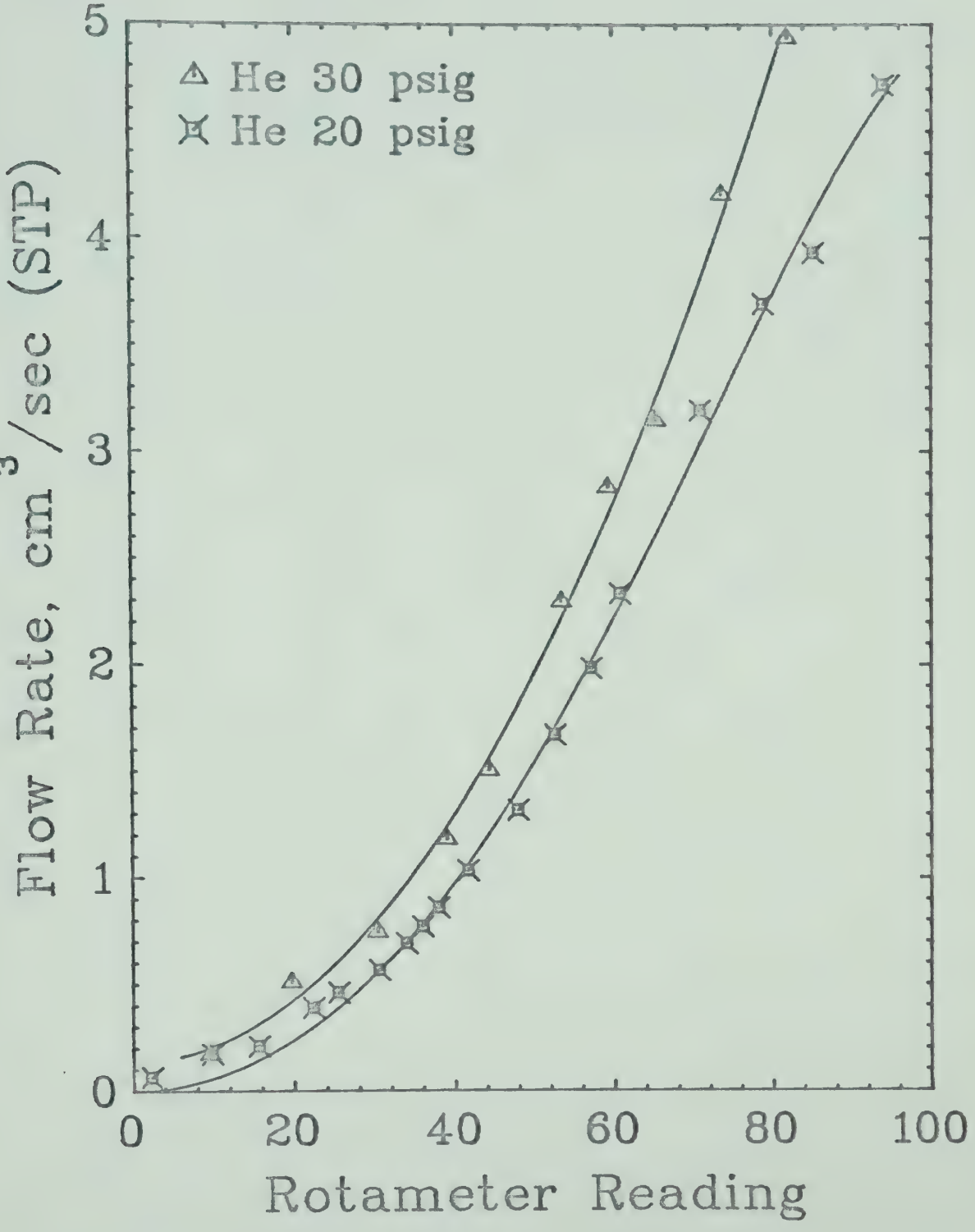

Figure C.2 Rotameter Calibration Curves for Helium (Matheson #610 tube)

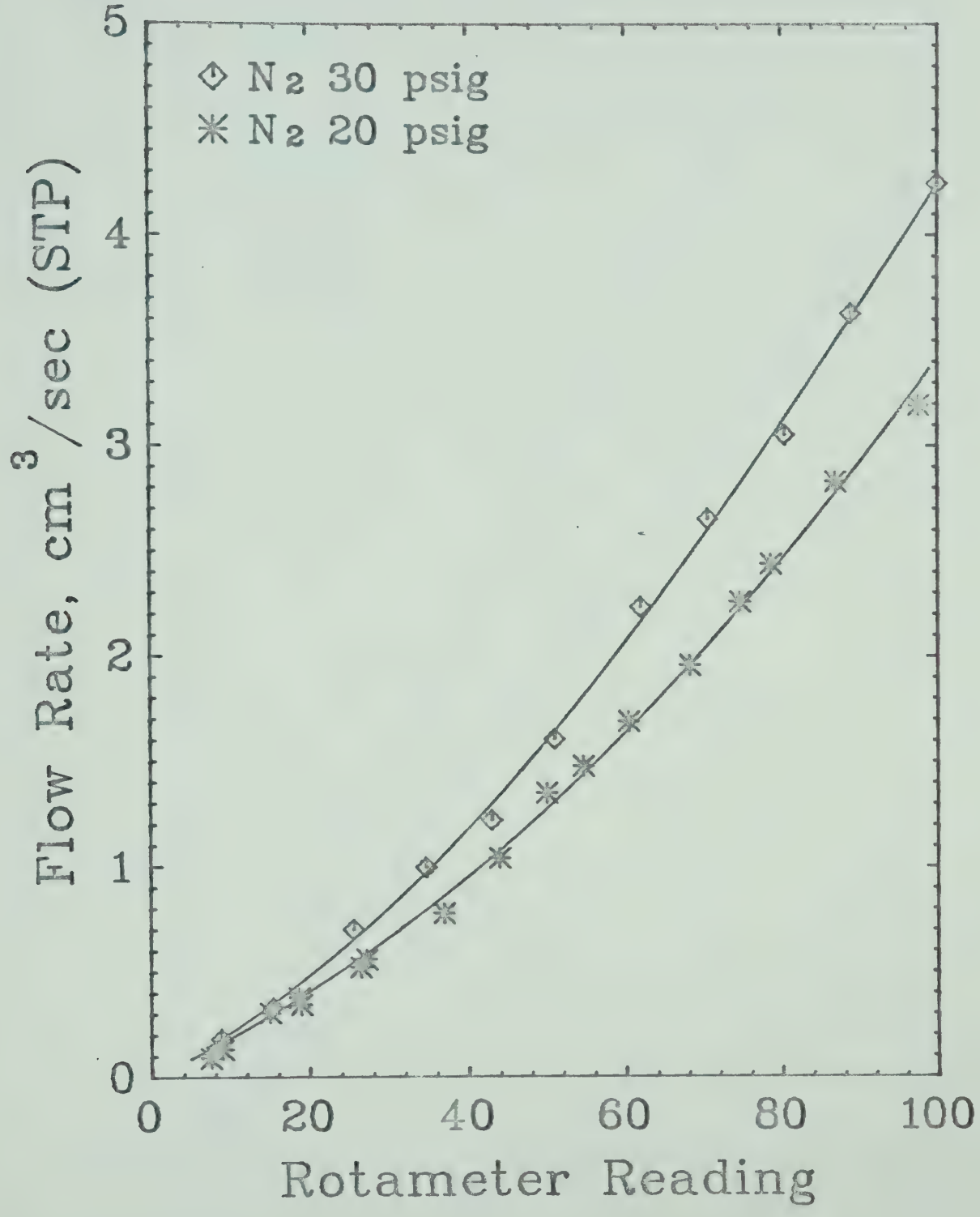

Figure C.3 Rotameter Calibration Curves for Nitrogen (Matheson #610 tube)

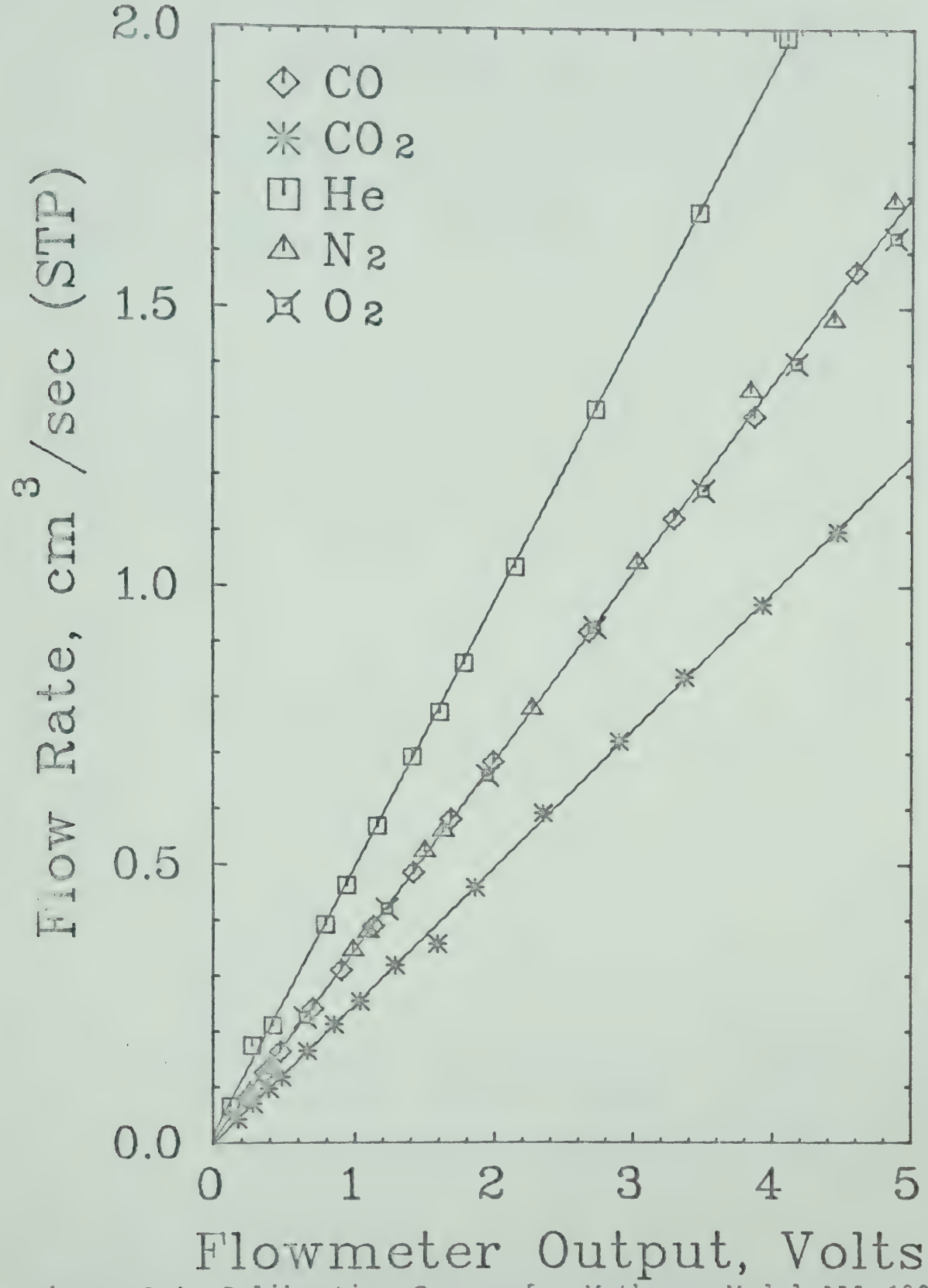

Figure C.4 Calibration Curves for Matheson Model ALL-100 Linear Mass Flowmeter (0-100 SCCM)

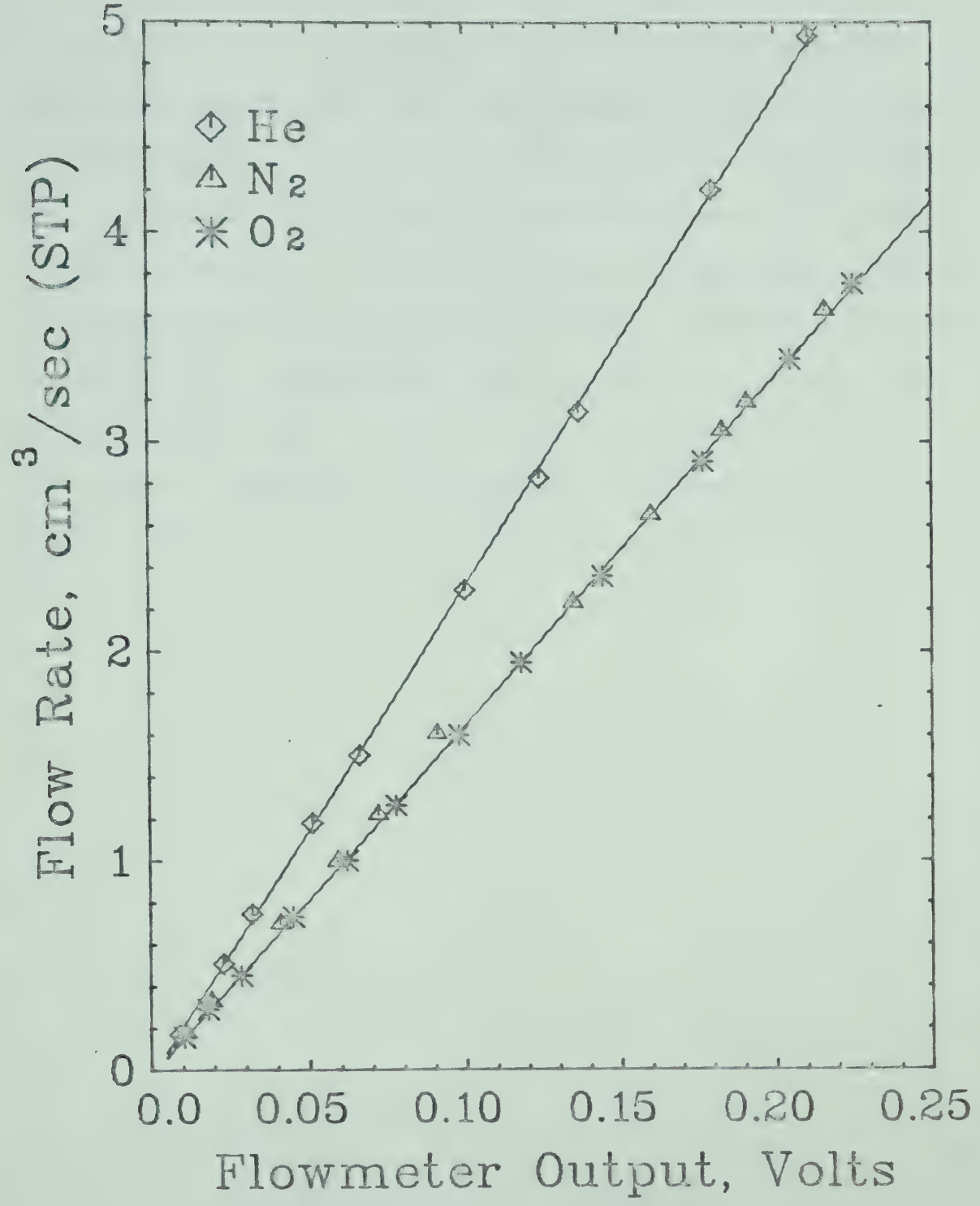

Figure C.5 Calibration Curves for Matheson Model 8116-0153 Linear Mass Flowmeter (0-5000 SCCM)

Appendix D Gas Chromatograph Calibration

In Tables D.1 to D.3 are given the calibration data for the gas chromatograph, in which the response factors of carbon dioxide, oxygen, and carbon monoxide relative to nitrogen are presented. No calibrations were performed for water, as it was not present in any of the reaction mixtures. These response factors are necessary in order to convert raw data in the form of area percent (or in arbitrary units) into actual compositions in the form of mole fractions. The calculation procedure which must be followed in order to perform this conversion is given following Table D.3.

Table D.1 GC Calibration Data for CO_2-N_2 Mixtures

$\frac{CO_2}{N_2}$, Actual	$\frac{CO_2}{N_2}$, Area	RF = $\frac{CO_2/N_2 \text{ Actual}}{CO_2/N_2 \text{ Area}}$
0.01297	0.01515 0.01501	0.856 0.864
0.01614	0.01877 0.01872 0.01870	0.860 0.862 0.863
0.01883	0.02180 0.02180 0.02165	0.864 0.864 0.870
0.02221	0.02584 0.02566 0.02556 0.02547	0.860 0.866 0.869 0.872
0.02714	0.03129 0.03122 0.03104	0.867 0.869 0.874
0.03768	0.04357 0.04343 0.04341 0.04325	0.865 0.868 0.868 0.871
0.05579	0.06393 0.06371 0.06342	0.873 0.876 0.880
Average Response Factor		0.867

Table D.2 GC Calibration Data for O_2-N_2 Mixtures

$\frac{O_2}{N_2}$, Actual	$\frac{O_2}{N_2}$, Area	RF = $\frac{O_2/N_2 \text{ Actual}}{O_2/N_2 \text{ Area}}$
0.2000	0.1890 0.1882 0.1877	1.058 1.063 1.065
0.3321	0.3144 0.3137 0.3106	1.056 1.059 1.069
0.7324	0.6805 0.6795 0.6794	1.076 1.078 1.078
Average Response Factor		1.067

Table D.3 GC Calibration Data for CO-N_2 Mixtures

$\frac{CO}{N_2}$, Actual	$\frac{CO}{N_2}$, Area	RF = $\frac{CO/N_2 \text{ Actual}}{CO/N_2 \text{ Area}}$
0.01866	0.01521 0.01491	1.227 1.252
0.02248	0.01808 0.01802 0.01788	1.243 1.248 1.257
0.03685	0.03019 0.03015 0.03013	1.221 1.222 1.223
0.09289	0.07638 0.07616 0.07574	1.216 1.220 1.226
0.17398	0.14083 0.13961 0.13891	1.235 1.246 1.252
Average Response Factor		1.235

GC Calculation Procedure

In order to perform the calculations it is necessary to assume that the thermal conductivity of a mixture of O_2, N_2 and CO is a linear function of the pure component thermal conductivities and mole fractions. Using this assumption, the split ratio (SR) between the two parallel branches of the column arrangement is give by:

$$SR = \frac{\text{Area}(O_2) + \text{Area}(N_2) + \text{Area}(CO) \quad \text{(from 5A M.S.)}}{\text{Area}(O_2+N_2+CO) \quad \text{(composite peak from P-S)}} \qquad (D.1)$$

where M.S. stands for molecular sieve, and P-S stands for Porapak T - Spherocarb. Once the split ratio has been calculated, the amount of CO_2 which has been held up in the 5A molecular sieve column can be determined from knowing the amount of CO_2 which passed through the Porapak T - Spherocarb part of the column, i.e.:

$$\text{Area}(CO_2 \text{ from 5A M.S.}) = SR*\text{Area}(CO_2 \text{ from P-S}) \qquad (D.2)$$

The calculation of the mole fraction of each component can now be performed by the following procedure:

$$CD = \text{Area}(O_2)*RF(O_2) + \text{Area}(N_2)*RF(N_2) + \text{Area}(CO)*RF(CO) + SR*\text{Area}(CO_2 \text{ from P-S})*RF(CO_2) \qquad (D.3)$$

$$\text{Mole Fraction } O_2 = \text{Area}(O_2)*RF(O_2)/CD \qquad (D.4)$$

$$\text{Mole Fraction } N_2 = \text{Area}(N_2)*RF(N_2)/CD \qquad (D.5)$$

$$\text{Mole Fraction CO} = \text{Area(CO)}*RF(CO)/CD \qquad (D.6)$$

$$\text{Mole Fraction } CO_2 = \text{Area}(CO_2 \text{ from P-S})*RF(CO_2)*SR/CD \qquad (D.7)$$

where RF stands for response factor. A numerical example of this calculation procedure is given below, where it is assumed that a mixture of CO_2, CO, O_2 and N_2 has caused the integrator to produce the following raw data:

Component	Area%	RF(from Tables D.1-D.3)
O_2+N_2+CO	35	—
CO_2	10	0.867
O_2	20	1.067
N_2	30	1.0
CO	5	1.235

From Equation D.1 the split ratio is found to be:

$$SR = (20+30+5)/35 = 1.5714$$

Thus the common divisor in the mole fraction calculation is given by:

$$CD = 20(1.067) + 30(1.0) + 5(1.235) + 1.5714(10)(0.867)$$
$$= 71.139$$

The mole fractions are now found from Eqs. D.4-D.7 to be:

$$mf(O_2) = 20(1.067)/71.139 = 0.300$$

$$mf(N_2) = 30(1.0)/71.139 = 0.422$$

$$mf(CO) = 5(1.235)/71.139 = 0.087$$

$$mf(CO_2) = 10(0.867)(1.5714)/71.139 = 0.191$$

Appendix E Computer Programs for Chapter 8

This appendix contains the source code of the computer program which was used to integrate the six ordinary differential equation model presented in Chapter 8. Also included is the program which was used to determine the number, and stability, of steady-states for the six ODE model.

```
C
C  THIS PROGRAM IS USED TO INTEGRATE THE SYSTEM OF SIX ODE'S
C  PRESENTED IN CHAPTER 8. THE INTEGRATION CAN BE PERFORMED
C  USING EITHER GEAR'S METHOD OR THE RKF METHOD.
C
FTN4,X
      BLOCK DATA NAME, NAMED BLOCK DATA AREAS
      DOUBLE PRECISION F,K1,KM1,K2,KM2,K3,G1,G2,G3
     *,A1,A2,A3,B1,B2,B3
      COMMON APARAMB F,K1,KM1,K2,KM2,K3,G1,G2,G3
     *,A1,A2,A3,B1,B2,B3
      COMMON /COUNT/ NPINT,IPINT,NDLAY,IMAX,IBUF(100)
     *,IDCBO(144),VQO
      COMMON /MAN/ NINT,IPLOT,NAMEO(3)
      END
      PROGRAM DIM6(,31005), 6 ODE MODEL FOR CO OXIDATION
      EXTERNAL F6,PDERV
      DIMENSION X(7)
      DOUBLE PRECISION Y(6),TIME,H,HMX,AER,RER,DTIME
     *,G(8,6),GSAVE(78),GMAX(6),GERR(6),GPW(72)
      COMMON /COUNT/ NPINT,IPINT,NDLAY,IMAX,IBUF(100)
     *,IDCBO(144),VQO
      COMMON /MAN/ NINT,IPLOT,NAMEO(3)
      CALL DTACH
      CALL INPUT(LUNO,TIME,H,HMX,AER,RER,DTIME,N,Y)
      NPINT=1
      IF(NDLAY.GT.0) NPINT=0
      DO 10 I=1,N
      GMAX(I)=0.01D0
 10   G(1,I)=Y(I)
      JS=0
      DO 50 IPINT=1,NINT
      IF(INTG.EQ.0)
     *CALL RKF(TIME,Y,N,F6,DTIME,H,HMX,AER,RER,IFLAG)
      IF(INTG.EQ.1)CALL SGEAR(N,TIME,DTIME,G,GSAVE,H,HMX
     *,RER,1,GMAX,GERR,IFLAG,JS,6,GPW,PDERV)
      IF(INTG.EQ.0) GO TO 30
      DO 20 I=1,N
 20   Y(I)=G(1,I)
 30   IF(IFLAG.NE.1) GO TO 60
      IF(IPINT.LT.NDLAY) GO TO 50
      X(1)=SNGL(TIME*VQO)
      DO 40 II=1,N
 40   X(II+1)=SNGL(Y(II))
      IF(IPINT/IPLOT*IPLOT.NE.IPINT) GO TO 50
      IF(IMAX.EQ.1) GO TO 50
      CALL CODE
      WRITE(IBUF,800) (X(I),I=1,7)
800   FORMAT(12(1PE13.5))
      CALL WRITF(IDCBO,IERR,IBUF,46)
      WRITE(LUNO,810) (X(I),I=1,7)
810   FORMAT(7(1PE11.3))
      NPINT=NPINT+1
 50   CONTINUE
```

```
      WRITE(LUNO,820) NPINT
820   FORMAT(" "," # OF POINTS =",I5)
      GO TO 70
 60   WRITE(LUNO,830) IFLAG,TIME,(Y(I),I=1,N)
830   FORMAT(" ",I3,7(D15.6,1X))
 70   CALL CLOSE(IDCBO)
      CALL OPEN(IDCBO,IERR,NAMEO,2,1,ICRO)
      CALL RWNDF(IDCBO)
      CALL CODE
      WRITE(IBUF,840) NPINT
840   FORMAT(I6)
      CALL WRITF(IDCBO,IERR,IBUF,3)
      CALL CLOSE(IDCBO)
      STOP
      END
      SUBROUTINE INPUT(LUNO,TIME,H,HMX,AER,RER,DTIME,N,Y)
      DIMENSION X(7),NAMEI(3),IDCBI(144),IBUFA(50),IRBUF(33)
      DOUBLE PRECISION Y(6),TIME,H,HMX,AER,RER,DTIME
      DOUBLE PRECISION F,K1,KM1,K2,KM2,K3,G1,G2,G3,A1,A2,A3
     *,B1,B2,B3,CO,O2,CO2,OS,COS,T
     *,RK1,RK2,RK3,RKM1,RKM2,E1R,E2R,E3R,DH1,DH2,DH3
     *,U,A,V,L,MASS,CP,TO,PO,QO,FCO,FO2,CONCT,DEXP,Q
      COMMON /PARAM/ F,K1,KM1,K2,KM2,K3,G1,G2,G3
     *,A1,A2,A3,B1,B2,B3
      COMMON /COUNT/ NPINT,IPINT,NDLAY,IMAX,IBUF(100)
     *,IDCBO(144),VQO
      COMMON /MAN/ NINT,IPLOT,NAMEO(3)
      EQUIVALENCE (NAMEI(1),IRBUF(2)),(ICRI,IRBUF(6))
      EQUIVALENCE (ICRO,IRBUF(10)),(LUN,IRBUF(14))
      LUNW=LOGLU(ISIS)
      LUNR=LUNW
      CALL IFMTE(LUNW)
      CALL GETST(IBUFA,-17,ILOG)
      CALL PARSE(IBUFA,ILOG,IRBUF)
      IF(ILOG.GT.0) GO TO 600
      WRITE(LUNW,800)
800   FORMAT(" NAME OF INPUT DATA FILE ")
      READ(LUNR,290) NAMEI
290   FORMAT(3A2,1X,I2)
      WRITE(LUNW,801)
801   FORMAT("ENTER INPUT CRN, OUTPUT CRN, AND OUTPUT LUN")
      READ(LUNR,*) ICRI,ICRO,LUN
600   LUNO=LUN
      CALL OPEN(IDCBI,IERR,NAMEI,0,1,ICRI)
      CALL READF(IDCBI,IERR,IBUF)
      CALL CODE
      READ(IBUF,*) N,INTG,IDIMG,INTAL
      CALL READF(IDCBI,IERR,IBUF)
      CALL CODE
      READ(IBUF,*) TIME,DTIME,H,HMX,AER,RER
      CALL READF(IDCBI,IERR,IBUF)
      CALL CODE
      READ(IBUF,*) CO,O2,CO2,OS,COS,T
      IF(IDIMG.EQ.0) GO TO 20
```

```
      CALL READF(IDCBI,IERR,IBUF)
      CALL CODE
      READ(IBUF,*) RK1,RKM1,RK2,RKM2,RK3
      CALL READF(IDCBI,IERR,IBUF)
      CALL CODE
      READ(IBUF,*) E1R,E2R,E3R,DH1,DH2,DH3
      CALL READF(IDCBI,IERR,IBUF)
      CALL CODE
      READ(IBUF,*) U,A,V,L,MASS,CP
      CALL READF(IDCBI,IERR,IBUF)
      CALL CODE
      READ(IBUF,*) TO,PO,QO,FCO,FO2
      CONCT=PO/(8.314D0*TO)
      Q=QO*(TO/273.D0)*(1.D+05/PO)
      G1=E1R/TO
      G2=E2R/TO
      G3=E3R/TO
      K1=RK1*A/Q
      K2=RK2*A/Q
      K3=RK3*A*DEXP(-G3)/(Q*FCO*CONCT)
      KM1=RKM1*A*DEXP(-G1)/(Q*FCO*CONCT)
      KM2=RKM2*A*DEXP(-G2)/(Q*FO2*CONCT)
      B1=Q*DH1*CONCT*FCO/(U*A*TO)
      B2=Q*DH2*CONCT*FO2/(U*A*TO)
      B3=Q*DH3*CONCT*FCO/(U*A*TO)
      A1=V*CONCT*FCO/(A*L)
      A2=2.D0*V*CONCT*FO2/(A*L)
      A3=U*A*V/(MASS*CP*Q)
      F=FCO+FO2
      VQO=V/Q
      GO TO 30
20    CALL READF(IDCBI,IERR,IBUF)
      CALL CODE
      READ(IBUF,*) K1,KM1,K2,KM2,K3
      CALL READF(IDCBI,IERR,IBUF)
      CALL CODE
      READ(IBUF,*) G1,G2,G3,B1,B2,B3
      CALL READF(IDCBI,IERR,IBUF)
      CALL CODE
      READ(IBUF,*) F,A1,A2,A3
      VQO=1.0D0
30    CALL READF(IDCBI,IERR,IBUF)
      CALL CODE
      READ(IBUF,*) NINT,IPLOT,NDLAY
      IF(INTAL.EQ.0) CALL INITL(CO,O2,T,COS,OS)
      WRITE(LUNO,330) TIME,DTIME,H,HMX,AER,RER
      IF(IDIMG.EQ.0) GO TO 40
      WRITE(LUNO,330) RK1,RK2,RK3,RKM1,RKM2
      WRITE(LUNO,330) E1R,E2R,E3R,DH1,DH2,DH3
      WRITE(LUNO,330) U,A,V,L,MASS,CP
      WRITE(LUNO,330) TO,PO,QO,FCO,FO2
40    WRITE(LUNO,330) CO,O2,CO2,OS,COS,T
      WRITE(LUNO,330) K1,KM1,K2,KM2,K3
      WRITE(LUNO,330) G1,G2,G3,B1,B2,B3
```

```
      WRITE(LUNO,330) F,A1,A2,A3
330   FORMAT(12(1PD13.5))
      WRITE(LUNO,345) NINT,IPLOT,N,INTG,NDLAY
345   FORMAT(6(5X,I4))
      Y(1)=CO
      Y(2)=O2
      Y(3)=CO2
      Y(4)=OS
      Y(5)=COS
      Y(6)=T
      X(1)=SNGL(TIME)
      DO 1 II=1,6
1     X(II+1)=SNGL(Y(II))
      CALL DFILE(IDCBI,ICRI,IDCBO,NAMEO,ICRO)
      CALL CODE
      WRITE(IBUF,350)NINT
350   FORMAT(I6)
      CALL WRITF(IDCBO,IERR,IBUF,3)
      IF(IDIMG.EQ.0) GO TO 50
      CALL CODE
      WRITE(IBUF,360) RK1,RK2,RK3,RKM1,RKM2
      CALL WRITF(IDCBO,IERR,IBUF,34)
      CALL CODE
      WRITE(IBUF,360) E1R,E2R,E3R,DH1,DH2,DH3
      CALL WRITF(IDCBO,IERR,IBUF,39)
      CALL CODE
      WRITE(IBUF,360) U,A,V,L,MASS,CP
      CALL WRITF(IDCBO,IERR,IBUF,39)
      CALL CODE
      WRITE(IBUF,360) TO,PO,QO,FCO,FO2
      CALL WRITF(IDCBO,IERR,IBUF,34)
 50   CALL CODE
      WRITE(IBUF,360) K1,KM1,K2,KM2,K3
360   FORMAT(12(1PE13.5))
      CALL  WRITF(IDCBO,IERR,IBUF,34)
      CALL CODE
      WRITE(IBUF,360) G1,G2,G3,B1,B2,B3
      CALL WRITF(IDCBO,IERR,IBUF,39)
      CALL CODE
      WRITE(IBUF,360) F,A1,A2,A3
      CALL WRITF(IDCBO,IERR,IBUF,26)
      CALL CODE
      WRITE(IBUF,360) TIME,DTIME,H,HMX,AER,RER
      CALL WRITF(IDCBO,IERR,IBUF,39)
      IF(NDLAY.GT.0) RETURN
      CALL CODE
      WRITE(IBUF,360) (X(I),I=1,7)
      CALL WRITF(IDCBO,IERR,IBUF,46)
      RETURN
      END
      SUBROUTINE INITL(CO,O2,T,COS,OS)
      DOUBLE PRECISION DEXP,DSQRT,CO,COS,O2,T,OS,RM1,R1CO,F
     *,RM2,R202,K1,KM1,K2,KM2,K3,G1,G2,G3,A1,A2,A3,B1,B2,B3
      COMMON /PARAM/ F,K1,KM1,K2,KM2,K3,G1,G2,G3
```

```
     *,A1,A2,A3,B1,B2,B3
      RM1=KM1*DEXP(G1*T/(1.D0+T))
      R1CO=K1*CO
      RM2=KM2*DEXP(G2*T/(1.D0+T))
      R2O2=K2*O2
      COS=0.0D0
      OS=0.0D0
      IF((CO.LT.1.D-10).AND.(O2.LT.1.D-10))RETURN
      IF((CO.GE.1.D-10).AND.(O2.GE.1.D-10)) GO TO 20
      IF(CO.GE.1.D-10) GO TO 10
      OS=1.D0/(1.D0+DSQRT(RM2/R2O2))
      RETURN
10    COS=1.D0/(1.D0+RM1/R1CO)
      RETURN
20    OS=1.D0/(1.D0+DSQRT(RM2/R2O2)*(1.D0+R1CO/RM1))
      COS=1.D0-OS-DSQRT(RM2/R2O2)*OS
      RETURN
      END
      SUBROUTINE F6(TIME,Y,YP)
      DOUBLE PRECISION Y(6),YP(6),TIME,DEXP
      DOUBLE PRECISION T,CO,O2,CO2,COS,OS,RCO,RCO2,RO2,QQO,Q
      DOUBLE PRECISION DT,DCO,DO2,DCO2,DCOS,DOS,T1,S
     *,F,K1,KM1,K2,KM2,K3,G1,G2,G3,A1,A2,A3,B1,B2,B3
      COMMON /PARAM/ F,K1,KM1,K2,KM2,K3,G1,G2,G3
     *,A1,A2,A3,B1,B2,B3
      CO=Y(1)
      O2=Y(2)
      CO2=Y(3)
      OS=Y(4)
      COS=Y(5)
      T=Y(6)
      S=1.D0-COS-OS
      T1=T+1.D0
      IF(S.LT.0.0D0) S=0.0D0
      RCO=K1*CO*S-KM1*DEXP(G1*T/T1)*COS
      RO2=K2*O2*S*S-KM2*DEXP(G2*T/T1)*OS*OS
      RCO2=K3*DEXP(G3*T/T1)*COS*OS
      QQO=1.D0+(F/(1.D0+2.D0*A1/A2))*(2.D0*A1
     **(RCO2-RCO)/A2-RO2)
      DCO=1.D0-QQO*CO-RCO
      DO2=1.D0-QQO*O2-RO2
      DCO2=-QQO*CO2+RCO2
      DOS=A2*RO2-A1*RCO2
      DCOS=A1*(RCO-RCO2)
      DT=A3*(B1*RCO+B2*RO2+B3*RCO2-T)
      YP(1)=DCO
      YP(2)=DO2
      YP(3)=DCO2
      YP(4)=DOS
      YP(5)=DCOS
      YP(6)=DT
      RETURN
      END
      SUBROUTINE PDERV(TIME,Y,YP,PW,M,IND)
```

```
      DOUBLE PRECISION Y(8,M),YP(M),PW(M,M),TIME,DEXP,DSQRT
     *DABS,DA,T,CO,O2,CO2,COS,OS,S,Q,T1,R1,R2,R3,T12
     *,DT,DCO,DO2,DCO2,DCOS,DOS,RCO,RCO2,RO2
     *,F,K1,KM1,K2,KM2,K3,G1,G2,G3,A1,A2,A3,B1,B2,B3
      COMMON /PARAM/ F,K1,KM1,K2,KM2,K3,G1,G2,G3
     *,A1,A2,A3,B1,B2,B3
      CO=Y(1,1)
      O2=Y(1,2)
      CO2=Y(1,3)
      OS=Y(1,4)
      COS=Y(1,5)
      T=Y(1,6)
      T1=T+1.0D0
      S=1.D0-COS-OS
      IF(S.LT.0.0D0) S=0.0D0
C     Q=QO+(8.314D0*A*TO/P)*(-RCO-RO2+RCO2)
      RCO=K1*CO*S-KM1*DEXP(G1*T/T1)*COS
      RO2=K2*O2*S*S-KM2*DEXP(G2*T/T1)*OS*OS
      RCO2=K3*DEXP(G3*T/T1)*COS*OS
      IF(IND.EQ.1) GO TO 100
      DCO=1.D0-F*CO-RCO
      DO2=1.D0-F*O2-RO2
      DCO2=-F*CO2+RCO2
      DOS=A2*RO2-A1*RCO2
      DCOS=A1*(RCO-RCO2)
      DT=A3*(B1*RCO+B2*RO2+B3*RCO2-T)
      YP(1)=DCO
      YP(2)=DO2
      YP(3)=DCO2
      YP(4)=DOS
      YP(5)=DCOS
      YP(6)=DT
      RETURN
100   CONTINUE
      R1=KM1*DEXP(G1*T/T1)
      R2=KM2*DEXP(G2*T/T1)
      R3=K3*DEXP(G3*T/T1)
      T12=T1*T1
      PW(1,1)=-F-K1*S
      PW(1,2)=0.0D0
      PW(1,3)=0.0D0
      PW(1,4)=K1*CO
      PW(1,5)=K1*CO+R1
      PW(1,6)=R1*G1*COS/T12
      PW(2,1)=0.0D0
      PW(2,2)=-F-K2*S*S
      PW(2,3)=0.0D0
      PW(2,4)=2.D0*R2*OS+2.D0*K2*O2*S
      PW(2,5)=2.D0*K2*O2*S
      PW(2,6)=R2*G2*OS*OS/T12
      PW(3,1)=0.0D0
      PW(3,2)=0.0D0
      PW(3,3)=-F
      PW(3,4)=R3*COS
```

```
      PW(3,5)=R3*OS
      PW(3,6)=R3*G3*COS*OS/T12
      PW(4,1)=0.0D0
      PW(4,2)=A2*K2*S*S
      PW(4,3)=0.0D0
      PW(4,4)=-2.D0*A2*K2*O2*S-2.D0*A2*R2*OS-A1*R3*COS
      PW(4,5)=-2.D0*A2*K2*O2*S-A1*R3*OS
      PW(4,6)=-A2*R2*G2*OS*OS/T12-A1*R3*G3*COS*OS/T12
      PW(5,1)=A1*K1*S
      PW(5,2)=0.0D0
      PW(5,3)=0.0D0
      PW(5,4)=A1*(-K1*CO-R3*COS)
      PW(5,5)=A1*(-K1*CO-R3*OS-R1)
      PW(5,6)=A1*(-R1*G1*COS/T12-R3*G3*OS*COS/T12)
      PW(6,1)=A3*B1*K1*S
      PW(6,2)=A3*B2*K2*S*S
      PW(6,3)=0.0D0
      PW(6,4)=A3*(-B1*K1*CO-2.D0*B2*(K2*O2*S+R2*OS)
     *+B3*R3*COS)
      PW(6,5)=A3*(-B1*(K1*CO+R1)-2.D0*B2*K2*O2*S+B3*R3*OS)
      PW(6,6)=A3*(-B1*R1*COS*G1/T12-B2*R2*G2*OS*OS/T12
     *+B3*R3*G3*OS*COS/T12-1.0D0)
      RETURN
      END
```

This program also requires the RKF, SGEAR, MXINV and DFILE subroutines listed in Appendix B.

```
      IMPLICIT REAL*8(A-H,K,O-Z)
C
C     PROGRAM CALCULATES X, Y, Z, OS, COS, T, GIVEN ALL OTHER
C     PARAMETERS FOR THE 6 ODE MODEL. AFTER CALCULATION OF
C     THE ABOVE CONSTANTS, THE EIGENVALUES ARE CALULATED.
C
      EXTERNAL FCN
      DIMENSION EVAL(2,6),TOS(3,99),WK(68),TSS(99),OSS(99)
     *,COSS(100),IERR(100),P(22)
      COMPLEX*16 W(6),ZSM,ZLG
      EQUIVALENCE (W(1),EVAL(1,1)),(ZSM,OS1),(ZLG,OS2),
     *(P(1),RK1),(P(2),RKM1),(P(3),RK2),(P(4),RKM2),(P(5),
     *RK3),(P(6),E1R),(P(7),E2R),(P(8),E3R),(P(9),DH1)
     *,(P(10),DH2),(P(11),DH3),(P(12),U),(P(13),A),(P(14),V)
     *,(P(15),RL),(P(16),RMASS),(P(17),CP),(P(18),TO)
     *,(P(19),PO),(P(20),QO),(P(21),FCO),(P(22),FO2)
      COMMON /P1/X,Y,Z,OS,COS,T
      COMMON /P2/ K1,KM1,K2,KM2,K3,A1,A2,A3
      COMMON /P3/ G1,G2,G3,B1,B2,B3,F
      CALL TRACER(-1,162)
C     READ(5,900) K1,KM1,K2,KM2,K3
C     READ(5,900) A1,A2,A3,B1,B2,B3
C     READ(5,900) G1,G2,G3,F
  900 FORMAT(9D13.5)
      READ(5,900) RK1,RKM1,RK2,RKM2,RK3
      READ(5,900) E1R,E2R,E3R,DH1,DH2,DH3
      READ(5,900) U,A,V,RL,RMASS,CP
      READ(5,900) TO,PO,QO,FCO,FO2,F
      READ(5,905) NDATA
  905 FORMAT(I4)
      DO 100 IDAT=1,NDATA
C     READ(5,900) A3,B3
      READ(5,910) IPAR,PAR
  910 FORMAT(I4,D13.6)
      P(IPAR)=PAR
      CONCT=PO/(8.314D0*TO)
      Q=QO*(TO/273.D0)*(1.D+05/PO)
      G1=E1R/TO
      G2=E2R/TO
      G3=E3R/TO
      K1=RK1*A/Q
      K2=RK2*A/Q
      K3=RK3*A*DEXP(-G3)/(Q*FCO*CONCT)
      KM1=RKM1*A*DEXP(-G1)/(Q*FCO*CONCT)
      KM2=RKM2*A*DEXP(-G2)/(Q*FO2*CONCT)
      B1=Q*DH1*CONCT*FCO/(U*A*TO)
      B2=Q*DH2*CONCT*FO2/(U*A*TO)
      B3=Q*DH3*CONCT*FCO/(U*A*TO)
      A1=V*CONCT*FCO/(A*RL)
      A2=2.D0*V*CONCT*FO2/(A*RL)
      A3=U*A*V/(RMASS*CP*Q)
      WRITE(6,805)
  805 FORMAT('1',//////)
      WRITE(6,806)RK1,RKM1,RK2,RKM2,RK3
```

```
806   FORMAT(10X,6(1PD11.4))
      WRITE(6,806) E1R,E2R,E3R,DH1,DH2,DH3
      WRITE(6,806) U,A,V,RL,RMASS,CP
      WRITE(6,806) TO,PO,QO,FCO,FO2
      WRITE(6,807)
807   FORMAT(///)
      WRITE(6,810) K1,KM1,K3
 810  FORMAT(T10,'K1 =',1PD12.4,T30,'K-1 =',1PD12.4,T50,'K3'
     *,' =',1PD12.4)
      WRITE(6,811) K2,KM2,F
 811  FORMAT(T10,'K2 =',1PD12.4,T30,'K-2 =',1PD12.4,T50,' F'
     *,' =',1PD12.4)
      WRITE(6,812) A1,A2,A3
 812  FORMAT(T10,'A1 =',1PD12.4,T30,' A2 =',1PD12.4,T50,'A3'
     *,' =',1PD12.4)
      WRITE(6,813) B1,B2,B3
 813  FORMAT(T10,'B1 =',1PD12.4,T30,' B2 =',1PD12.4,T50,'B3'
     *,' =',1PD12.4)
      WRITE(6,814) G1,G2,G3
 814  FORMAT(T10,'G1 =',1PD12.4,T30,' G2 =',1PD12.4,T50,'G3'
     *,' =',1PD12.4)
      TMAX=B1+B3+B2*A1/A2
      DO 20 I1=1,5
      DO 10 I2=1,5
      TOS(1,(I1-1)*5+I2)=(1.0D0*TMAX/5.D0)*DFLOAT(I2-1)
     *+0.10*TMAX
      TOS(2,(I1-1)*5+I2)=(1.0D0/5.D0)*DFLOAT(I1-1)+0.10D0
 10   TOS(3,(I1-1)*5+I2)=0.95D0-TOS(2,(I1-1)*5+I2)
 20   CONTINUE
      DO 22 IJ=1,25
      NSIG=8
      N=3
      IMAX=75
      IER=0
      CALL UERSET(0,LEVOLD)
      DO 21 INC=1,3
 21   TOS(INC,IJ)=TOS(INC,IJ)*10000.D0
      CALL ZSCNT(FCN,NSIG,N,IMAX,PAR,TOS(1,IJ),FNORM,WK,IER)
      DO 26 INC=1,3
 26   TOS(INC,IJ)=TOS(INC,IJ)/10000.D0
 22   IERR(IJ)=IER
      NSS=0
      DO 25 IJ=1,25
      IF(IERR(IJ).EQ.129) GO TO 25
      IF((TOS(1,IJ).LE.0.).OR.(TOS(1,IJ).GE.(TMAX)))GO TO 25
      IF((TOS(2,IJ).LE.0.).OR.(TOS(2,IJ).GE.(1.D0)))GO TO 25
      IF(NSS.EQ.0) GO TO 24
      DO 23 IK=1,NSS
      REL=1.D-06
      IF((DABS((TOS(1,IJ)-TSS(IK))/TSS(IK)).LT.REL).AND.
     *((DABS(TOS(2,IJ)-COSS(IK))/COSS(IK)).LT.REL)) GO TO 25
 23   CONTINUE
      NSS=NSS+1
      TSS(NSS)=TOS(1,IJ)
```

```
      COSS(NSS)=TOS(2,IJ)
      OSS(NSS)=TOS(3,IJ)
      GO TO 25
24    CONTINUE
      NSS=1
      TSS(NSS)=TOS(1,IJ)
      COSS(NSS)=TOS(2,IJ)
      OSS(NSS)=TOS(3,IJ)
25    CONTINUE
      DO 30 IJ=1,NSS
      T=TSS(IJ)
      COS=COSS(IJ)
      OS=OSS(IJ)
      X=(1.D0-T/TMAX)/F
      Y=(1.D0-A1*T/(A2*TMAX))/F
      Z=K3*DEXP(G3*T/(1.D0+T))*OS*COS/F
      IF((OS+COS.GT.1.01D0).OR.(OS+COS.LT.-0.01D0))GO TO 30
      IF((X+Z.GT.1.02D0).OR.(X+Z.LT.0.98D0)) GO TO 30
      CALL EVALUE(W)
      WRITE(6,826) T,X,Y
826   FORMAT(////,T10,'T = ',1PD13.6,T30,'X = ',1PD13.6,
     *T50,'Y  = ',1PD13.6)
      WRITE(6,827) Z,OS,COS
827   FORMAT(T10,'Z = ',1PD13.6,T30,'OS= ',1PD13.6,T50,
     *'COS= ',1PD13.6,/)
      WRITE(6,830) (EVAL(1,J),J=1,6)
830   FORMAT(T5,6(1PD10.3,2X))
      WRITE(6,830) (EVAL(2,J),J=1,6)
 30   CONTINUE
100   CONTINUE
200   CONTINUE
      STOP
      END
      SUBROUTINE EVALUE(W)
      IMPLICIT REAL*8(A-H,K,O-Z)
      DIMENSION RJ(6,6),WK(6),BB(6)
      COMPLEX*16 W(6),ZZ(6,6)
      COMMON /P1/X,Y,Z,OS,COS,T
      COMMON /P2/ K1,KM1,K2,KM2,K3,A1,A2,A3
      COMMON /P3/ G1,G2,G3,B1,B2,B3,F
      IER=0
      S=1.D0-COS-OS
      T1=T+1.D0
      T12=T1*T1
      R1=KM1*DEXP(G1*T/T1)
      R2=KM2*DEXP(G2*T/T1)
      R3=K3*DEXP(G3*T/T1)
      RJ(1,1)=-F-K1*S
      RJ(1,2)=0.0D0
      RJ(1,3)=0.0D0
      RJ(1,4)=K1*X
      RJ(1,5)=K1*X+R1
      RJ(1,6)=R1*G1*COS/T12
      RJ(2,1)=0.0D0
```

```
      RJ(2,2)=-F-K2*S*S
      RJ(2,3)=0.0D0
      RJ(2,4)=2.D0*R2*OS+2.D0*K2*Y*S
      RJ(2,5)=2.D0*K2*Y*S
      RJ(2,6)=R2*G2*OS*OS/T12
      RJ(3,1)=0.0D0
      RJ(3,2)=0.0D0
      RJ(3,3)=-F
      RJ(3,4)=R3*COS
      RJ(3,5)=R3*OS
      RJ(3,6)=R3*G3*COS*OS/T12
      RJ(4,1)=0.0D0
      RJ(4,2)=A2*K2*S*S
      RJ(4,3)=0.0D0
      RJ(4,4)=-2.D0*A2*(K2*Y*S+R2*OS)-A1*R3*COS
      RJ(4,5)=-2.D0*A2*K2*Y*S-A1*R3*OS
      RJ(4,6)=-A2*R2*G2*OS*OS/T12-A1*R3*G3*COS*OS/T12
      RJ(5,1)=A1*K1*S
      RJ(5,2)=0.0D0
      RJ(5,3)=0.0D0
      RJ(5,4)=-A1*(K1*X+R3*COS)
      RJ(5,5)=-A1*(K1*X+R1+R3*OS)
      RJ(5,6)=-A1*(R1*G1*COS/T12+R3*G3*COS*OS/T12)
      RJ(6,1)=A3*B1*K1*S
      RJ(6,2)=A3*B2*K2*S*S
      RJ(6,3)=0.0D0
      RJ(6,4)=A3*(-B1*K1*X-2.D0*B2*(K2*Y*S+R2*OS)+B3*R3*COS)
      RJ(6,5)=A3*(-B1*(K1*X+R1)-2.D0*B2*K2*Y*S+B3*R3*OS)
      RJ(6,6)=A3*(-B1*R1*G1*COS/T12-B2*R2*G2*OS*OS/T12
     *+B3*R3*G3*OS*COS/T12-1.D0)
      CALL EIGRF(RJ,6,6,0,W,ZZ,6,WK,IER)
      IF(IER.LT.32) RETURN
      WRITE(6,810) IER
  810 FORMAT(//,T20,'IER FROM EIGRF = ',I4)
      RETURN
      END
      SUBROUTINE FCN(XX,FF,N,PAR)
      IMPLICIT REAL*8(A-H,K,O-Z)
      DIMENSION XX(N),FF(N),PAR(1)
      COMMON /P2/ K1,KM1,K2,KM2,K3,A1,A2,A3
      COMMON /P3/ G1,G2,G3,B1,B2,B3,F
      TMAX=B1+B3+B2*A1/A2
      IF(XX(1).LT.0.0D0) XX(1)=0.0D0
      IF(XX(1).GT.TMAX*10000.D0) XX(1)=TMAX*10000.D0
      T=XX(1)/10000.D0
      COS=XX(2)/10000.D0
      OS=XX(3)/10000.D0
      F1=DEXP(G1*T/(1.D0+T))
      F2=DEXP(G2*T/(1.D0+T))
      X=(1.D0+KM1*F1*COS)/(F+K1*(1.D0-OS-COS))
      Y=(1.D0+KM2*F2*OS*OS)/(F+K2*((1.D0-OS-COS)**2))
      T1=T/(1.D0+T)
      S=1.D0-COS-OS
      F3=DEXP(G3*T1)
```

```
      FF(1)=B1*(1.D0-F*X)+B2*(1.D0-F*Y)+B3*K3*F3*COS*OS-T
      FF(2)=K1*X*S-KM1*DEXP(G1*T1)*COS-K3*DEXP(G3*T1)*COS*OS
      FF(3)=A2*(K2*Y*S*S-KM2*DEXP(G2*T1)*OS*OS)-A1*K3*F3
     **COS*OS
      FF(1)=FF(1)*10000.D0
      FF(2)=FF(2)*100.D0
      FF(3)=FF(3)*100.D0
      RETURN
      END
```

B30339